Theoretical modelling of transition states for asymmetric processes

Linney, Lynda

Award date:
1995

Awarding institution:
University of Bath

Theoretical Modelling of Transition States for Asymmetric Processes

Submitted by Mrs Lynda Linney

for the degree of PhD

of the University of Bath

1995

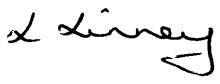

ProQuest LLC
789 East Eisenhower Parkway
P.O. Box 1346
Ann Arbor, MI 48106-1346

Contents

Chapter 1: Summary

The aims of this work are threefold.

(1) To rationalise the causes of asymmetric induction in known reactions of high stereoselectivity.

(2) To predict enantioselectivities for reactions with new substrates, prior to experiment.

(3) To design new catalysts for asymmetric reduction.

A mechanism for the reduction of acetone catalysed by oxazaborolidine-borane adducts (figure 1-1) was determined using the AM1 hamiltonian.

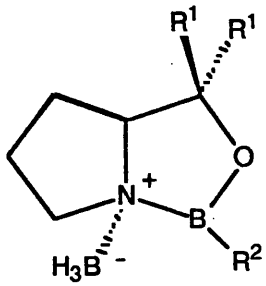

R^1 = H, Ph, β-Nap
R^2 = H, Me, Ph

Figure 1-1

The results from this method accurately reproduced known experimental data and provided valuable insight into the mechanism. The calculations indicated that energetic differences between the epimeric hydride transfer transition states (figure 1-2) were responsible for the stereoselectivity.

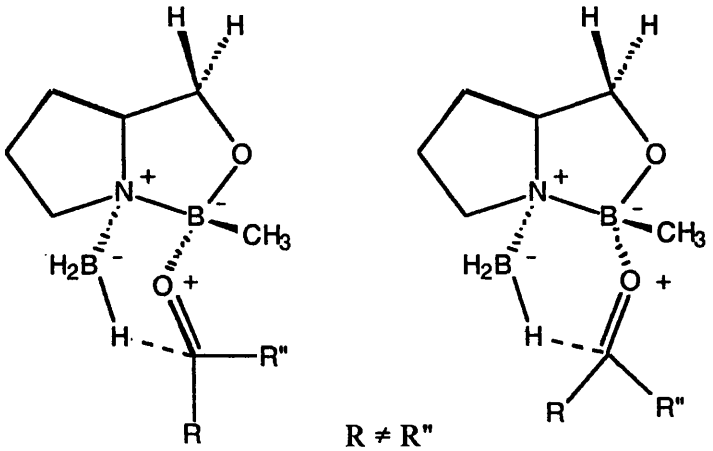

R ≠ R"

Figure 1-2

The selectivity arises from interactions between the boron substituent of oxazaborolidine and the substituents of the ketone, the nature of interaction being dependant on the configuration of the transition state. The predicted selectivity followed the trends noted in published experimental work, but the magnitude of the control was often lower than that observed experimentally.

With this knowledge obtained from the oxazaborolidine system, a new catalyst was designed (figure 1-3).

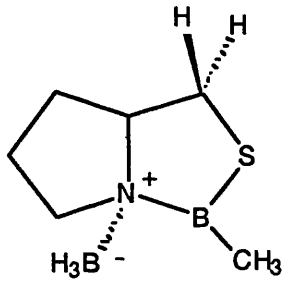

Figure 1-3

The theoretically predicted stereoselectivity was higher than that of the comparable oxazaborolidine system. Experimental work is underway to synthesise this catalyst and observe the enantiomeric excess (e.e.) obtained from the reduction of acetophenone.

The reduction of substituted exocyclic enones by oxazaborolidine-borane adducts had not been studied before. Theoretical e.e.s were predicted for a variety of enones. The experimental work to confirm these results is being undertaken by Professor Tim Gallagher's group.

A collaboration was undertaken with Dr. Martin Wills to study the reduction of ketones by phosphinamide-borane adducts. This study determined the catalytic mechanism and provided insight into the limited stereoselectivity exhibited by these catalysts.

A study of the alkylation reactions catalysed by amino-alcohol-zinc complexes did not identify a mechanism, but highlighted serious problems with the parameterisation of zinc.

Chapter 2: A Review of the Theory Behind the Computational Chemistry Used in This Research and of the Theoretical Basis of the Cited Experimental Work

Electronic structure and molecular mechanics calculations have multiple roles in modern-day chemistry. They supply information about the structures, relative stabilities and other properties of molecules. In this regard, they serve to supplement traditional experimental methods.

Electronic structure calculations are also called on to furnish information about mechanisms and product distribution of chemical reactions. Whilst these calculations provide quantitative information about transition states and reaction mechanisms, qualitative models provide a description for systems which are too large to be described by the more rigorous treatment.

It is their ability to describe chemical reactivity and product selectivity which most clearly distinguishes electronic structure methods (quantum mechanics) from empirical molecular mechanics schemes.

2.1 Molecular Mechanics

Molecular mechanics (MM) assumes that a molecule can be treated as a body comprised of atoms held together by bonds which are approximated to harmonic oscillators. Contributions to the molecule's electronic energy from bond stretching and bending, rotations about internal bonds, van der Waals attractions and repulsions between nonbonded atoms, and electrostatic interactions due to polar groups are all considered. These contributions are summed to give the potential energy, V, for the motion of the nuclei within the molecule:

$$V = V_{str} + V_{\theta} + V_{\omega} + V_{vdw} + V_{es} \quad \text{.....Equation 2-1}$$

V_{str} is the potential energy of bond stretching and is expressed as quadratic function of the displacement of each bond length:

$$V_{str} = \tfrac{1}{2}\sum_i k_s(l_i - l_o)^2 \quad \text{.....Equation 2-2}$$

where k_s is the force constant for that bond, and l_o is the equilibrium bond length (which is provided in the molecular mechanics program).

The bond bending contribution is function of the deviation of the angle from the equilibrium angle θ_o:

$$V_\theta = \tfrac{1}{2}\sum_i k_\theta(\theta_i - \theta_o)^2 \quad \text{.....Equation 2-3}$$

The V_ω term is present for internal rotation about single bonds. In ethane, which has a three fold rotational axis, V_ω is approximated to:

$$V_\omega = \tfrac{1}{2}V_o(1-\cos 3\omega) \quad \text{.....Equation 2-4}$$

where V_o is the barrier height and ω is the torsion angle.

The contribution of the van der Waals energy is calculated from the sum of interactions between nonbonded atoms. The Lennard-Jones 6-12 potential, as shown in equation 2-5, is often employed.

$$V_{vdw} = \frac{a}{R^{12}} - \frac{b}{R^6} \quad \text{.....Equation 2-5}$$

where a and b are constants and R is the inter-atomic distance.

V_{es} is often modelled as the sum of interactions between empirically determined fractional point charges Q_α located at the nuclei:

$$V_{es} = \sum_\alpha \sum_{\beta>\alpha} \frac{Q_\alpha Q_\beta}{R_{\alpha\beta}} \quad \text{.....Equation 2-6}$$

where R_{ab} is the distance between nuclei α and β. An alternative is to place an electric dipole moment of empirically determined magnitude at the centre of the

polar bonds and then V_{es} is expressed as the sum of the interactions between the dipoles.

The force constants and other parameters needed to calculate the potential are selected to reproduce known geometries, energies and vibrational spectra. As sufficient data are required to derive parameters, MM cannot be applied to novel types of compounds. Results of high level *ab initio* calculations are often used to derive parameters where no experimental data are available.

Once a starting geometry has been supplied the program varies the structure until V is minimised. The success of a MM method depends upon the force field employed. The MM2 and MM3 force fields, developed by Allinger[1] for hydrocarbons are widely used; AMBER[2] and CHARMM[3] provide force fields for proteins and nucleic acids.

Whilst MM provides an excellent tool for studying the conformations of large molecules, it cannot be used to investigate transition states, and is therefore of little use to the organic chemist who wishes to investigate the maxima and minima present on a reaction pathway.

2.2. Quantum Mechanical Methods

Quantum mechanics (QM) provides solutions to the electronic Schrödinger equation.[4] The time-independent form is used when considering stationary states of molecules:

$$\hat{H}\psi = E\psi \quad \text{.....Equation 2-7}$$

The Schrödinger equation is an eigenvalue problem. This means that the effect of the operator ($\hat{H}$) on some function (ψ) of the electronics and nuclear co-ordinates is identical to multiplying that function by a constant (E = energy). $\hat{H}$ is the Hamiltonian operator which is the sum of the kinetic and potential energy, V. For one particle moving in three-dimensional space, equation 2-7 is modified to:

$$-\frac{\hbar^2}{2m}\nabla^2\psi + V\psi = E\psi \quad \text{.....Equation 2-8}$$

where $\hbar = (h/2\pi)$, h is Planck's constant and ∇^2 is the Laplacian operator:

$$\nabla^2 \equiv \frac{\partial^2}{\partial x^2} + \frac{\partial^2}{\partial y^2} + \frac{\partial^2}{\partial z^2} \quad \text{.....Equation 2-9}$$

In three-dimensional space with n particles, the potential is expressed in terms of $3n$ co-ordinates, so the Hamiltonian is:

$$\hat{H} = -\sum_{i=1}^{n} \frac{\hbar^2}{2m}\nabla_i^2 + V(x_1,.....,z_n) \quad \text{.....Equation 2-10}$$

The integration of the wave function, ψ, over all the co-ordinates gives the probability of finding an electron in all space:

$$\int |\psi|^2 d\tau = 1 \quad \text{.....Equation 2-11}$$

The eigenfunctions for a one-electron species are orbitals (or hydrogen-like orbitals). They are also referred to as spatial orbitals as their surface encloses a specified amount of probability (figure 2-1). For example, a p_z wave function has a node which means that there is zero probability of finding an electron at r = 0.

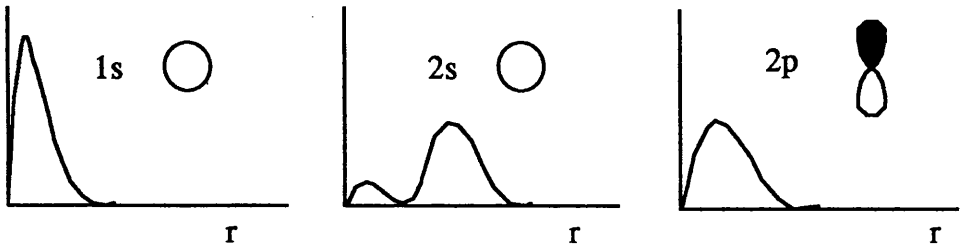

The graphs show the probability of finding an electron at a distance r from the nucleus (radial dependance).
The sketches show the angular-dependence of the wave function.

Figure 2-1

Electrons have spin eigenfunctions of $\frac{1}{2}$ and $-\frac{1}{2}$. A spin function is either α or β (up or down) or a linear combination of α and β. In a one-electron system, the complete wave function is the product of the spatial function $\psi(x,y,z)$ and a spin

function. An orbital which provides a description of the spatial and spin function is called a spin-orbital.

To ensure the Pauli exclusion principle applies, which states no two electrons can occupy the same spin-orbital, an approximate wave function for a system of many electrons can be written as a Slater determinant of spin-orbitals; interchange of two electrons interchanges two rows in the determinant, which multiplies that wave function by -1, thus ensuring antisymmetry.

Another important theorem is the variation theorem. This theorem states that improvements in the wave function will result in a decrease in energy.

Whilst for hydrogen the exact solution to Schrödinger's equation can be calculated, for many-electron atoms the best approach is to use the Hartree-Fock (HF) procedure. The HF method approximates the atomic wave function as a product of one-electron spin orbitals. It finds the best possible forms for the orbitals by an iterative calculation in which each electron is assumed to move in the field produced by the nucleus and the average charge cloud due to the other electrons - this iterative approach is called a self-consistent-field (SCF) method.

HF calculations are usually done by expanding each orbital as a linear combination of basis functions and iteratively solving the HF equation:

$$\hat{F}u_i = \varepsilon_i u_i \quad \text{.....Equation 2-12}$$

where $\hat{F}$ is the Fock operator (which unlike the Hamiltonian operator includes terms for exchange and coulomb integrals), u_i is the i^{th} spin orbital and ε_i is the energy of the spin-orbital.

The coulomb integral represents the potential energy of the interaction between an electron and the electron density cloud from another electron. The exchange integrals has no simple physical interpretation but ensures that the wave function is antisymmetric with respect to electron exchange. Slater-type orbitals were originally used as basis functions but when multi-atom systems were studied

problems arose in evaluating the needed integrals and Gaussian-type functions were developed.

When studying molecules, only a purely electronic Hamiltonian need be considered as the nuclei are considered as fixed and the nuclear motions can be ignored (Born-Oppenheimer Approximation). The electronic Hamiltonian is the sum of the operators for kinetic energy, electron-nuclear attractions and electron-electron repulsions. In the many electron atom, the SCF method constructs an approximate wave function using spin-orbitals, of which the spatial part is an atomic orbital (AO). In molecules, the spatial part is a molecular orbital (MO) which is a linear combination of atomic orbitals (LCAO).

Roothaan modified this approach by using a linear combination of basis functions rather than AO's:

$$\phi_i = \sum_s c_{is}\chi_s \quad \text{.....Equation 2-13}$$

where ϕ is the MO, s is the label of the basis function, i the label of the MO and χ is the basis function.

Substituting equation **2-12** into **2-13** gives:

$$\sum_s c_{is}\hat{F}\chi_s = \varepsilon_i \sum_s c_{is}\chi_s \quad \text{.....Equation 2-14}$$

which on multiplication by χ_r and integration gives the Hartree-Fock-Roothaan Equation:

$$\sum_s c_{is}(F_{rs} - \varepsilon_i S_{rs}) = 0 \quad \text{.....Equation 2-15}$$

where F_{rs} is the Fock operator, ε_i the orbital energies and S_{rs} the overlap integral between the basis functions r and s.

This equation is solved using an iterative approach as the Fock operator is dependant on the orbitals ϕ_i which are dependant on unknown coefficients c_{is}. To solve this equation the Fock matrix is expressed in terms of basis functions, r, s, t

and u and these combine to form one-, two-, three- or four-centre integrals depending on whether the basis functions are different and on the same nuclei.

An initial guess for a starting geometry is generated for the occupied-MO expressions as linear combinations of basis functions. This set of MOs is used to compute the Fock operator and an initial value of ε_i is calculated. This provides an improved set of coefficients, which leads to an improved set of MOs, leading to an improved Fock operator, and so on. This process continues until there is no further improvement in the coefficients and energies.

Quantum mechanical methods can be subdivided into *ab initio* and semi-empirical approaches.

2.2.1 Ab initio Methods

Ab initio methods solve the Schrödinger equation without the use of any approximations. The success of this approach depends on the use of an adequate basis set to provide a reasonable description of the MO. As already mentioned, the use of Slater type orbitals (STOs) was superseded by Gaussian type functions (GFTs). The current practice is to take each basis set as a linear combination of a small number of Gaussians. This combination is referred as a contracted Gaussian-type function (CGFT), and the small number of Gaussians as primitive Gaussians.

Minimal CGFT sets are formed by fitting STOs, which are then approximated to a linear combination of N Gaussian functions. The most common value of N is three, this being the STO-3G basis set. Split valence basis sets use different number of Gaussians to describe the inner-shell and valence orbitals. For example in the 6-31G set, the inner shell is represented by a CGFT comprised of six primitive Gaussians and in the valence shell there are two basis functions, one comprised of three primitive Gaussians and the other is a single diffuse Gaussian.

Polarisation functions use a linear combination of six primitives and adds a single set of six d-type Cartesian Gaussian polarisation function for each non-

hydrogen atom. This is denoted as the 6-31G* or 6-31G(*d*). 6-31G** or 6-31(*d,p*) has the d-type functions used in 6-31G* basis set and adds a set of three *p*-type Gaussian polarisation functions on each hydrogen atom.

To improve accuracy in anionic species, diffuse functions are added. The 6-31+G* adds to 6-31G* four highly diffuse functions (s, p_x, p_y, p_z) on each non-hydrogen atom whilst 6-31++G* includes highly diffused s functions on each hydrogen atom.

The large number of basis functions needed to provide a good description of the MO makes *ab initio* calculations very expensive in terms of computer time and often impractical for anything other than small molecule systems.

A failure of the Hartree-Fock approach is in its neglect of electron correlation. In equation **2-12** the exchange and coulomb integrals account for the interactions between electrons. These integrals allow for the interaction of one electron with another, with the second electron being represented as a smoothed-out averaged electron density. This prevents finding electrons in the same region of space, but it does not allow for the instantaneous electron correlation of electrons. The Hartree-Fock functions has some correlation effects as it satisfies the antisymmetry requirement of the Pauli principle, so their is little probability of finding electrons with the same spin in the same region of space.

This makes the Hartree-Fock energy higher than true energy of the system. Electron correlation effects can be accounted for by either implicit of explicit promotion of electron(s) from occupied molecular orbitals into unoccupied (virtual) orbitals. The configuration interaction (CI) method uses explicit electron promotion whereas Møller-Plesset (MP) perturbation theory involves implicit promotion. In the MP approach, the basis functions in the Fock operator (equation **2-15**) are a combination of both occupied and unoccupied orbitals. For example in MP2, a second order approximation, two occupied orbitals have been replaced by two virtual orbitals. In both these methods, the effect of electron correlation is added to the HF-energy.

The effectiveness of both CI and MP methods depends upon the availability of d-type functions. Occupied molecular orbitals for molecules containing light elements generally have only small contributions from d-type atomic orbitals whereas many of the low level virtual orbitals involve significant contributions from d-type functions. For this reason, the smallest basis set which can be used for meaningful electron correlation corrections is 6-31G*.

2.2.2 Semi-empirical Methods

The semi-empirical methodology provides a means for modelling larger systems as it uses a simpler Hamiltonian and experimentally derived parameters are employed to reduce the number of integrals calculated.

The earliest semi-empirical method was Hückel theory which was developed to study planar conjugated systems. This one electron method assumed that the π-electrons could be treated separately by incorporating the effects of the σ electrons and the nuclei into an effective π-electron Hamiltonian. This was later extended to study non-planar molecules.

A two-electron method was devised by Pariser, Parr and Pople which only considered the valence electrons. The complete neglect of differential overlap[5] (CNDO) and intermediate neglect of differential overlap[6] (INDO) methods, devised by Pople and co-workers, were the first developments of this method. In both these methods only the valence electrons were described by a minimal basis set of STOs and all the three- and four-centred electron-repulsion integrals were ignored. CNDO represented an improvement over Hückel theory as it could represent electron-electron interactions.

INDO was an improved approach as it did not neglect differential overlap between AOs on the same atom in the one-centre electron-repulsion integrals, but still neglected them in two-centre electron integrals.

MINDO,[7] modified INDO, was devised by Dewar and co-workers an improved parameter set but it still could not represent lone-pair/lone-pair interactions.

Pople also suggested neglect of diatomic differential overlap (NDDO) in which overlap is neglected only between AOs centred on different atoms, but parameterisation gave disappointing results. MNDO,[8] developed by Dewar, was based on this approach and parameters were optimised to reproduce heats of formation, dipole moments, ionisation potentials and molecular geometries. MNDO was unable to reproduce hydrogen bonding, which was fatal when studying systems of biological interest, and it also produced spurious results when interactions were just longer than bonding distances.

Using spherical Gaussians to mimic correlation effects, Dewar managed to correct the core-core interactions to remove the spurious results in the long-range interactions. This new method, AM1[9] (Austin Model one), successfully represented hydrogen bonding.

Stewart reparameterised MNDO to give PM3[10] (parametric method number 3) which calculated all one-centre, two-electron integrals. Parameters were derived from molecular data rather than atomic spectral data.

Semi-empirical methods can reproduce heats of formations and geometries in good agreement with the experimental results. Due to the approximations used when considering the valence electrons, the method is considerably less expensive than an *ab initio* approach and is applicable to large systems.

Unlike the *ab initio* approach, energies calculated using the more recent hamiltonians require no further calculations for the effects of electron-correlation, as the effects are included by virtue of the parameterisation.

One failing that was noticed during this research was that the partial charges derived from the Mulliken population were often incorrect. In the Mulliken procedure,[11] the partial charge of an atom is determined from the difference between the expected electron density based on the atomic charge of that atom and that

calculated by the density matrix. The density matrix is obtained when equation **2-15** is expressed in terms of integrals over the basis functions:

$$F_{rs} = H_{rs}^{core} + \sum_{t=1}^{N}\sum_{u=1}^{N} P_{tu}[(rs\,|\,tu) - \tfrac{1}{2}(ru\,|\,ts)] \quad \text{.....Equation 2-16}$$

where $(rs|tu)$ are the two-electron repulsion integrals, P_{tu} is electron density matrix:

$$P_{tu} = 2\sum_{j=1}^{n/2} c_{tj}^{*} c_{uj} \qquad t = 1,2,....,b \quad u = 1,2,...,b \quad \text{.....Equation 2-17}$$

As the Mulliken population method predicted that the electron density at the sp^2-carbon of acetophenone was higher than in 4'-methoxyacetophenone, another method for calculating charge distribution was used.

The method used calculated the charge distribution from the molecular electrostatic potential, ε_p. The molecular electrostatic potential represents the energy of interaction of a unit positive charge at some point in space, p, with the nuclei and electrons of a molecule.

$$\varepsilon_p = \sum_{A}^{nuclei} \frac{Z_A}{R_{AP}} - \sum_{t}^{N}\sum_{u}^{N} P_{tu} \int \frac{\chi_t(r)\chi_u(r)}{r_p} \quad \text{.....Equation 2-18}$$

where Z_A are the atomic numbers, P_{tu} is the density matrix and R_{AP} and r_p are the distances separating the point charges from the nuclei and electrons respectively. The first summation is over the atomic centres and the second is over the basis functions.

A density matrix based on the electrostatic potential is then calculated in three stages: a grid of points is defined surrounding the molecule, the electrostatic potential is calculated at each grid point using equation **2-18**, a least-squares fitting routine fits all the points in the grid to an 'approximate electrostatic potential' in which the nuclear charges and electron distribution are replaced by a set of atom centred charges, Q_A, subject to an overall charge balance.

$$\varepsilon_p^{approx} = \sum_{A}^{nuclei} \frac{Q_A}{R_{AP}} \quad \text{.....Equation 2-19}$$

In MOPAC 93,[12] the currently implemented electrostatic potential approach was devised by Kollman and co-workers.[13] In their approach, the points are positioned at 1.4, 1.6, 1.8 and 2.0 times the van der Waals radii from each atom. In subsequent chapters, all partial charges have been determined using this method.

If the only application of quantum mechanics had been to determine the energy of molecules and certain physical properties, it would not have had such a significant impact on modern chemistry. The ability to locate structures on potential energy surfaces has made QM an indispensable tool for the modern chemist.

2.3 Potential Energy Surfaces

Central to the theoretical description of chemical phenomena is the Born-Oppenheimer approximation, which states that the motion of the electrons in a molecule is uncoupled from the motion of the nuclei. It is the Born-Oppenheimer approximation that leads to the concept of a potential energy surface (PES). As the motion of electrons is separated from the motion of nuclei, a potential energy can be determined for each possible arrangement of the nuclei in a molecule. The PES is the function that describes how the potential energy changes as the nuclei move relative to one another.

Two common representations of PES are given in figure 2-2. The top one, (a), is a transect diagram. The heavy dark line is the minimum energy path (MEP) which connects reactants to products *via* a transition state (TS). The lower, (b), is a contour map.

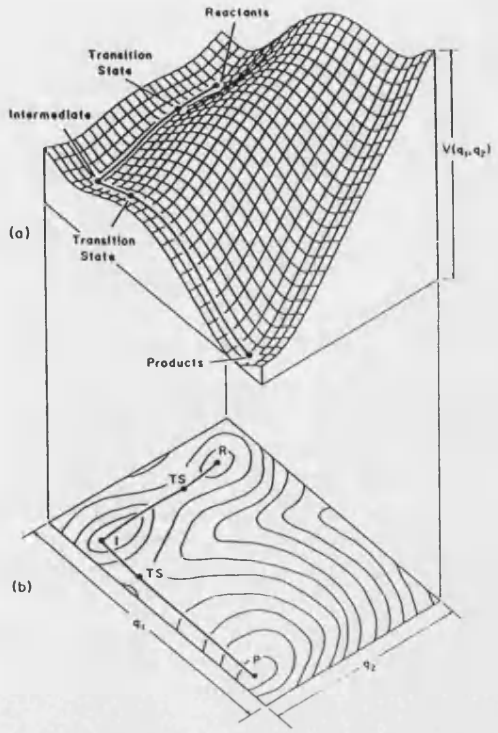

Figure 2-2

The similarity between the energy contours and the height contours used by the Ordinance Survey explains why MEPs are often referred to as valleys and TSs as mountain passes.

If the transect diagram was cut along the MEP, the view of removed cross-section would be the familiar one-dimensional potential diagram (figure 2-3).

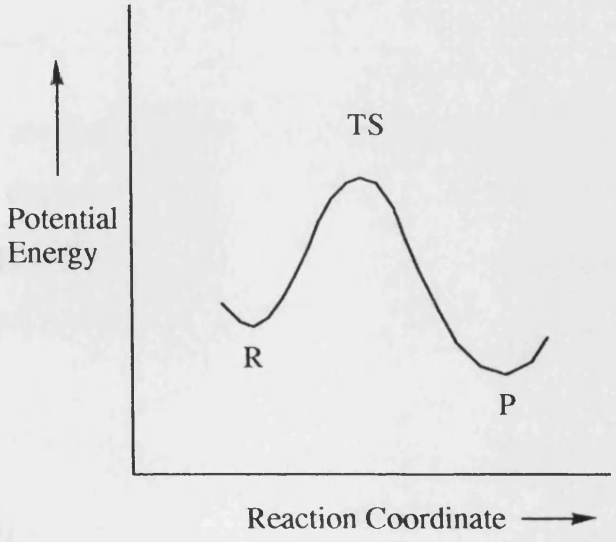

Figure 2-3

The one-dimensional diagram describes a reaction-step in terms of a continuous motion along the reaction co-ordinate. Describing TS as lying on a continuous path between reactants and products is transition state theory.[14] The Arrhenius equation provides a method to relate the barrier height, activation energy, to the rate of the reaction.

$$k_{obs} = A \exp\left(\frac{-E_a}{RT}\right) \text{ or } -E_a = RT \ln\left(\frac{k_{obs}}{A}\right) \quad \text{.....Equation 2-20}$$

where k_{obs} is the observed rate constant, R is the ideal gas constant, T is the temperature, A is the pre-exponential factor and E_a is the activation energy.

The advantage of QM over traditional experimental methods is that it can provide the geometries of the minima as well as the relative energetics (thermodynamics). Whilst kinetic studies can provide the activation energy for a reaction and isotope effects can give an indication of the position of the TS along the reaction co-ordinate, only QM allows the TS to be directly studied.

The reactants, products and TSs are all stationary points. On the one-dimensional representation this implies that the change in energy with respect to the change in coordinates is zero. The mathematical form of this is given in equation 2-21.

$$\frac{dE}{dR} = 0 \quad \text{.....Equation 2-21}$$

In an N atom system, there are 3N degrees of freedom. As the rotational and translation degrees of freedom can be ignored, a consequence of the Born-Oppenheimer approximation, this leaves 3N-6 internal degrees of freedom. On a multi-dimensional surface a stationary point can be defined as:

$$\frac{\partial E}{\partial R_i} = 0 \quad \text{.....Equation 2-22}$$

where R_i represents the 3N-6 independent co-ordinates.

In the one-dimensional case, the minima are points for which the second derivative of the energy with regard to the geometrical co-ordinate are greater than zero and TSs (maxima) are points for which the second derivative is less than zero. With many dimensions, the situation is more complicated because the single second derivative is replaced by a matrix of partial second derivatives.

$$\begin{pmatrix} \frac{\partial^2 E}{\partial R_1^2} & \frac{\partial^2 E}{\partial R_1 R_2} & \cdots \\ \frac{\partial^2 E}{\partial R_2 R_1} & \frac{\partial^2 E}{\partial R_2^2} & \\ \vdots & & \frac{\partial^2 E}{\partial R_{3N-6}^2} \end{pmatrix} \quad \text{.....Equation 2-23}$$

This can be solved by an alternative set of geometrical co-ordinates (ξ_i) for which the matrix of second derivatives is now diagonal, i.e.

$$\begin{pmatrix} \frac{\partial^2 E}{\partial \xi_1^2} & & 0 \\ & \frac{\partial^2 E}{\partial \xi_2^2} & \\ 0 & & \frac{\partial^2 E}{\partial \xi_{3N-6}^2} \end{pmatrix} \quad \text{.....Equation 2-24}$$

The ξ_i are referred to as normal co-ordinates. Within this new co-ordinate system, the minima are characterised by all positive second derivatives and the transition states by all positive second derivatives except for one corresponding to the reaction co-ordinate (ξ_r) for which the second derivative is negative.

$$\text{Minima}: \frac{\partial^2 E}{\partial \xi_i^2} > 0 \; i = 1,2, ..., 3N-6. \qquad \text{Maxima}: \frac{\partial^2 E}{\partial \xi_{ri}^2} < 0$$

Using this approach, the multi-dimension problem has been simplified to a situation which is no more complex than that for the one dimensional case.

2.4 Obtaining Geometries for Stationary Points on the PES

Geometry optimisation is an iterative process. The energy and its first derivative with respect to all geometrical co-ordinates are calculated for the provided guess geometry. This information is then used to project a new geometry. This process is repeated until a lowest energy or optimised geometry is obtained. There are three main criteria which must be satisfied to ensure that the obtained geometry is acceptable; the geometry changes between successive steps must not lower the energy by more than a specified amount; the energy gradient (see equation **2-22**) must be close to zero; and successive iterations must not change any geometrical parameter by more than a small value.

Once these criteria have been satisfied, the calculation of matrix of second derivatives is used to confirm the nature of species.

The algorithms that will be discussed for geometry optimisation are those which were used within this thesis and are found in either MOPAC 93 and/or AMPAC 4.0 and 4.5.[15]

2.4.1 Geometry Optimisation for Minima on the PES

The default optimisation routine for minima in MOPAC and AMPAC is the Broyden-Fletcher-Goldfarb-Shanno[16] (BFGS) method. In this method, the geometry is altered so that the energy decreases and gradient (the first derivative of the energy with respect to the co-ordinates) tends to zero. When small alterations of the geometry do not result in a significant decrease in energy or gradient, the optimised geometry has been located.

Whilst this approach will locate a minima, it does not necessarily locate the lowest energy conformer of that the molecule. For example, rotation about a bond might locate an energetically more favourable structure.

The possible conformations about a particular bond can be investigated by changing the dihedral angle of one of the substituents in small steps. In this calculation, the angle of interest is fixed at the defined bond angle whilst the rest of the molecule, or a defined portion, is allowed to re-optimise. Then the angle is altered by a defined amount, and the optimisation repeated.

Consider 2-butene (figure 2-4), assume that the *cis*-geometry was located by the optimisation method.

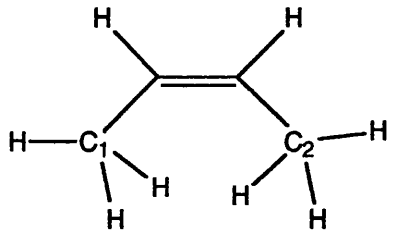

Figure 2-4

In the *cis*-geometry, the dihedral angle C_1-C=C-C_2 is 0°. If this angle was altered in 10° steps from 0° to 180° and the rest of structure allowed to minimise at each stage, an energy profile for rotation about the C=C would be obtained. This profile would have a minimum at 0°, a maximum at 90° and a lower energy minimum at 180°, relating to the *trans*-geometry.

By the use of this calculation, which is referred to as a reaction co-ordinate calculation, a lower energy conformer of the molecule would be located.

This type of process could also be used to determine if the hydrogens attached to the methyl groups preferred to eclipsed or staggered with respect to the double bond.

2.4.2 Transition State Geometry Optimisation

The location of a transition state, or saddle point, is often more difficult than finding an equilibrium geometry. The usual concepts of covalency and hybridisation do not help as the structure is often not well described by these conventional bonding ideas. The best way to locate the TS is to start with a

reasonable approximation of the structure. This 'best guess' can be obtained by several methods:

1. Optimisation of the maximum found on a reaction co-ordinate calculation.

This approach uses a bond distance or bond angle, which when varied, converts the reactants to the products. Consider the S_N2 reaction between a nucleophile, Nuc, and R_3C-Y. Decreasing distance between Nuc and C would result in an increase in the distance between C and Y. Therefore, if the energy was determined for small decreases in Nuc-C bond length, an energy profile for the S_N2 displacement would be obtained (figure 2-5).

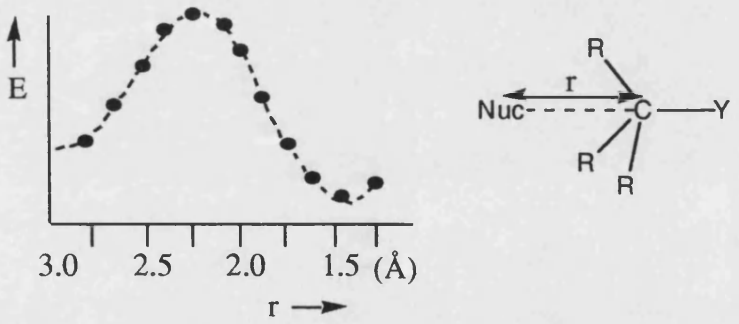

Figure 2-5

The maximum energy structure can then be used as the 'guess structure'. This can be refined by using Bartel's non-linear least squares gradient minimisation routine[17] (NLLSQ) method or by eigenvector following.

NLLSQ locates a TS by minimising the sum of the squares of the gradient vector. This method can also locate minima, albeit much slower than BFGS, but caution must be exercised as it can also locate shoulders on the PES. If the second derivatives of the energy with respect to the co-ordinates are determined, *via* a FORCE calculation, each stationary point can be defined as either a minimum, maximum or some other type of structure.

The 'best guess' structure often has the correct negative eigenvalue, but the gradient of molecule is far from zero or there are other spurious eigenvalues relating to motions of groups not involved in the bond-making or breaking step. The eigenvector-following routine,[18] EF/TS, can be used to follow the direction of correct curvature to locate the TS. This method can only be applied when the guess structure is in close proximity to the TS, it can not be used to locate the TS if the 'best guess' structure is closer to the minima than the TS.

The optimisation of the maximum of the reaction co-ordinate method can fail if there is a sharp discontinuity in the reaction profile (figure 2-6).

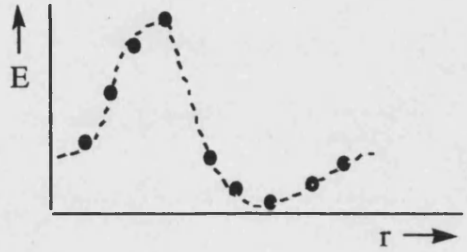

Figure 2-6

A sharp discontinuity will occur when a small displacement of the defined co-ordinate results in significant geometrical reorganisation. Optimisation of the maximum will rarely located the desired TS. This can sometimes be resolved by repeating the reaction co-ordinate calculation but starting from the products and returning to the reactants.

2. Dewar's method of working forwards from the reactants and backwards from the product.

If the reactant and product geometries are known, SADDLE[19] can be used to locate an approximate T.S. An pictorial representation of this method is shown in figure 2-7.

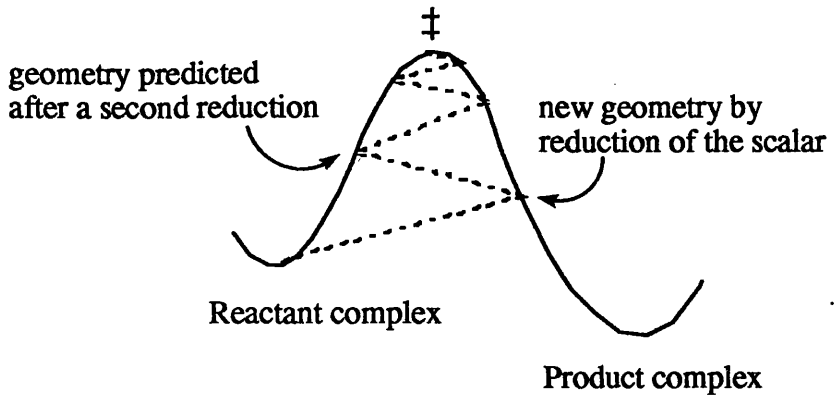

Figure 2-7

The heat of formation of both systems are calculated and a vector relating to a direct path between reactants and products is calculated. The scalar of the vector is reduced by about ten percent, and new vector identifies a new geometry. If this geometry is higher in energy than that of the original product, the process is repeated to locate a higher energy reactant geometry. This method effectively 'climbs' up the energy surface to locate an approximate structure of the T.S. which can then be refined using either NLLSQ or the eigenvector following routine.

3. The use of analogous TSs from previous work.

This approach can be applied to a series of TSs where the only difference between the systems is a change of substituent, which does not exert a significant steric or electronic effect on the TS. For example, consider the two TSs shown in figure 2-8.

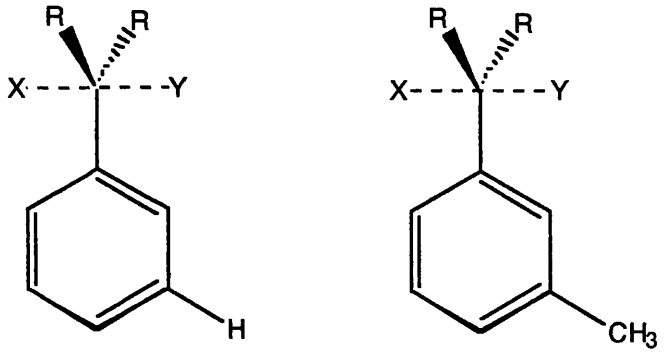

Figure 2-8

The unsubstituted TS can be used as a template for the complicated system. The hydrogen is replaced by the methyl group and the new structure minimised using NLLSQ. It is often advisable to add the substituent and optimise the position of this substituent using BFGS whilst keeping the remainder of the geometry fixed. When the lowest energy orientation of the substituent has been located, the whole system can be subjected to a full geometry optimisation.

This method will not work if the electronic nature of the substituent changes the nature of the TS. For example, the hydride transfer to acetophenone cannot be used as a template for hydride transfer to 4'-nitroacetophenone, as the electron-withdrawing nature of the substituent will alter the TS.

2.5 Studying Complex Reaction Mechanisms

The methods discussed so far have been used to determine the geometry of isolated minima and maxima. A complex reaction mechanism can be subdivided into a series of elementary reaction steps.

In an elementary step, there is a single pathway linking the reactants to the products *via* the TS. The neighbouring minima to the TS are located by intrinsic reaction co-ordinate calculations[20] (IRCs). An IRC calculation follows the path of steepest descent from the TS, in terms of a mass-weighted co-ordinate system, to either neighbouring minima. Both the forward and reverse pathway can be followed by specifying the sign of the initial displacement vector.

In this thesis, several complex reaction mechanisms have been studied (see chapters 4, 9 and 11). Each mechanism was divided into several elementary steps. To determine the continuous path from start to finish, an approximate structure of the reactants was optimised. Using a reaction co-ordinate calculation, a 'best guess' TS was obtained. This approximate TS was then refined using either NLLSQ or the eigenvector following routine. If only one imaginary vibrational frequency was identified by the FORCE calculation, the IRC=1 and IRC=-1

calculations were performed to locate the reactant and product complexes for that elementary step. The product complex geometry for that step was then used as the reactant geometry for the next elementary step in the mechanism.

Using this approach for all the elementary steps, a complex reaction mechanism can be studied.

2.6 The Determination of the Enantiomeric Excess of the Products

This thesis will focus on the enantiocontrol exhibited by several asymmetric catalysts. The enantiocontrol arises from free energy differences in the TSs of the rate determining step. This is a statement of the Curtin-Hammett Principle.[21]

Consider a stereospecific reaction (figure 2-9) in which conformers A and B are in rapid equilibrium and react to give X and Y respectively.

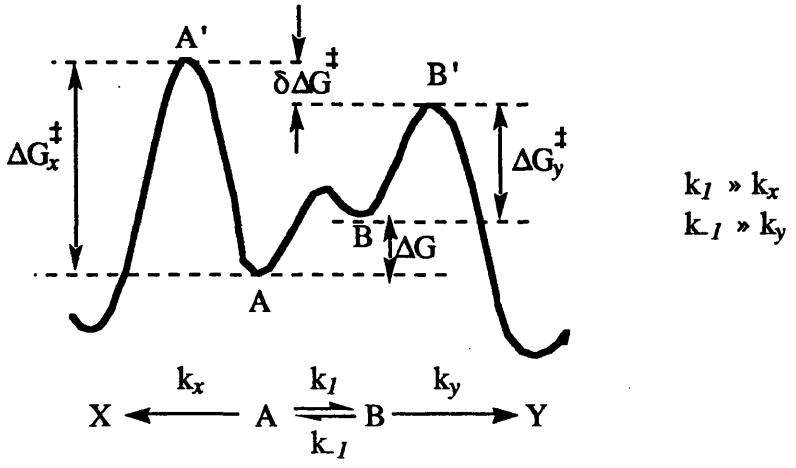

Figure 2-9

The equilibrium constant between A and B is given by:

$$K = \frac{[B]}{[A]} = \frac{k_1}{k_{-1}} \quad \text{.....Equation 2-25}$$

The relative amount of X and Y is given by:

$$\frac{d[X]}{dt} = k_x[A'] \qquad \frac{d[Y]}{dt} = k_y[B'] \quad \text{.....Equation 2-26}$$

$$\frac{d[Y]}{d[X]} = \frac{k_y}{k_x}.K \quad \text{.....Equation 2-27}$$

Replacing equilibrium and rate constants by free energy terms gives:

$$\frac{d[Y]}{d[X]} = \frac{e^{-\Delta G_y^{\ddagger}/RT}}{e^{-\Delta G_x^{\ddagger}/RT}}.e^{-\Delta G/RT} = e^{\delta\Delta G^{\ddagger}/RT} \quad \text{.....Equation 2-28}$$

The relative amount of the two products is thus only dependant on the difference in the free energy of activation for the two routes related to a common origin; it is not dependant of the stability of the two conformers.

For the stereoselective reactions studied in this thesis (see chapters 6 and 7), the enantiomeric excess (e.e.) was dependant on the free energy differences between four hydride transfer TSs, two conformers of a six-membered ring in both epimeric forms. For example, see figure 2-10.

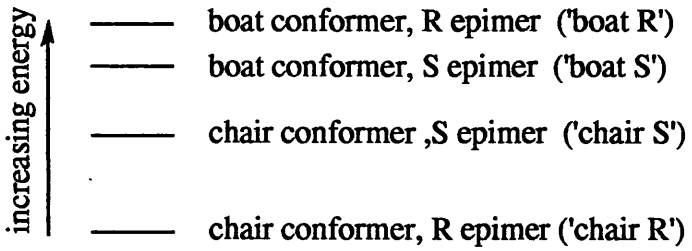

Figure 2-10

The enthalpy difference between the 'chair R' TS and the other higher energy TSs can be calculated from the energies provided by MOPAC or AMPAC. To calculate the enantiomeric excess (e.e.) of a product, the free energy differences between the TSs have to be calculated. The entropy differences between the TSs are calculated using CAMVIB and CAMISO.[22]

These two programs evaluate molecular partition functions, zero-point energies and thermodynamic properties from the vibrational frequencies determined

in the FORCE calculation. Spurious translational and rotational contributions to vibrational frequencies, arising from the determination of the Cartesian force constants by numerical finite differencing of analytical gradients using rectilinear displacements, are eliminated by a projection method, and the resulting vibrational frequencies are entirely consistent with the masses and moments of inertia obtained from the molecular geometries.

The free energy differences can then be calculated as the enthalpy and entropy differences are known. The relative populations are then calculated using equation 2-29.

$$\text{relative population} = \exp\left(\frac{-\delta(\Delta G)}{RT}\right) \quad \text{.....Equation 2-29}$$

where $\delta(\Delta G)$ is the free energy difference between the TS and the lowest energy TS, R is the ideal gas constant and T is the temperature.

Using this approach, the relative population of the lowest energy TS, in this example 'chair R', is one. The populations are then normalised, so that the sum of the populations are equal to one. From these normalised populations, the e.e. can be calculated using equation 2-30.

e.e. = [normalised population of the R TSs - normalised population of the S TSs] x 100 .....Equation 2-30

2.7 Kinetic Isotope Effects

It is not the aim of this introduction to provide a review of all experimental physical organic methods that furnish information about reactions mechanisms. Many excellent text books serve this purpose.[23] The only technique that will be reviewed is that of kinetic isotope effects. Kinetic isotope effects were available for some of the systems studied, so a review of this method is pertinent to this thesis.

Kinetic isotope effects arise from the fact that the zero-point energy of a molecule containing a heavier isotope is lower than that of the lighter, unsubstituted molecule. Consequently, less energy is required to dissociate a carbon-hydrogen bond than a carbon-deuterium bond (figure 2-11).

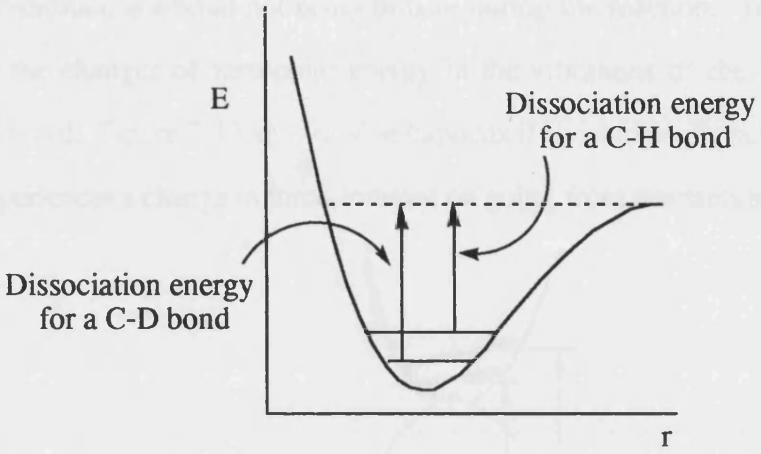

Figure 2-11

Therefore if a C-H bond is cleaved in the rate determining step, substitution of deuterium for hydrogen will result in rate decrease. Therefore, the ratio of rate constants for the unsubstituted and substituted reaction, k_H/k_D, would be greater than one.

Isotopic labelling provides a valuable tool for mechanistic determination. For example, the bromination of acetone was known to be independent of the bromine concentration so it was postulated that the rate determining step was ketone tautomerisation (figure 2-12).

Figure 2-12

As the rate determining step involved cleavage of a C-H bond, repeating the reaction with deuterated acetone should have a significant effect on the rate - k_H/k_D was found to be 7. k_H/k_D typically lie between 1 (no isotope effect) and 8 and are greatest when the hydrogen is symmetrically bonded to the atoms between which it

is being transferred or in a straight line between the two atoms. k_H/k_D values of less than 1 are called inverse kinetic isotope effects.

Kinetic isotope effects can be observed in reactions which do not involve cleavage of a C-H bond. A secondary isotope effect is one that results from isotopic substitution at a bond not being broken during the reaction. These effects arise from the changes of zero-point energy in the vibrations of the isotopically substituted bond. Figure 2-13 shows what happens if an isotopically substituted C-H bond experiences a change in force constant on going from reactants to the TS.

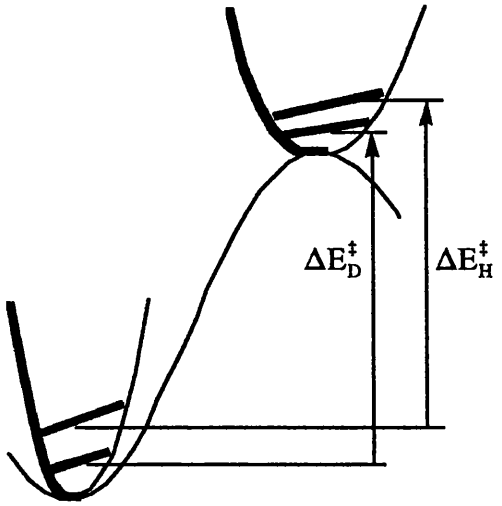

Figure 2-13

As the force constant has decreased in the TS, as a result of weaker bonding, there is a smaller difference between hydrogen and deuterium zero-point energy. Therefore k_H/k_D is greater than one, but of a small magnitude.

Secondary isotope effects are most commonly observed when deuterium substitution is made at a carbon which undergoes a change in hybridisation during the reaction. Consider the solvolysis of isopropyl bromide shown in figure 2-14.

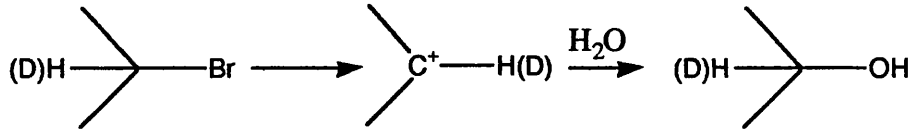

Figure 2-14

In this reaction, the reactants are sp^3 hybridised and the TS is sp^2 hybridised. A significant decrease in the force constant for the out-of-plane bend (figure 2-15) is associated with this change in hybridisation.

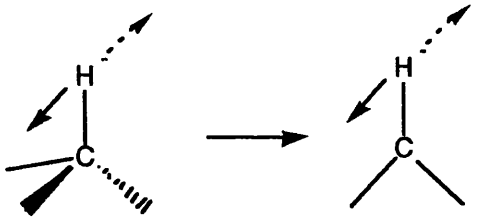

bend
1350 cm^{-1}

out-of-plane bend
800 cm^{-1}

Figure 2-15

The energy difference between the zero-point energies is less in the T.S., so the reaction is slowed by substitution of deuterium for hydrogen, and the k_H/k_D is 1.34, which is typical for sp^3 - sp^2 changes. This is often referred to as a secondary α-deuterium isotope effect as the substitution occurred at the α-position.

β-secondary isotope effects can also observed (figure 2-16).

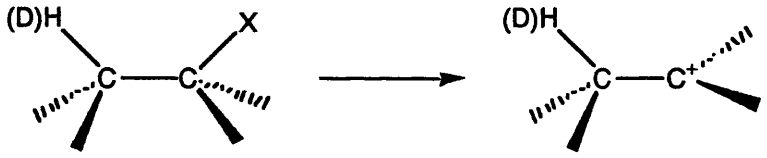

Figure 2-16

The C-H(D) bond is weakened and the frequencies lowered by hyperconjugation. The most significant reduction of frequency is in the bending mode. k_H/k_D can vary in the range 0.7 to 1.4 and are dependant upon the dihedral angle between the C-H(D) bond and the vacant *p* orbital on the β-carbon.

2.8 The Objectives of this Research

There were two distinct aspects to this research. The general aims were to *rationalise* the causes of asymmetric induction in known reactions of high stereoselectivity and to *design* new catalysts for asymmetric synthesis.

The following objectives had to be achieved:

1. critical evaluation of existing computational methodology for modelling of TSs in complex molecular systems, by means of...

2. theoretical investigation of the mode of action of chiral oxazaborolidine and organozinc catalysts.

3. theoretical modelling of TSs of new stereoselective reactions in collaboration with experimental chemists at the Universities of Bath and Bristol.

Chapters 3, 5, 8 and 10 provide a review of the pertinent literature for the computational study discussed in the proceeding chapter.

Chapter 4 discusses the computational study of the mechanism for the reduction of ketones by oxazaborolidine-borane adducts. All structures in this chapter have the prefix **oab-**, except for the those in the study of the uncatalysed reduction which have the prefix **uncat-**.

Chapter 6 discusses the computational investigation into the determination of the origins of stereoselectivity, all structures have the prefix **chi-**.

Chapter 7 describes the study of new stereoselective reactions, the structures having the prefix **new-**.

Chapter 9 reports the findings of the computational study of the reduction of ketones by phosphinamide-borane adducts. All structures in this chapter have the prefix **npo-**.

Chapter 11 focuses on the computational study of dialkylzinc chemistry. The organozinc-dialkylzinc complexes have the prefix **nzo-** whereas the oxazaborolidine-dialkylzinc complexes have the prefix **nbo-**.

Chapter 3: The Reduction of Prochiral Ketones by Chiral Oxazaborolidine-Borane Adducts: A Review of the Literature

3.1 Introduction to Oxazaborolidine Chemistry

Oxazaborolidines (OABs) are extensively used as asymmetric catalysts.[24] Their main application is as OAB-borane adducts which are used in the reduction of aromatic prochiral ketones to yield secondary alcohols of high optical purity. OABs have also been used as catalysts for other reactions including Diels Alder cycloaddition reactions[25] and alkylation reactions.[26] The success of OAB chemistry stems from the ease in which the N-B-O moiety can be incorporated into a chiral environment, typically the nitrogen and oxygen are provided by a β-amino alcohol.

Itsuno and co-workers effected the first reduction using an oxazaborolidine-borane adduct.[27a] They investigated the reduction of propiophenone by the complexes formed between β-amino alcohols and borane-tetrahydrofuran. Figure 3-1 shows the enantiomeric excess of the generated (R)-1-phenylpropan-1-ol.

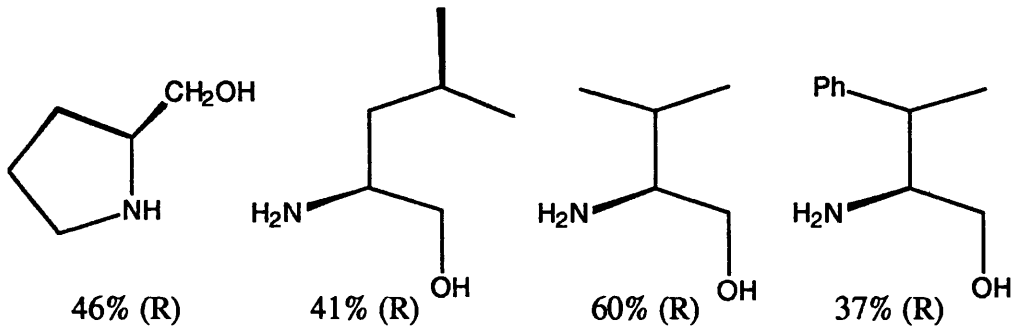

Figure 3-1

From the results of this and subsequent studies,[27b-e] Itsuno proposed that the resulting complexes contained a relatively rigid five-membered ring system. He suggested 'that this chiral complex may be a chiral catalyst, not a reagent' - this type ofreaction is now referred to as ligand-accelerated catalysis.

In 1987 Corey *et al.* proposed the structure of Itsuno's complex, which was later confirmed by ^1H NMR and X-ray crystallography.[28] With the insight provided by the structure, Corey developed a bicyclic oxazaborolidine, which is often referred to as the CBS (Corey-Bakshi-Shibata) catalyst, and proposed a possible mechanism for the reduction (figure 3-2).[29]

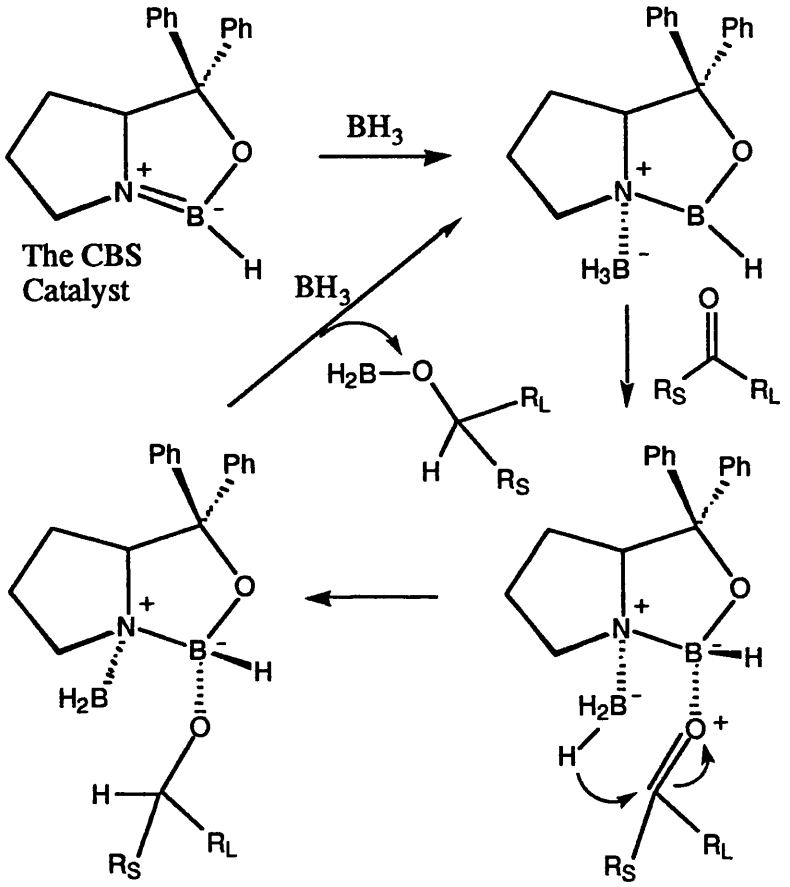

Figure 3-2

These systems are often called 'chemzymes', as the ketone and borane are bound in close proximity, and after the reduction has occurred the oxazaborolidine releases the product, by analogy with enzymes.

After the structure had been proposed, a multitude of OABs were synthesised, some of which are shown in figure 3-3. The enantiomeric excesses are quoted for the reduction of acetophenone by the borane adduct of the OAB shown.[29,30a-i]

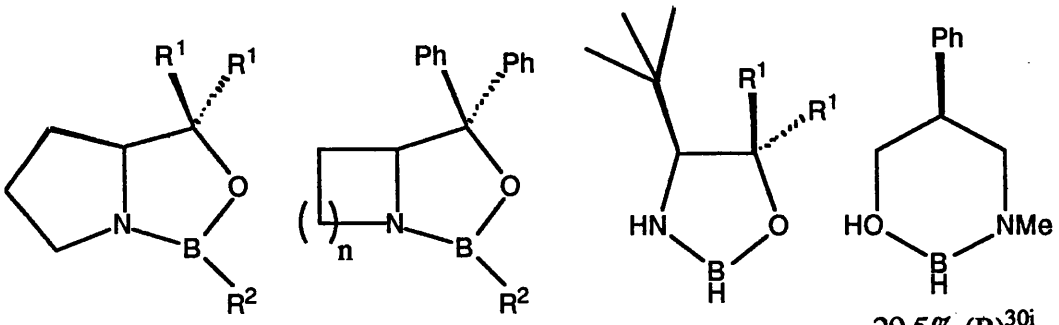

R^1	R^2	e.e
Ph	H	97% (R)[29]
Ph	Me	97% (R)[30a]
Ph	Ph	96% (R)[30b]
H	H	8% (R)[30c]
		95% (R)[30d]

n	e.e.
0	94% (R)[30e]
1	98% (R)[30f]
3	87% (R)[30g]

R^1	e.e
H	80% (R)[30h](R)
Ph	89% (R)[30h](R)

29.5% (R)[30i]

Figure 3-3

3.2 Experimental Insight into the Catalysed Reduction Mechanism

The mechanism proposed by Corey involved four elementary steps: formation of the borane adduct; binding of the carbonyl group; hydride transfer via a six-membered boat transition structure; addition of borane to release the alcohol (after work up) and to regenerate the catalyst.

Experimental elucidation of the mechanism has focused on formation of the borane adduct and the hydride transfer step.

3.2.1 Formation of the Borane Adduct

The addition of borane to the oxazaborolidine results in the formation of a borane adduct which is soluble in a variety of aprotic solvents, such as benzene, dichloromethane, chloroform or toluene. A variety of boron-based hydride sources have been used including borane-dimethyl sulfide complex, borane-tetrahydrofuran (borane-THF) complex and catecholborane.

Mathre *et al.* noted that an equilibrium existed between the adduct and free oxazaborolidine plus borane (figure 3-4).[31] As a consequence a small amount of free oxazaborolidine was always seen. In Lewis-basic solvents, such as tetrahydrofuran, the free borane formed a complex with the solvent and thus the percentage of the OAB-borane adduct present in the solution was concentration dependent.

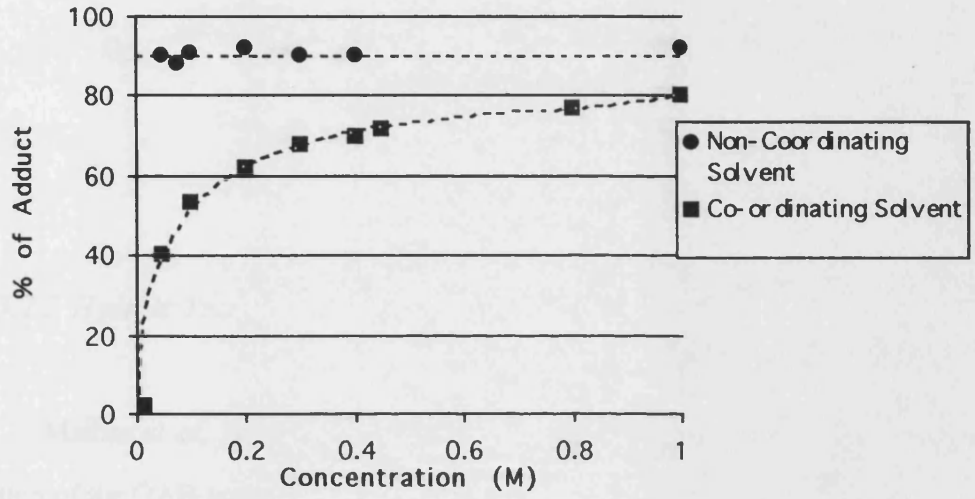

Figure 3-4

As the borane-THF complex can reduce prochiral ketones to a racemic alcohol, Mathre concluded that the concentration dependent equilibrium would have to be considered in the optimisation of oxazaborolidine catalysed reductions performed in THF.

Tlahuext and Contreras stated that the addition of diborane decreased the double bond character of the nitrogen to boron bond in the OAB resulting in an increase in the acidity of the boron.[32] This increase would favour intramolecular co-ordination of a hydride to the boron atom and it was proposed that the resulting bridged structure could be in an equilibrium with a dimer formed by a three centre, two electron B-H-B bridge (figure 3-5).

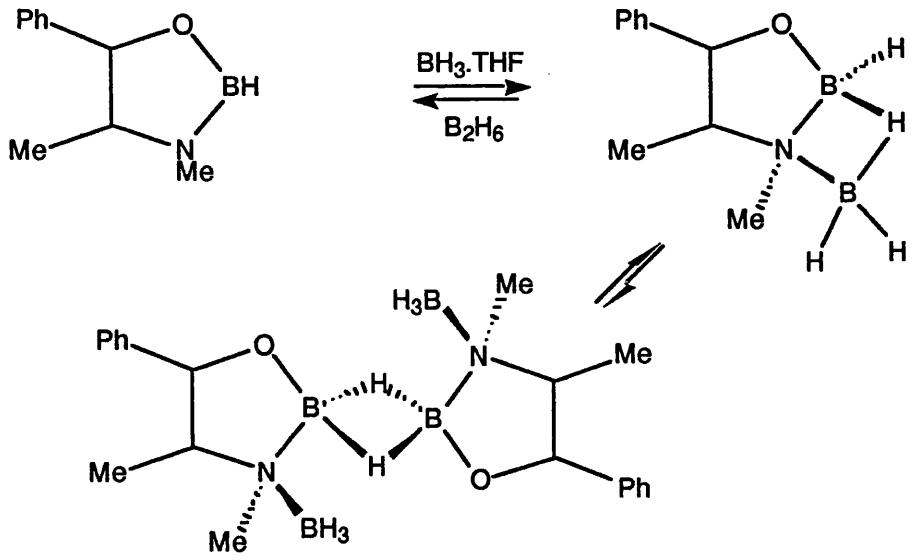

Figure 3-5

3.2.2 Hydride Transfer

Mathre *et al.* investigated the effect of stoichiometry and solvent on the reaction of the OAB-borane adduct with acetophenone.[32] In both protic and aprotic solvents the reaction went to completion when the borane-adduct to ketone ratio was 1:2. From this it was concluded that two of the three hydrogen atoms of the borane were readily available for participation in the reduction step. Cai and co-workers discovered that the addition of triethylamine and some alcohols could be added to the reaction mixture to prevent the second hydride transfer.

Corey and co-workers[33] measured the relative rates of reduction of acetophenone and its *para*-nitro and *para*-methoxy derivatives by an OAB-borane adduct: 1.0, 3.4 and 1.8 respectively. From this it was concluded that, as there was only a small rate difference, 'neither the ketone-catalyst co-ordination nor hydride transfer to carbonyl steps were strictly rate limiting for these substrates.' The reduction of acetophenone by a 1:1 mix of ^{1}H and ^{2}H borane-OAB adduct revealed a kinetic isotope effect (k_H/k_D) for the hydride transfer step of 1.7 from which Corey concluded that this was indicative of an early transition state for the highly exothermic hydride transfer step.

As the reactivities of α,α,α-trifluoro and α,α,α-trichloroacetophenone were found to comparable to acetophenone, Corey stated that the increased electrophilicity of the carbonyl carbon compensated for the lower Lewis basicity and greater steric shielding of the carbonyl oxygen. The value of k_H/k_D decreased to 1.1 for the reduction of α,α,α-trifluoroacetophenone by a 1:1 mixture of catecholborane-^{1}H and catecholborane-^{2}H-OAB adduct from which the conclusion was drawn that the association of the ketone to the borane adduct was rate limiting.

3.3 Mechanistic Insights from Theoretical Studies

The most comprehensive investigation of the reduction mechanism of OAB-borane adducts has been undertaken by Nevalainen.[34] Simple models were used in his *ab initio* studies to represent the pertinent interactions. His studies were performed using a variety of basis sets, but the lack of a consistent model and basis set prevents a detailed discussion of the energetic and geometrical changes during one catalytic turnover. The results summarised in this section are for the most complex system studied using the 6-31G split-valence basis set, with polarisation functions, where included.

3.3.1 The Effect of a Lewis-Basic Solvent on the OAB

Nevalainen used the systems shown in figure 3-6 to calculate the energy of solvation for the OAB.[34c] Water was used as a model for tetrahydrofuran.

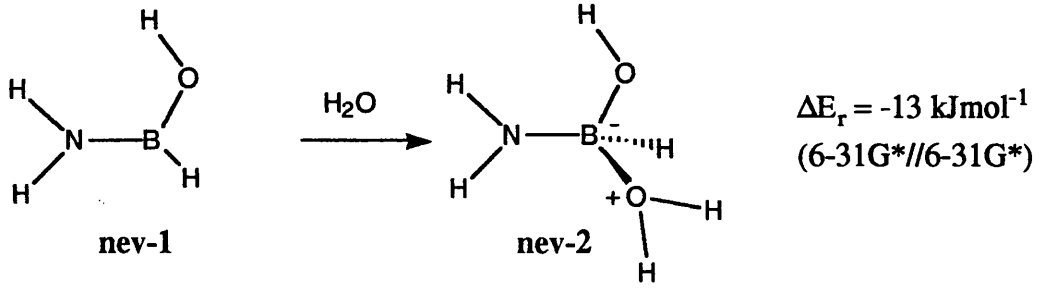

Figure 3-6

Only 'loose' complexes were formed in which the water-boron interaction was greater than 3 Å, with the stabilisation appearing to be due to hydrogen-bond formation rather than co-ordination to boron. As expected with such a weak interaction, no significant changes in geometry were observed in either the water or the oxazaborolidine moiety.

3.3.2 Formation of the Borane Adduct.

The formation of the borane adduct was studied by considering the addition of borane-water, as a model of borane-THF, to the simple OAB shown in figure 3-7.[34a]

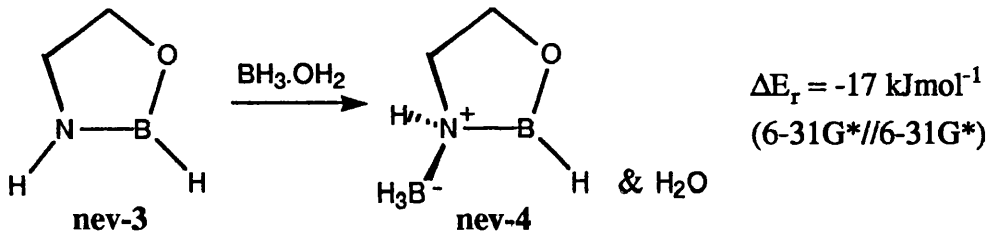

nev-3 nev-4

Figure 3-7

The decrease in donation from nitrogen to the OAB boron resulted in an increase in the acidity of boron, a change which favours the donation of electrons from the sp^2-oxygen of a ketone.

Polarisation of the charge distribution within the borane moiety increased during binding, with the hydrogens becoming more negatively charged and boron more positive. As the reducing power of the borane-adduct increased with the increasing polarisation of the borane moiety, the non-catalysed reduction of a ketone by free borane-THF should not compete with the intramolecular reaction.

Nevalainen also studied possible co-ordination of borane to the oxygen of the oxazaborolidine moiety.[34k,m] Although co-ordination was structurally possible, the N-adducts were found to be more favourable by about 19 kJ mol^{-1} (6-31G*//6-31G*). He noted that 'even if O-adducts were formed the orientation of the borane (with respect to the ketone) would be wrong for hydride transfer too occur.'

The OAB-borane adduct was found to be stabilised by the formation of a solvated species (figure 3-8). A loose complex, **nev-5a**, was formed by the co-ordination of the solvent *anti* to the N-BH_3 bond, but this was found to be energetically more favoured than the tight complex formed *via syn* co-ordination, **nev-5b.**

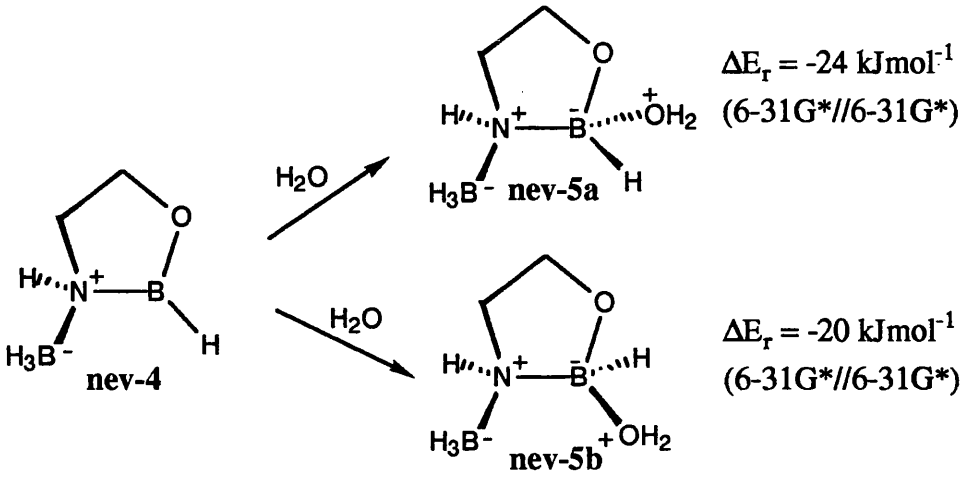

Figure 3-8

In both structures, there was a marked decrease in the N-BH_3 bond distance compared to the 'non-solvated' structure.

All attempts to optimise models of the bridged structures found by Tlahuext and Contreras[32] resulted in the formation of a eclipsed moiety, with no hydride bridge, which was 3.6 kJ mol^{-1} higher in energy than the staggered form (figure 3-9).[34i]

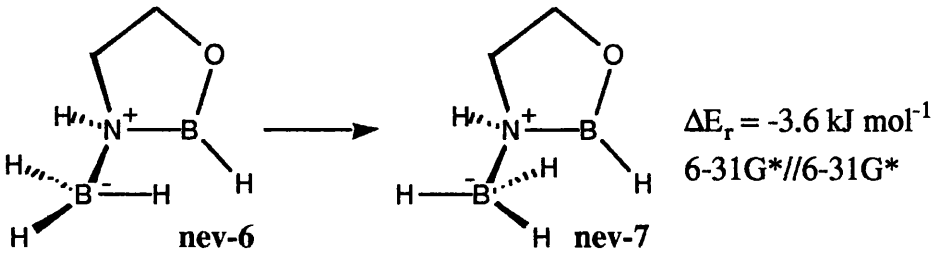

Figure 3-9

The formation of a tightly bound dimeric system was not observed, rather a weak aggregate with the B-H distance greater than 3 Å.

Although the combination of two OAB monomers to form a dimer was calculated to be energetically favoured, the energy required to displace a molecule of

water from each monomer was predicted to be greater than the energy released on dimerisation.

Aggregation of OAB-borane adducts was predicted to be energetically favoured. Nevalainen proposed that the addition of borane to a solution of dimeric oxazaborolidines would increase the stability of the dimer, whereas the addition of catecholborane would not significantly alter the degree of aggregation. He stated that this postulate was supported by experimental observations: in non-polar solvents the reaction temperature can not exceed -78°C, whereas in THF borane can be used as the hydride source at 23°C, as the higher temperature and choice of solvent prevents aggregation.

3.3.3 Co-ordination of the Ketone

Formaldehyde was used as a simplified model for a prochiral ketone, and the reaction shown in figure 3-10 was considered to determine the changes in energetics related to the ketone binding.[34c]

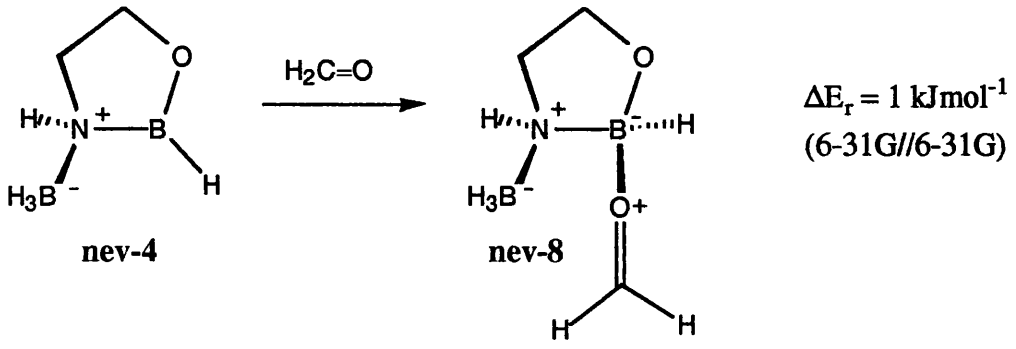

Figure 3-10

As the electron demand of the ring boron decreased on binding, the electron density of nitrogen increased resulting in a decrease in the N-BH_3 bond length. This further polarised the borane moiety.

The effect of the Lewis-basic solvent was determined by considering the two reactions shown in figure 3-11:

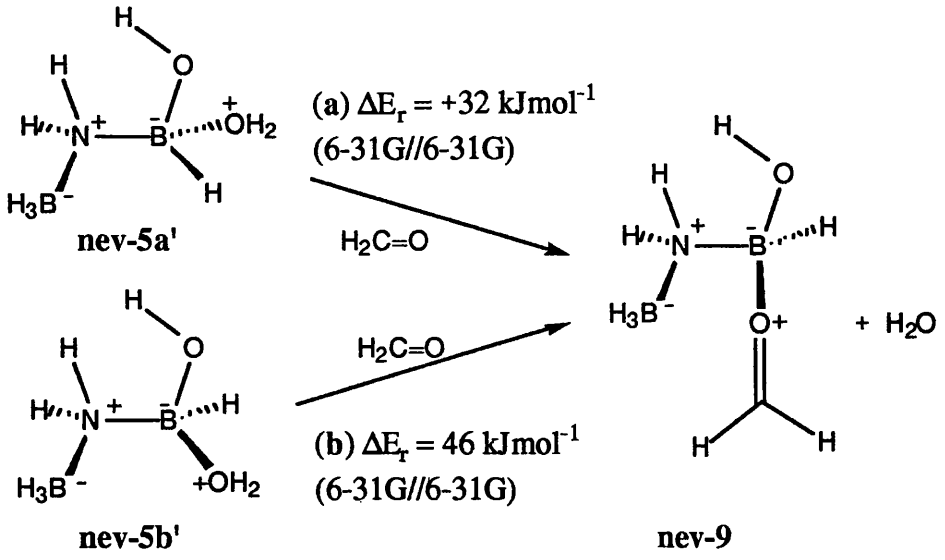

Figure 3-11

In pathway (a), the boron of the OAB moiety was still sp^2-hybridised and the approach of the ketone to the co-ordination site was unhindered. In the adduct of pathway (b) the dipole moment 'points in the wrong direction to attract a ketone to approach the boron of the oxazaborolidine ring.'

For the uncatalysed reaction, the binding of the ketone to the hydride source can be represented as

$$H_3B\text{-}OH_2 + H_2C{=}O \rightarrow H_2C{=}OBH_3 + H_2O$$

The overall energy change for this reaction was calculated to be +18 kJ mol^{-1} (6-31G//6-31G). He concluded that the low barrier for the uncatalysed reaction explained the experimental observation that the enantioselectivity decreased with increasing concentrations of borane-THF.

In a later study on the orientation of the bound ketone, Nevalainen located another conformer in which the carbonyl bond was parallel to the N-B linkage of the OAB (figure 3-12), rather the perpendicular as for **nev-8.** [34h]

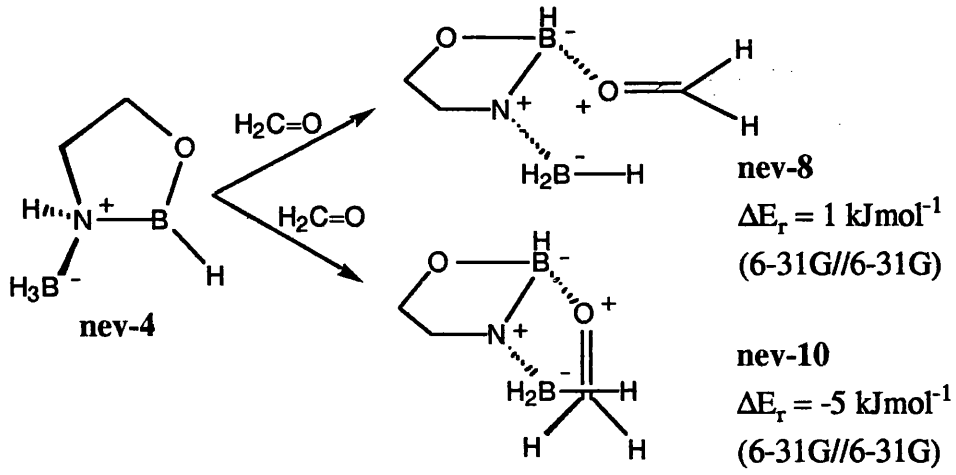

Figure 3-12

Nevalainen applied Hine's Principle of Least Nuclear Motion[35] to determine which of the two conformers was most likely to undergo hydride transfer (figure 3-13). The changes in specific bond lengths which arose from ketone binding were compared with those predicted to occur during hydride transfer.

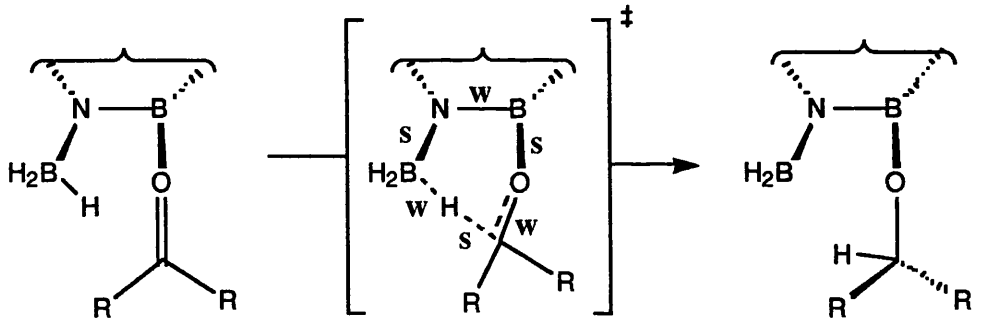

Figure 3-13

nev-10 was found to be closer to the transition structure as those bonds weakened by the hydride transfer had lengthened more during the co-ordination of the carbonyl group, and those strengthened by transfer had decreased by more than those in **nev-8**.

3.3.4 After Hydride Transfer.

After the hydride transfer step, Nevalainen located several possible pathways for the regeneration of the catalyst.

The hydride transfer (figure 3-14) was found to be a highly exothermic reaction.[34d]

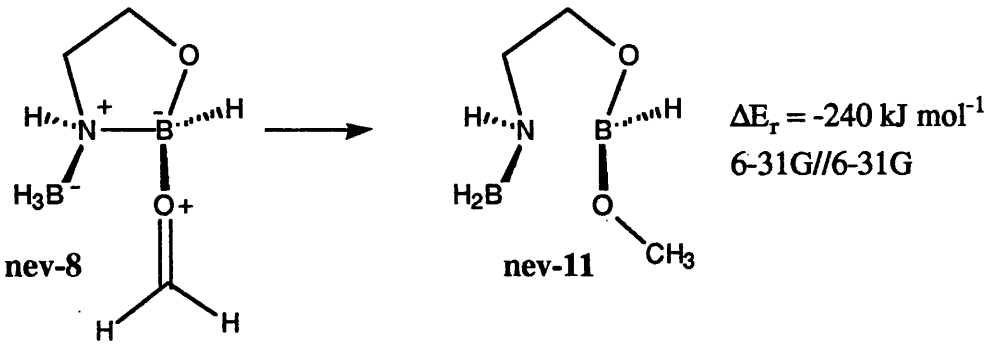

Figure 3-14

All attempts to optimise a structure which had the N-B bond intact resulted in 'spontaneous decomposition' into **nev-11.** The last structure located before decomposition occurred, for which the energy gradient was 6.26 kJ mol^{-1} Å^{-1}, was 88 kJ mol^{-1} higher in energy than **nev-11** (4-31G*//4-31G*). On the basis of his earlier studies of solvent effects, Nevalainen stated that the co-ordination of a Lewis basic solvent to the -BH_2 group would prevent decomposition as the electron demand of the -BH_2 moiety would decrease, resulting in a strengthened *endo*-cyclic N-B bond.

The N–B bond of the OAB was reformed during the step shown in figure 3-15.[34d]

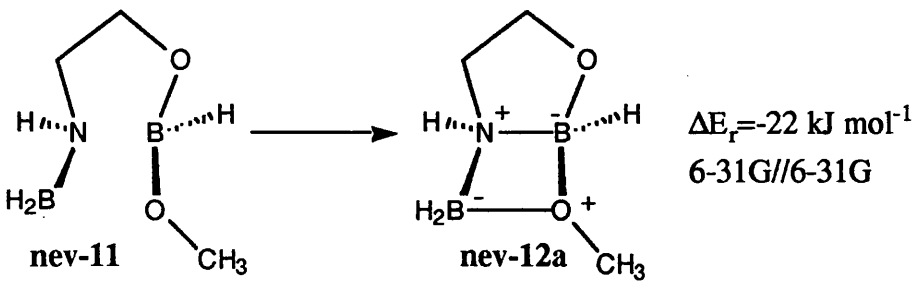

Figure 3-15

By studying the Mulliken overlap populations of the atoms in oxazadiboretane ring, Nevalainen determined that the boron of the OAB to the oxygen of alkoxyborane moiety had the minimum overlap. He concluded that this bond could be cleaved to form an OAB-alkoxyborane moiety (figure 3-16). [34e] The regeneration of the OAB and liberation of alkoxyborane was endothermic, irrespective of whether the alkoxyborane was removed in one or two steps.

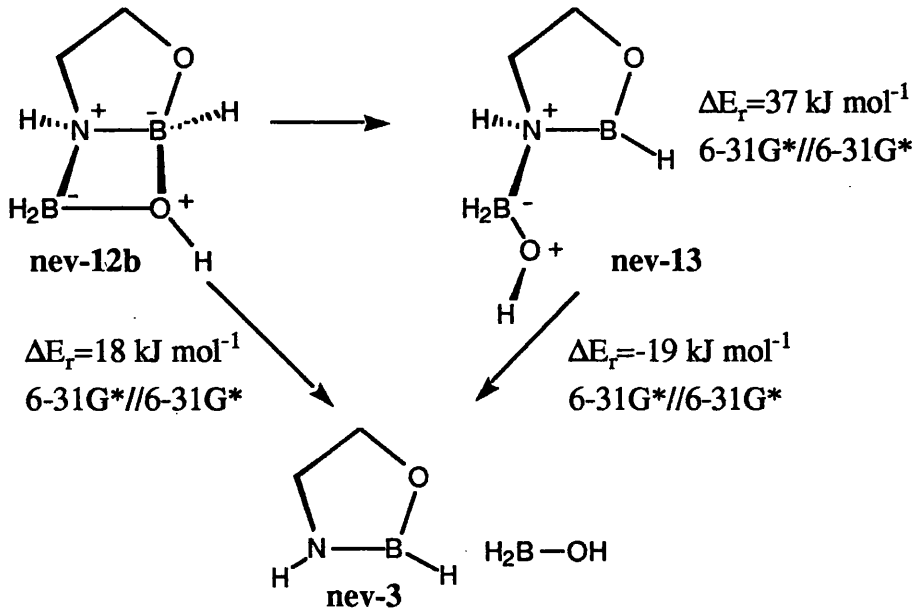

Figure 3-16

Studies on the 'alkoxyborane'-OAB adduct **nev-13** showed that the hydrogens were more negatively charged implying a higher propensity to deliver a hydride than the borane adduct. If another hydride transfer occurred, Nevalainen predicted that a dialkoxyborane-OAB adduct would be a weaker Lewis-acid than either of the previous adducts, making a third hydride transfer unlikely and cleavage of the *exo*-cyclic N-B bond would occur.

The removal of the methoxyborane from **nev-12a** was calculated to require +54 kJ mol^{-1} of energy (6-31G//6-31G). [34d] An alternative, lower energy route[34o] (figure 3-17) involved the addition of more borane to form **nev-14a** or **nev-14b.** The liberation of the alkoxyborane from **nev-14a** either **nev-14b** resulted in the regeneration of the OAB-borane adduct.

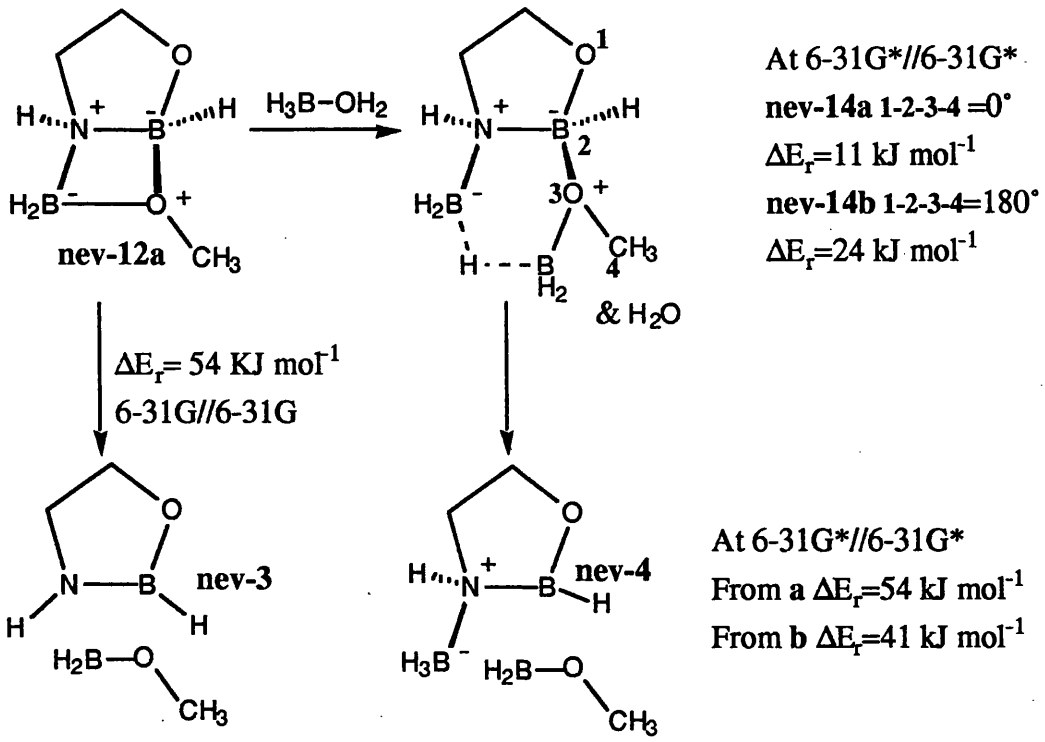

Figure 3-17

Based on earlier solvent studies, Nevalainen predicted that the 'barrier' to the release of alkoxyborane would be +9 kJ mol^{-1} from **nev-14a** and -4 kJ mol^{-1} from **nev-14b** in the presence of a Lewis-basic solvent.

If no basic solvent was present, the catalytic cycle would stop as the reco-ordination of the alkoxyborane would be more favoured than ketone co-ordination.

Nevalainen has also proposed a mechanism involving a hydride shift (figure 3-18).[34q]

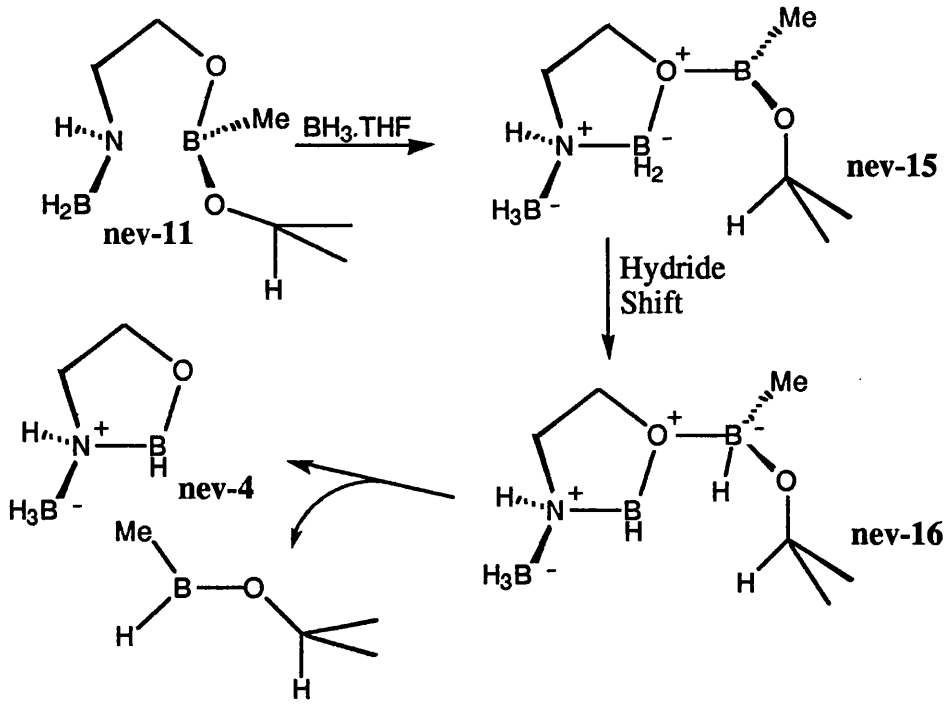

Figure 3-18

Whilst models of these structures have been studied, there was no consistent set of models or basis set from which the energy changes could be calculated. Despite this, Nevalainen stated that the addition of borane-THF for form **nev-15** was a favoured process. An analogous hydride transfer to **nev-15** to **nev-16** released about 13 kJ mol^{-1} (6-31G//6-31G). As of yet, there have been no studies for the regeneration step from **nev-16**.

Chapter 4: A Computational Study of the Mechanism for the Reduction of Acetone by Chiral Oxazaborolidine-Borane Adducts

For the determination of the mechanism, the OAB-borane adduct derived from (S)-prolinol was chosen. This system was selected because at the start of this investigation it was known to be a good catalyst, but to impart poor stereocontrol.[27a] Acetone was selected as the ketone thus removing the possibility of diastereomeric TSs. The labelling scheme used throughout this discussion is shown in figure 4-1. If more than one molecule of any of the species is present, the most recently added moiety will be denoted by 'n'.

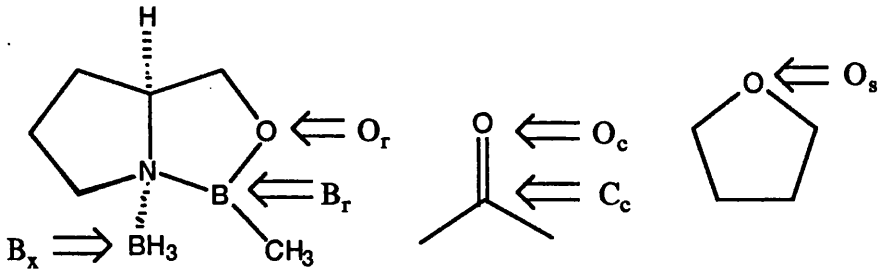

Figure 4-1

4.1 The Uncatalysed Reduction of Acetone

The reduction of acetone by borane-THF, as shown in figure 4-2, was the logical choice of reference point against which the role of the OAB in the catalysed reduction can be assessed.

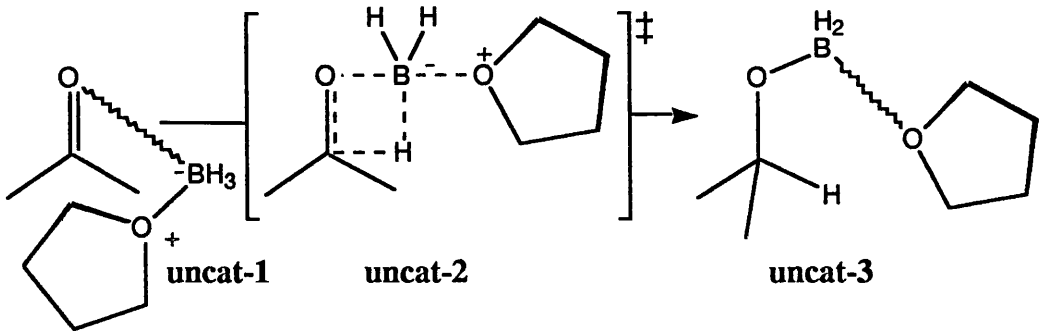

Figure 4-2

The ball-and-stick representations for these species are shown on the next page. Carbon and hydrogen are depicted as non-shaded circles with a black and green border respectively. Oxygen and boron are depicted by shaded circles which are pink and brown respectively.

The calculated enthalpies and optimised geometrical parameters for the reactant complex, **uncat-1**, the TS **uncat-2** and the product, **uncat-3**, are given in table 4-1.

Table 4-1: The energetics (kcal mol^{-1}) and important geometrical distances (Å) for the uncatalysed reduction of acetone by THF-borane

	uncat-1	uncat-2	uncat-3
ΔH_f	-98.69	-74.92	-134.36
ΔH_{rel} [a]	-2.02	21.75	-37.69
B-O_c	5.222	1.722	1.336
B-O_s	1.768	2.219	3.636
B-H_t	1.197	1.273	2.465
O_c-C_c	1.236	1.318	1.447
C_c-H_t	3.648	1.646	1.129

[a] Enthalpy of formation relative to isolated borane-THF [-47.66 kcal mol^{-1}] + acetone [-49.01 kcal mol^{-1}] = -96.67 kcal mol^{-1}

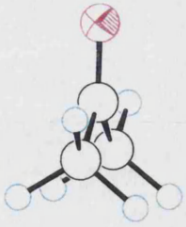

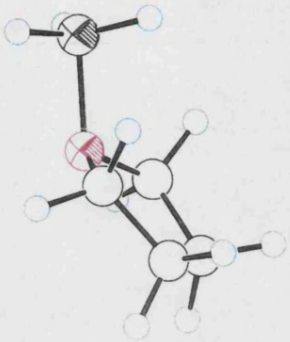

uncat-1

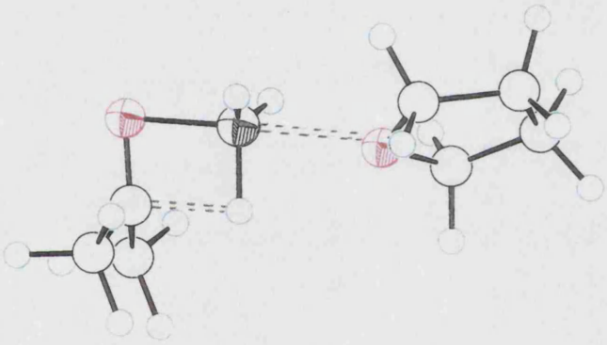

uncat-2

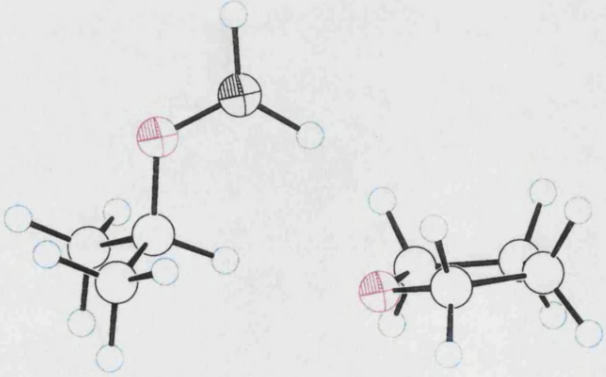

uncat-3

In the initial work on borane reductions, Brown[36] proposed a two step mechanism for the reduction of ketones: namely co-ordination of borane-THF to the carbonyl oxygen followed by hydride transfer. In this study, this type of two step mechanism was not located either by the intrinsic reaction calculation or by a direct reaction co-ordinate calculation in which the distance between the oxygen and the boron was decreased in small increments. The latter of these two studies produced a profile with no turning points which implied that a concerted hydride transfer occurred.

White *et al.*[37] studied the reduction of acetone by a borane-morpholine complex from which they concluded that there was no evidence for or against the breaking of the boron-nitrogen bond in the rate determining step, but that cleavage must occur shortly after hydride transfer if the isopropoxy group was to be formed. It was suggested that 'some loosening of the boron-nitrogen bond accompanies co-ordination of boron to oxygen with some concerted hydride transfer also occurring in the transition state.'

From the equation $n = \exp[(d_1 - d_n)/c]$, where d_1 and d_n are bond lengths of order 1 and n respectively and $c = 0.2$, the Pauling bond order n can be calculated. The value of c was determined from the AM1 structure of diborane as this has two bond distances and orders which can be measured, namely a single bond ($d_1 = 1.192$ Å) and the bridged B-H bond ($d_{0.5} = 1.329$ Å).

The Pauling bond order for B-H_t in the TS was 0.67 implying that minimal B-H bond cleavage had occurred. The calculated KIE at 23°C was $k_H/k_D = 1.26$ for the reduction by borane-d_3-THF. This value was lower than expected, which could be attributed to the small extent of B-H bond cleavage in the TS and the non-linear geometry of the hydride transfer.

The origin of low KIE values in hydride transfer reactions has been the subject of much investigation. White *et al.* attributed the value of $k_H/k_D = 1.1$ for the reduction of acetone by borane-d_3-morpholine to the small amount of B-H bond cleavage in the TS. Hawthorne *et al.*[38] concluded that the value of $k_H/k_D = 1.52$ for

the hydrolysis of pyridine diphenylborane was due to a non linear geometry for hydride transfer. In their study of the hydrolysis of pyridine arylboranes, Davis *et al.*[39] noted that the inverse primary kinetic isotope effect arose from significant secondary isotope effects. The inverse primary KIE noted by Wigfield *et al.*[40] for reductions by lithium tri*tert*-butoxyaluminodeuteride was attributed to the relatively loose Al-H bond being replaced by a tighter C-H bond.

To ensure that the calculated KIE for the uncatalysed, reference reaction was not being reduced by significant secondary isotope effects, three further isotope effect calculations were performed. A value of the $k_H/k_D = 1.24$ was obtained for only the transferring hydride being isotopically labelled, $k_H/k_D = 1.02$ for the two non-transferring hydrogens; the corresponding equilibrium isotope effects were $K_H/K_D = 0.72$ and were $K_H/K_D = 1.06$ respectively. From these calculations, the conclusion was drawn that the value of $k_H/k_D = 1.26$ for the reduction of acetone by borane-d_3-THF arose from weak B-H bond being replaced by a stronger C-H interaction.

4.2 The Oxazaborolidine

The AM1 geometry for the OAB had a butterfly-like structure with the two five-membered rings adopting an almost planar conformation. The ball-and-stick representation of this molecule, **oab-0**, is shown on the next page along with the crystal structure found by Corey for a related oxazaborolidine-borane adduct.[28] The only significant difference between the structures was the planarity observed in the AM1 structure in contrast to the puckered conformation observed in the crystal structure. This was not unexpected as the AM1 hamiltonian is known to underestimate the energetic advantage of the puckered conformations for small ring systems.[41]

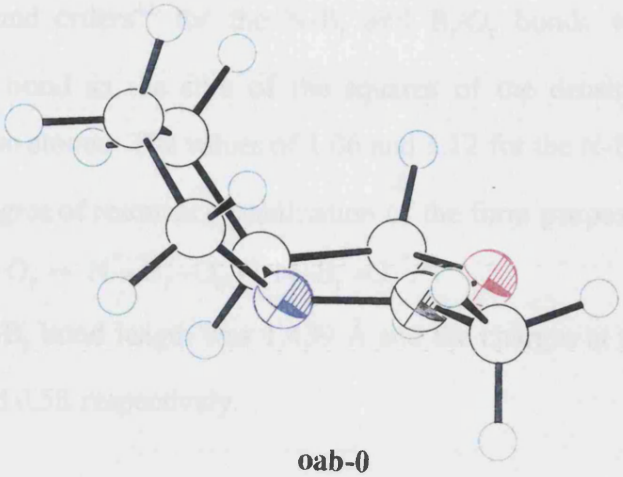

oab-0

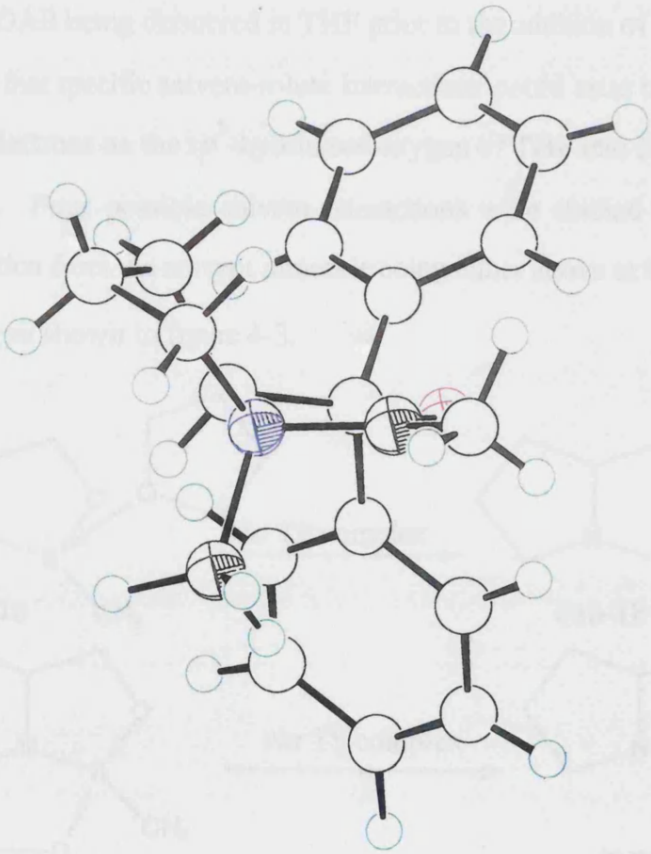

crystal structure

The bond orders[42] for the N-B_r and B_r-O_r bonds were calculated by considering a bond as the sum of the squares of the density matrix elements between the two atoms. The values of 1.06 and 1.12 for the N-B_r and B_r-O_r bonds suggested a degree of resonance stabilisation of the form proposed by Nevalainen, namely $N–B_r–O_r \leftrightarrow N^+=B_r^-–O_r \leftrightarrow N–B_r^-=O_r^+$.[34a]

The N-B_r bond length was 1.439 Å and the charges at nitrogen and boron were -0.56 and 0.58 respectively.

4.3 Specific Solvation of the Catalyst

The experimental procedure typically employed for these catalytic reductions involved the OAB being dissolved in THF prior to the addition of the ketone. It can be envisaged that specific solvent-solute interactions could arise by donation of the lone pair of electrons on the sp^3-hybridised oxygen of THF into the empty *p*-orbital on boron B_r. Four possible solvent interactions were studied - a long or short B_r-O_s interaction from the solvent molecule being either above or below the plane of the OAB ring as shown in figure 4-3.

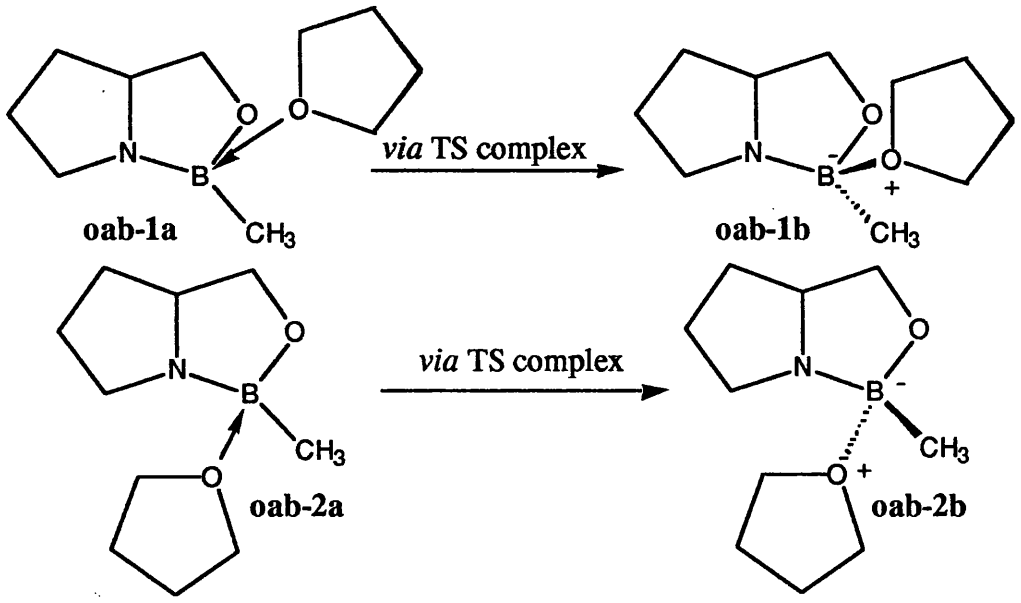

Figure 4-3

The complex formed when the THF was positioned above the convex face, **oab-1a**, with a long range interaction B_r-O_s (4.2 Å) was 1.50 kcal mol^{-1} more stable than isolated OAB and THF. The corresponding interaction from the convex face, **oab-2a**, provided less stabilisation, 0.88 kcal mol^{-1} and a slightly longer B_r-O_s distance (4.4 Å). The THF molecules had a large degree of conformational freedom in both complexes, the different orientations of the THFs being highlighted in the ball-and-stick representations of **oab-1a** and **oab-2a** on the next page. Due to the relative position of the solvent from the OAB, the charge distribution and geometry of the OAB did not alter significantly.

Tighter complexes, with shorter B_r-O_s distances were located but they were found to be endothermic relative to isolated OAB and THF. Formation of **oab-1b** involved a barrier was 5.9 kcal mol^{-1} ($\upsilon^{\ddagger}$ = 102*i* cm^{-1}) and was itself 4.2 kcal mol^{-1} less stable than isolated OAB and THF. The barrier for the formation of **oab-2b** was lower, 5.3 kcal mol^{-1} ($\upsilon^{\ddagger}$ = 131*i* cm^{-1}) and only 2.9 kcal mol^{-1} less stable than isolated OAB and THF. Co-ordination of the solvent changed the hybridisation of the B_r from sp^2 to sp^3 hybridised and thus weakened the overlap with the lone pairs on the neighbouring nitrogen and oxygen, O_r. Table 4-2 highlights the structural changes that occurred in the OAB during the formation of tight solvent complexes.

Table 4-2: The variation in bond lengths (Å) associated with solvation of the OAB

	oab-0	**oab-1b**	**oab-2b**
N-B_r	1.438	1.459	1.472
B_r-O_r	1.400	1.413	1.417

The formation of the tighter interaction with the solvent would ultimately hinder binding of the ketone to the OAB due to the reduction in the Lewis acidity of the boron B_r.

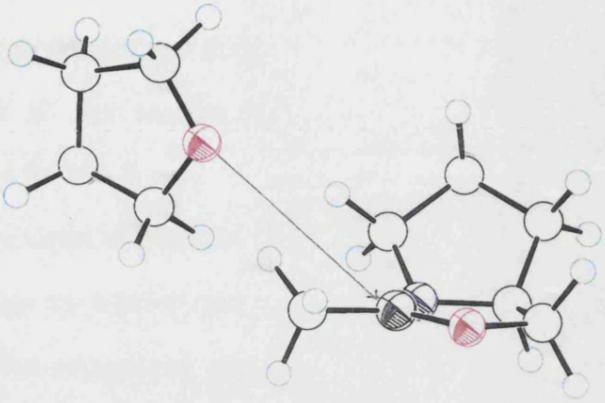

oab-1a

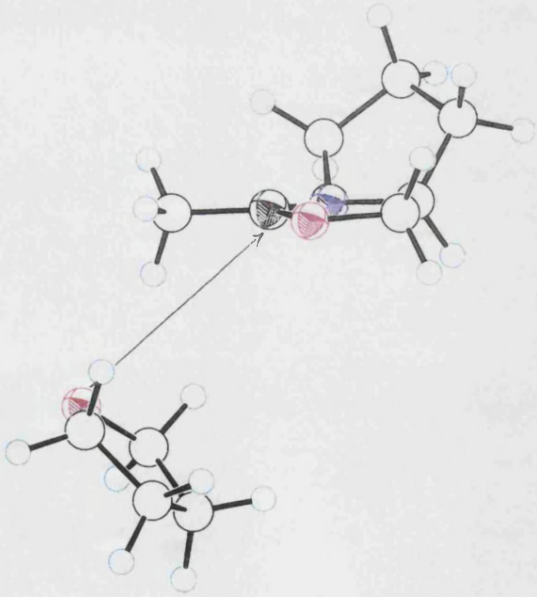

oab-2a

4.4 Formation of the OAB-Borane Adduct

The formation of borane adducts was considered from all four OAB-THF complexes. The formation of the OAB-borane adduct occurred in an S_N2 process with the lone pair on nitrogen displacing the solvent molecule from the borane-THF complex. For all four solvent complexes, a long range interaction between the nitrogen N and the boron, B_x, of the borane-THF complex was located before the barrier was overcome to form the OAB-borane adducts.

Although the barriers for the nucleophilic attack did not significantly vary between the four complexes, the adducts arising from **oab-1b** and **oab-2b** were about 10 kcal mol^{-1} less stable than those arising from **oab-1a** or **oab-2a.** As co-ordination of a solvent molecule on the convex face, as in **oab-2a,** would ultimately result in approach of the ketone from the concave face of the OAB and thus remote from the hydride source, only formation of OAB-borane adduct from the concave, long-range OAB-THF complex, **oab-1a,** would occur during a catalytic cycle.

The important structural changes for the elementary step (figure 4-4) for the formation of the OAB-borane adduct from **oab-1a** are given in table 4-3. A side view of the ball-and-stick representations for this step are shown on the next page.

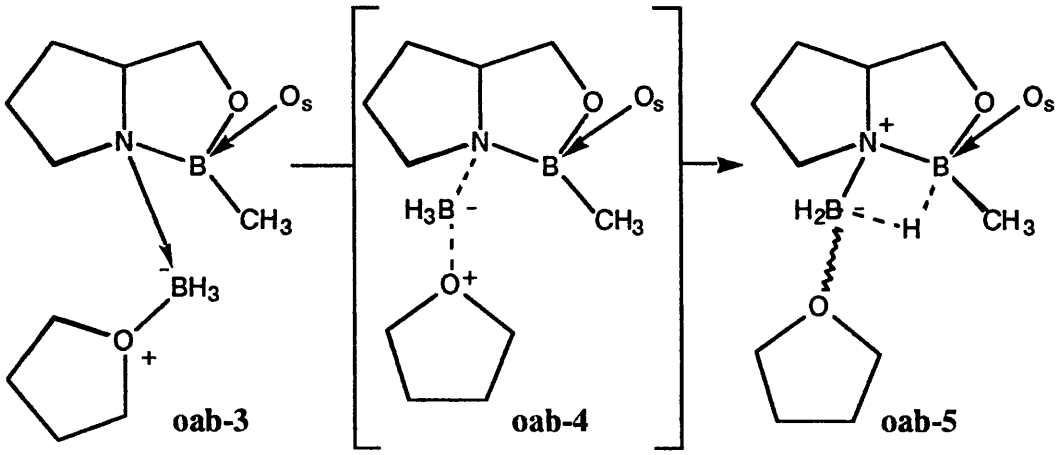

Figure 4-4

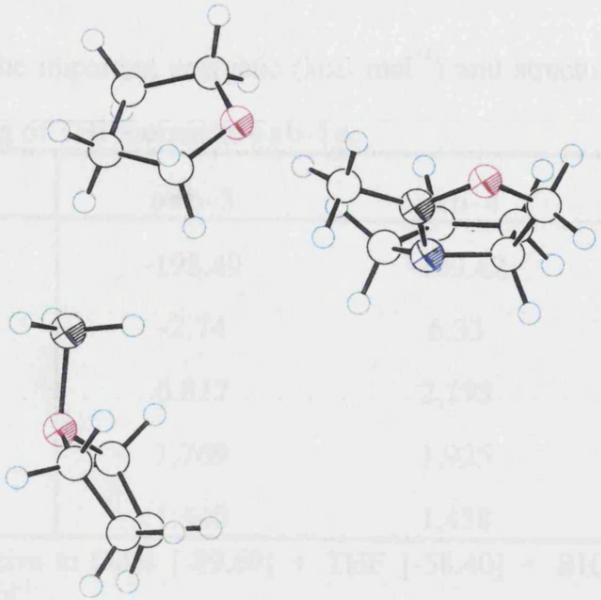

oab-3

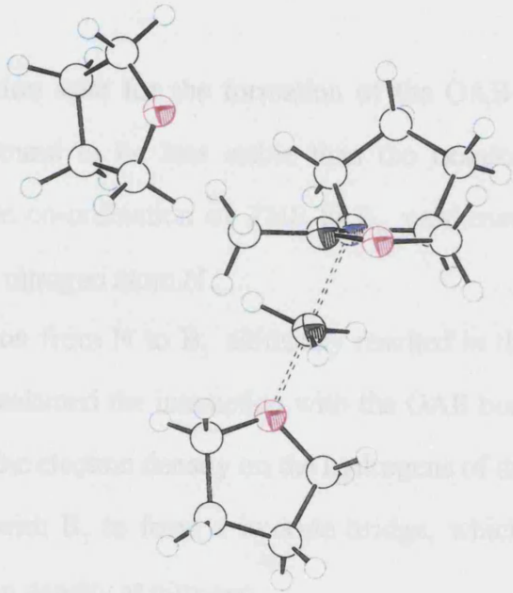

oab-4

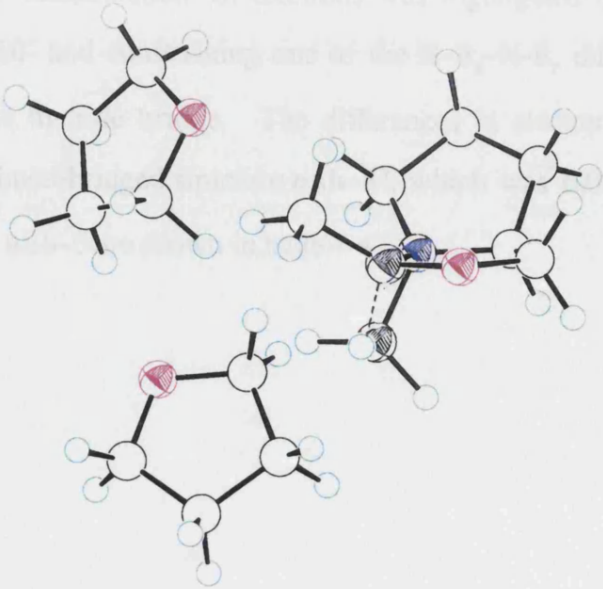

oab-5

Table 4-3: The important energetic (kcal mol^{-1}) and structural changes arising from the binding of THF-borane to **oab-1a.**

	oab-3	**oab-4**	**oab-5**
ΔH_f	-198.49	-189.42	-214.57
ΔH_{rel} [a]	-2.74	6.33	-18.82
$N–B_x$	6.817	2.198	1.551
$B_x–O_s$	1.769	1.925	5.124
$N–B_r$	1.440	1.458	1.576

[a] Enthalpy relative to OAB [-89.69] + THF [-58.40] + BH_3–THF [-47.66] = -195.75 kcal mol^{-1}

The transition state for the formation of the OAB-borane, **oab-4**, ($\upsilon^{\ddagger}$ = -330 cm^{-1}) was found to be less stable than the isolated species. During the transformation, the co-ordination of THF to B_x weakened with the donation of electrons from the nitrogen atom N.

The donation from N to B_x ultimately resulted in the N becoming electron deficient which weakened the interaction with the OAB boron, B_r. The donation into B_x increased the electron density on the hydrogens of the borane moiety, which can then interact with B_r to form a hydride bridge, which overall minimises the decrease of electron density at nitrogen.

This 'redistribution' of electrons was highlighted by rotating the borane moiety by 60° and constraining one of the H-B_x-N-B_r dihedrals to 180° which removed the hydride bridge. The differences in electron density between the bridged and non-bridged structure **oab-5'**, which was 6.02 kcal mol^{-1} higher in energy than **oab-5** are shown in table 4-4.

Table 4-4: The variation in charge distribution between **oab-5** and **oab-5'**

	q(N)	$q(B_r)$	$q(B_x)$	$q(H_t)$
oab-5	0.12	0.33	-0.27	-0.05
oab-5'	0.59	0.24	-0.06	-0.17

Comparing the geometrical parameters (table 4-5) of these two structures with the crystal structure showed that the non-bridged structure more closely resembled the solid state form of the OAB-borane adduct. The ball-and-stick representations of the front view of **oab-5** and **oab-5'** are shown on the next page.

Table 4-5: A comparison of selected bond lengths between **oab-5'**, **oab-5** and the crystal structure.

	crystal structure	AM1 (**oab-5'**)	AM1 (**oab-5**)
$N\text{-}B_r$	1.486	1.517	1.576
$N\text{-}B_x$	1.621	1.603	1.551
$B_r\text{-}O_r$	1.546	1.375	1.442
$B_r\text{-}CH_3$	1.335	1.534	1.551
$H_t\text{-}B_x\text{-}N\text{-}B_r$	65.2	61.3	-6.2

Literature precedent existed for both structures. Tlaheuxt and Contreras noted that the ^{11}B NMR resonances of N-methyl ephedrine appeared at a abnormally high field,[32] as do the resonances in diborane. From this they concluded that the formation of the OAB-borane adduct weakened the nitrogen-boron bond within the OAB, increasing the acidity of the boron, 'promoting an intramolecular co-ordination of one hydride into the boron atom.'

Nevalainen's investigation provided contradictory results. In initial studies he found that a bridging interaction stabilised aminoborane by -53 kJ mol^{-1} but later studies implied that hydroxyaminoborane could not adopt bridged structures.[34a,h]

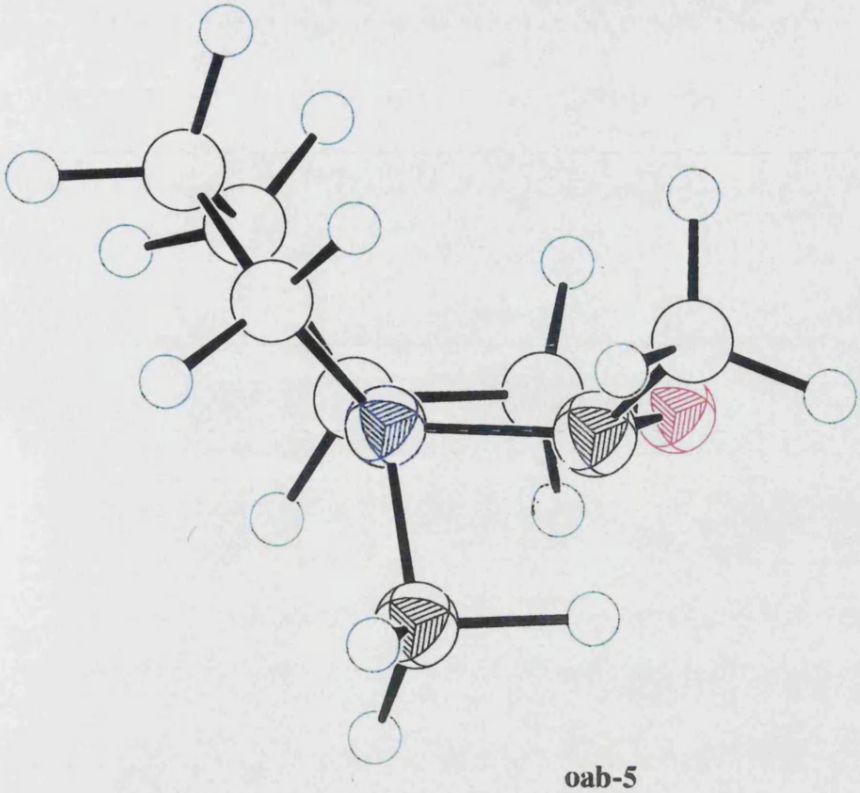

oab-5

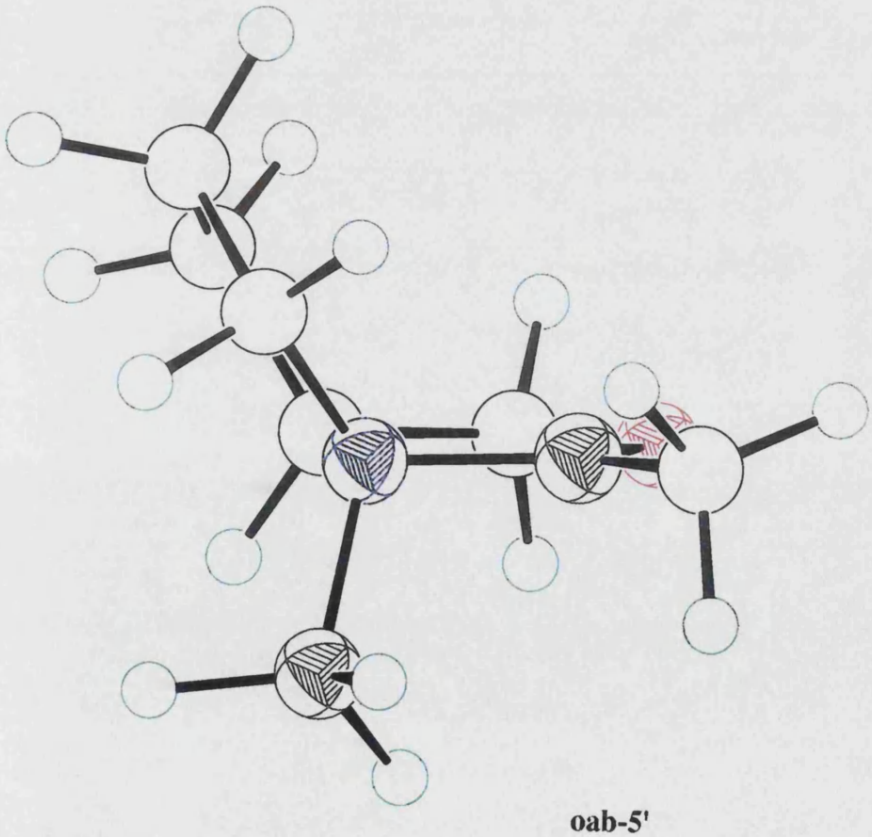

oab-5'

In order to resolve this issue, four related systems (figure 4-5) were studied using AM1, HF/6-31G** and MP2/6-31G**. *Ab initio* calculations were performed using Gaussian 92.[43] Each structure was subjected to a full geometry optimisation.

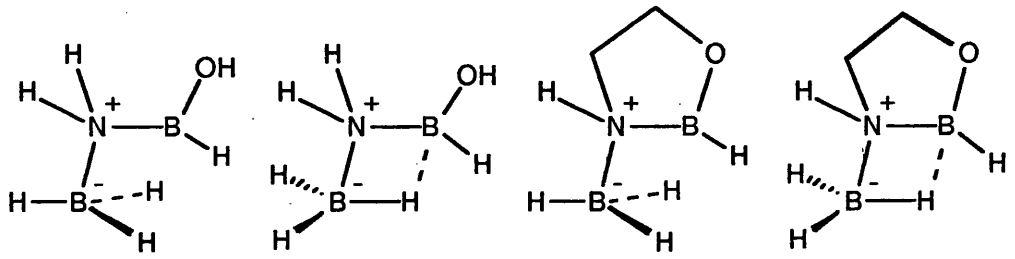

(i) (ii) (iii) (iv)

Figure 4-5

The energies for all four structures at each level of theory are given in table 4-6 - the *ab initio* energies are quoted in hartrees where 1 hartree = 627.510 kcal mol^{-1}.

Table 4-6: Total energies (hartree) for *ab initio* and heats of formation (kcal mol^{-1}) for AM1 optimised structures

	MP2/6-31G**	HF/6-31G**	AM1
(i)	-183.38957[a]	-182.83666	-108.45[c]
(ii)	-183.39739	-182.83384	-117.12
(iii)	-260.54487[b]	-259.72311	-78.32[d]
(iv)	-260.55138	-259.71997	-88.49

[a] $\upsilon^{\ddagger} = 101i\ cm^{-1}$, [b] $H\text{-}B_x\text{-}N\text{-}B_r$ constrained to 180°, [c] $\upsilon^{\ddagger} = 127i\ cm^{-1}$, [d] $\upsilon^{\ddagger} = 150i\ cm^{-1}$

The bridged structures (ii) and (iv) were predicted to be minima at each level of theory. The HF/6-31G** method also predicted that (i) and (iii) were minima, about 2 kcal mol^{-1} lower in energy than the bridged structures. However, the MP2/6-31G** and AM1 method predicted that the non-bridged structures were TSs for rotation about the $N\text{-}B_x$ bond. Both the latter two methods include electron

correlation - MP2 implicitly includes the most important effects of electron correlation whilst it is included in AM1 by virtue of its parameterisation.

The bridging energies are presented in table 4-7.

Table 4-7: The energetic differences (kcal mol^{-1}) between the bridged and unbridged structures

	MP2/6-31G**	HF/6-31G**	AM1
E (ii) - E (i)	-4.91	1.77	-8.67
E (iv) - E (iii)	-4.09	1.97	-10.17

This result clearly showed that the bridging interaction was favoured and highlighted the need to include electron correlation in *ab initio* calculations. Single point MP2/6-31G** calculations were performed on the HF/6-31G** structures and the same trends as the full optimisation at the electron correlated level were observed. In contrast with HF/6-31G**, AM1 provided the correct description of the bridging interaction but overestimated the energetic advantage.

Whilst this study confirmed that bridging interaction within **oab-5** was not an artefact of the AM1 method, the lack of hydride bridge within in the crystal structure needed to be addressed. The crystal structure was obtained from the Cambridge Structural Database, and the unit cell was projected using Roche's 'in house package', Moloc. In a tightly packed unit cell, which comprised thirty six OAB-borane adducts, the hydride bridging interaction had been replaced by interactions between the each of the hydrogens of the BH_3 group and a hydrogen attached to the phenyl group of a neighbouring OAB moiety. A ball-and-stick representation of a portion of the unit cell is shown on the next page.

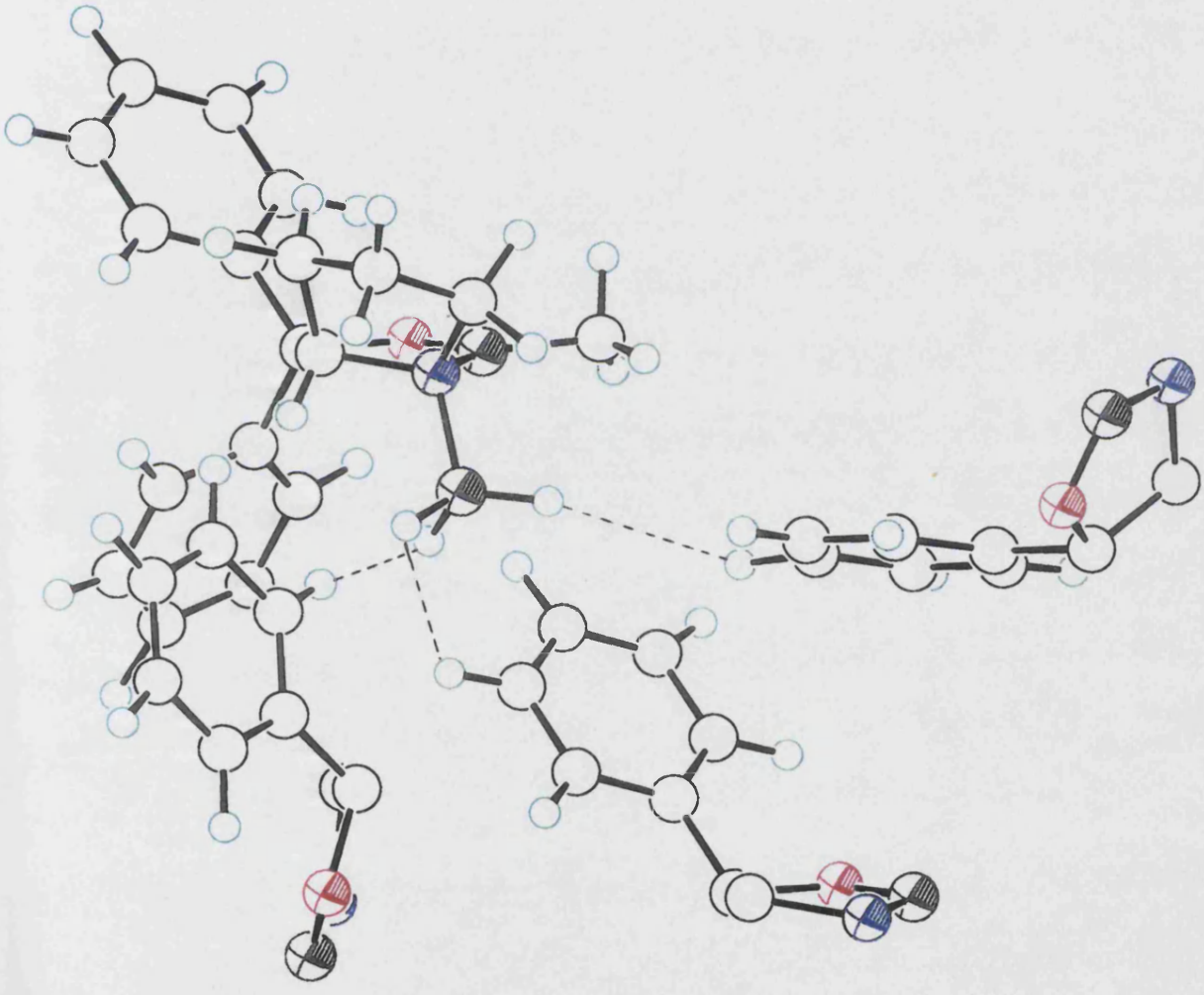

Four of the OAB-borane adducts within the unit cell

Shows the interaction of the -BH_3 group with three neighbouring phenyl groups

Note: lower phenyl groups and the pyrrolidine ring removed for clarity

4.5 The Binding of Acetone

As with the solvation interactions between O_s and B_r, the ketone binding can also be characterised by both long-range and short-range interactions between B_r and the sp^2-hydridised oxygen atom O_c of the carbonyl group.

Although it had been concluded that the approach of acetone from the exposed concave face of a convex-solvated OAB-borane adduct would position the ketone in a remote location from the hydride source, the elementary steps were still investigated. The approach of the ketone identified a long-range structure (B_r-O_c = 3.766 Å) *via* a 3.1 kcal mol^{-1} barrier (TS: B_r-O_c = 2.417 Å, $\upsilon^{\ddagger}$ = 127*i* cm^{-1}) to a short-range interaction (B_r-O_c = 1.939 Å) in which the carbonyl carbon was nearly 4.5 Å from the nearest hydrogen atom of the borane moiety. The barrier for the reverse reaction was calculated to be 2.5 kcal mol^{-1} which indicated that solvation from the convex face would not remove the ketone from the catalytic cycle as ketone binding was reversible.

The preferable location for the ketone involved approach from the convex face, so that it was positioned *syn* to the hydride source. Chair and both conformers could be distinguished in the TS for binding of the ketone ($\upsilon^{\ddagger}$= 121*i* cm^{-1} for the boat TS and 148*i* cm^{-1} for the chair); the six-membered-ring comprising the atom H_t–B_x–N–B_r–O_c–C_c where H_t is the hydride that is transferred in the subsequent transition state.

The geometries and energetic changes that occur during binding (figure 4-6) are presented in table 4-8, where b indicates the boat conformer and c the chair conformer.

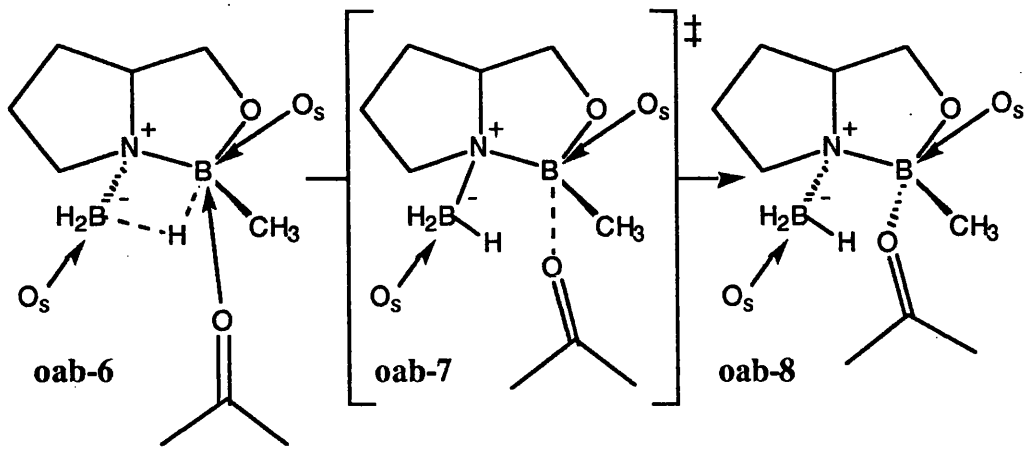

Figure 4-6

Table 4-8: The important energetic (kcal mol-1) and geometrical changes (Å) arising from ketone co-ordination

	Boat Conformations			Chair Conformations		
	oab-6b	**oab-7b**	**oab-8b**	**oab-6c**	**oab-7c**	**oab-8c**
ΔH_f	-264.44	-254.09	-256.98	-265.36	-253.39	-258.05
ΔH_{rel} [a]	-19.68	-9.33	-12.22	-20.60	-8.63	-13.29
B_r-O_c	5.472	2.326	1.827	5.814	2.362	1.856
N-B_r	1.573	1.535	1.559	1.573	1.536	1.560
N-B_x	1.549	1.598	1.599	1.548	1.596	1.590
C_c-O_c-B_r-N	12.3	15.3	79.9	3.2	-28.4	-87.3
H_t-B_x-N-B_r	-6.0	-56.8	-63.3	-6.6	-61.4	-55.4

[a] Enthalpy of formation relative to isolated OAB [-89.69] + THF [-58.40] + BH_3.THF [-47.66] + MeCOMe [-49.01] = -244.76 kcal mol^{-1}

The ball-and-stick representations for the TSs and ternary OAB-borane-ketone adducts are given on the next page. The side view clearly shows the different orientations of the ketone. For clarity, the hydrogens have been removed from the two THF molecules.

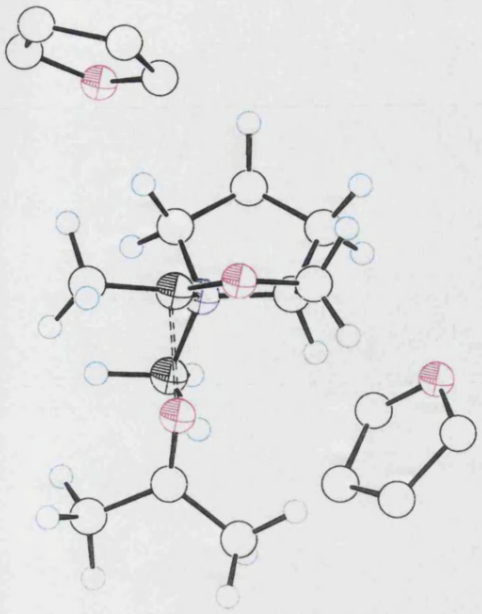

oab-7c

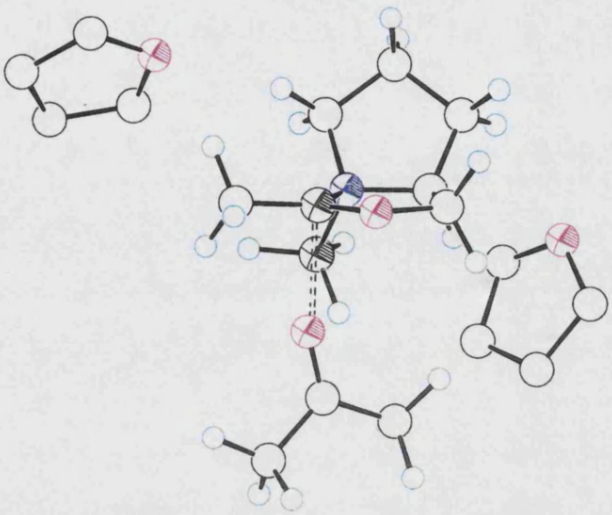

oab-7b

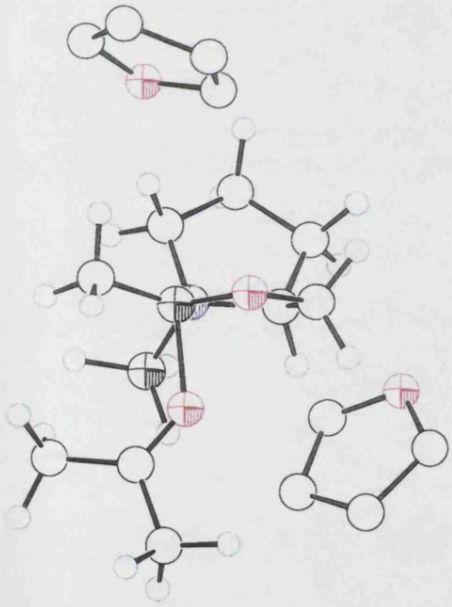

oab-8c

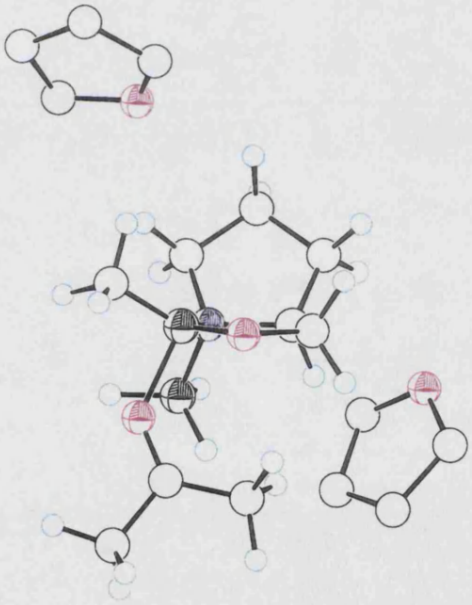

oab-8b

Rotation of the borane moiety occurred as the ketone approached. Both the long-range and short-range ketone complexes preferred the chair conformer by about 1 kcal mol^{-1}. In both of the short-range complexes, the nearest hydrogen H_t was only a little more than 2.5 Å from the carbonyl carbon C_c.

Figure 4-7 shows the variation in the electronic distribution that occurred during the approach of the ketone to B_r to form **oab-8b**.

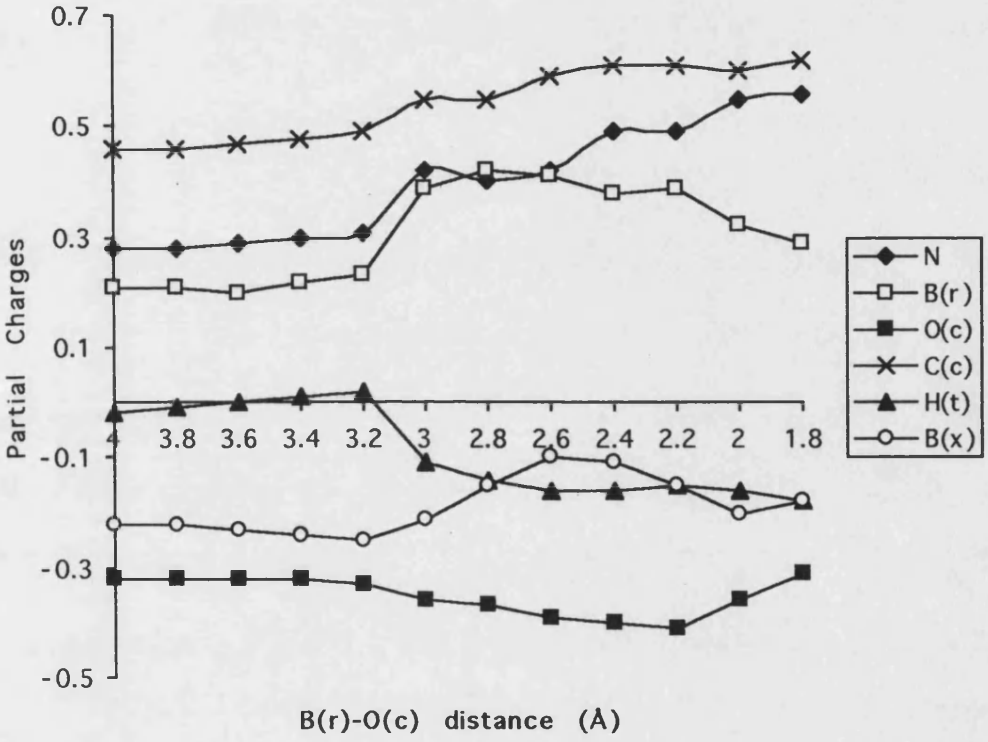

Figure 4-7

Only slight changes occurred between B_r-O_c = 4.0 Å to 3.2 Å as the hydride bridge was still present. The carbonyl carbon C_c became more electron deficient during the binding and the electron density increased on the hydride, both changes promoting the hydride transfer. The approach of the ketone to B_r had similar trends irrespective of the final conformer formed, but the magnitudes of the charges differed between **oab-8b** and **oab-8c** (table 4-9).

Table 4-9: The charge distribution in **oab-8b** and **oab-8c**

	oab-8b	oab-8c
q(N)	0.44	0.40
$q(B_r)$	0.20	0.37
$q(O_c)$	-0.29	-0.47
$q(C_c)$	0.62	0.72
$q(H_t)$	-0.16	-0.12
$q(B_x)$	-0.17	-0.18

4.6 Hydride Transfer

The hydride-transfer step was found to be significantly exothermic and involved an early transition state for both the boat ($\upsilon^{\ddagger} = 448i$ cm^{-1}) and chair ($\upsilon^{\ddagger} = 451i$ cm^{-1}) conformers. Two different orientations for each TS are shown in the ball-and-stick representations on the next page.

After transfer the pathways had significant differences. The intermediate formed after hydride transfer from the boat conformer had small amount of N-B_r bond cleavage and on a barrier-less rotation about the O_c-C_c bond an oxazadiboretane, which had a four membered-ring comprising of N–B_r–O_c–C_c, was formed.

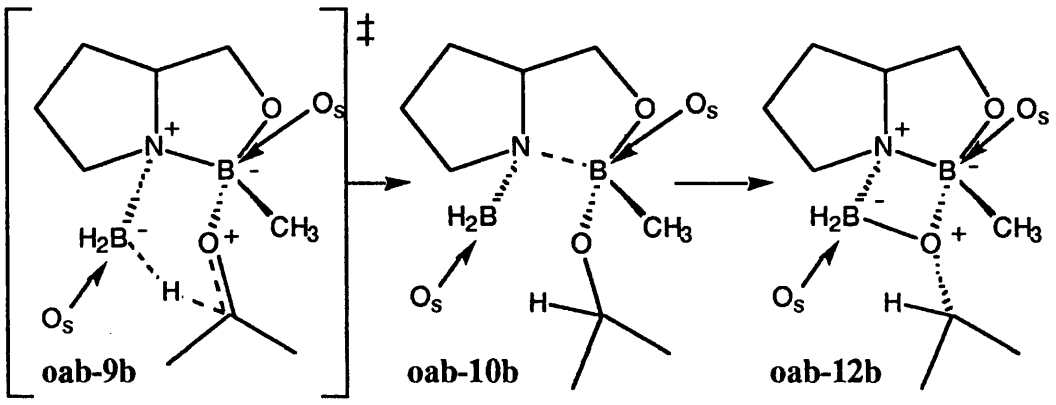

Figure 4-8

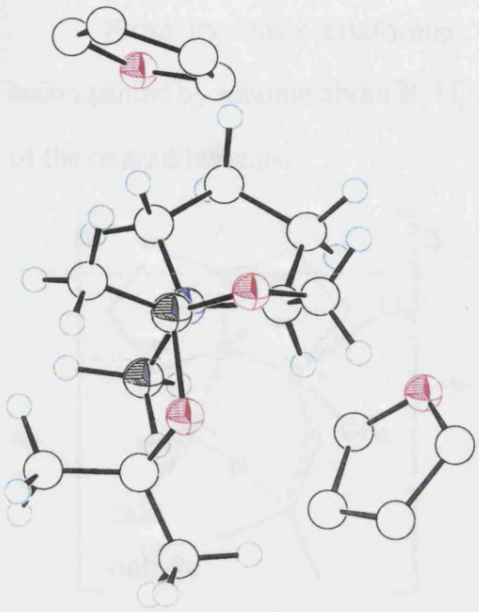

oab-9c
side view

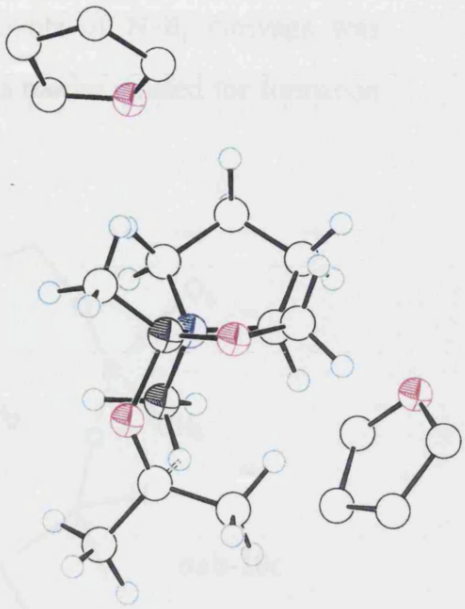

oab-9b
side view

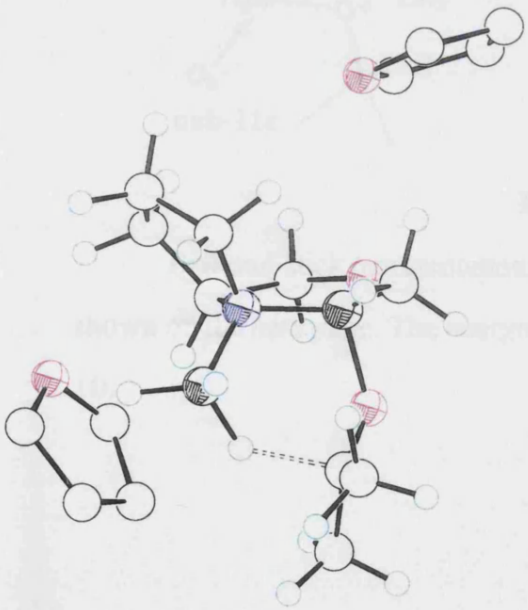

oab-9c
front view

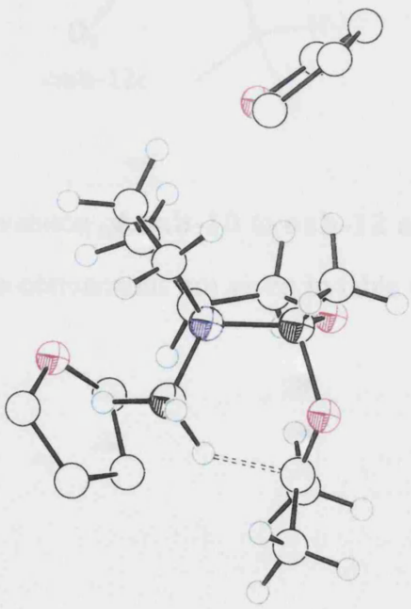

oab-9b
front view

From the chair conformer, significant amounts of N-B_r cleavage was accompanied by rotation about B_r-O_c and O_c-C_c and a barrier existed for formation of the oxazadiboretane.

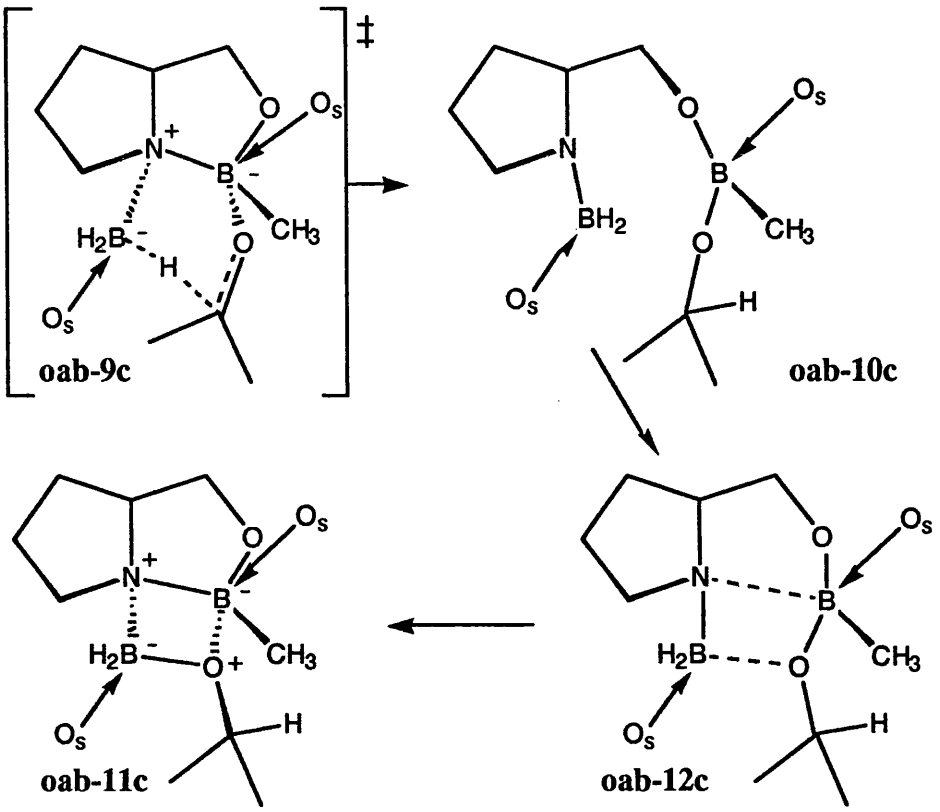

Figure 4-9

Ball-and-stick representations for the conversion of **oab-10** to **oab-12** are shown on the next page. The energetics for these conversions are given in table 4-10.

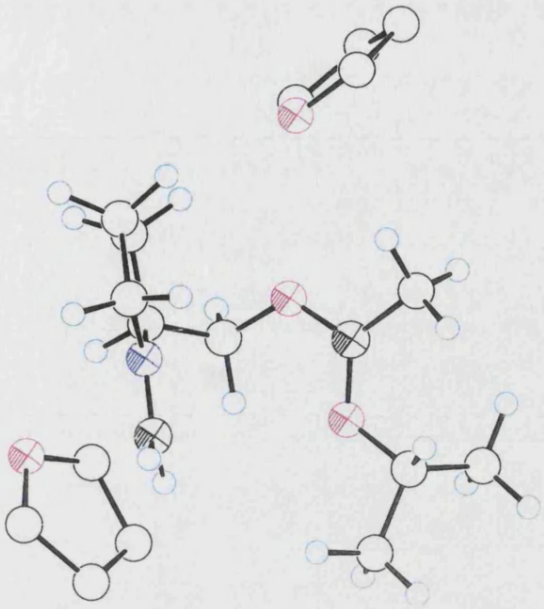

oab-10c

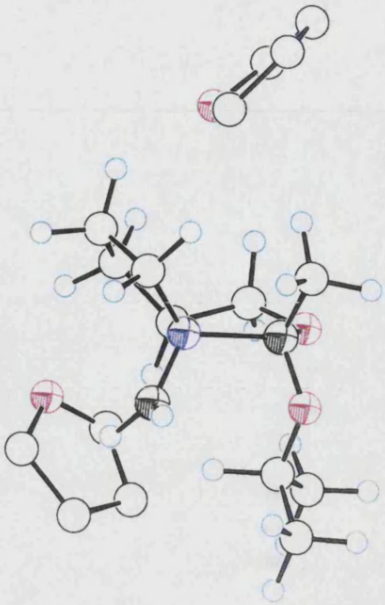

oab-10b

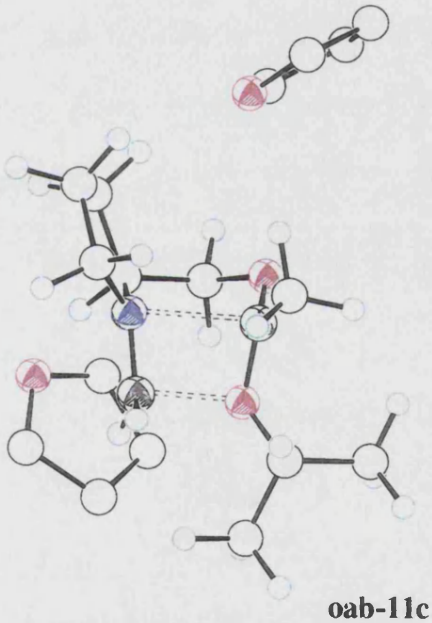

oab-11c

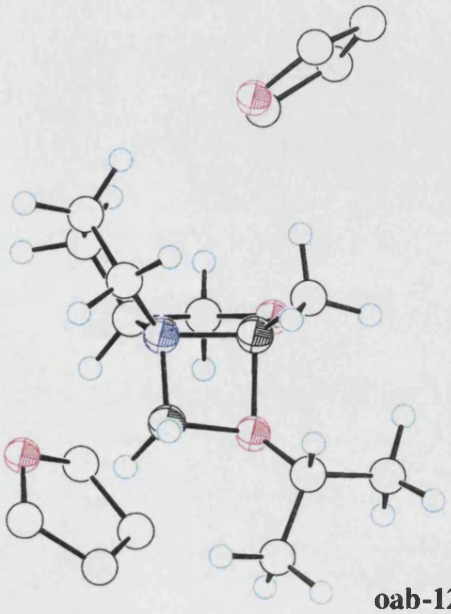

oab-12c

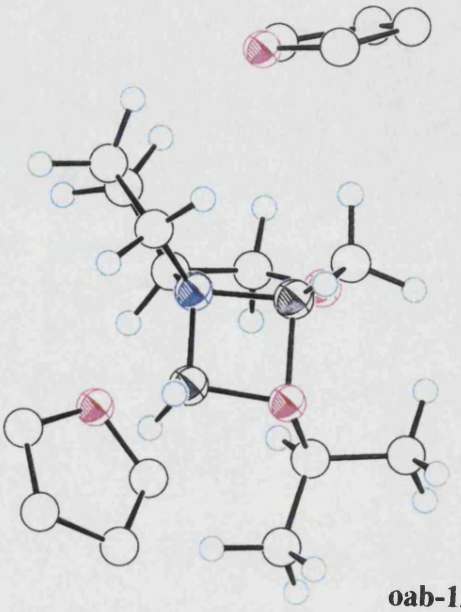

oab-12b

Table 4-10: The important energetic (kcal mol^{-1}) and geometric changes (Å) from hydride transfer to oxazadiboretane formation

	boat conformations (**oab-**)			chair conformations (**oab-**)			
	9b	**10b**	**12b**	**9c**	**10c**	**11c**	**12c**
ΔH_f	-251.40	-266.08	-299.51	-252.86	-292.38	-278.74	-297.65
ΔH_{rel}[a]	-6.64	-21.32	-54.75	-8.10	-47.62	-33.98	-52.89
N-B_r	1.598	1.751	1.592	1.597	3.609	2.208	1.597
B_r-O_c	1.687	1.442	1.674	1.710	1.367	1.440	1.672
O_c-C_c	1.289	1.408	1.440	1.288	1.436	1.442	1.436
C_c-H_t	1.701	1.155	1.127	1.681	1.126	1.126	1.126
H_t-B_x	1.254	1.738	-	1.258	4.553	-	-
B_x-N	1.575	1.482	1.572	1.566	1.352	1.428	1.562
B_x-O_c	-	2.761	1.593	-	3.575	1.880	1.602

[a] Enthalpy of formation relative to isolated OAB [-89.69] + THF [-58.40] + BH_3.THF [-47.66] + MeCOMe [-49.01] = -244.76 kcal mol^{-1}

The Pauling bond orders for the B_x-H_t were **n** = 0.73 and 0.74 for the boat and chair TS respectively, giving an indication of how 'early' the transition state occurred.

The calculated heat of formation for the chair TS, **oab-9c**, was 1.54 kcal mol^{-1} lower in energy than for the boat TS, **oab-9b**. Corey *et al.* had proposed that the hydride transfer adopted the boat conformation,[29] although no explanation had been proffered for this suggestion, or indeed, at which stage the orientation leading to a chair conformer became disfavoured.

Although the THF co-ordination to both conformers of the hydride transfer TS appeared to be weak and non-specific, the presence of these solvent molecules minimised the degree of 'ring-opening' (N-B_r was greater 4 Å without either THF molecules). The variation in the amount of N-B_r ring cleavage was related to differences in the charge distribution in the hydride transfer TS. Table 4-11 shows

the partial charges in **oab-8b** and **oab-8c** and the change with respect to the ketone complexes.

Table 4-11: The charge distribution in the hydride transfer TSs and a comparison with the preceding ternary OAB-borane-acetone complexes

	oab-9b	**Δ(9b-8b)**	**oab-9c**	**Δ(9c-8c)**
q(N)	0.48	+0.04	0.49	+0.09
$q(B_r)$	0.13	-0.07	0.33	-0.07
$q(O_c)$	-0.30	-0.01	-0.49	-0.02
$q(C_c)$	0.55	-0.07	0.76	+0.04
$q(H_t)$	0.03	+0.19	-0.06	+0.06
$q(B_x)$	-0.38	-0.21	-0.28	-0.11

The most significant differences were in the electron density at C_c, H_t and B_x. The lower electron density on H_t and higher density on C_c in **oab-9b** implied that more electron rearrangement had occurred in the boat TS. The larger electron population on B_x in **oab-9b** allowed for more electron donation from that atom to the electron deficient nitrogen. Therefore as the reaction proceeded, the nitrogen could donate to boron B_r, keeping the N-B_r bond intact. Leading from the chair TS, the lower availability of electron density on B_x to stabilise an already more electron deficient N-B_r interaction resulted in cleavage. The electron density located on O_c did not change significantly between the ketone complex to the hydride transfer TS or the next intermediate, either conformer of **oab-10**.

Both oxazadiboretanes had a planar N_r-B_r-O_c-B_x ring but the orientation of the isopropyl groups differed. In **oab-12b** the isopropyl group occupied the *endo* position (C_c–O_c–B_r–$N_r \approx 110°$) compared to the *exo* adopted in **oab-12c** (C_c–O_c–B_r–$N_r \approx -130°$). The differences in the orientation are highlighted by the ball-and-stick representation shown on the next page.

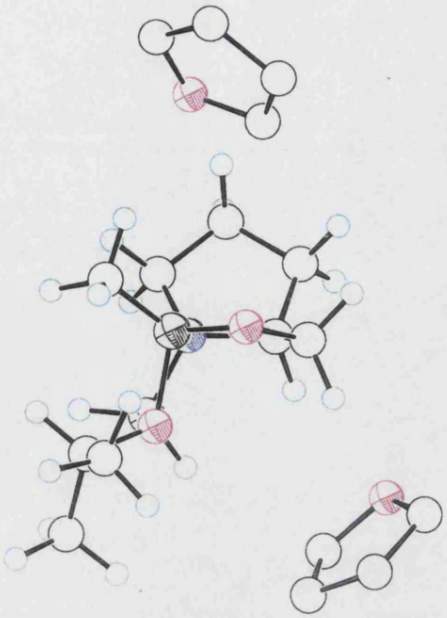

oab-12c
side view

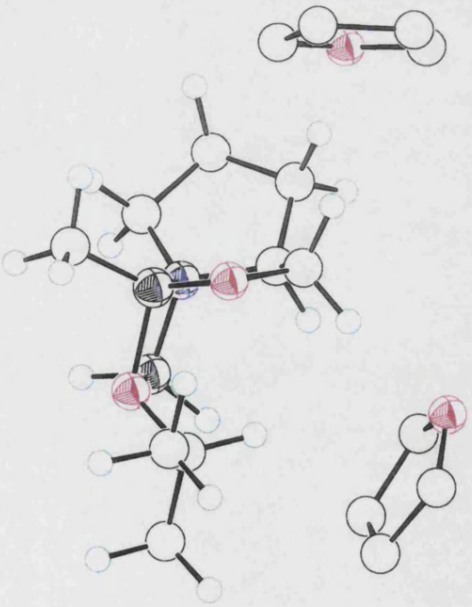

oab-12b
side view

4.7 Regeneration of the Catalyst and Product Release

Corey's initial mechanism had indicated that the addition of borane had completed the catalytic cycle.[29] The only pertinent experimental observations related to the possibility of a second hydride transfer.[31,44] A brief study of the second hydride transfer was made to compare the barrier for another hydride transfer with those for the regeneration pathway. A detailed study of subsequent hydride transfers was not pursued as experimental observations implied that the second hydride transfer was not rate limiting.

Three cleavage points of the oxazadiboretane were identified which could ultimately release the alkoxyborane, namely cleavage of N-B_x, B_r–O_c or B_x–O_c.

4.7.1 Breaking the N–B_x bond

No mechanism involving the cleavage of the N-B_x by the approach of a second moiety of borane-THF to nitrogen could be located. On closer inspection of the charge distribution within the oxazadiboretane, the S_E2 mechanism was unlikely to occur as the nitrogen atom N was electron deficient. Structures containing B-H-B bridging interactions between B_x and the newly introduced borane-THF were located and although they were less stable than the oxazadiboretanes, there was no weakening of the interactions which held the alkoxyborane to the OAB.

4.7.2 Cleavage of the B_r-O_c Bond

Nevalainen[34e] had located a structure resulting from the cleavage of the B_r-O_c bond which was 37 kJ mol^{-1} higher in energy than the oxazadiboretane (6-31G*//6-31G*). In this study, all attempts to find a transition state for the cleavage of the B_r-O_c bond were unsuccessful.

In the oxazadiboretanes **oab-12b** and **oab-12c**, B_r had a similar charge as in the hydride bridged structure **oab-5**: 0.31 and 0.40 compared to 0.33, so the possibility of cleavage being coupled with the approach of a second ketone was investigated.

The approach of a second ketone to the boron B_r of **oab-12c** lead from a structure containing long-range interaction between acetone and oxazadiboretane, **ket2-1** *via* a barrier of 26.45 kcal mol^{-1} (**ket2-2** $\upsilon^{\ddagger}$= 177*i* cm^{-1}) to an OAB-alkoxyborane-ketone complex, **ket2-3**. The barrier to a second hydride transfer was 7.7 kcal mol^{-1} (**ket2-4** $\upsilon^{\ddagger}$= 463*i* cm^{-1}) which was approximately 2.2 kcal mol^{-1} higher barrier than the first hydride transfer, but lower in energy than the binding TS. An oxazadiboretane, **ket2-5**, was formed directly from the TS.

The overall changes (figure 4-10) are summarised in table 4-12. The ball-and-stick representations of **ket2-2** to **ket2-5** are shown on the next page.

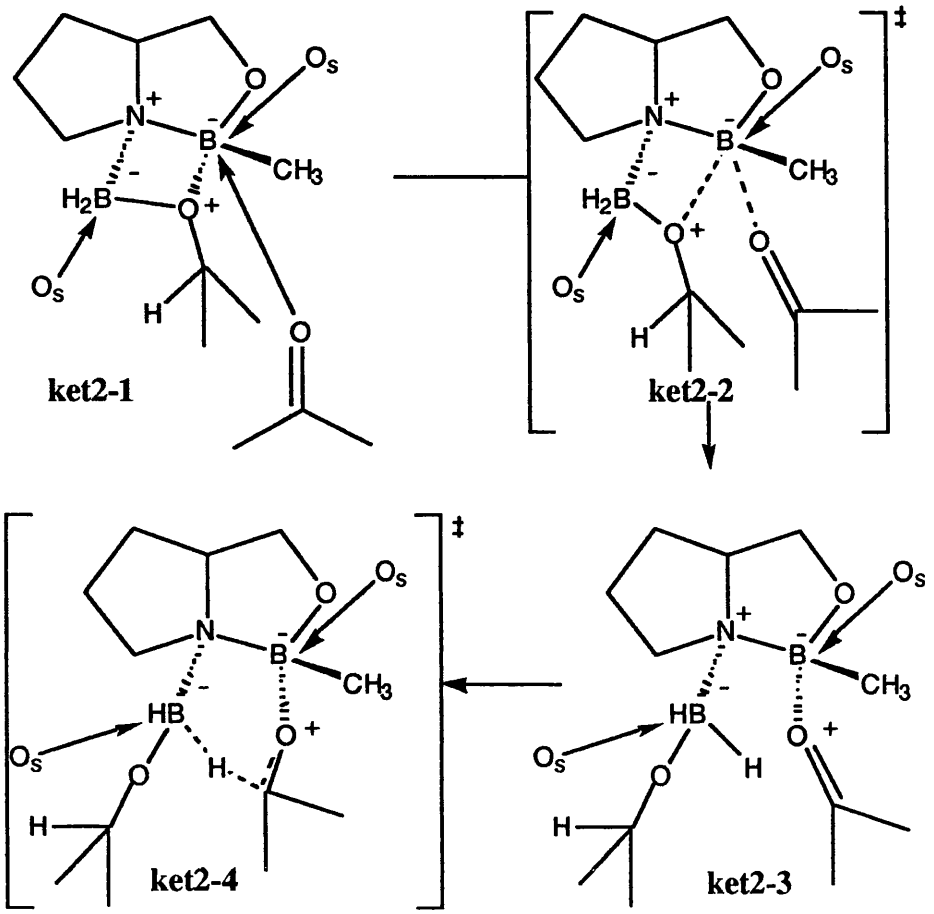

Figure 4-10

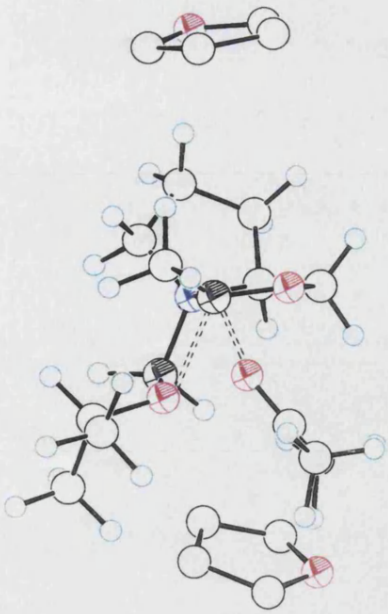

ket2-2

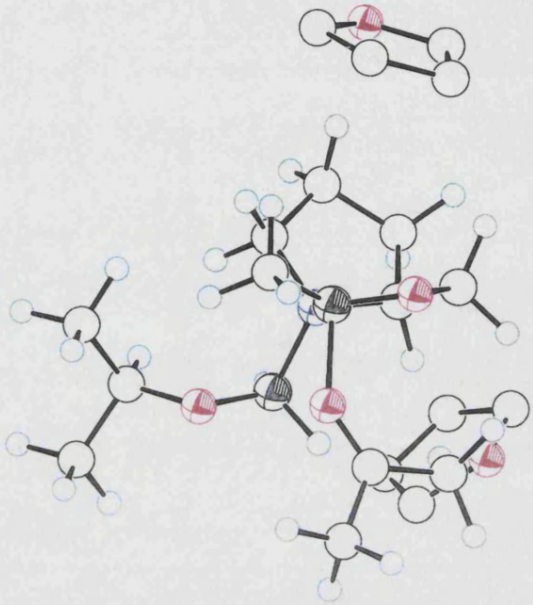

ket2-3

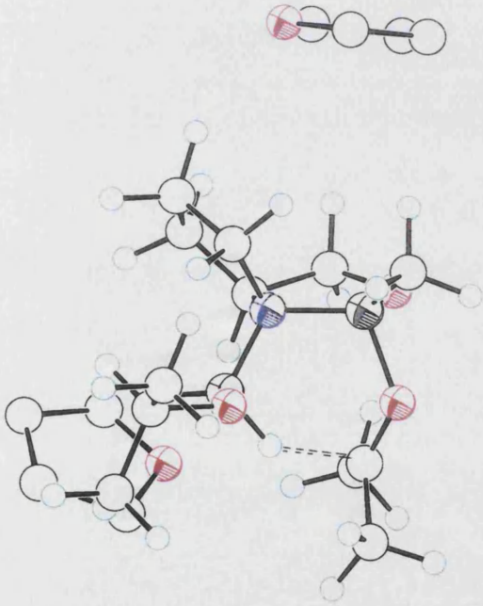

ket2-4

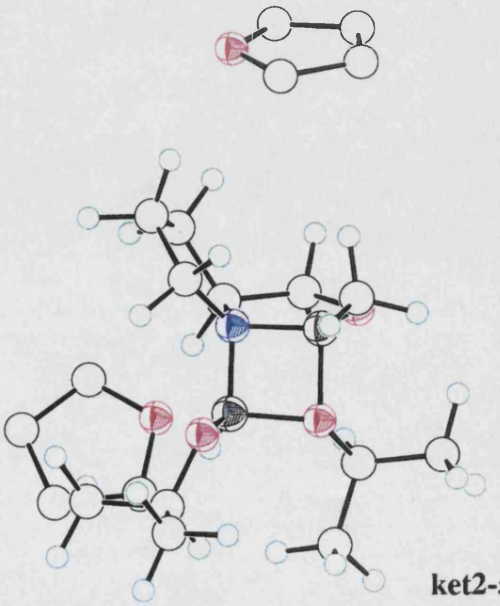

ket2-5

Table 4-12: The energetic changes (kcal mol^{-1}) and geometrical changes (Å) arising from the co-ordination and reduction of a second molecule of acetone

	ket2-1	ket2-2	ket2-3	ket2-4	ket2-5
ΔH_f	-349.51	-323.06	-337.70	-330.01	-377.69
ΔH_{rel} [a]	-55.74	-29.29	-43.93	-36.24	-83.92
B_r–O_c	1.681	2.134	3.103	-	-
B_r–$O_{c(n)}$	4.454	2.073	1.831	1.648	1.649
$C_{c(n)}$–$H_{t(n)}$	-	-	2.502	1.621	1.126
B_x–$H_{t(n)}$	-	-	1.214	1.264	2.768
N–B_x	1.565	1.603	1.672	1.610	1.583

[a] Enthalpy of formation relative to OAB [-89.69] + THF [-58.40] + BH_3.THF [-47.66]+ 2 MeCOMe [-98.02] = -293.77 kcal mol^{-1}

4.7.3 Cleavage of the B_x-O_c Bond

Inspection of the charge distribution within the oxazadiboretane N-B_r-O_c-B_x ring, revealed that O_c was electron rich. The approach of a second moiety of borane-THF to O_c was found to involve a long range interaction between O_c of the oxazadiboretane and B_n of the newly added borane-THF, *via* a barrier of 5.55 kcal mol^{-1} ($\upsilon^{\ddagger} = 119i\ cm^{-1}$) for addition to the boat oxazadiboretane and 6.97 kcal mol^{-1} to the equivalent chair conformer ($\upsilon^{\ddagger} = 88i\ cm^{-1}$) to a short range complex **oab-15** (O_c-$B_n \approx 2$ Å), figure 4-11. The barrier was higher for addition to the chair oxazadiboretane, **oab-12c**, because the isopropyl group was in the *exo*-position. Therefore the B_r–O_c bond had rotate to minimise the interaction between the borane-THF and the isopropyl group.

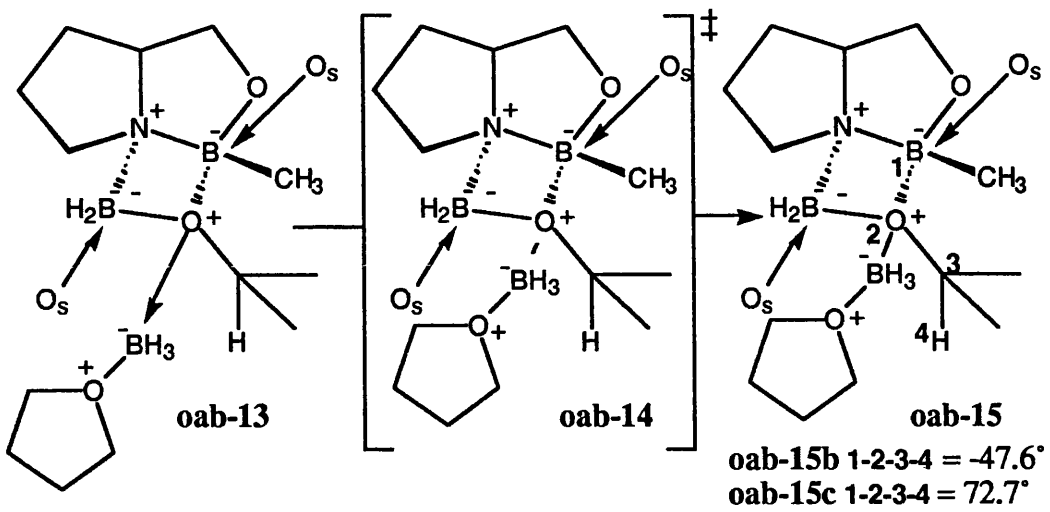

Figure 4-11

Although the resulting structure had the isopropyl group in an *endo* orientation, there were still noticeable differences between the structures resulting from the different conformations of the hydride transfer transition state.

Unlike the original co-ordination of the hydride source to nitrogen, an S_N2 displacement of the THF molecule by the oxygen O_c had not occurred. The energetics of the long-range complexes **oab-13**, the TS **oab-14** and the short range complex **oab-15** are given in table 4-13. The ball-and-stick representations of **oab-14** and **oab-15** are given on the next page.

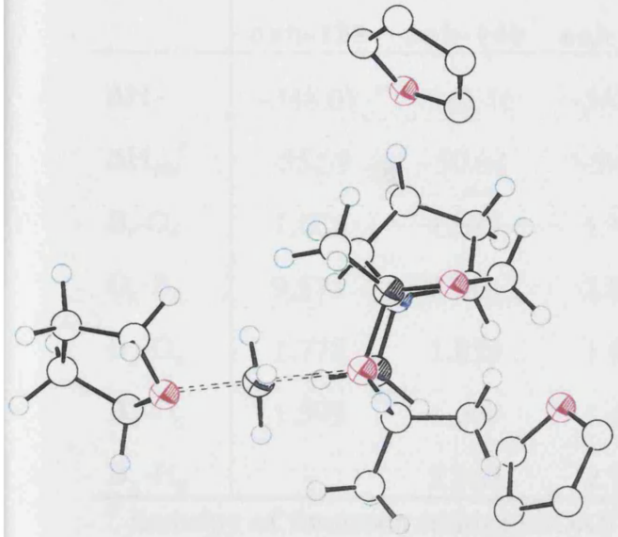

oab-14c

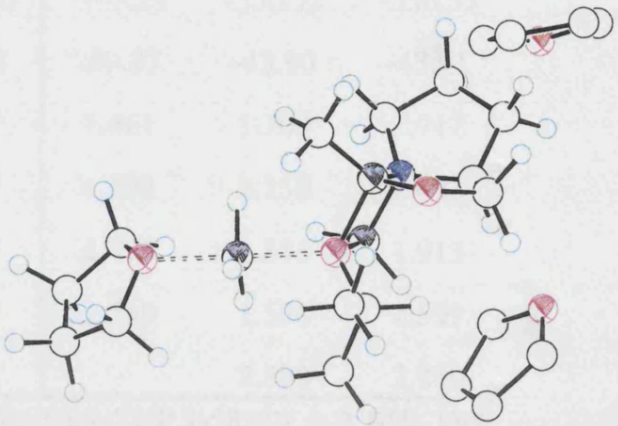

oab-14b

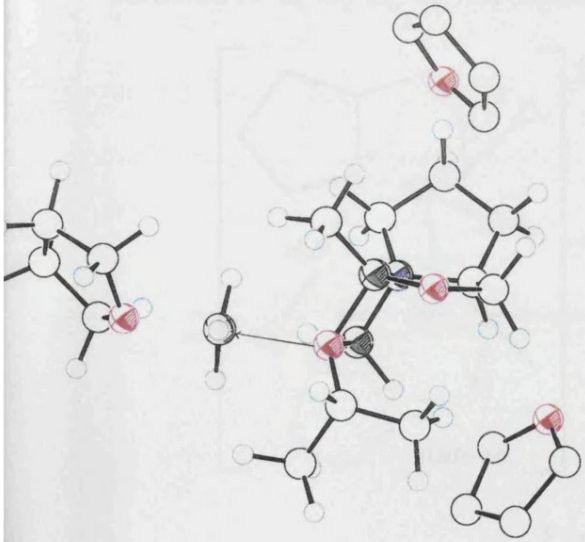

oab-15c

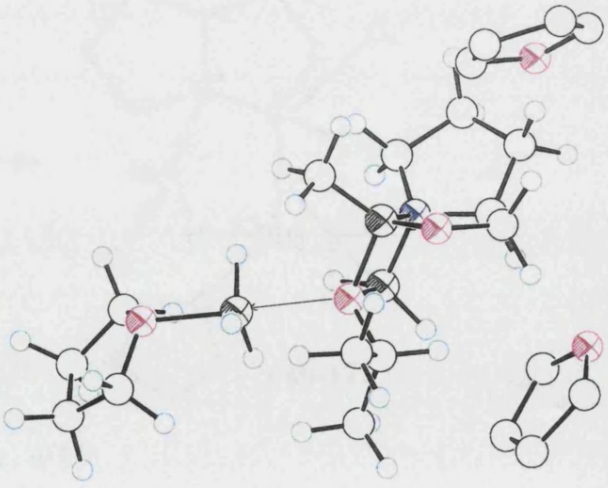

oab-15b

Table 4-13: The important energetic (kcal mol^{-1}) and geometric changes arising from the co-ordination of THF-borane to the oxazadiboretanes

	oab-13b	oab-14b	oab-15b	oab-13c	oab-14c	oab-15c
ΔH_f	-348.01	-342.46	-342.80	-343.29	-336.32	-336.33
ΔH_{rel} [a]	-55.59	-50.04	-50.38	-50.87	-43.90	-43.91
B_r-O_c	1.666	1.685	1.717	1.661	1.700	1.712
O_c-B_n	9.574	2.261	2.017	4.892	2.150	2.073
B_n-O_s	1.778	1.859	1.927	1.776	1.888	1.913
B_x-O_c	1.599	1.609	1.617	1.580	1.596	1.599
B_x-H_n	-	2.962	2.841	-	2.898	2.869

[a] Enthalpy of formation relative to OAB [-89.69] + THF [-58.40] + 2 BH_3.THF [-95.32] + MeCOMe [-49.01] = -292.42 kcal mol^{-1}

A barrier of 21.6 kcal mol^{-1} from **oab-15b** and 15.1 kcal mol^{-1} from **oab-15c** existed for the formation of a hydride-bridged six-membered ring comprising the atoms N–B_r–O_c–B_n–H_n–B_x (figure 4-12).

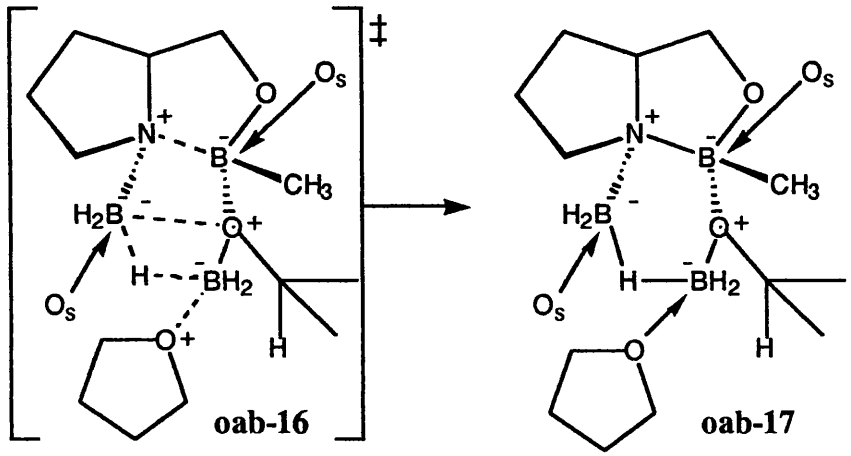

Figure 4-12

The TS, **oab-16**, ($\upsilon^{\ddagger}$ = 365*i* cm^{-1}) marked the convergence of the boat and chair pathways. In the TS the bond between boron B_n and oxygen of THF O_s weakened, and was cleaved in the product.

The formation of loosely-bonded larger ring system resulted in the weakening of the N-B_r interaction. This bond increase resulted in a decrease of the B_r-O_c and N-B_x bond lengths. The six-membered ring adopted a distorted boat conformer in which the interaction between the solvent THF molecule and boron B_n was weak and non-specific.

Table 4-14 shows the energetic and structural changes resulting from the formation of hydride-bridge. The front view of the ball-and-stick representations of both conformers of **oab-15**, TS **oab-16**, and tricyclic structure **oab-17** are shown on the next page.

Table 4-14: The important energetic (kcal mol-1) and structural (Å) changes arising from the formation of the 5/5/6 ring system, **oab-17**

	oab-16	**oab-17**
ΔH_f	-321.25	-350.37
ΔH_{rel} [a]	-10.01	-39.13
N-B_r	1.655	1.600
B_r-O_c	1.572	1.688
O_c-B_n	1.770	1.529
B_n-H_n	1.213	1.315
H_n-B_x	1.954	1.293
B_x-N	1.506	1.566
B_x-O_c	2.135	2.453
B_n-O_s	2.099	4.231

[a] Enthalpy of formation relative to isolated OAB [-89.69] + THF [-58.40] + 2 BH_3.THF [-95.32] + MeCOMe [-49.01] = -292.42 kcal mol^{-1}

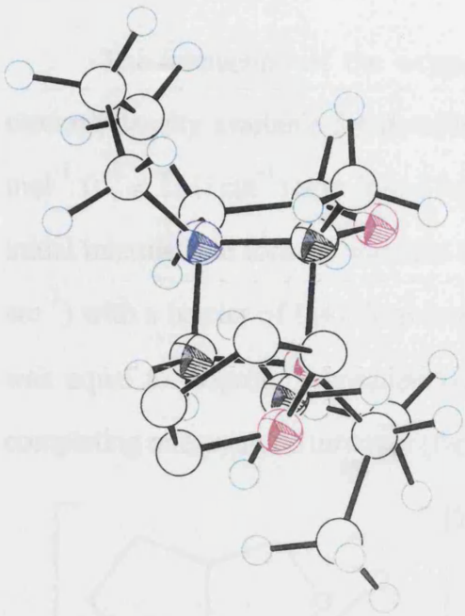

oab-15c

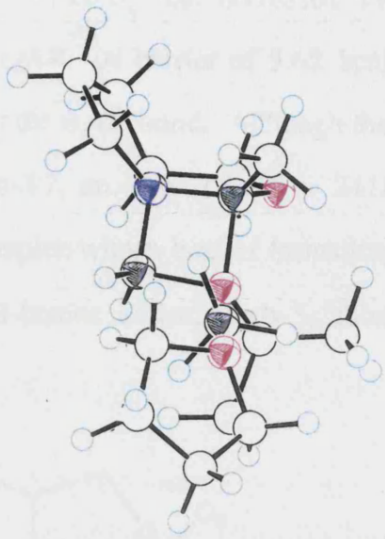

oab-15b

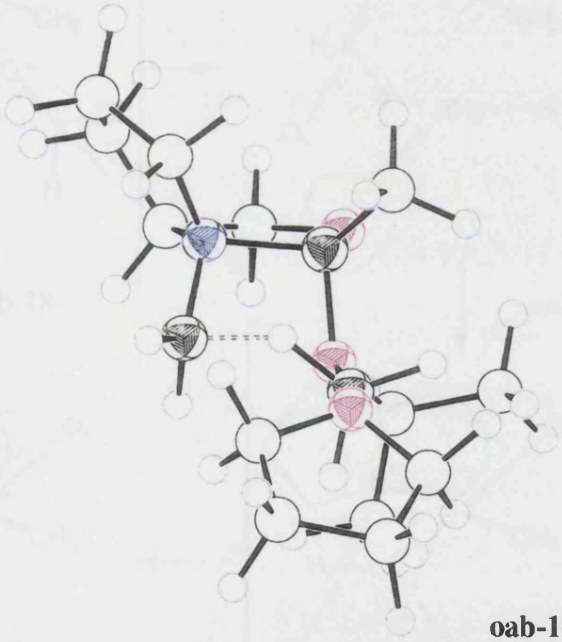

oab-16

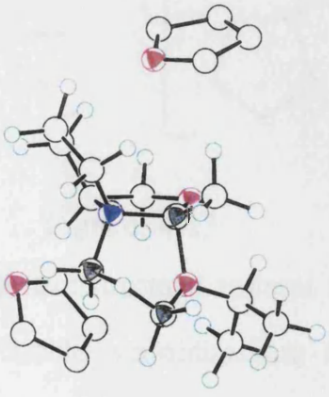

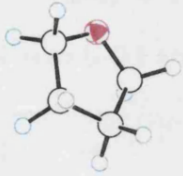

oab-17

The interaction of the oxygen O_c with the boron B_n had decreased the electron density available for donation to B_r of the OAB. A barrier of 5.62 kcal mol^{-1} ($\upsilon^{\ddagger} = 151i\ cm^{-1}$) was found for the cleavage of the B_r-O_c bond. Although the initial intermediate formed was less stable than **oab-17**, an early TS ($\upsilon^{\ddagger} = 241i\ cm^{-1}$) with a barrier of 0.47 kcal mol^{-1} lead to a complex whose heat of formation was equal to isopropoxyborane-THF and the OAB-borane adduct, **oab-5**, thus completing one catalytic turnover (figure 4-13).

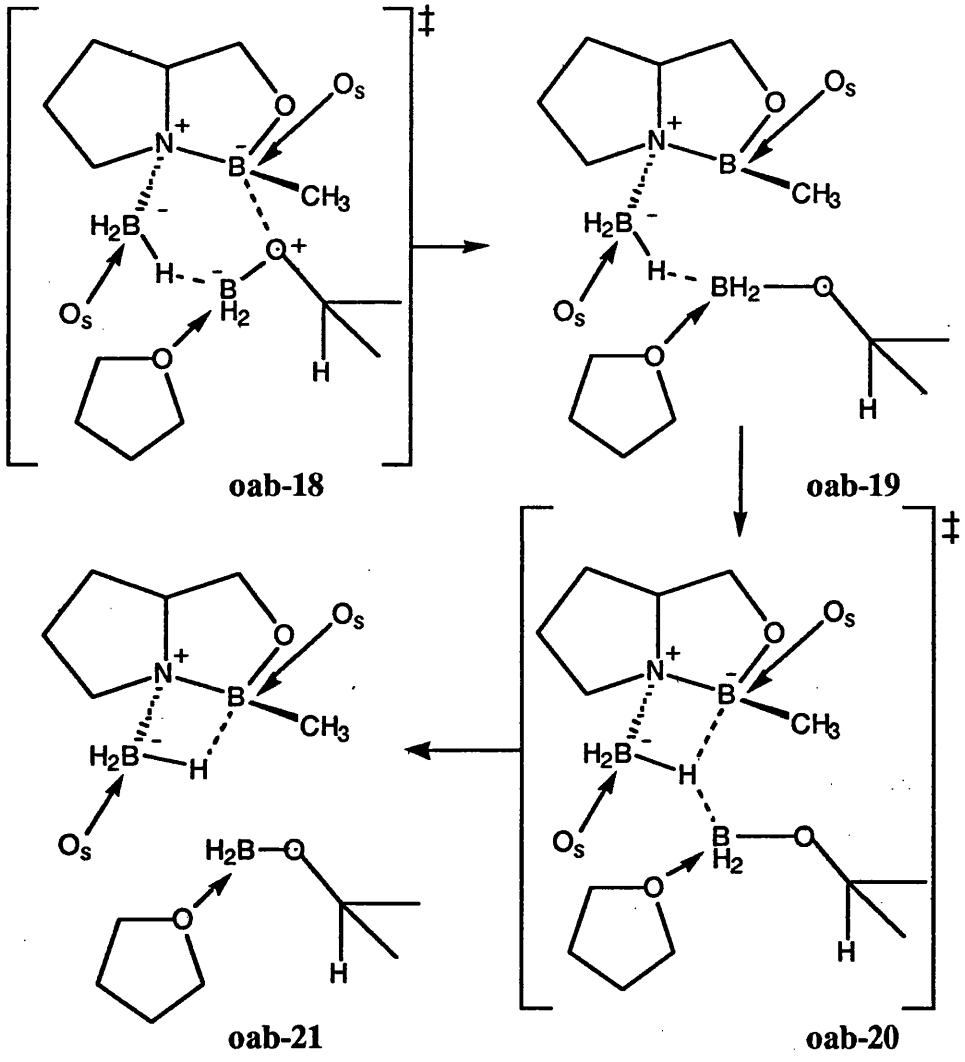

Figure 4-13

The energetics and important structural features for the TS for the B_r-O_c bond breaking, **oab-18**, the unstable intermediate **oab-19**, the early TS **oab-20** and the final complex **oab-21** are given in table 4-15. The ball-and-stick representations for the conversion of **oab-18** to **oab-21** are on the next page.

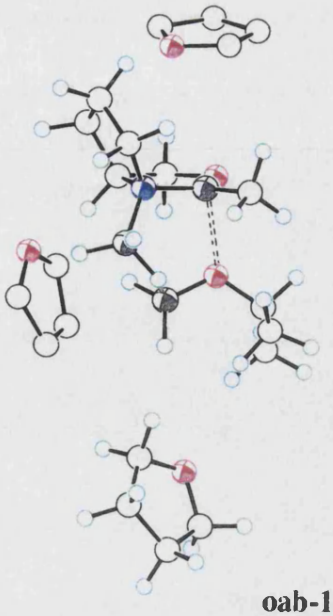

oab-18

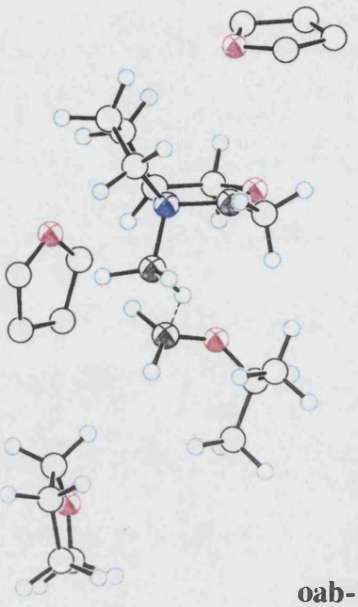

oab-19

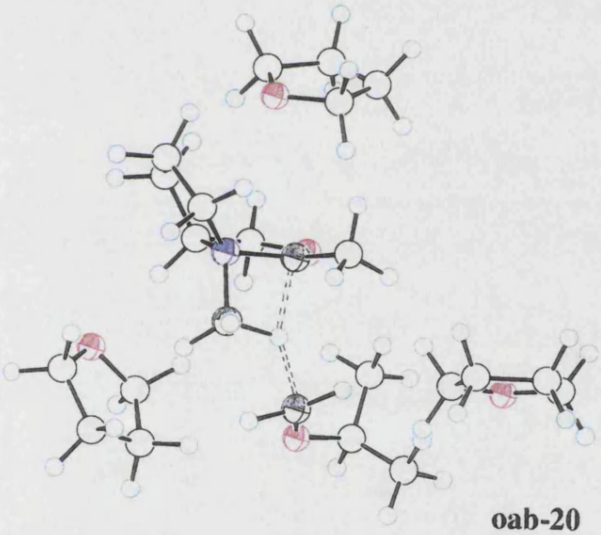

oab-20

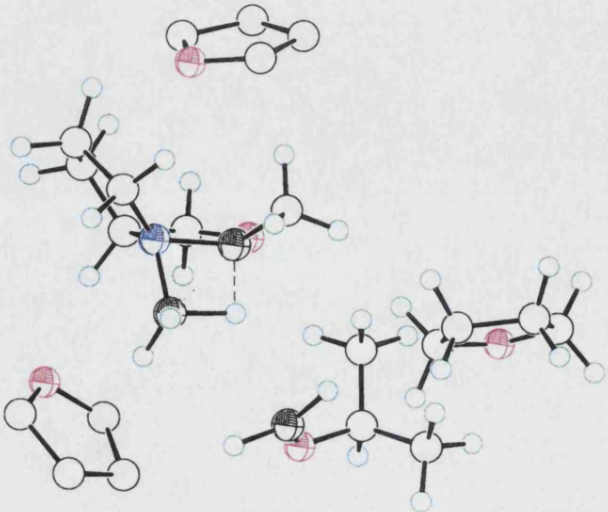

oab-21

Table 4-15: The important energetic (kcal mol^{-1}) and structural (Å) changes for the final steps of the catalytic cycle

	oab-18	oab-19	oab-20	oab-21
ΔH_f	-341.01	-346.63	-346.16	-349.88
ΔH_{rel} [a]	-48.59	-54.21	-53.74	-57.46
B_r-O_c	2.410	4.047	3.998	4.242
B_r-H_n	2.629	2.558	1.800	1.375
B_x-H_n	1.256	1.244	1.262	1.337
B_n-H_n	1.385	1.459	1.673	2.408
B_n-O_c	1.414	1.390	1.364	1.339

[a] Enthalpy of formation relative to isolated OAB [-89.69] + THF [-58.40] + 2 BH_3.THF [-95.32] + MeCOMe [-49.01] = -292.42 kcal mol^{-1}

The location of **oab-21** marked the completion of one possible catalytic cycle. In a system as complex as the OAB-borane-ketone adducts, it would be naive to assume that this is the definitive mechanism, but based on the energetics, it is reasonable to postulate that this may be one of the low energy pathways.

4.8 Discussion of the Identified Reaction Pathway

This study clearly indicated that the hydride-bridged OAB-borane adduct, **oab-5**, was the start and finish point of a catalytic cycle involving a single hydride transfer. This was not an unreasonable postulate due to the greater stability of the OAB-borane adduct than the solvated OAB-borane complex.

As **oab-5** was the initial structure, table oab-16 and graph (figure 4-14) show the energetic changes during one catalytic cycle based on the reference point of OAB-borane adduct [-214.57] + MeCOMe [-49.01] + BH_3-THF [-47.66] = -311.24 kcal mol^{-1}.

Table 4-16: The relative energetic changes during one catalytic turnover

via boat conformer	**oab-6b**	**oab-7b**	**oab-8b**	**oab-9b**	**oab-10b**		**oab-12b**	**oab-13b**	**oab-14b**	**oab-15b**
for hydride transfer	-0.86	9.49	6.60	12.18	-2.5		-35.93	-36.77	-31.22	-31.56
via chair conformer	**oab-6c**	**oab-7c**	**oab-8c**	**oab-9c**	**oab-10c**	**oab-11c**	**oab-12c**	**oab-13c**	**oab-14c**	**oab-15c**
for hydride transfer	-1.78	10.19	5.53	10.72	-28.74	-15.16	-34.07	-32.05	-25.08	-25.09
after convergence of	**oab-16**	**oab-17**	**oab-18**	**oab-19**	**oab-20**	**oab-21**				
pathways	-10.01	-39.13	-29.77	-35.39	-34.92	-38.64				

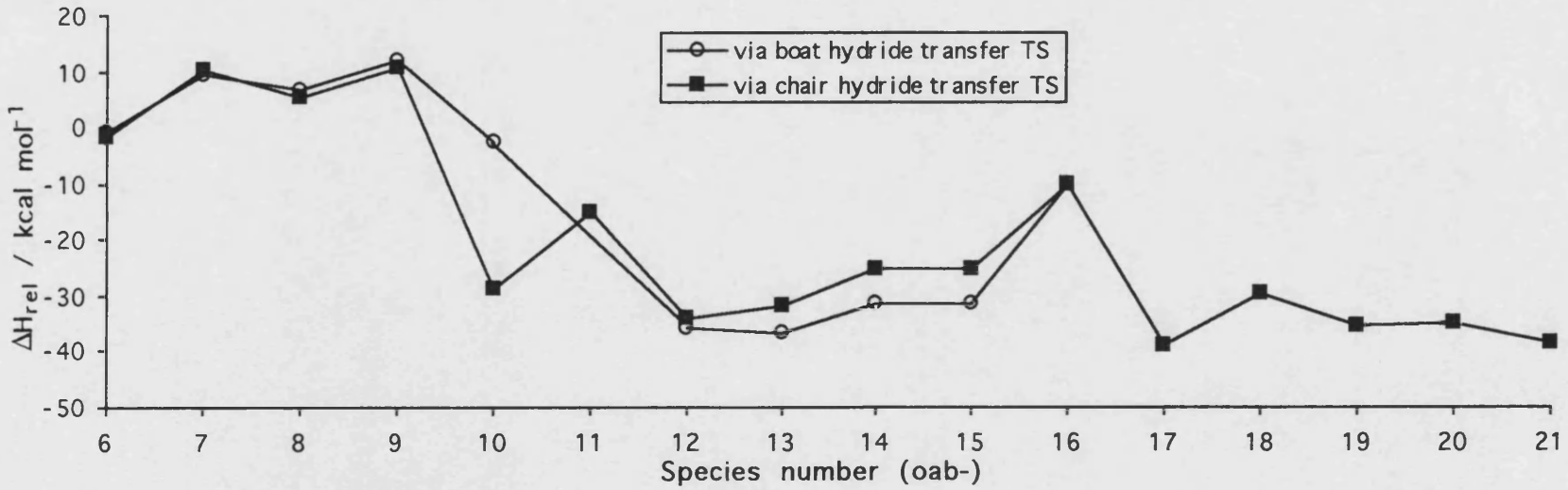

Figure 4-14

From the graph, it was clear that the formation of the hydride transfer transition structure was the rate determining step for both pathways. This implied that enantiomeric excesses observed for the reduction of a prochiral ketone were related to the energetic differences between diastereomeric hydride transfer TSs.

The TS for the formation of the OAB-borane-ketone adduct was only slightly lower in energy: from the chair conformer of the ternary adduct **oab-8c**, the barriers for hydride transfer *versus* dissociation were comparable, 5.19 kcal mol^{-1} and 4.66 kcal mol^{-1} respectively. From the comparable boat conformer, **oab-8b**, the barrier for hydride transfer was 5.48 kcal mol^{-1} compared to 2.89 kcal mol^{-1} for dissociation of the ternary complex. The possibility of an equilibrium prior to the hydride transfer TS was considered during the calculation of the kinetic isotope effect. A steady state approximation was used in the calculation of the KIE (figure 4-15).

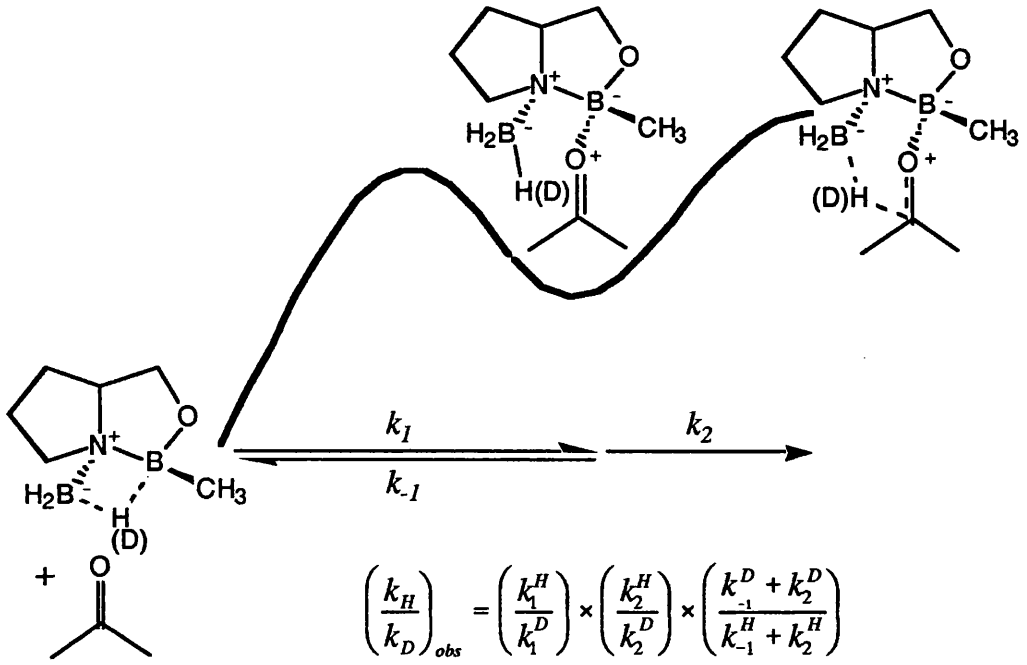

Figure 4-15

Using this steady state treatment, at 23°C the KIEs were 1.81 and 1.72 for the boat and chair conformers respectively.

The KIEs were also calculated from the appropriate isotopomers of OAB-borane adduct and the hydride transfer TS, without regard for the ketone co-

ordination step. Values of $k_H/k_D = 1.89$ and $k_H/k_D = 1.74$ were obtained for the boat and chair conformers respectively. The near agreement between these results and those obtained using the steady state treatment implied that the hydride-transfer step was essentially rate-determining and that ketone co-ordination was not kinetically significant.

The experimental value obtained by Corey *et al.* was 1.7 at 23°C from which they concluded that the TS was early and hydride transfer was highly exothermic.[33]

As with the uncatalysed reduction, there was the possibility of inverse secondary effects reducing the observed primary KIE. Analysis of the KIE of $k_H/k_D = 1.89$ for the boat conformer to be showed it to be comprised of a primary effect $k_H/k_D = 1.76$ for the transferring hydride and a small $k_H/k_D = 1.10$ for the non-transferring hydrogens. For the chair conformer, $k_H/k_D = 1.74$ was composed of a primary KIE of $k_H/k_D = 1.66$ and a secondary KIE of $k_H/k_D = 1.05$. These results indicated that the low KIE was not the result of a dominant secondary isotope effect, but the replacement of a weak B-H bond a stronger C-H interaction.

With the experimental KIE observations supporting the proposed mechanism, the origins of catalysis by OAB-borane adducts could be addressed. Care was needed when selecting a reference reaction as the co-ordination of the solvent differed between the uncatalysed and catalysed hydride transfer TS. In the uncatalysed TS, the solvent had a strong and specific interaction with the borane whereas in the catalysed TS the co-ordination was loose and non-specific.

To obtain an accurate comparison, both transition structures were located without solvent present. The boat TS was selected as the model for the catalysed reaction as this was the higher energy conformer and therefore the slower of the two catalytic pathways.

From the charge distributions in the hydride transfer TS it can be concluded that the reduction was catalysed by an increase in the nucleophilicity of the transferring hydride H_t and the decrease in electron density at the carbonyl carbon

C_c. The dipolar N-B_r bond interacts with the zwitterion-like charge distribution of the uncatalysed TS (figure 4-16); the redistribution of the electrons around the OAB six-membered ring occurring during the approach of O_c of the ketone to the boron B_r of the OAB.

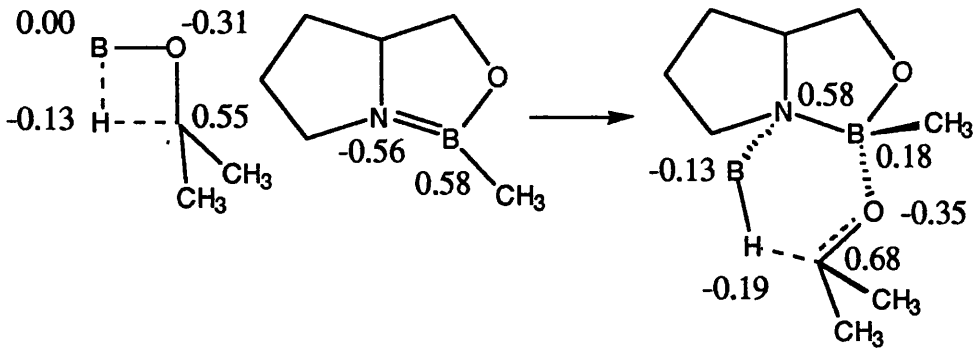

Figure 4-16

The dipolar nature of the N-B bond of the OAB was also studied by considering the cleavage of the six-membered ring into two fragments, one relating to the OAB-portion and the other to a distorted 'uncatalysed TS'. A single SCF calculation was performed on each portion to allow the charges to be calculated (figure 4-17).

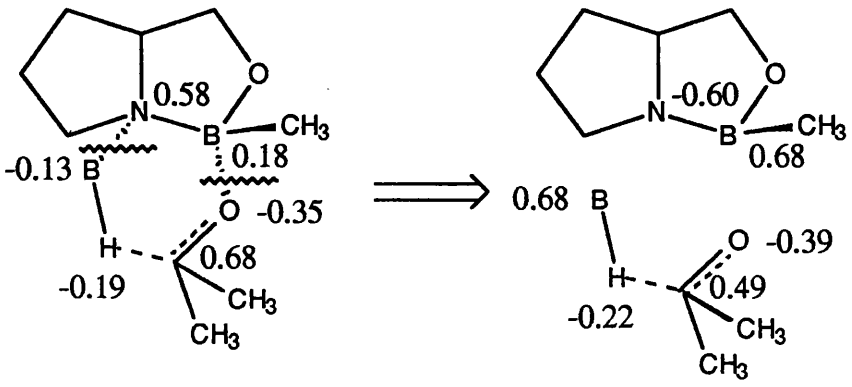

Figure 4-17

The charge distribution in the fragments clearly reflected the donation from the nitrogen to boron B_x and from the sp^2-oxygen O_c to ring boron, B_r.

Whilst the analysis of the charge distribution provided a qualitative insight into why catalysis occurred, a more detailed analysis was required to determine why

such a significant rate enhancement occurred. Two reactions were used to assess the energetic changes during hydride transfer (figure 4-18).

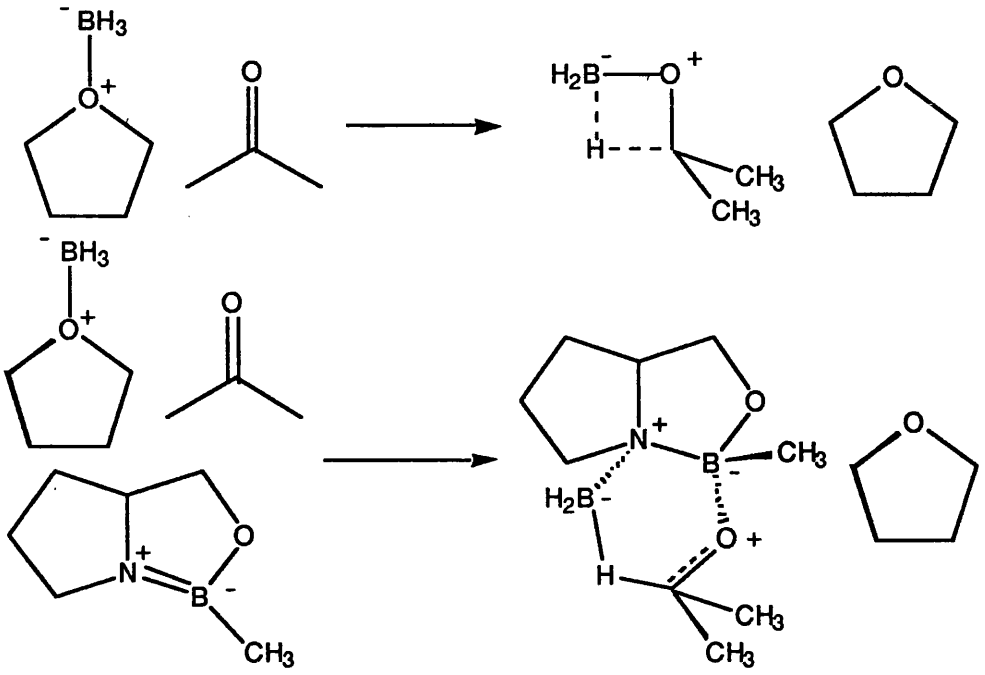

Figure 4-18

The energy required for these conversions were 18.66 kcal mol^{-1} for the uncatalysed reaction and -3.08 kcal mol^{-1} for the catalysed reduction, 21.74 kcal mol^{-1} less demanding than the uncatalysed reduction.

The energy required to distort the geometry from the four-membered TS to the geometry adopted in the catalysed reaction was 38.86 kcal mol^{-1} (figure 4-19) The energy of the 'distorted TS' was obtained from a single SCF calculation with the co-ordinates of the atoms being in the same relative positions as in the OAB-catalysed TS. The energy required to distort the OAB to the conformation found in the catalysed TS was 27.15 kcal mol^{-1}.

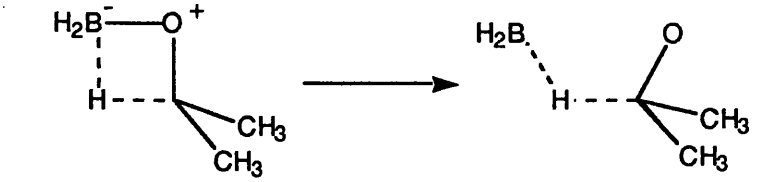

ΔH_f = -19.61 kcal mol^{-1} ΔH_f = 19.25 kcal mol^{-1}

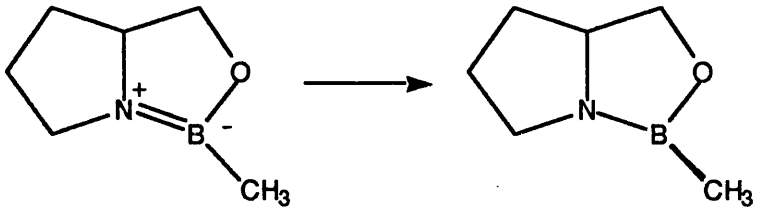

ΔH_f = -89.81 kcal mol^{-1} ΔH_f = -62.66 kcal mol^{-1}

Figure 4-19

Therefore the total distortion energy was 66.01 kcal mol^{-1}.

Comparing the sum of the energy of the two fragments with that of the catalysed TS, -43.41 kcal mol^{-1} versus -131.04 kcal mol^{-1}, implied that interactions between the two fragments would released 87.63 kcal mol^{-1}.

Therefore the catalysed reaction can be considered as unfavourable distortions, requiring 66 kcal mol^{-1}, being counteracted by advantageous interactions releasing 87.7 kcal mol^{-1}; an overall release of 21.7 kcal mol^{-1}, the amount by which the barrier to hydride transfer had been shown to be reduced.

With a mechanism determined and the rate determing step identified, the issue of why OAB-borane adducts are highly enantiospecific could be investigated.

Chapter 5: The Reduction of Prochiral Ketones by Chiral Oxazaborolidine-Borane Adducts: A Review of the Literature

5.1 Experimental Investigations Pertinent to the Origins of Selectivity

This section will review experiments which have focused upon the origins of selectivity and which factors affect the levels induction exerted. It is not the aim of this section to provide a list of enantiomeric excesses obtained from the reduction of prochiral ketones.

5.1.1 The Effect of the Substituents of the OAB on Induction

Comprehensive studies of the effect of substituents on selectivity have been carried out by two independent groups. Garcia and co-workers[45] and Cho *et al.*[46] have varied the substituents attached to the 2-, 3- and 5-positions (figure 5-1).

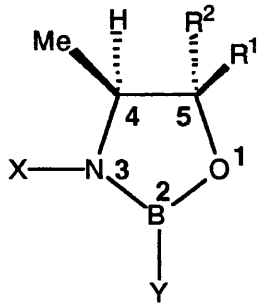

Varying the nitrogen substituent (X)

R^1=Ph , Y=R^2= H

X	H	Me	n-Bu	i-Pr
e.e	72	83	22	3

Varying substituents at the 5-position (R^1,R^2)

Y=X=H

R^1, R^2	H	Me	Ph
e.e	17	25	84

Varying the boron subtituent (Y)

R^1=Ph, R^2=H, X=Me

Y	Me	n-Bu	Ph
e.e	61	55	42

Figure 5-1

Both groups noticed a marked decrease in yields and selectivity with the increase in steric bulk or the presence of electron withdrawing groups attached to

nitrogen. Garcia noted that reaction rates decreased with increasing bulk of the boron-substituent, but the enantioselectivity did not significantly alter. Cho's research noticed a greater decrease in enantioselectivity with the change of this substituent.

Both studies revealed the particular sensitivity of the induction to the substituent at the 5-position.

Garcia also investigated the origins of the minor enantiomer. The major enantiomer resulted from an *exo* conformation of the ketone with respect to the oxazaborolidine ring. Garcia postulated that the minor isomer could result from either the *endo* conformer or a complex formed from the borane co-ordinating with the oxygen of the oxazaborolidine. As studies of dioxoborolidines revealed no catalytic activity, he concluded that the *endo* conformation must produce the minor isomer.

5.1.2 The Effect of the Ketone Substituents on Induction

Mathre and co-workers[31] noted that the nature of the *para*-substituent on substituted acetophenones affected enantioselectivity and reaction rate. A slight decrease in enantioselectivity was observed on changing from an electron-donating to an electron-withdrawing group. They concluded that the electron-donating substituents stabilised the ternary ketone-oxazaborolidine-borane complex, thus increasing the steric interactions responsible for enantioselectivity. The slight decrease of reaction rate when an electron-donating group was replaced by an electron-withdrawing group was attributed to a greater increase in the rate of hydride transfer compared to the decrease in the ketone complexation equilibrium constants.

The enantioselectivity was found to be more sensitive to changing the boron substituent from methyl to ethyl, 96.6 to 95.6%, than changing the smaller substituent on the ketone from a methyl to an ethyl group, 98.8% to 99.0%.

5.1.3 The Effect of Temperature on Enantiomeric Excesses

The effect of temperature on enantioselectivity has been an area of conflicting findings. Mathre and co-workers[31] commented that 'as expected, the level of enantioselection increases by decreasing the reaction temperature' whereas Corey *et al.*[33] noted that the enantioselectivity increased with increasing temperature.

Stone[47] attempted to explain this apparent contradiction by performing a careful investigation into the reduction of acetophenone and cyclohexyl methyl ketone using OAB with a variety of boron-substituents, namely methyl (B-Me), butyl (B-Bu) and phenyl (B-Ph). He found that the selectivity/temperature dependence was influenced by the boron substituent and the ketone. When the reduction was carried out at -15°C, he found that the selectivity was not particularly dependent on the boron substituent for the reduction of the acetophenone, but particularly sensitive for cyclohexylmethyl system. This was in direct contrast to the findings at 23°C.

Stone also found that the selectivity at lower temperature was also solvent dependent. He compared the reduction of acetophenone using the B-Ph oxazaborolidine in THF and toluene. He found that between -40 and 0°C the selectivity in the reaction performed in THF was considerably less than in toluene, but between 20 and 60°C the enantioselectivities were comparable.

5.1.4 The Effect of Side Reactions and Impurities on Enantioselectivity

In contrast to the pioneering work of Itsuno,[27a] Buono and co-workers[48] discovered that borane-adduct derived from (S)-proline could be used as highly efficient asymmetric induction catalyst. They found that enantiomeric excess was strongly temperature dependent; a summary of their findings is given in table 5-1.

Table 5-1: The reduction of acetophenone with borane and 2 mol % (S)-proline

Temp. (°C)	25	35	66	110
e.e.	8	37	42	59

By increasing the amount of catalyst from two to ten mole percent, the e.e. increased from 59% to 95% at 110°C. Buono proposed that the catalyst was obtained from a dimeric structure, being supported by the findings of Mathre and co-workers,[31] and was itself in equilibrium with another dimer (figure 5-2). If the second dimer was favoured at lower temperatures, the lower enantioselectivities could be explained by competition with the uncatalysed reaction.

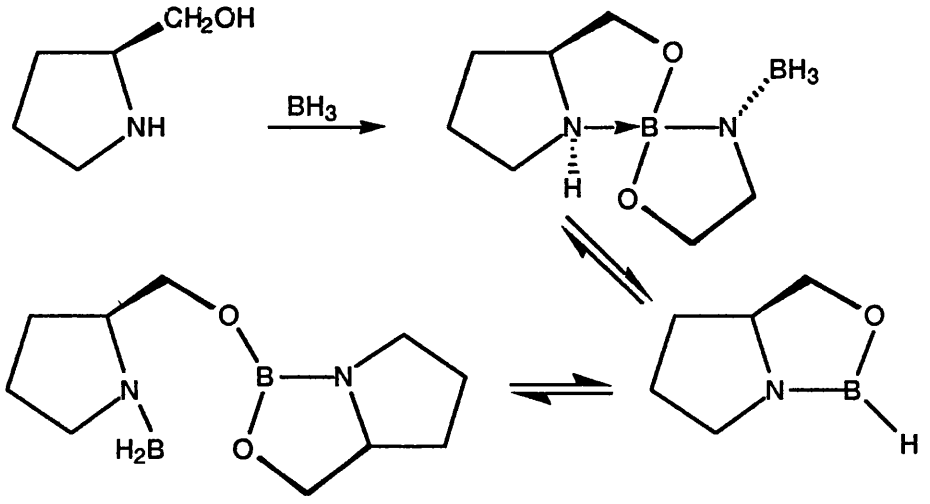

Figure 5-2

Brown and co-workers also found an example of reversible dimerisation involving a ring-opening and closure (figure 5-3).[49] From his studies, Brown concluded that the 'structure of oxazaborolidines is highly sensitive to substitution in the ring, and that a dimeric species with potential reducing power is easily accessible under the conditions of typical catalytic reactions.'

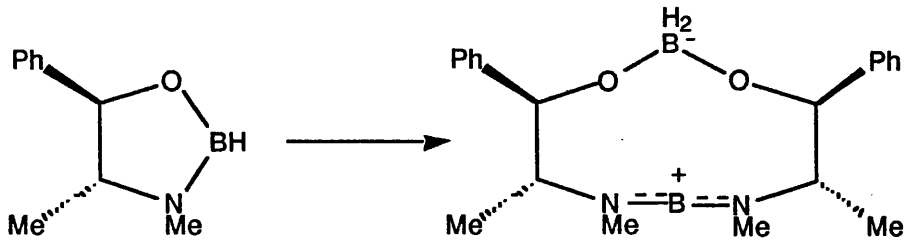

Figure 5-3

Mathre and co-workers[50] performed a thorough investigation to obtain the optimum experimental conditions for reproducible results. They observed that reagents needed to be dried thoroughly prior to reduction because the presence of water had a significantly detrimental effect on the optical purity of the alcohol. A mere one milligram of water, compared to one gram of ketone, was all that was needed to reduce the enantiomeric excess from 95% to 50%. In contrast, the presence of methanol in the reaction mixture did not affect the level of asymmetric induction.

They also noted that the presence of methylboronic acid, which was used to prepare the OAB from diphenyl-substituted prolinol, reduced the e.e. to 70%. It was proposed that the presence of the acid or water resulted in decay in selectivity rather than hydrolysis of the catalyst.

In a later study, Mathre and co-workers[31] found that the enantioselectivity was dependent on the degree of substitution of the hydride source. He proposed that the lower apparent enantioselectivity observed for the second hydride transfer may be the result of competitive non-oxazaborolidine catalysed reduction or an alternative catalytic cycle whereby the alkoxyborane generated during the first hydride transfer remained co-ordinated to the oxazaborolidine and provided the second hydride.

An investigation by Cai *et al.* confirmed the latter of these proposals.[44a] When triethylamine was added, the alkoxyborane intermediate was trapped before the second hydride transfer could occur, and thus increasing the enantioselectivity of the reaction. As this method stopped the catalytic process by the formation of a tight complex, an alternative additive was sought which did not inhibit the cycle.

A variety of alcohols[44b] were added to the reaction mixture and it was found that the addition of isopropyl alcohol increased then enantioselectivity for 2-substituted-4-chromanones, but not for α-tetralone or unsubstituted-4-chromanones (figure 5-4).

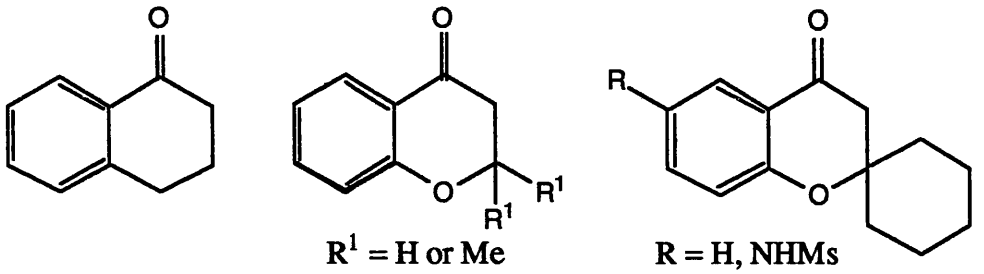

R^1 = H or Me

R = H, NHMs

α-tetralone

R^1 = H
unsubstituted 4-chromanone

2-substituted 4-chromanone

Figure 5-4

Low temperature NMR studies are underway by Cai to elucidate the effect of the alcohol on the mechanism.

5.2 Theoretical Modelling To Determine the Origins of Enantioselectivity

Despite Nevalainen's considerable analysis of possible intermediates on the reaction pathway, he has not undertaken any studies of the hydride transfer transition structures. His only references to this important step were in terms of qualitative changes.

5.2.1 Semi-Empirical MO Investigation into the Origins of Induction

Liotta and co-workers[51] have used the MNDO hamiltonian to locate the hydride transfer TS and the preceding ternary OAB-borane-ketone complex for the catalysts and ketones shown in the figure 5-5.

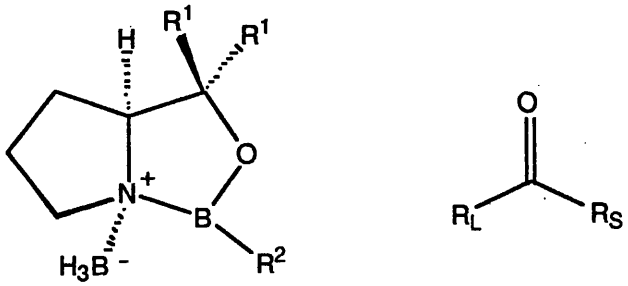

R^1 = H, Ph, α- & β-Naph, *i*-Pr,*o*-MeOPh

R^2 = H, Me, Et ; R_L = Ph, *t*-Bu ; R_S = Me, Et

Figure 5-5

Rate constants were determined for the conversion of the enantiomeric ketone complexes into diastereomeric chair, half-chair and boat transition structures. These rate constants were then used to predict e.e.s which were in good agreement with the experimentally observed values, a summary of their findings is shown in table 5-2.

Table 5-2: A comparison of the Liotta's theoretical e.e.s with experimental e.e.s for a range of oxazaborolidines and ketones

R^1	R^2	R_L	R_S	calcd. e.e.	exptl. e.e.[1]
Ph	H	Ph	Me	98	97.0
Ph	H	Ph	Et	80	90.0
Ph	Me	Ph	Me	93	96.5
Ph	Me	*t*-Bu	Me	96	97.3
H	H	Ph	Me	2	poor
H	Me	Ph	Me	42	poor

[1] As cited in Liotta and co-workers' paper[51]

The chair TS was found to have the lowest overall activation energy for all the systems studied. The barrier to forming the half-chair was consistently 5 kcal mol^{-1} higher in energy than that for the lowest energy conformer and was thus discarded from the calculation of enantiomeric excess.

The study concluded that variation of the boron substituent had a 'fine-tuning' effect on selectivity, due to increased steric congestion favouring the *exo*-R_L orientation but the nature of the prolinol substituent was the single most important determinant of selectivity.

5.2.2 Ab Initio MO Study of the Origins of Stereocontrol

Quallich and co-workers[52] have undertaken a combined *ab initio* MO and experimental study of oxazaborolidine-borane adducts derived from the substituted ephedrines (figure 5-6).

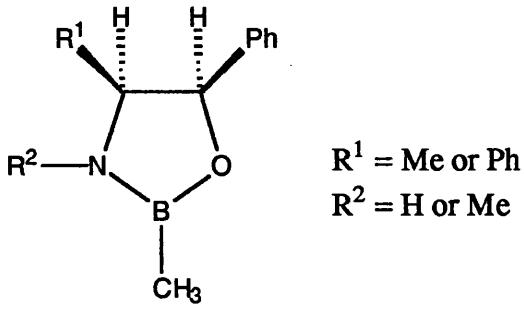

Figure 5-6

The experimental observations for the reduction of α-tetralone and *tert*-butyl methyl ketone were compared to the theoretical findings at the 3-21G, 6-31G* and MP2/6-31G* levels for the reduction of *tert*-butyl methyl ketone. The aim of the study was to determine the relationship between catalyst structure and e.e., the role of the geminal diphenyl substituents and the effect of nitrogen substitution on selectivity.

To validate the results provided by 3-21G basis set, the energies and structures of OAB-borane-ketone complexes from this level were compared with those obtained using the higher basis sets. As the HF/3-21G structures did not differ significantly from those calculated using the correlated MP2/6-31G* method, the former was utilised to determine the enantiomeric excesses for reduction of *tert*-butyl methyl ketone. The enantiomeric excesses were determined by considering

the difference in free energies between the *exo* and *endo* transition structures and compared favourably with the experimentally observations.

They concluded that the molecular recognition between the boron and the ketone, and the blocking of one face by the phenyl substituents were the key elements in the high enantioselectivities obtained. Increasing the substitution on nitrogen resulted in a decrease in enantioselectivity because of conformational changes in the prolinol ring forcing the phenyl substituent to adopt a higher energy conformer.

Chapter 6: The Origin of the Selectivity Observed in the Reduction of Ketones by Chiral Oxazaborolidine-Borane Adducts: A Computational Study

The study of the mechanism in chapter 4 had indicated that the hydride transfer TS was the rate limiting step (see also section 6.1). Therefore, the enantiomeric excess (e.e.) resulting from the reduction of a prochiral ketone could be calculated from the free energy differences for the hydride transfer TSs. Relative free energies were calculated for higher energy TSs with respect to the lowest energy, enantiomeric TS. From the free energy, a relative population was obtained using equation **6-1.**

$$\text{population relative to the most stable enantiomer} = \exp\left(\frac{-\delta(\Delta G)}{RT}\right)$$

.....Equation **6-1**

where $\delta(\Delta G)$ is the difference in free energy of the species with respect to the most stable enantiomer, R is the ideal gas constant and T the temperature.

The populations are then scaled so that the total population is equal to one and the e.e. determined from the difference in the populations of the (R) and (S) enantiomers.

enantiomeric excess = [population of the (R) enantiomer - population of the (S) enantiomer] x 100.....Equation **6-2**

Enthalpy, entropies, free energies and populations were all calculated to four decimal places whilst e.e. were calculated to one decimal place. In the tables that follow, enthalpy and free energies are only quoted to two decimal places, so any differences that do not tally are as a result of rounding errors.

The specific interactions of THF solvent molecules have not been considered due to the conformational freedom of these molecules, and the significant effect of small energy changes on the enantiomeric excess.

6.1 The Interconversion of the Boat and Chair TS

As mentioned in the introduction (chapter 2), the e.e. can be determined from the free energy difference of species with the highest free energy which are found on the reaction pathway. Whilst the study of the mechanism had shown that the co-ordination of the ketone was not rate limiting, there was the possibility that the barrier for the interconversion of the boat and chair conformers could be higher than barrier for hydride transfer.

The ternary OAB-borane-ketone complexes of the boat and chair conformers of the R epimer were optimised for the reduction of acetophenone by an OAB-borane adduct (figure 6-1).

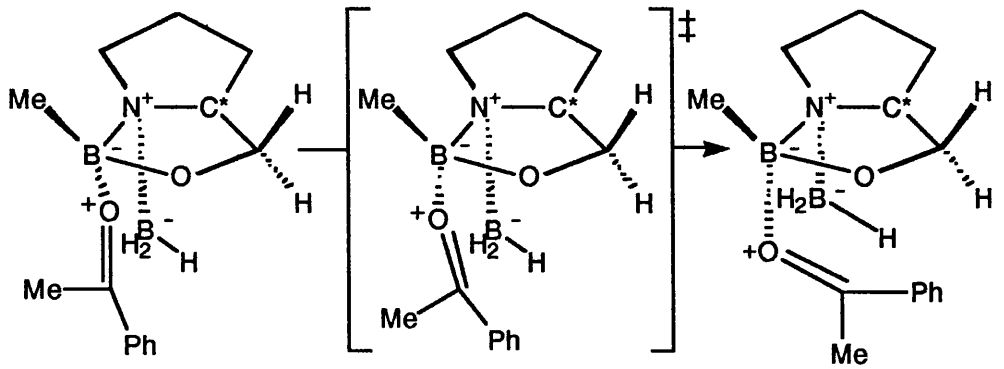

Figure 6-1

Whilst the structure **chi-4** appeared to related to the interconversion of the boat and chair conformers, analysis of the calculated vibrational frequencies identified one imaginary frequency but of very small magnitude ($\upsilon^{\ddagger}$ = 29 cm^{-1}). Small displacements of the geometry relating to forward and reverse motions along the reaction co-ordinate, followed by full optimisation identified the boat and chair conformers of the ketone complex. All attempts to locate a TS with a more

meaningful vibrational frequency failed so the located geometry has been accepted as an approximate TS for the conversion. Table 6-1 provides the important geometrical and energetic changes.

Table 6-1: The enthalpy (kcal mol^{-1}) and important dihedral angles (°) for the conversion of the boat conformer to the chair conformer for hydride transfer

	chi-3	**chi-4**	**chi-5**
ΔH_f	-102.18	-98.71	-98.89
C_c-O_c-B_r-N	-79.7	3.3	53.8
O_c-B_r-N-C	-80.5	-93.3	-104.9

As will be discussed in the next section, the 'boat R' hydride transfer TS was the least stable epimer for this OAB-borane adduct (ΔH_f = -88.56 kcal mol^{-1}) The TS **chi-4** was 3.2 kcal mol^{-1} lower in energy than the 'boat R' hydride transfer TS, confirming that e.e. could be determined on the basis of relative free energy difference between TS epimers.

6.2 The Reduction of Acetophenone by Various OAB-Borane Adducts

All the reductions were studied at 25°C as this was the temperature at which the most experimental data was available. Boat and chair conformers for the hydride transfer TS were located for the reduction of acetophenone, with both R and S stereochemistry. In the R epimers the phenyl group of acetophenone was positioned *endo* with respect to the oxazaborolidine ring and *exo* in the S epimers. The four orientations are shown in figure 6-2 and in the ball-and-stick representations on the next page (R^1=Ph, R^2=Me).

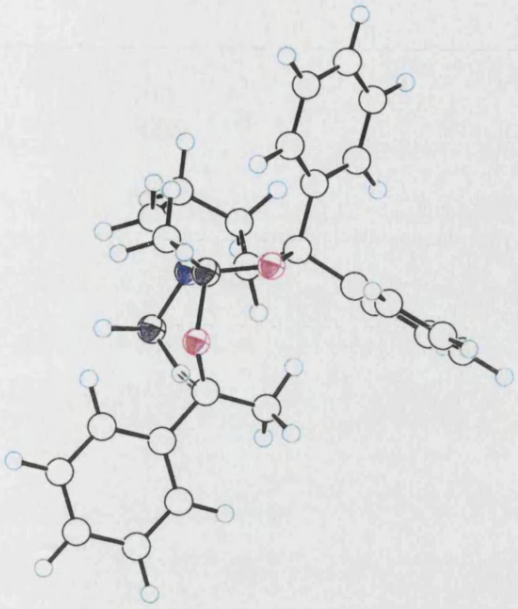

'Boat S' hydride transfer TS

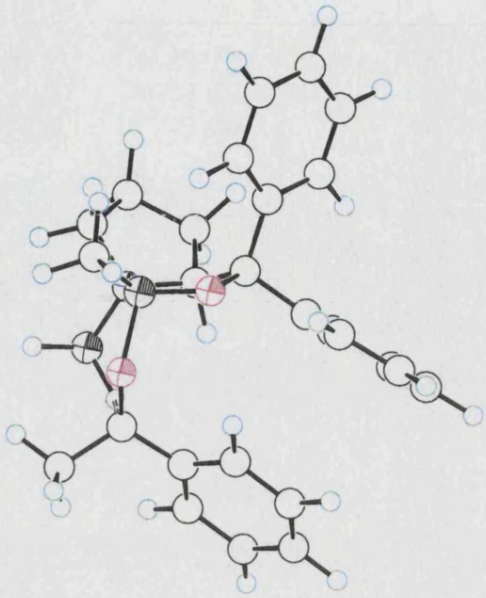

'Boat R' hydride transfer TS

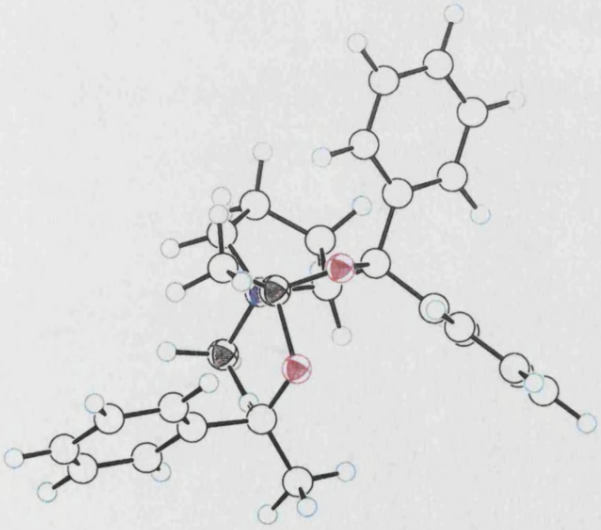

'Chair S' hydride transfer TS

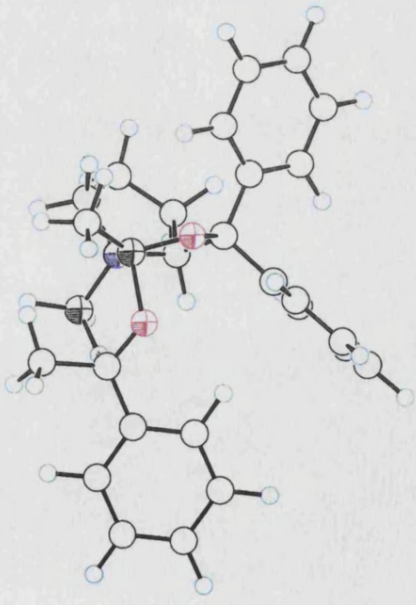

'Chair R' hydride transfer TS

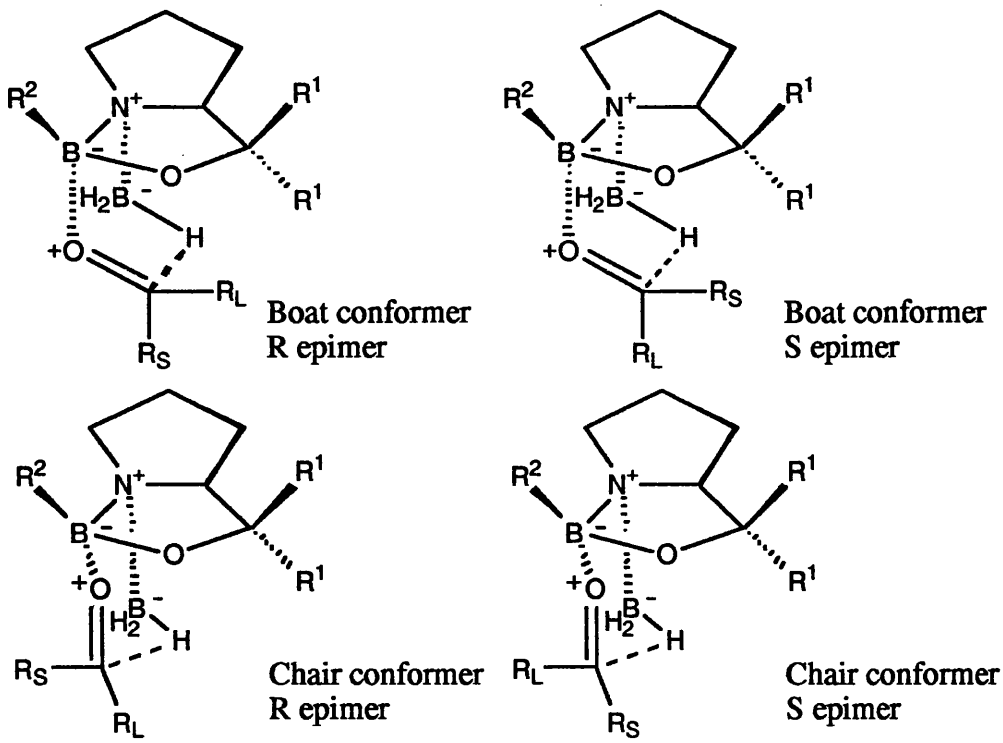

Figure 6-2

Unless otherwise noted the TSs will be referred to as 'boat R', 'boat S', 'chair R' and 'chair S' respectively.

6.2.1 Reduction of Acetophenone by OAB-borane Adducts Derived from (S)-Prolinol

The first catalyst system to be analysed was that with R^1 = H (figure 6-3).

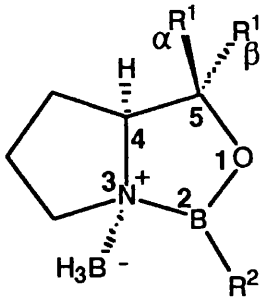

R^1 = H
R^2 = H: **chi-1a**
R^2 = Me: **chi-1b**
R^2 = Ph: **chi-1c**
R^2 = ^{t}Bu: **chi-1d**

Figure 6-3

Table 6-2 shows the variation of the enthalpy, relative enthalpy, relative free energy and relative population of the four conformers with varying boron substituent.

Table 6-2: The energetics for the reduction of acetophenone by **chi-1a, chi-1b, chi-1c** and **chi-1d** (kcal mol^{-1})

	ΔH_f	$\delta(\Delta H_f)$	$\delta(\Delta G)$	population	$\upsilon^{\ddagger}$ (cm^{-1})
chi-1a					
boat S	-89.06	1.10	1.48	0.0649	421*i*
boat R	-88.56	1.60	1.54	0.0582	409*i*
chair S	-89.12	1.04	1.29	0.0897	408*i*
chair R	-90.16	0.00	0.00	0.7872	409*i*
chi-1b					
boat S	-95.62	1.62	1.79	0.0424	438*i*
boat R	-95.51	1.74	1.77	0.0438	432*i*
chair S	-95.26	1.99	1.88	0.0368	437*i*
chair R	-97.25	0.00	0.00	0.8770	418*i*
chi-1c					
boat S	-57.29	1.29	1.09	0.1197	424*i*
boat R	-56.84	1.74	1.08	0.1205	406*i*
chair S	-55.48	3.10	2.64	0.0087	424*i*
chair R	-58.57	0.00	0.00	0.7511	432*i*
chi-1d					
boat S	-99.03	0.29	0.35	0.1186	441*i*
boat R	-98.90	0.43	-0.17	0.4573	422*i*
chair S	-96.95	2.38	1.90	0.0137	430*i*
chair R	-99.33	0.00	0.00	0.3404	426*i*

The enthalpy of the OAB-borane adducts, the barrier for hydride transfer *via* the 'chair R' conformer, the theoretical and experimental e.e. at 25°C are given in table 6-3.

Table 6-3: The effect of the boron substituent (R^2) on the e.e when R^1=H

	ΔH_f (OAB-BH_3)	ΔH_{rel} (CR)[a]	e.e. at 25°C	exptl. e.e. at 25°C
chi-1a	-83.74	8.69	69.1% (R)	8% (R)
chi-1b	-93.99	11.86	83.2% (R)	none available
chi-1c	-56.45	12.99	74.3% (R)	none available
chi-1d	-101.25	17.04	59.5% (R)	none available

[a] Enthalpy relative of the 'chair R' TS to the appropriate OAB-borane adduct + PhCOMe [-15.12 kcal mol^{-1}]

For all four OAB-borane adducts, the 'chair R' TS was the lowest energy epimer. The energy of the 'chair R' TS, with respect to the OAB-borane adduct, decreased as R^2 was altered.

For the conversion of R^2 from hydrogen to methyl to phenyl, the population of the 'boat R' epimer did not significantly enhance the enantiocontrol. For these three substituents, there was a larger change in the energy of the 'chair S' epimer than in the 'boat S' TS.

The variation of B_r-O_c bond distance and changes in the sum of the bond angles about B_r with variation of R^2 for the 'chair R' epimer (table 6-2) provided insight into the origin of stereoselectivity.

In isolated OAB, the sum of the angles about B_r (N-B_r-O_r, N-B_r-C and C-B_r-O_r) about B_r was 360°, consistent with a planar geometry. With the approach of the ketone to boron, it would tend to a sp^3-hybrised structure. If the boron was completely sp^3-hybridsed the sum of angles would be 328° 24'. Therefore the degree of pyramidalisation or planarity about boron can be obtained from the bond angles.

Table 6-4: The changes in B_r-O_c bond distance (Å) and angles (°) about B_r in the 'chair R' TS with the variation of boron substituents.

	chi-1a	chi-1b	chi-1c	chi-1d
B_r-O_c	1.675	1.713	1.701	1.744
X-B-X	345.2	346.2	345.8	347.0

The e.e. followed the trends observed in bond length and in the sp^2-character of B_r for the **chi-1a, chi-1b,** and **chi-1c.** The planarity about boron B_r increased in the following order: **chi-1a < chi-1c < chi-1b < chi-1d.** The increased planarity placed the boron substituent in closer proximity to the ketone substituents. This explained the close correlation of the e.e. to the population of the 'chair S' TS as the aromatic ring of the ketone and the boron-substituent were in similar regions of space.

In **chi-1d** there was a significant decrease in the bond length coupled with the expected increase in planarity around B_r, but the stereoselectivity decreased. This was as direct consequence of the decrease in stability of the 'chair R' epimer, rather than an increase in the stability of the other TSs.

6.2.2 The Reduction of Acetophenone by OAB-Borane Adducts Derived From the Diphenyl Substituted (S)-Prolinol

The next catalyst family to be analysed was those in which R^1 = Ph (figure 6-4).

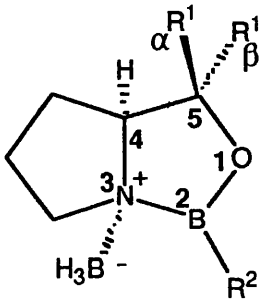

R^1 = Ph
R^2 = H: **chi-2a**
R^2 = Me: **chi-2b**
R^2 = Ph: **chi-2c**
R^2 = ^{t}Bu: **chi-2d**

Figure 6-4

Table 6-5 shows the variation in the enthalpy, relative enthalpy, relative free energy and population of the four conformers with the change in boron substituent, R^2.

Table 6-5: The energetics for the reduction of **chi-2a, chi-2b, chi-2c** and **chi-2d** (kcal mol^{-1})

	ΔH_f	$\delta(\Delta H_f)$	$\delta(\Delta G_{298})$	population	$\upsilon^{\ddagger}(cm^{-1})$
chi-2a					
boat S	-19.11	0.77	1.27	0.0894	403*i*
boat R	-14.24	5.64	5.00	0.0001	375*i*
chair S	-18.74	1.14	0.95	0.1519	404*i*
chair R	-19.88	0.00	0.00	0.7586	423*i*
chi-2b					
boat S	-24.88	1.92	1.59	0.0575	436*i*
boat R	-20.48	6.31	4.97	0.0001	458*i*
chair S	-24.90	1.89	1.28	0.0979	428*i*
chair R	-26.79	0.00	0.00	0.8445	434*i*
chi-2c					
boat S	13.67	1.68	1.76	0.0468	419*i*
boat R	18.79	6.77	6.13	0.0000	368*i*
chair S	15.01	3.02	1.83	0.0417	417*i*
chair R	11.99	0.00	0.00	0.9115	436*i*
chi-2d					
boat S	-25.10	2.54	1.63	0.0455	411*i*
boat R	-21.03	6.61	4.64	0.0000	432*i*
chair S	-26.03	1.60	0.63	0.2438	417*i*
chair R	-27.64	0.00	0.00	0.7105	426*i*

The enthalpy of the OAB-borane adducts, the barrier for hydride transfer *via* the 'chair R' conformer, the theoretical and experimental e.e. at 25°C are given in table 6-6.

Table 6-6: The effect of the **chi-2** boron substituent on the e.e.

	ΔH_f (OAB-BH_3)	ΔH_{rel} (CR)[a]	e.e. at 25°C	exptl. e.e. at 25°C
chi-2a	-14.46	9.70	51.7% (R)	97% (R)
chi-2b	-24.70	13.02	68.9% (R)	97% (R)
chi-2c	13.09	14.02	82.3% (R)	96% (R)
chi-2d	-31.82	19.30	42.1% (R)	-

[a] Enthalpy relative of the 'chair R' TS to the appropriate OAB-borane adduct + PhCOMe [-15.12 kcal mol^{-1}]

The 'chair R' TS was again the lowest energy structure. The 'boat R' epimer was effectively not populated for all four OAB-borane adducts because of the unfavourable interaction between the aromatic group associated with the ketone and the diphenyl group attached to the catalyst. The relative population of the 'boat S' was not significantly affected by the change in the boron-substituent. As with the first class of catalysts, R^1=H, the e.e. was mainly affected by changes in the 'chair S' epimer since the aromatic group and group attached to boron B_r were in similar regions of space.

Inspection of the changes in the B_r-O_c bond distance and changes in the sum of the bond angles about B_r with variation of R^2 for the 'chair R' epimer, table 6-7, revealed a similar trend to the other class of catalysts.

Table 6-7: The changes in B_r-O_c bond distance (Å) and angles (°) about B_r found in the 'chair R' TS with the variation of boron substituents.

	chi-2a	**chi-2b**	**chi-2c**	**chi-2d**
B_r-O_c	1.654	1.688	1.678	1.733
X-B-X	343.7	344.5	344.4	346.4

The planarity about boron B_r increased in the following order: **chi-2a** < **chi-2c** ≈ **chi-2b** < **chi-2d.** The same explanation of increasing bond length resulting in increased steric interactions between the catalyst and the bulky ketone substituent can be applied to this system.

For both R^1 substituents, the R^2 = Me or Ph imparted more control than R^2 = H. The main difference was the relative control exerted by R^2 = Me or Ph. When R^1 = H, the catalyst with R^2 = Me, **chi-1b**, exerted more enantiocontrol than the R^2 = Ph system, **chi-1c**. The opposite observation was found when R^1 = Ph, with the e.e. for **chi-2b** being about 13% lower than that **chi-2c**.

If the e.e.s for R^1 = Ph were calculated on the basis of enthalpic differences alone, that is the entropic differences were ignored, the values obtained for R^2 = Me and R^2 = Ph were similar, 85.2% (R) and 87.8% (R) respectively. Compared to the values of 68.9% (R) and 82.3% (R) predicted from the difference in free energy, it was clear that the entropic contribution to **chi-2b** had significantly increased the population of one (or both) of the (S)-conformers.

Analysis of the data (table 6-5) revealed that the free energy difference between 'chair R' and 'chair S' TSs was less than the enthalpy difference between these epimers. The entropy difference, 2.05 cal mol^{-1} K^{-1}, implied that the 'chair S' TS was looser than the other stereoisomer. From a comparison of the geometries, this 'looseness' appeared to be in the binding of the ketone. The B_r-O_c distance was 1.727 Å in the 'chair S' TS compared to 1.688 in the 'chair R' TS and the C-H_t distances were 1.709 Å and 1.698 Å for the 'S' and 'R' respectively.

Comparing the two families of catalysts, it was noted that systems derived from (S)-prolinol, **chi-1**, were not inferior in terms of their ability to exert stereocontrol. This was in direct contrast to experimental observations of Itsuno[27a] and Corey.[29]

Buono[48] had found that the e.e. of the (S)-prolinol catalyst could be improved by increasing the reaction temperature and the concentration of the catalyst. This evidence implied that the catalyst was not inherently flawed but unwanted side reactions lowered the stereoselectivity at lower temperatures; the side reactions being non-competitive for the more substituted catalyst.

In the investigation of the mechanism (see chapter 4.6) the N-B_r bond in the intermediate directly after the hydride transfer TS was markedly weaker. Analysis of intrinsic reaction co-ordinates from the hydride transfer TSs (figure 6-5) revealed that phenyl groups prevented the increase in the N-B_r bond length.

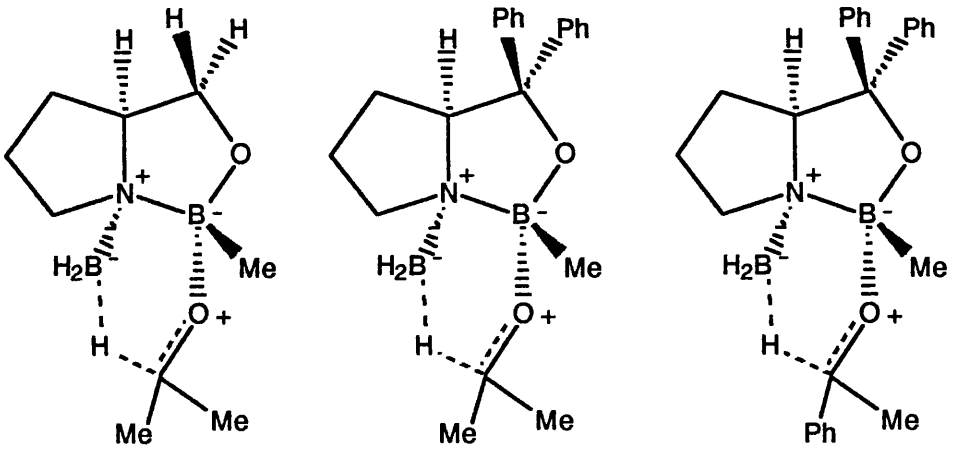

chi-6 **chi-7** **chi-8** both epimers

Figure 6-5

In all three TSs, specific interactions from solvent molecules were not included. The intermediate occurring after hydride transfer *via* the chair TS from **chi-6** and **chi-7** had a weak N-B_r interaction, 4.264Å and 1.810Å respectively, whereas an oxazadiboretane was formed directly from **chi-8**, in which the N-B_r bond was 1.583 Å. From this it was clear the diphenyl group prevented cleavage

of the N-B_r bond, probably due to a higher barrier for rotation about the O_r-$C(Ph_2)$ bond.

Buono[48] had commented that the OAB-borane adduct was in an equilibrium with a complex which was directly involved in the catalytic cycle. From this study, it could be postulated that the 'ring-opened' form, **oab-10c**, (figure 6-6) of the catalyst is in fact the species observed in Buono's NMR study.

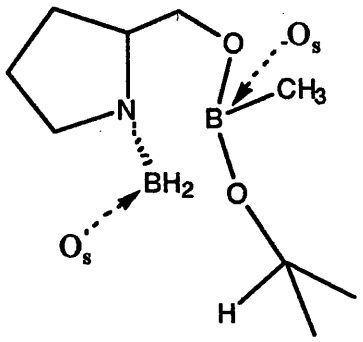

oab-10c
(see chapter 4-6)

Figure 6-6

In the 'ring-opened' form the oxygen O_r was found to be electron rich and could interact with borane-THF. This would place a hydride source in close proximity to B_r which was electron deficient and thus a possible binding site for Lewis-basic groups, such as carbonyl oxygen. The changes in energetics and important bond lengths for the binding of borane-THF, ketone binding and hydride transfer (figure 6-7) are summarised in table 6-8.

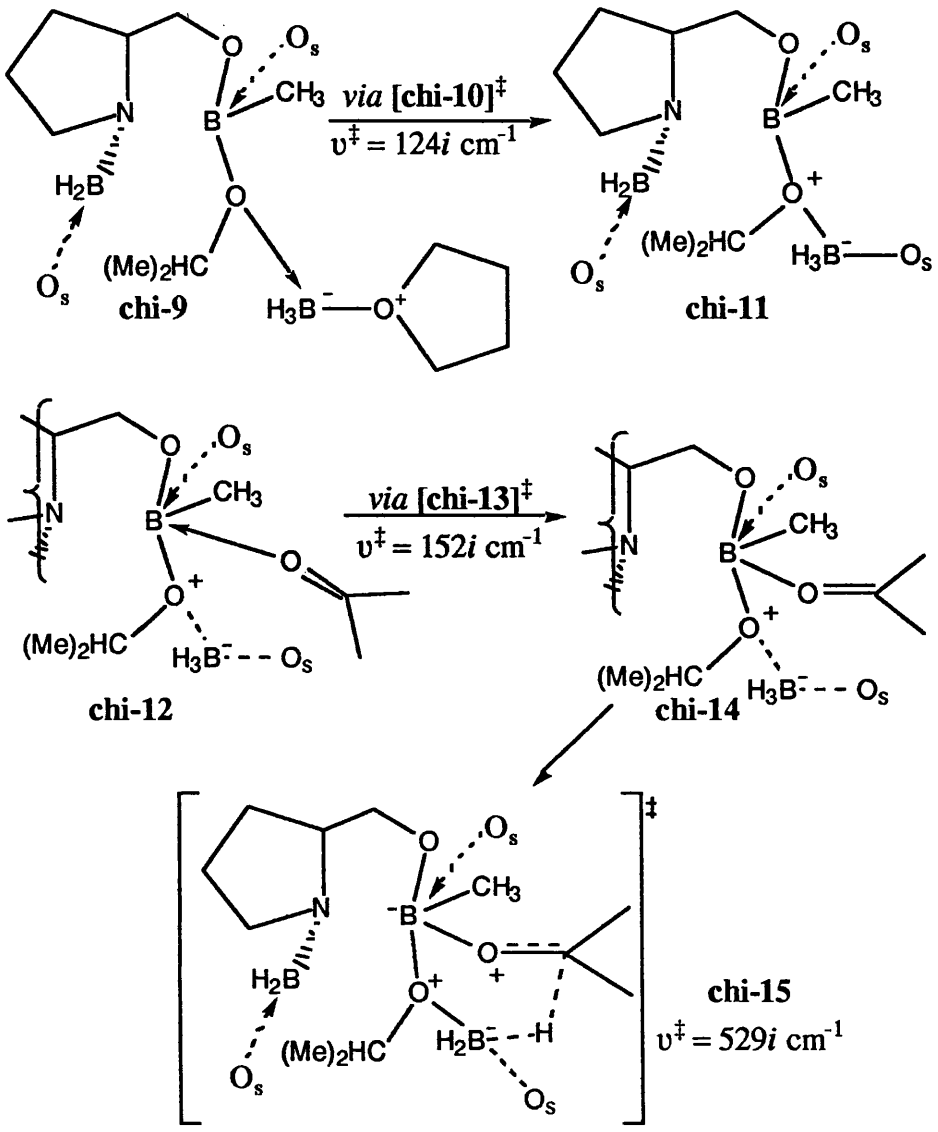

Figure 6-7

The ball-and-stick representation of **chi-15** is given on the next page.

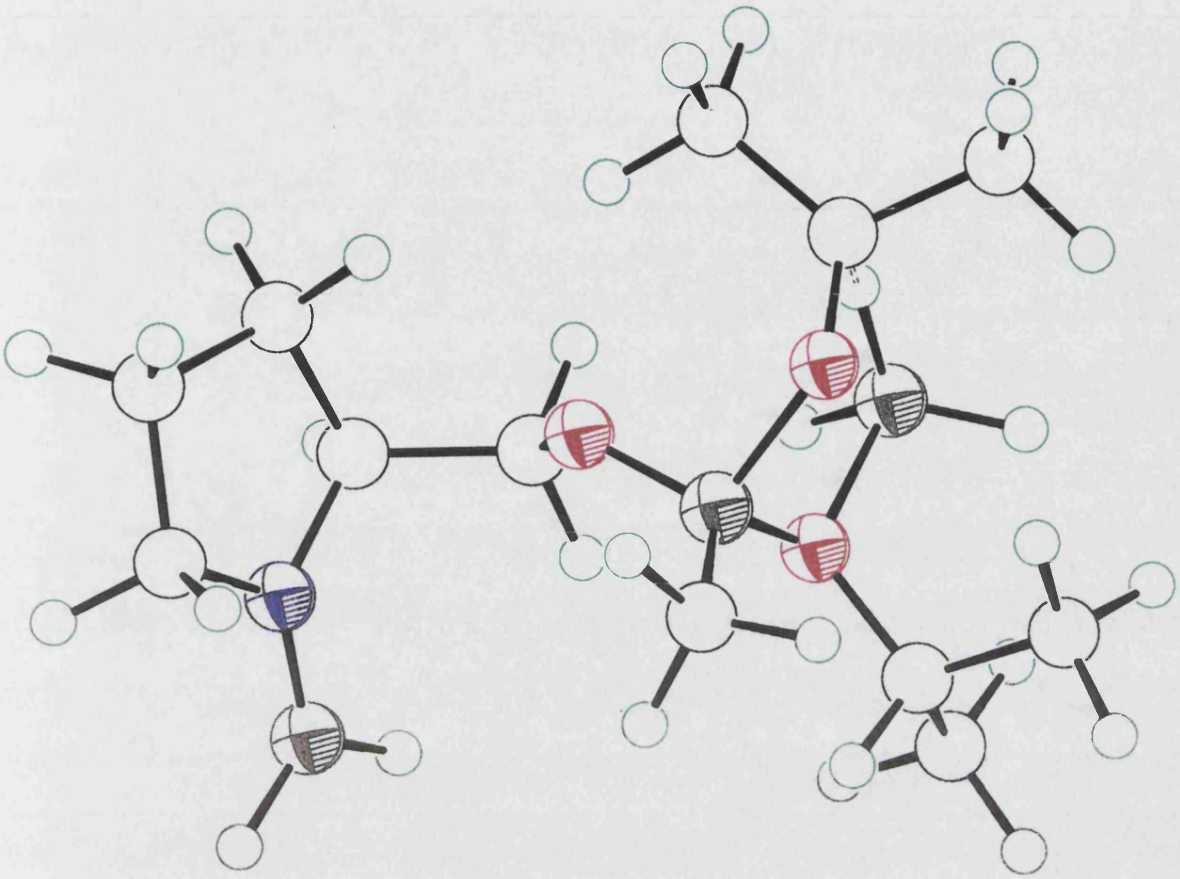

chi-15
THF molecules removed for clarity

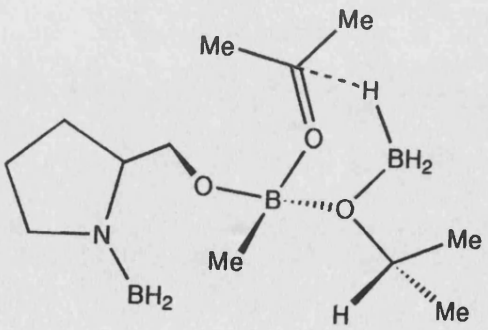

Table 6-8: The important energetic (kcal mol^{-1}) and structure (Å) changes the reduction of acetone bound to **oab-10c**

	chi-9	**chi-10**	**chi-11**	**chi-12**	**chi-13**	**chi-14**	**chi-15**
ΔH_f	-344.01	-337.66	-337.78	-389.22	-383.10	-386.25	-375.72
ΔH_{rel}[a]	-51.59	-45.24	-45.36	-47.79	-41.67	-44.82	-34.29
O_c-B_n	4.033	2.221	2.076	2.043	2.056	2.014	1.777
B_n-O_s	1.767	1.884	1.883	1.900	1.907	1.901	2.091
B_r-$O_{c(n)}$	-	-	-	3.976	2.276	1.901	1.669
$C_{c(n)}$-H_t	-	-	-	-	-	2.477	1.576
B_n-H_t	-	-	-	-	-	1.201	1.256

[a] Enthalpy relative to OAB [-89.69] + THF [-58.40] + 2 BH_3-THF [-95.32] + 2 MeCOMe [-98.02] = -341.43 kcal mol^{-1}

As in the OAB mechanism, long-range and short-range interactions were found between borane-THF and an electron rich donor atom, and between electron deficient boron, B_r and the carbonyl oxygen. Hydride transfer was rate limiting but **chi-15** was approximately 0.5 kcal mol^{-1} lower in energy than the TS (**oab-11c**) for formation of the oxazadiboretane. The barrier for the conversion of **chi-9** to **chi-15** was 6.47 kcal mol^{-1} lower than the barrier for the uncatalysed reduction.

The hydride transfer TS, **chi-15**, had more flexibility than either of the boat or chair hydride transfer TS. Therefore the e.e. by this mechanism would be lower.

At 25°C, the free energy of the **oab-11c**, the TS for the formation of the oxazadiboretane was 2.52 kcal mol^{-1} higher than **oab-10c.** The TS, **chi-10**, for the binding of borane-THF was only 0.01 kcal mol^{-1} higher in free energy.

At the optimum temperature of 110°C,[48] the formation of both TSs as predicted by the free energy to be favourable, -2.28 and -2.75 kcal mol^{-1} for **oab-11c** and **chi-10** respectively. This implied that the ratio of acetone that underwent

reduction *via* a less rigid TS compared to that on the more rigid OAB-borane adduct would be approximately 3:2, resulting in a lower e.e.

Buono found that increasing the percentage of the OAB from two to ten mole percent, whilst keeping the percentage of borane-THF at two mole percent, increased the e.e. to greater than 95%. As the different ratio would only affect the binding of the borane-THF, not the formation of the oxazadiboretane, the free energy was recalculated allowing for the different concentrations. The ratios were used in the calculation are shown in figure 6-8.

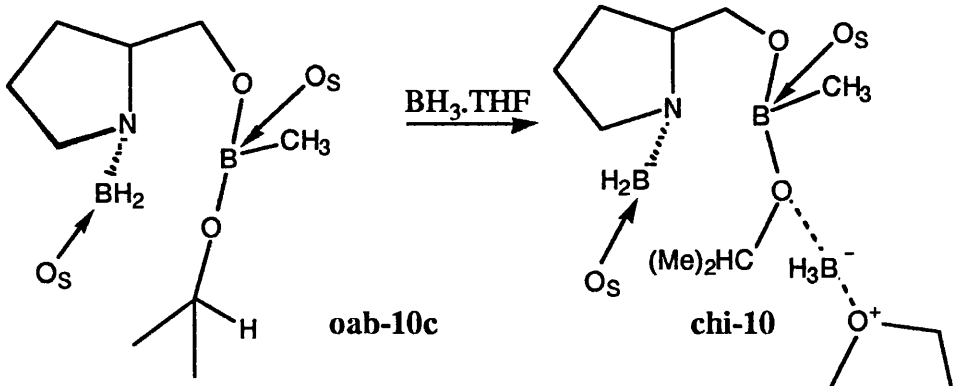

5 (oab-10c) + BH_3.THF ⟶ chi-10 + 4 (oab-10c)

Figure 6-8

The entropy for molecules of less than one molar can be calculated using equation **6-3**.

S at x molar = S (1 molar) - R ln (x) .....Equation **6-3**

where x is the new concentration and the R the ideal gas constant.

The concentration of BH_3-THF was 0.83 mmol and **oab-10c** was 4.15 mmol (assuming a hundred percent conversion of the OAB-borane adduct to **oab-10c**).[48] Table 6-9 shows the enthalpy, entropy at 1 molar, entropy at the appropriate and free energy for all four molecules.

Table 6-9: The thermodynamic data (ΔH & ΔG: kcal mol^{-1}, S = cal mol^{-1} K^{-1}) for the formation of **chi-10**

	ΔH_f	S (1molar)	S (*x* molar)	ΔG (383.15K)
oab-10c	-292.38	244.06	254.95	-390.06
BH_3-THF	-47.66	90.31	104.40	-87.66
chi-10	-337.66	294.55	308.64	-455.92

$$\therefore \Delta G = [\{-455.92 + (4 \times -390.06)\} - \{(5 \times -390.06) + -87.66\}]$$
$$= 21.77 \text{ kcal mol}^{-1}$$

Therefore, the TS for binding borane-THF required 21.77 kcal mol^{-1} at the higher OAB-borane adduct concentration. The reformation of the OAB did not require borane-THF, so the free energy difference of -2.28 kcal mol^{-1} would be unaffected by the concentrations change. This implied that this route would be energetically favoured over co-ordination of the borane. The removal of the competing pathway would result in the maximum e.e. being obtained and the true enantiocontrol of the catalyst observed.

6.3 Reduction of Other Ketones by **chi-2b** (R^1 = Ph, R^2 = Me)

With the insight provided by comparison of various OAB-borane adducts, the role of the substituents on the ketone was analysed.

6.3.1 The Reduction of Para-Substituted Acetophenones

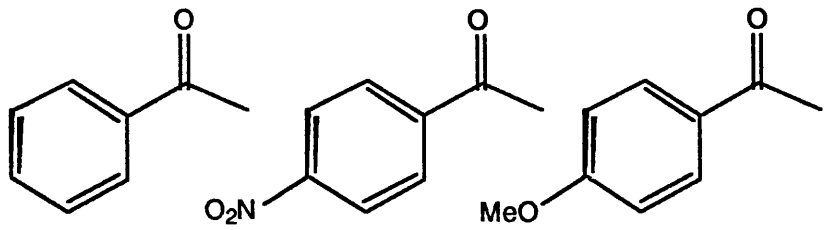

chi-16 **chi-17** **chi-18**

Figure 6-9

Mathre and co-workers[31] had noted that e.e. and rates were sensitive to alterations in the substituent at the *para* position on the aromatic ring of acetophenone. 'A slight decrease in enantioselectivity going from an electron-donating to an electron-withdrawing substituent' was attributed to increased steric interactions due to a more stable ternary ketone-oxazaborolidine-borane complex. In competition reactions, the relative rates for the reduction of acetophenone, 4'-nitro- and 4'-methoxyacetophenone were 1, 1.36 and 1.42 respectively.

Corey *et al.* [33] studied similar systems and concluded that the small rate difference was indicative that 'neither ketone-catalyst co-ordination nor hydride transfer were strictly rate limiting.' They stated that the relative rates for the binding step were anticipated to be *p*-OMe > *p*-H >*p*-NO_2 and the reverse for hydride transfer.

The binding TS of the ketone to the OAB-borane adduct, OAB-borane-ketone complex and hydride transfer TS were located for acetophenone, 4'-nitro- and 4'-methoxyacetophenone. The heats of formation and relative enthalpies are given in table 6-10.

Table 6-10: A summary of the energetic changes (kcal mol^{-1}) for the reduction of acetophenone and the *para*-substituted acetophenones

	ketone binding TS		OAB-BH_3-ketone		hydride transfer TS	
	ΔH_f	ΔH_{rel}[a]	ΔH_f	ΔH_{rel}[a]	ΔH_f	ΔH_{rel}[a]
p-H BS	-25.21	14.58[b]	-29.31	10.48	-24.88	14.91
p-H BR	-23.57	16.21[c]	-28.39	11.40	-20.48	19.30
p-H CS	-27.14	12.64[d]	-28.46	11.33	-24.90	14.89
p-H CR	-27.22	12.57[e]	-31.28	8.51	-26.79	12.99
p-NO_2 BS	-22.22	12.48[f]	-24.54	10.16	-20.08	14.62[g]
p-NO_2 BR	-20.39	14.31[h]	-25.08	9.62	-16.50	18.20[i]
p-NO_2 CS	-23.59	11.12[j]	-23.97	10.73	-20.41	14.29[k]
p-NO_2 CR	-22.94	11.77[l]	-25.85	8.86	-21.95	12.75[m]
p-OMe BS	-63.77	14.66[n]	-68.08	10.36	-63.67	14.77[o]
p-OMe BR	-63.54	14.89[p]	-66.87	11.57	-58.90	19.53[q]
p-OMe CS	-65.55	12.89[r]	-66.88	11.55	-63.35	15.08[s]
p-OMe CR	-65.71	12.72[t]	-70.13	8.31	-65.59	12.84[u]

[a] Enthalpy relative to OAB-borane adduct [-24.67] + appropriate ketone [PhCOMe = -15.12, *p*-NO_2 PhCOMe = -10.04, *p*-OMe PhCOMe = -53.77], [b] $\upsilon^{\ddagger}$=143*i* cm^{-1}, [c] $\upsilon^{\ddagger}$=143*i* cm^{-1}, [d] $\upsilon^{\ddagger}$=87*i* cm^{-1}, [e] $\upsilon^{\ddagger}$=99*i* cm^{-1}, [f] $\upsilon^{\ddagger}$=132*i* cm^{-1}, [g] $\upsilon^{\ddagger}$=441*i* cm^{-1}, [h] $\upsilon^{\ddagger}$=123*i* cm^{-1}, [i] $\upsilon^{\ddagger}$=495*i* cm^{-1}, [j] $\upsilon^{\ddagger}$=99*i* cm^{-1}, [k] $\upsilon^{\ddagger}$=432*i* cm^{-1}, [l] $\upsilon^{\ddagger}$=133*i* cm^{-1}, [m] $\upsilon^{\ddagger}$=430*i* cm^{-1}, [n] $\upsilon^{\ddagger}$=139*i* cm^{-1}, [o] $\upsilon^{\ddagger}$=441*i* cm^{-1}, [p] $\upsilon^{\ddagger}$=122*i* cm^{-1}, [q] $\upsilon^{\ddagger}$=463*i* cm^{-1}, [r] $\upsilon^{\ddagger}$=103*i* cm^{-1}, [s] $\upsilon^{\ddagger}$=430*i* cm^{-1}, [t] $\upsilon^{\ddagger}$=90*i* cm^{-1}, [c] $\upsilon^{\ddagger}$=437*i* cm^{-1}.

Competition reactions had been used by Mathre[31] to determine the relative reduction rates. As the 'chair R' conformer was the most stable epimer for all three ketones, the theoretical 'observed' rate constant of reduction of each ketone was calculated using equation **6-4**.

$$\text{observed rate constant} = \frac{(k_1 k_2)/k_{-1}}{1 + (k_2/k_{-1})} \quad \text{.....Equation 6-4}$$

where k_1 is rate constant for ketone co-ordination, k_{-1} is rate constant for dissociation of the OAB-borane-ketone complex and k_2 is rate constant for hydride transfer.

From this equation, the rates relative to the reduction of acetophenone, **chi-16**, were 1.38 and 1.61 at -20°C for **chi-17** and **chi-18.**

The relative rates calculated directly from the energy difference between the OAB-borane adduct plus ketone and the 'chair R' hydride transfer TS did not differ significantly for the result obtained from using equation **6-4.** This implied that the rate enhancement arose from differences in the hydride transfer TS, and not the prior step.

The value of 0.75 was obtained for Pauling bond order n for the B-H_t bond the 'chair R' TS for all three systems. This implied that the rate differences could not be attributed to the TS for the substituted systems occurring 'earlier' on the reaction profile.

To determine the origin of the rate enhancement, the 'chair R' hydride transfer TSs were 'broken' into the OAB and uncatalysed reduction components (figure 6-10). This provided insight into the stabilisation provided by the OAB to the 'distorted' uncatalysed reduction TS.

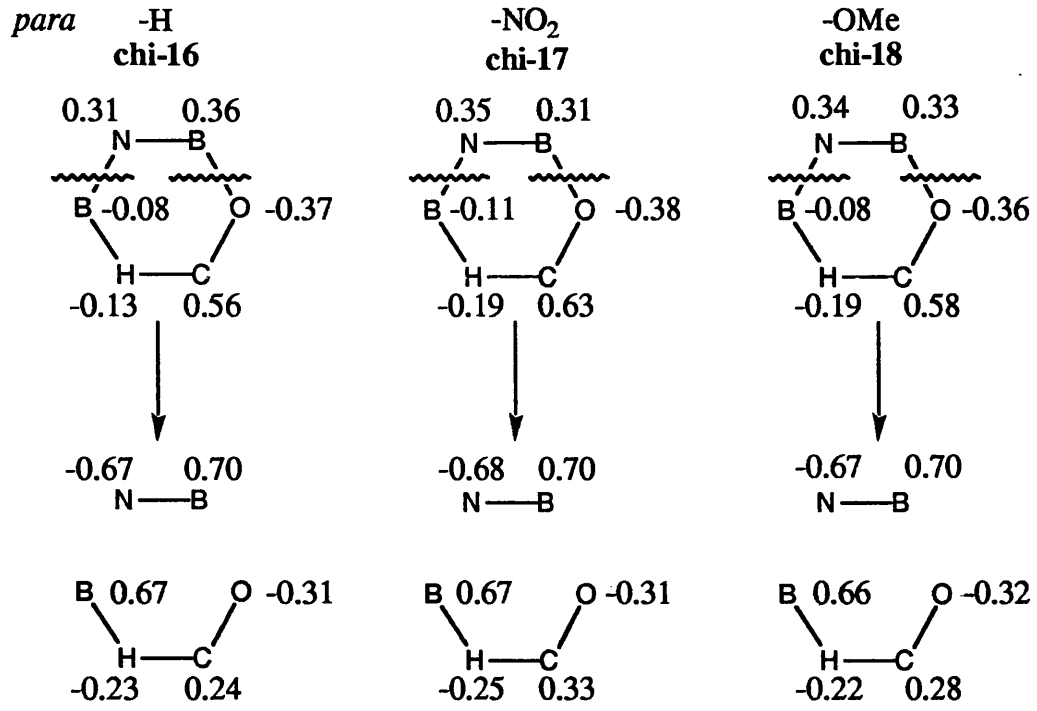

Figure 6-10

Analysis of the charge separation of the forming H_t-C_c bond revealed a larger difference for the substituted systems, 0.58 for **chi-17** and 0.50 for **chi-18**, compared with 0.47 for **chi-16**. Increased charge separation would result in a rate enhancement.

This analysis implied that the reduction of **chi-17** should occur faster than **chi-18**. Inspection of the enthalpic barrier for hydride transfer for the 4'-nitroacetophenone was actually lower than that for the electron donating system, which was not unexpected due to the more electrophilic-nature of the carbon centre. The free energy for the hydride transfer to 4'-methoxyacetophenone was lower than that of the electron-withdrawing system as a result of a larger entropic contribution. The enthalpy, entropy and free energy differences, relative to the OAB-borane adduct plus ketone, for the reduction of **chi-16**, **chi-17** and **chi-18** are shown in table 6-11.

Table 6-11: The thermodynamic data (-20°C) for the hydride transfer *via* the 'chair R' TS of **chi-16, chi-17** and **chi-18**, relative to the ketone plus OAB-borane adduct. (ΔH & ΔG: kcal mol^{-1}, S = cal mol^{-1} K^{-1})

	$\Delta H^{\ddagger}$	$\Delta S^{\ddagger}$	$\Delta G^{\ddagger}$
chi-16	12.99	12.05	9.94
chi-17	12.75	11.73	9.78
chi-18	12.84	12.40	9.70

The uncatalysed reduction of these ketones were also studied. The enthalpic barriers to hydride transfer were 3.69 kcal mol^{-1}, 4.52 kcal mol^{-1} and 3.67 kcal mol^{-1} for acetophenone, 4'-nitro and 4'-methoxyacetophenone respectively. The rates of reduction relative to acetophenone were 0.27 and 1.67 4'-nitro and 4'-methoxyacetophenone, respectively.

The trends in the rates reflected the trends in the barriers to hydride transfer, 19.20 kcal mol^{-1}, 20.07 kcal mol^{-1} and 19.10 kcal mol^{-1} for acetophenone, 4'-nitro and 4'-methoxyacetophenone respectively. The charge distribution in the uncatalysed TSs was studied (figure 6-11).

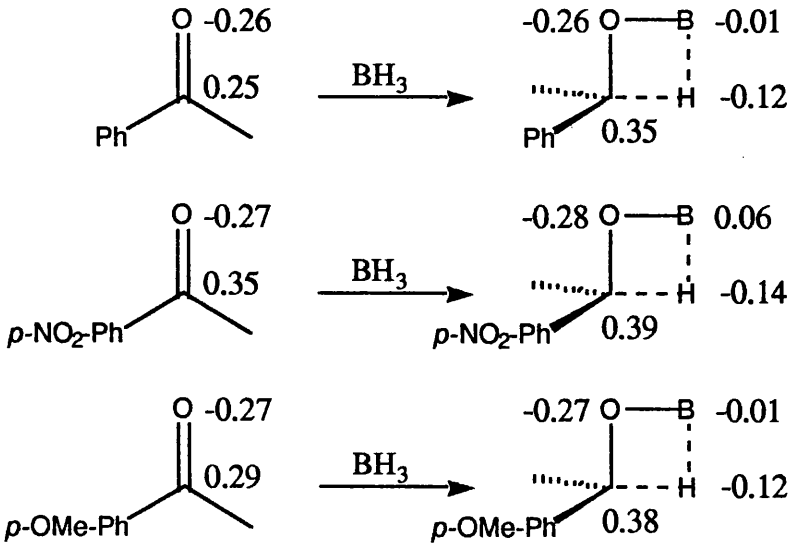

Figure 6-11

As with the catalysed reduction, the relative rate of reduction was dependant on the charge difference in the forming C-H bond: the larger the difference, the faster the reaction.

The e.e. were calculated for the catalysed reduction of these ketones. The relative enthalpy, free energy and populations at -20° C for all four epimers of the hydride transfer TS of each ketone are given in table 6-12.

Table 6-12: The relative energetics of the conformers (kcal mol^{-1}) adopted during the reduction of **chi-16, chi-17** and **chi-18**

	$\delta(\Delta H_f)$	$\delta(\Delta G_{253})$	population
chi-16			
BS	1.92	1.66	0.0333
BR	6.31	5.21	0.0000
CS	1.89	1.39	0.0570
CR	0.00	0.00	0.9097
At -20°C calculated e.e. = 81.9% (R) experimental 98.8% (R)			
chi-17			
BS	1.88	1.72	0.0286
BR	5.45	4.47	0.0001
CS	1.54	1.08	0.1022
CR	0.00	0.00	0.8691
At -20°C calculated e.e. = 73.8% (R) experimental 98.7% (R)			
chi-18			
BS	1.92	1.71	0.0313
BR	6.69	5.61	0.0000
CS	2.24	1.73	0.0303
CR	0.00	0.00	0.9384
At -20°C calculated e.e. = 87.7% (R) experimental 99.6% (R)			

The experimentally observed trends[33] between **chi-16, chi-17** and **chi-18** were also noticeable in the calculated e.e. The 'chair R' TS was the most stable epimer and e.e. was most sensitive to changes in the population of the 'chair S' conformer.

As the *para*-substituent was altered from electron-withdrawing through to electron-donating, the distance between boron B_r and the oxygen O_c of the carbonyl group decreased. The boron could not adopt a more pyramidal geometry to reduce the interaction between the boron-methyl and the ketone, as this would have resulted in an unfavourable interaction between the methyl group and the α-phenyl group on the 5-position. Therefore the energy of the 'chair S' TS increased as a result of the increased interaction between the aromatic ring of the ketone and the boron-methyl group, which thus increased the e.e.

6.3.2 The Reduction of Aliphatic Ketones

The reduction of aliphatic ketones OAB-borane adducts typically yields alcohols of low optical purity, for example the reduction of 2-heptanone by the CBS catalyst produces the (R)-alcohol in only 34% e.e. From this study, it was concluded that poor selectivity arose from the similarity of the size of a methyl group to a larger homologue, straight-chain alkane.

The only aliphatic ketones in which high induction was experimentally observed was in the reduction of *tert*-butyl methyl ketone and cyclohexyl methyl ketone (figure 6-12). When the reductions were performed at -10°C, the e.e. of the appropriate alcohol was 97.3% (R)[29] and 64% (R)[50] respectively.

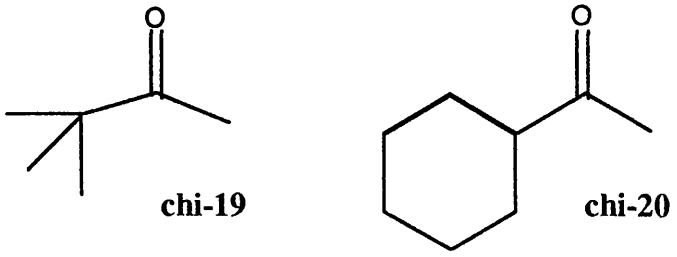

chi-19 **chi-20**

Figure 6-12

Table 6-13: The energetics of the hydride transfer TSs (kcal mol^{-1}) adopted during the reduction of **chi-19** and **chi-20**

	ΔH_f	$\delta(\Delta H_f)$	$\delta(\Delta G_{263})$	population	$\upsilon^{\ddagger}$ (cm^{-1})
chi-19					
boat S	-71.43	1.84	1.77	0.0330	447*i*
boat R	-62.19	11.09	11.75	0.0000	458*i*
chair S	-66.02	7.25	6.34	0.0000	452*i*
chair R	-73.27	0.00	0.00	0.9670	425*i*
enantiomeric excess at -10°C = 93.4% (R)					
chi-20					
boat S	-84.20	1.81	1.56	0.0370	426*i*
boat R	-83.04	2.97	3.03	0.0022	371*i*
chair S	-85.55	0.46	0.60	0.2318	435*i*
chair R	-86.01	0.00	0.00	0.7290	428*i*
enantiomeric excess at -10°C = 46.2% (R)					

In the reduction of *tert*-butyl methyl ketone, only the 'chair R' and 'boat S' TS had significant populations, an observation also made by Quallich *et al.*[52] in their *ab initio* study of OAB-borane adducts derived from ephedrine. The *endo* orientation of the bulky *tert*-butyl group made the 'boat R' TS energetically disfavoured, whilst the significant steric interaction between the bulky alkyl group and the boron-methyl substituent decreased the population of the 'chair S' conformer.

In the reduction of cyclohexyl methyl ketone, the proximity of the 5-β-phenyl group to the substituents of the ketone in both epimers of the boat conformation resulted in these conformers being higher energy than those in the chair conformer.

The chair epimers were of similar energy as the cyclohexyl group in the 'chair S' epimer adopted an orientation similar to that of the methyl group attached to 'chair R'. Consequently, the boron-methyl had a similar interaction with both epimer which explained the low e.e. The ball-and-stick representations of the chair conformers are shown on the next page.

6.4 The Reduction of Prochiral Ketones by OAB-Catecholborane Adducts

Corey *et al.* studied the reduction of α,α,α-trihalomethyl ketones by an OAB-catecholborane adduct.[33] They proposed that the rate constant for hydride transfer was increased in these ketones, 'even to the point that complexation is rate limiting'. The low value of the KIE for the reduction of α,α,α-trifluoroacetophenone by the adduct formed from a 1:1 mixture of ^{1}H- and ^{2}H-catecholborane was cited as supporting evidence, $k_H/k_D = 1.1$ at -78°C.

The catalyst employed by Corey had an *n*-butyl group as the boron substituent. This substituent adopts a conformation to minimise the interaction with the ketone, so it offers the same steric influence as a methyl group. Thus the OAB-catecholborane adduct, **chi-21**, was used for this study (figure 6-13). To assess any differences arising from a different hydride source, the reduction of acetophenone was studied in conjunction with the trihalomethyl ketones.

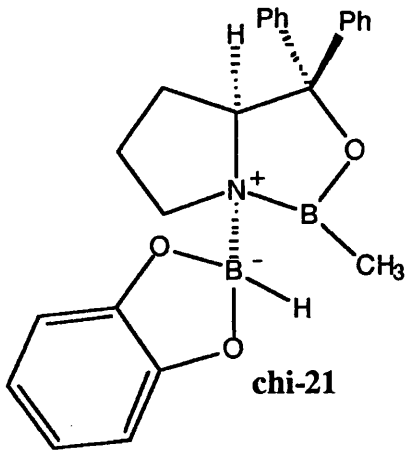

chi-21

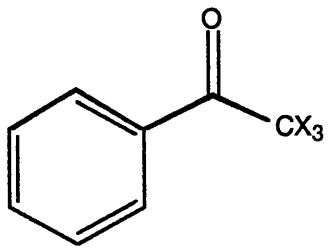

chi-22a: X=H
chi-22b: X=F
chi-22c: X=Cl
chi-22d: X=Br

Figure 6-13

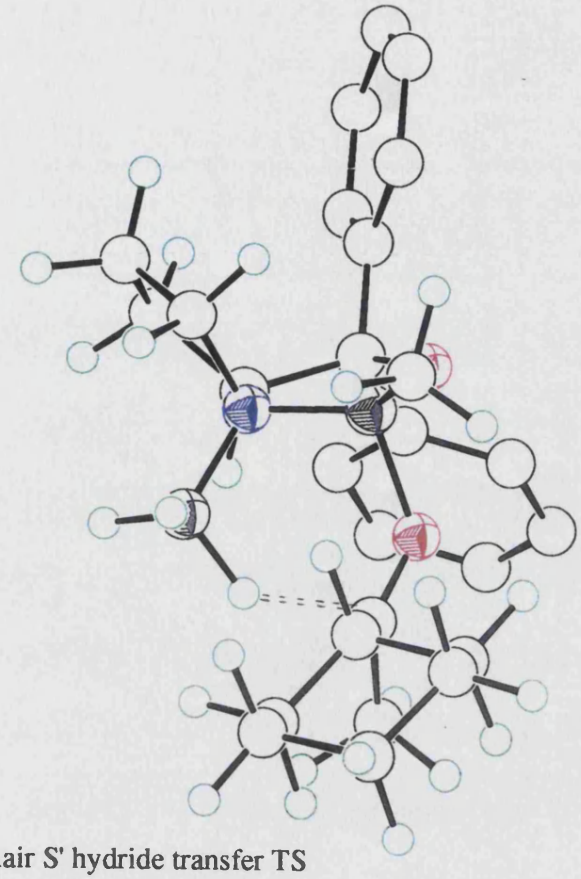

'Chair S' hydride transfer TS

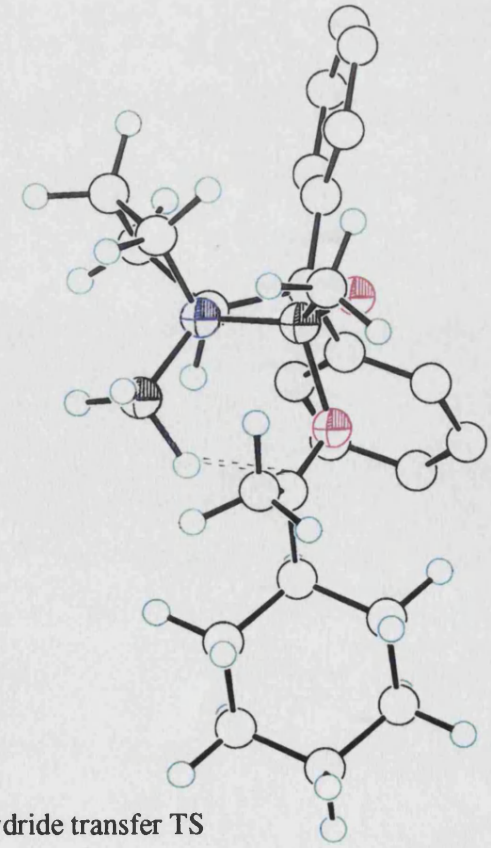

'Chair R' hydride transfer TS

6.4.1 The OAB-Catecholborane Adduct

Unlike the OAB-borane adduct, the OAB-catecholborane adduct did not contain a hydride bridge. Table **6-14** compares charge distribution of the catecholborane adduct **chi-21** with **chi-2b'**, the non-bridged version of **chi-2b** in which borane group was rotated about the N-B_x bond by 60° and one of the hydrogen's dihedral angle constrained to 180° (H-B_x-N-B_r).

Table 6-14: A comparison of the charge distribution in the OAB-borane and OAB-catecholborane adducts

	chi-21	**chi-2b'**
N	0.20	0.22
B_r	0.46	0.43
B_x	-0.16	-0.12
H	0.08	-0.14

The only significant difference was in the lack of electron density associated with the hydride of the OAB-catecholborane adduct. The electrophilic nature of the hydrogen attached to the catecholborane explained the lack of the hydride bridge. As the binding of the ketone to the OAB-borane adduct resulted in a redistribution of the electron density, it was possible that the hydride would be nucleophilic after the co-ordination of the ketone.

6.4.2 The Reduction of Acetophenone

Rather than locating the ternary ketone complex directly, the hydride transfer TSs were optimised and then an IRC calculation identified the neighbouring minimum. As with earlier studies, the 'chair R' TS was the lowest energy epimer, but a 'boat R' hydride transfer TS could not be located. The energetic differences of the three important epimers are given in table 6-15.

As the 'boat R' epimer had always been significantly higher in energy and the important borane substituent had not been altered, it was expected that the e.e. would not differ between the OAB-catecholborane or OAB-borane adducts.

Table 6-15: The important energetics (kcal mol^{-1}) for the conformers adopted during reduction of **chi-22a**

	ΔH_f	$\delta(\Delta H)$	$\delta(\Delta G_{296})$	population	$\upsilon^{\ddagger}$ (cm^{-1})
BS	-106.57	2.04	1.75	0.0438	413*i*
CS	-106.52	2.09	1.27	0.0993	417*i*
CR	-108.61	0.00	0.00	0.8569	444*i*
enantioselectivity at 23°C = 71.4% (R)					

As predicted the e.e. did not alter with the change in reducing agent, 71.4% compared with 68.9% for the OAB-borane adduct.

The change of hydride source had not significantly altered the relative energetics of the conformers, but the stability of the species during the elementary steps of ketone binding and hydride transfer differed significantly (table 6-16).

Table 6-16: The dependence of the stability (kcal mol^{-1}) of the species prior to and during the transfer on the nature of the hydride source

	chi-21[a]	**chi-2b**[b]	**chi-2b'**[c]
ketone binding TS	3.02	12.57	3.84
ternary ketone complex	0.49	8.51	-0.22
hydride transfer TS	14.40	12.99	4.27

[a] Enthalpy relative to OAB-catecholborane adduct [-107.89] + PhCOMe [-15.11] = -123.00 kcal mol^{-1}, [b] Enthalpy relative to OAB-borane adduct [-24.67] + PhCOMe = -39.78 kcal mol^{-1}, [c] Enthalpy relative to OAB-borane adduct without bridging interaction [-15.94] + PhCOMe = -31.05 kcal mol^{-1}.

The higher energies of the TS for ketone binding and of the ketone complex for **chi-2b** arose from the loss of the stabilising hydride bridge in OAB-borane adduct. Comparing the catecholborane with the non-bridged systems revealed a similar stability for the binding TS and the ternary complex.

The major difference between the systems, which could not be attributed to the loss of the hydride bridge, was the increased barrier to hydride transfer. The barrier for hydride transfer involving catecholborane was about 9.5 kcal mol^{-1} higher than that from borane.

The position of the hydride transfer TS along the reaction pathway was dependant on the hydride source. This difference was reflected the Pauling bond orders for the B_x-H_t bond of n = 0.62 for the 'chair R' hydride transfer TS with the OAB-catecholborane adduct **chi-21**, and n = 0.74 for the 'chair R' TS with the OAB-borane adduct **chi-2b** (or **chi-2b'** as the position of the hydride transfer TS along the reaction pathway was not dependant on the presence of a hydride bridge in the OAB-borane adduct).

The hydride transfer TSs were divided into the contributions from the OAB and a 'distorted' uncatalysed hydride transfer (figure 6-14).

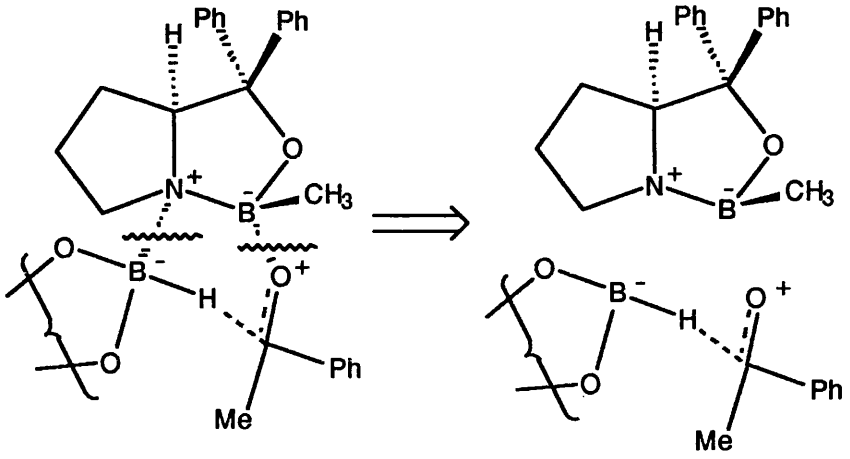

Figure 6-14

Analysis of the charge distribution (table 6-17) reflected the 'later' TS for **chi-21**. The carbonyl carbon C_c was less electron deficient whilst the hydride H_t was electron deficient.

Table 6-17: A comparison of the charge distribution in the hydride transfer TS fragments of **chi-21** and **chi-2b** (or **chi-2b'**)

	chi-21	**chi-2b**
q(N)	-0.67	-0.67
$q(B_r)$	0.71	0.70
$q(O_c)$	-0.30	-0.31
$q(C_c)$	0.13	0.24
$q(H_t)$	0.02	-0.23
$q(B_x)$	0.47	0.67

The difference in the position of the hydride transfer had to result from a lower driving force for the reaction. A study of the charge distribution in the ketone complexes, in which C-H_t was approximately 2.6 Å for both systems, revealed a lower electron density on the hydride in **chi-21** than in **chi-2**, 0.00 and -0.16 respectively.

6.4.3 The Reduction of Trihalomethyl Ketones

In the TSs for the reduction of acetophenone, the phenyl group was positioned in the *endo* position in the R epimers, and *exo* in the S. In the trihalomethyl systems, the phenyl group was in the *exo* position in the R epimer and *endo* in the S, as the $-CX_3$ group has the higher priority under the Cahn-Ingold-Prelog rules. As the most stable epimer had the phenyl group in the *endo* position, the $-CX_3$ group was effectively larger than the aromatic substituent.

The 'boat S' TS could not be located and the 'boat R' TS was not subjected to a full geometry optimisation because continued optimisation did not significantly lower the gradient and the structures obtained were significantly higher in energy than the chair epimers.

The pertinent thermodynamic data for the reduction of the trihalomethyl ketones is given in table 6-18.

Table 6-18: The important energetics (kcal mol^{-1}) for the conformers adopted during reduction of **chi-22b, chi-22c** and **chi-22d**

	ΔH_f	$\delta(\Delta H)$	$\delta(\Delta G)^a$	population	$\upsilon^{\ddagger}$ (cm^{-1})
chi-22b					
BR	-240.95[b]	7.33[b]	-	-	-
CS	-247.77	0.51	0.84	0.1027	419*i*
CR	-248.28	0.00	0.00	0.8973	418*i*
chi-22c					
BR	-96.22[b]	11.69[b]	-	-	-
CS	-105.67	2.24	2.17	0.0125	454*i*
CR	-107.91	0.00	0.00	0.9875	436*i*
chi-22d					
BR	-57.94[b]	12.73[b]	-	-	-
CS	-67.89	2.78	2.81	0.0035	473*i*
CR	-70.67	0.00	0.00	0.9965	459*i*

[a] ΔG at the experimental temperatures: **chi-22b** = -78°C, **chi-22c** & **chi-22d** = -23°C. [b] not subjected to full geometry optimisation

The barrier for hydride transfer *via* the 'chair R' conformer and the theoretical e.e. at the experimental temperature for acetophenone and the three trihalomethyl ketones are given in table 6-19. The e.e. were recalculated at 25°C to provide a comparison a constant temperature and a comparison with the reduction of acetophenone by OAB-borane adducts.

Table 6-19: A summary for the reduction of prochiral ketones by **chi-21**, an OAB-catecholborane adduct

	$\Delta H_{rel}(CR)^a$	e.e. (exptl. temp)	exptl. e.e.	e.e. (25°C)
chi-22a	14.40	71.4% (R)[b]	96% (R)	69.9% (R)
chi-22b	19.31	79.5% (R)[c]	90% (R)	70.2% (R)
chi-22c	19.24	97.5% (R)[d]	96% (R)	94.8% (R)
chi-22d	20.56	99.3% (R)[d]	98% (R)	98.3% (R)

[a] Enthalpy relative to **chi-21** [-107.89 kcal mol^{-1}] + the appropriate ketone [**chi-22a** = -15.12 **chi-22b** = -159.70 **chi-22c** = -19.26 **chi-22d** = 16.66]; [b] temperature = 23°C; [c] temperature = -78°C; [d] temperature = -23°C.

The e.e. increased with the increasing steric bulk of the methyl group, i.e. CBr_3 > CCl_3 > CF_3 > CH_3. The stability of both of the chair epimers decreased with increasing bulk, but the e.e. was linked to the decrease in stability of the 'chair S' as the changing substituent was in closer proximity to the boron-methyl group.

As the CX_3 group became more bulky, the orientation of the ketone altered to minimise the interaction between the boron-methyl group and the trihalomethyl group forcing the *endo* phenyl group of the ketone into a similar region of space as the β-phenyl group attached to the 5-position of the catalyst. Figure 6-15 and table 6-20 illustrate the important geometric changes.

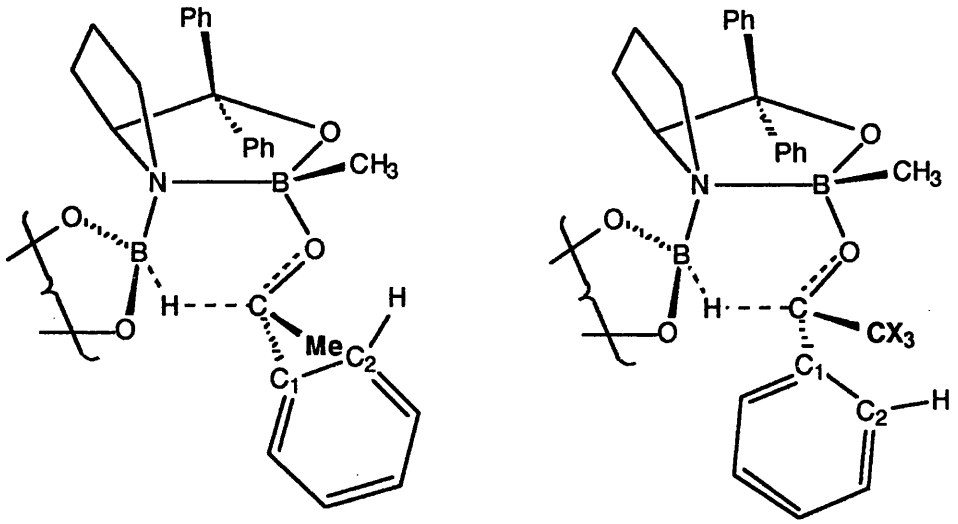

Phenyl group in *exo*-position
i.e. R epimer when acetophenone and S epimer for trihaloacetophenone

Figure 6-15

The ball-and-stick representation of the hydride transfer TSs are shown on the next page.

Table 6-20: A comparison of bond distances (Å) and dihedral angles (°) found in the chair epimers with the phenyl group in the *exo*-orientation

	chi-22a[a]	**chi-22b**[b]	**chi-22c**[b]	**chi-22d**[b]
B_r-O_c	1.640	1.799	1.774	1.752
C_c-O_c-B_x-N	-11	6	19	21
C_2-C_1-C_c-O_c	13	15	48	49

[a] R epimer, [b] S epimer

IRC calculations were performed on the 'chair S' TSs for trihalomethyl systems, and compared to the results from 'chair R' TS of **chi-22a** of the TS as the phenyl group attached to the ketone occupied the *endo* position in all systems.

Investigation of the intrinsic reaction co-ordinate from the trihalomethyl ketones did not locate the expected ternary complex, instead a complex with long range interactions between B_r-O_c and C_c-H_t.

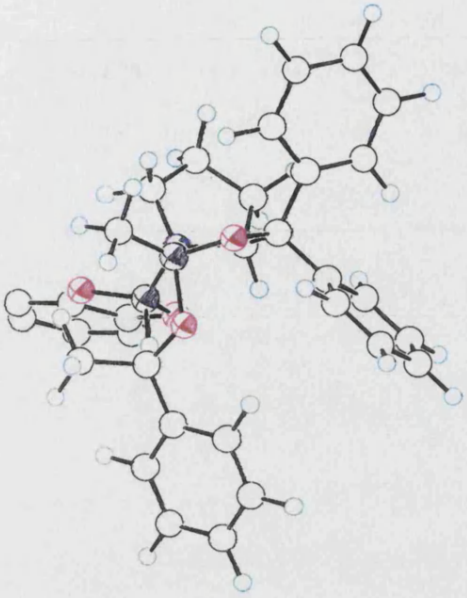

chi-22a
'Chair R' hydride transfer TS

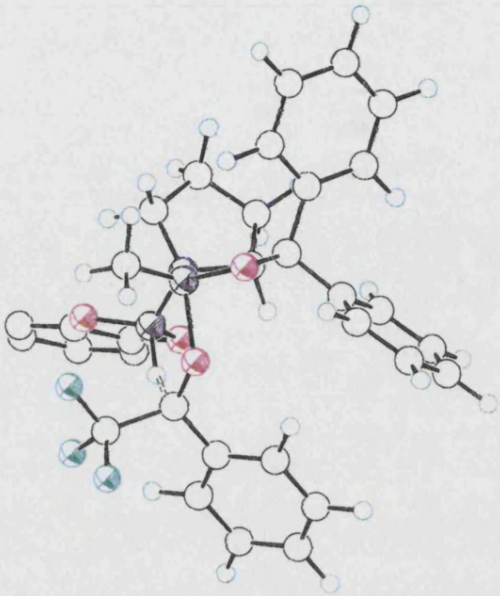

chi-22b
'Chair S' hydride transfer TS

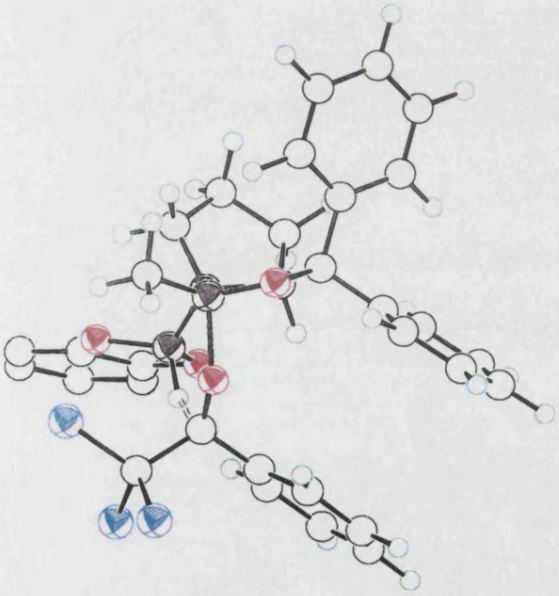

chi-22c
'Chair S' hydride transfer TS

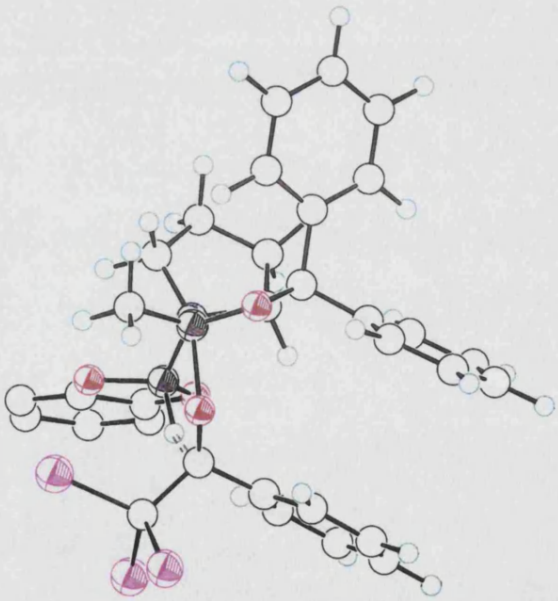

chi-22d
'Chair S' hydride transfer TS

These complexes were 19.06, 19.12 and 23.93 kcal mol^{-1} lower in energy than the S epimer hydride transfer TS for **chi-22b, chi-22c** and **chi-22d** respectively. Table 6-21 provides the heat of formation for these complexes and a comparison of the important geometrical features.

Table 6-21: The enthalpy (kcal mol^{-1}) and important bond distances (Å) in the complexes located by the reverse IRC

	chi-22b	**chi-22c**	**chi-22d**
ΔH_f	-266.84	-129.04	-91.82
ΔH_{rel} [a]	0.75	-1.89	-0.59
B_r-O_c	3.79	3.83	3.50
H_t-C_c	3.29	3.15	2.77

[a] Enthalpy relative to OAB-catecholborane adduct [-107.89] + appropriate ketone [$PhCOCF_3$ = -159.70, $PhCOCCl_3$ = -19.26, $PhCOCBr_3$ = 16.66]

The lack of ketone complex implied that either the presence of the trihalomethyl group had in some way altered the geometry or the nature of the ketone destabilised the ternary-ketone complex to the extent that it was no longer present. Table 6-22 compares the geometry and charge distribution of the ketones. The labelling scheme used in table 6-22 is shown in figure 6-16.

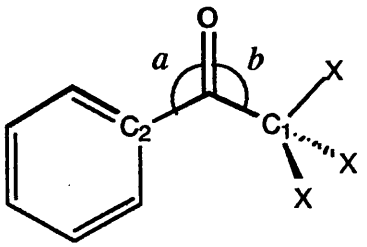

Figure 6-16

Table 6-22: The bond distances (Å), angles (°) and charge distribution of acetophenone and the trihalomethyl ketones

	chi-22a	chi-22b	chi-22c	chi-22d
C_c-C_1	1.496	1.572	1.540	1.528
C_c-C_2	1.479	1.465	1.476	1.480
a	121.5	124.9	122.5	122.2
b	121.0	117.0	120.1	121.2
$q(O_c)$	-0.26	-0.18	-0.30	-0.24
$q(C_c)$	0.25	0.24	0.95	1.02
$q(C_1)$	-0.44	0.07	-1.53	-2.05
$q(C_2)$	-0.02	-0.06	-0.45	-0.46

In acetophenone and trifluroacetophenone, both substituents of the ketone were coplanar with the carbonyl group and the molecules had C_{2v} symmetry. In the trichloro and tribromoacetophenone, both substituents were distorted out of the plane (figure 6-17).

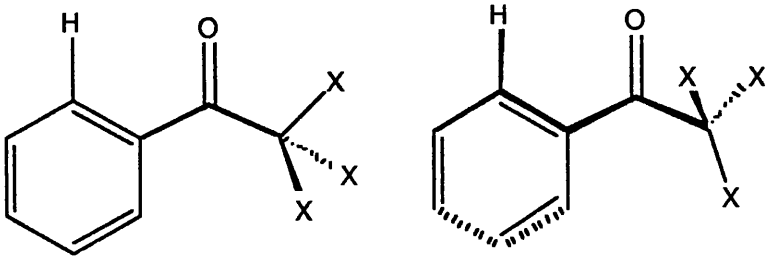

X = H or F X = Cl or Br

Figure 6-17

The absence of the ternary ketone complex for **chi-22b**, in contrast to acetophenone, can be attributed to the lower Lewis-basicity of the carbonyl oxygen. The differences in electron density at the carbonyl oxygen of **chi-22c** and **chi-22d** with respect to acetophenone, were smaller in magnitude. These differences could not explain the lack of the ketone complex.

Investigations by Corey *et al.* into the crystal structure of trihalomethyl ketones[53] revealed that the carbonyl oxygen was 'displaced significantly (typically about 9°) towards the trihalomethyl group'. He attributed this phenomenon a hyperconjugative interaction (figure 6-18).

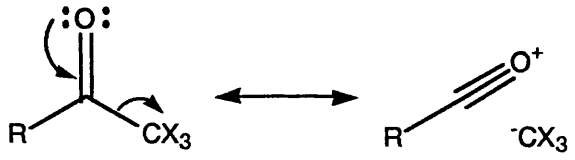

Figure 6-18

Both **chi-22c** and **chi-22d** (table 6-22) revealed an electronic perturbation in accordance with Corey's proposal which must disfavour the formation of the ternary complex.

From the findings of the IRC calculations, it was clear that Corey's assumption that the small KIE was linked to the ketone binding TS being rate determining was incorrect. The KIEs were calculated (table 6-23) at the same temperature at which the Corey had performed the reductions.

Table 6-23: The KIE for hydride transfer at the experimental temperature

	chi-22a	**chi-22b**	**chi-22c**	**chi-22d**
k_H/k_D	1.21 at 23°C	1.18 at -78°C	1.15 at -23°C	1.18 at -23°C

From these results it is evident that the reduction in k_H/k_D arose from the change of hydride source, rather than the presence of the trihalomethyl group. The equilibrium isotope effect was calculated between the OAB-catecholborane adduct plus acetophenone and the oxazadiboretane product and was found to be an inverse

effect, K_H/K_D = 0.80. This confirmed that the reduction of the primary KIE was due to a weak B-H bond being replaced by a stronger C-H bond.

6.5 The Origin of the Lower Selectivity of the Second Hydride Transfer

The experimental observation of a lower e.e. for the second hydride transfer can be addressed by the brief investigation performed in chapter 4.7.2. Even with acetone as a model of a prochiral ketone, it was noted that the hydride transfer TS was more stable than the TS for the formation of the OAB-alkoxyborane-ketone complex. This implied that the binding of the ketone was the rate determining step. The induction exerted by the boron-substituent would not be significantly different between epimers, due to the weaker interaction between the catalyst and the ketone, resulting in a lower e.e.

6.6 The Reduction in e.e. in the Presence of Water and Methylboronic Acid

Whilst Mathre *et al.* had noted that the addition of water or methylboronic acid adversely affected the levels of induction,[50] the only conclusion that was drawn was that the selectivity 'decayed' rather than that the catalyst was destroyed.

The additions of water and of methylboronic acid to the OAB-borane adduct were studied to see how these additives perturbed the structure. The approach of water was only considered from the concave face of the catalyst because co-ordination on the convex face would prevent the approach of the ketone to the catalyst.

Water formed a tightly bound complex with the OAB-borane adduct in which bridging by the borane hydrogen was replaced by an interaction with the lone pair on water (B_r-O_{water} = 1.847Å).

The barrier (figure 6-19) for the formation of the water-complex was 5.02 kcal mol^{-1} ($\upsilon^{\ddagger} = 407i\ cm^{-1}$) from OAB-borane adduct plus water.

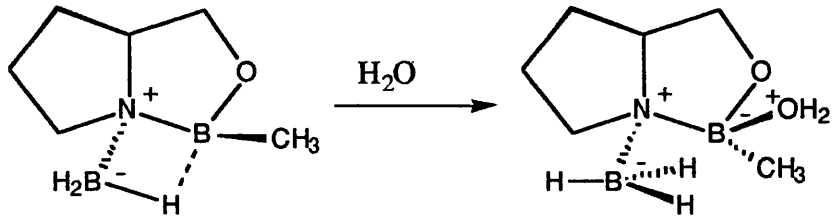

Figure 6-19

The barrier for the binding of water was 8 kcal mol^{-1} lower than the barrier for ketone binding to the OAB-borane adduct. The ball-and-stick representations of the water-bound complex and the ketone binding TS are shown on the next page.

From the tightly bound water complex, a 13.89 kcal mol^{-1} barrier existed ($\upsilon^{\ddagger}$ = 208*i* cm^{-1}) for the formation of the OAB-borane-ketone complex. The hydride transfer TS ($\upsilon^{\ddagger}$ = 433*i* cm^{-1}) was lower in energy than the ketone binding TS; the enthalpy difference was 1.32 kcal mol^{-1} and the free energy difference was 2.75 kcal mol^{-1}.

This change of rate determining step explained the reduction of e.e. as the boron substituent was too remote from the ketone to differentiate between the epimers. The energy difference between the 'chair R' and 'chair S' was 0.9 kcal mol^{-1} at the binding TS compared to 2.1 kcal mol^{-1} at hydride transfer.

Methylboronic acid was a weaker nucleophile than water, and did not form a tight complex with the OAB-borane adduct (B_r-O_{acid} = 3.900 Å).

The lowering of the e.e. resulted from the acid acting as a catalyst: the boron was electron deficient and the hydride source could be bound in close proximity to the ketone (figure 6-20). Table 6-24 summarises the important energetic and geometrical changes for this alternative reaction mechanism.

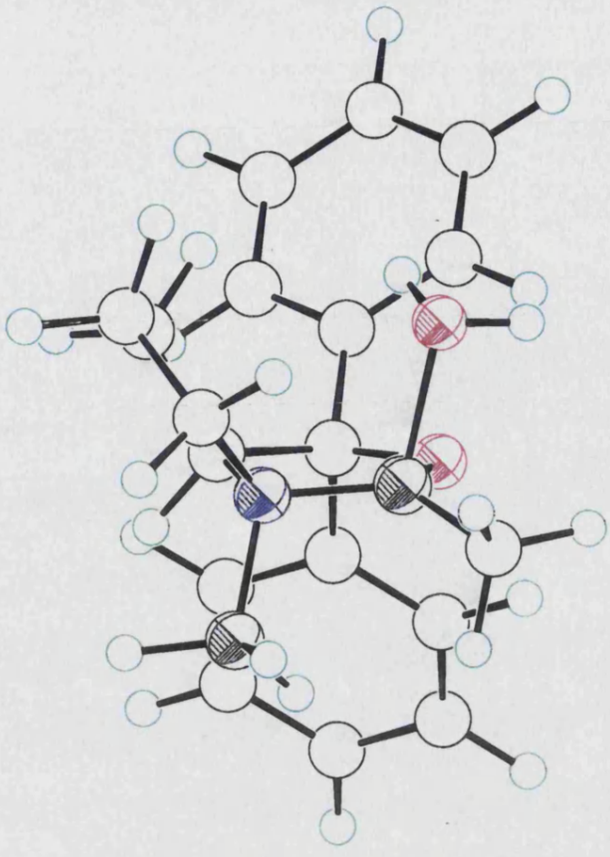

water-oxazaborolidine-borane adduct

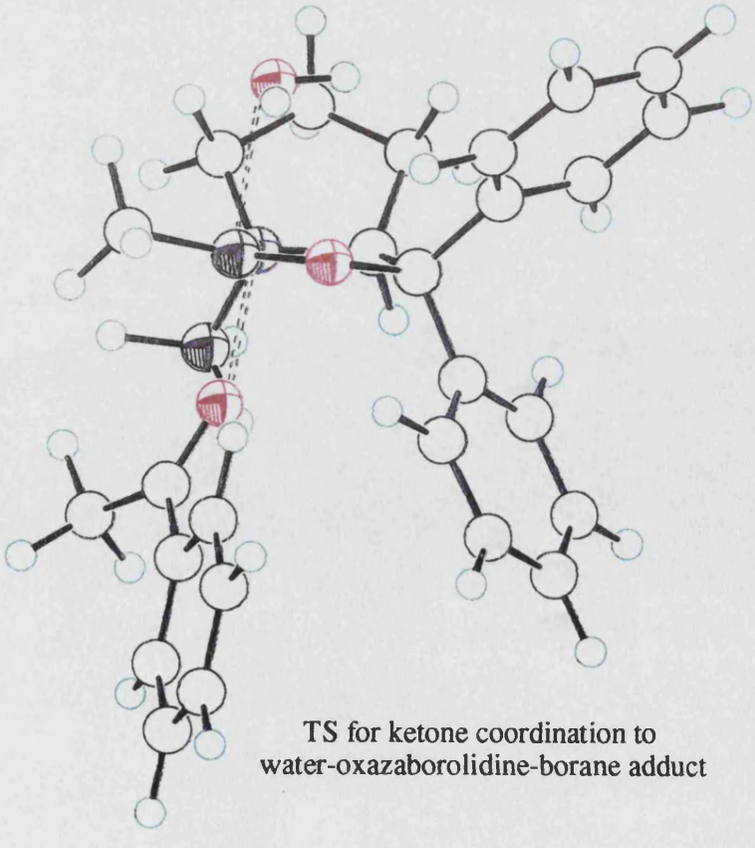

TS for ketone coordination to
water-oxazaborolidine-borane adduct

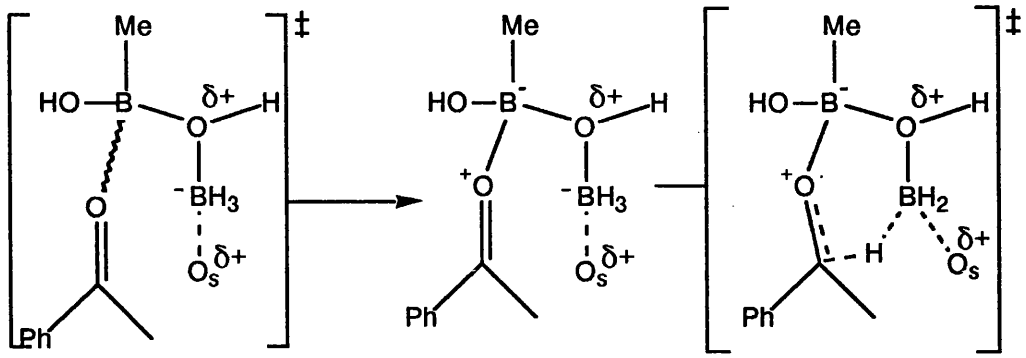

chi-23 chi-24 chi-25

Figure 6-20

The ball-and-stick representation of **chi-25** is shown on the next page.

Table 6-24: The important energetic (kcal mol^{-1}) and geometrical changes (Å) resulting from binding of acetophenone to a borane-methylboronic acid complex and the subsequent hydride transfer

	chi-23	chi-24	chi-25
ΔH_f	-183.49[b]	-187.26	-181.82[c]
ΔH_{rel}[a]	2.63	-1.14	4.30
O_{acid}-B	1.735	1.701	1.569
B_{acid}-O_c	2.387	1.859	1.692
C_c-H_t	-	2.532	1.671
B-H	1.201	1.203	1.252

[a] Enthalpy relative to acid-borane adduct [-171.01] + PhCOMe [-15.11] = -186.12 kcal mol^{-1}, [b] $\upsilon^{\ddagger} = 110i\ cm^{-1}$, [c] $\upsilon^{\ddagger} = 497i\ cm^{-1}$

This complex was catalytic, with the barrier to hydride transfer being lower than for the uncatalysed or OAB-catalysed reaction, 4.30 kcal mol^{-1} *versus* 19.20 kcal mol^{-1} and 12.99 kcal mol^{-1} (table 6-10 'chair R' TS) for the uncatalysed and catalysed reductions, respectively.

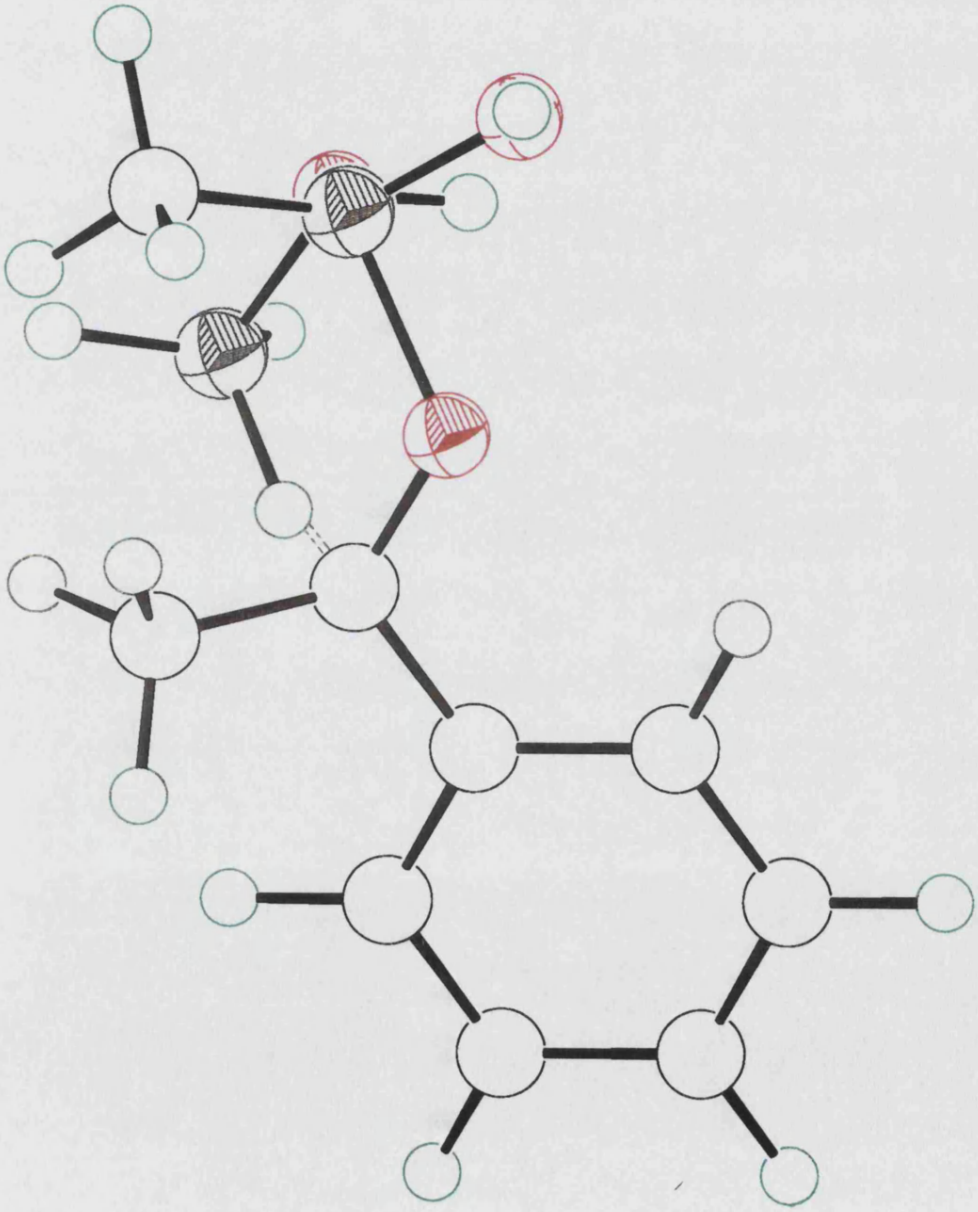

chi-25

Hydride transfer from methylboronic acid / borane adduct

The induction from the boron-methylboronic acid adduct would be lower due to the lack of rigidity in the TS. Therefore, the high degree of control exerted by the OAB-borane would be masked by the product from this less rigid system, resulting in a lower e.e. for the reduction of prochiral ketones by OAB-borane adducts with added methylboronic acid.

6.7 Comparison with Other Theoretical MO Investigations

At a quick glance, the MNDO hamiltonian as applied by Liotta and co-workers[51] appears to be more 'successful'. The theoretical enantiomeric excesses quoted were in excellent agreement with the experimental observations, for example the e.e. obtained for reduction of acetophenone by **chi-2b** was 93% compared to the experimental 96.5%. Their assumption that the e.e. could be derived from the rate constants for the conversion of the ternary OAB-borane-ketone to the hydride transfer TS contravenes the Curtin-Hammett principle.

If the MNDO hamiltonian is used together with a correct treatment of the kinetics, the results obtained are not as impressive. The predicted e.e. for the reduction of acetophenone by **chi-1b** (OAB derived from (S)-prolinol, with B-Me group) was only 16%, compared with the 42% found by their approach. The AM1 hamiltonian predicted the e.e. to 69% for the same catalyst.

Only a qualitative comparison of the *ab initio* results of Quallich and co-workers[52] and the results discussed here can be drawn due to the different OAB-catalyst model. Contrasting the only common ketone, namely *tert*-butyl methyl ketone, the theoretical e.e. was in close agreement with the experimental e.e in both studies. It must be noted that e.e. in the *ab initio* study were only calculated at the 3-21G level, probably due to the inherent problems of finding TSs using the Gaussian program. Close inspection of the relative enthalpies finds that the 2.18 kcal mol^{-1} energy difference, in favour of the *endo* TS, observed at the 3-21G level

was altered to 1.02 kcal mol^{-1} in favour of the *exo* TS, when single point MP2/6-31G*//6-31G* was performed!

Whilst the AM1 hamiltonian was not always accurate in predicting the exact magnitude of the stereocontrol, it did at least predict the correct enantiomer and experimental trends were reproduced albeit with more significant differences. All known KIE values were successfully reproduced and insight into their origin provided.

Unlike the conclusions of previous work by other authors, this study does not imply that the diphenyl groups attached to the 5-position are the most important substituent for imparting induction. In fact, when the substituent attached to boron was hydrogen or methyl, the predicted e.e. was greater when the substituents at the 5-position were hydrogen rather than phenyl groups.

With the insight gained from the analysis of the mechanism, namely that a successful catalyst has an electron deficient binding site in close proximity to a hydride source with increased nucleophilicity, and study of the origins of stereocontrol, in which the role of the boron substituent was highlighted, the challenge of predicting e.e. for systems prior to the experimental work and the design of improved catalysts was the next focus of this work.

Chapter 7: Theoretical Calculations on the Reduction of Prochiral Ketones Performed Prior to Experiment

In previous chapters, the experimental work had been published prior to the computational studies, the results of the studies implying that the AM1 hamiltonian provided a suitable method for studying the reduction of prochiral ketones by OAB-borane adducts. In this section the work described was of a predictive nature, with the studies being completed in advance of the experimental work.

7.1 The Reduction of Exocyclic Enones

Previous enantioselective reductions of exocyclic enones have used baker's yeast[54] or lithium aluminium hydride in the presence of N-methylephedrine and 2-(ethylamino)pyridine.[55] No attempts to use OAB-borane adducts had been reported prior to this study. The theoretical e.e.s were calculated in advance of the experimental work, the work being carried out by Professor Tim Gallagher's group at the University of Bristol.

The borane adduct used to study the reduction of the exocyclic enones was **chi-2b** (figure 7-1).

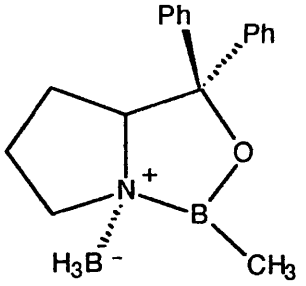

chi-2b
See chapter 6.2

Figure 7-1

Nine exocyclic enones were selected (figure 7-2), four based on cyclohexanone and six on cyclopentanone. For both ring sizes, the E- and Z-geometries of the exocyclic double bond were considered, with two substituents.

For the cyclopentanone system, a cyclopentyl group was attached to the terminus of the double bond.

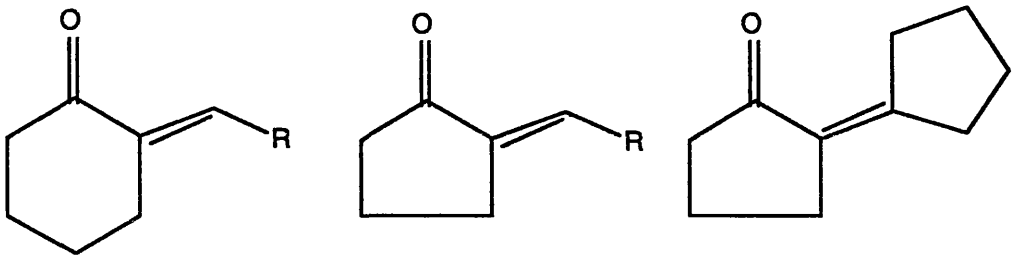

R = Me or Ph
E and Z-geometries about the double bond

only one double bond isomer

Figure 7-2

7.1.1 The Reduction of Substituted Cyclohexanones

Table 7-1 summarises the important energetics and relative populations of all the hydride transfer TS found for the reduction of **new-1** to **new-4** (figure 7-3).

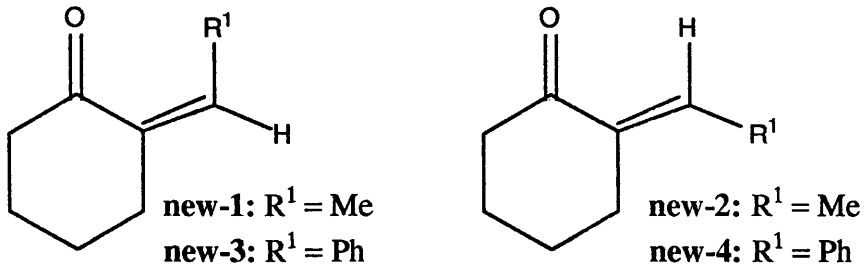

new-1: R^1 = Me
new-3: R^1 = Ph

new-2: R^1 = Me
new-4: R^1 = Ph

Figure 7-3

Table 7-1: The energetics for reduction of **new-1, new-2, new-3** and **new-4** (kcal mol^{-1})

	ΔH_f	$\delta(\Delta H)$	$\delta(\Delta G_{273})$	population	$\upsilon^{\ddagger}$ (cm^{-1})
new-1					
BS	-55.15	3.73	3.39	0.0032	399*i*
BR	-47.11	11.77	11.16	0.0000	272*i* & 39*i*
CS	-55.51	3.37	2.87	0.0075	411*i*
CR	-58.59	0.00	0.00	0.9893	446*i*
new-2					
BS	-56.73	3.51	3.35	0.0032	448*i*
BR	-50.77	9.47	8.95	0.0000	300*i*
CS	-57.63	2.61	2.52	0.0136	398*i*
CR	-60.24	0.00	0.00	0.9832	434*i*
new-3					
BS	-19.27	1.89	1.14	0.0758	468*i*
BR	-11.51	9.65	9.17	0.0000	241*i* & 32*i*
CS	-19.76	1.40	0.16	0.3990	453*i*
CR	-21.16	0.00	0.00	0.5252	430*i*
new-4					
BS	-23.64	2.22	3.36	0.0032	445*i*
BR	-15.69	11.28	10.77	0.0000	356*i*
CS	-24.23	2.74	2.38	0.0170	399*i*
CR	-26.97	0.00	0.00	0.9798	430*i*

The small, extra imaginary frequencies calculated for 'boat R' TS of **new-1** and **new-3** were not removed as the 'boat R' TS was considerably higher in energy than the other configurations. The removal of the small frequency would not have significantly altered the energetics.

Table 7-2 shows the calculated e.e. for reduction of the ketones and the barrier to hydride transfer *via* the most populated conformers.

Table 7-2: A comparison of the reduction of substituted cyclohexanones

	$\Delta H_{rel}(BS)^a$	$\Delta H_{rel}(CS)^a$	$\Delta H_{rel}(CR)^a$	e.e at 0°C
new-1	16.80	16.43	13.06	97.9% (R)
new-2	15.56	14.66	12.05	96.6% (R)
new-3	18.56	18.07	16.67	5.0% (R)
new-4	15.28	14.82	11.95	96.0% (R)

[a] Enthalpy relative to OAB-borane adduct [-24.70] + appropriate ketone [**new-1** = -47.27, **new-2** = -47.62, **new-3** = -13.16, **new-4** = -14.25 kcal mol^{-1}]

For all four ketones, the chair conformers were lower in energy than the comparable boat epimer.

The relative populations of the TSs (table 7-1) and therefore the e.e. (table 7-2) did not differ significantly between the Z- and E-methylidenecyclohexanone, **new-1** and **new-2**, and E-phenylidenecyclohexanone, **new-4**. The small differences in e.e resulted from small changes in population of the 'chair S' TS. This implied that the steric demands of the double-bond substituent closest to the boron-methyl group did not differ significantly between the three ketones.

The population of the 'boat S' TS was the same for all three ketones, only 0.0032. The low value was indicative of the unfavourable interaction between the unsubstituted edge of the enone and the β-phenyl group attached to the 5-position of the catalyst. When this epimer adopted the chair conformation, the orientation changed such that the enone was further away from the β-phenyl group but in closer proximity the boron-methyl. The differences between the interactions of the cyclohexanone ring with the β-5-Ph group are illustrated in figure 7-4.

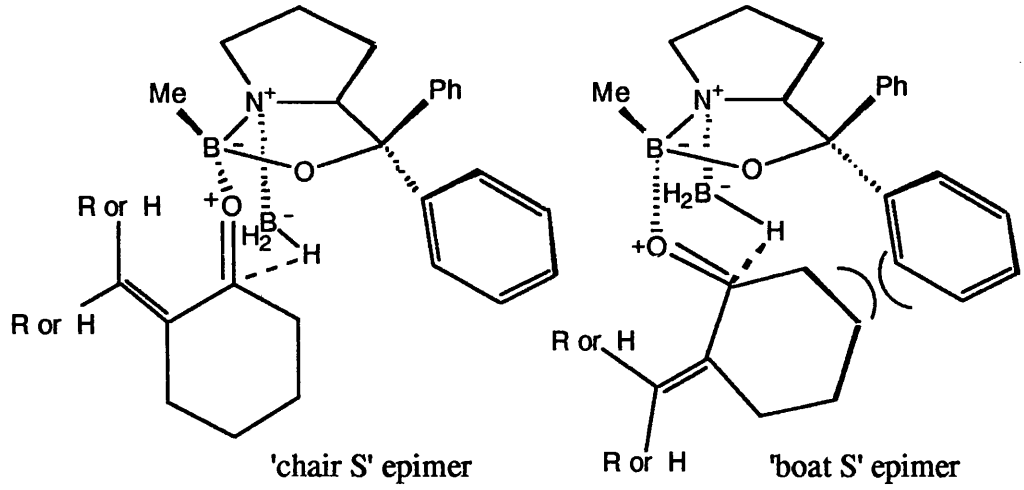

Figure 7-4

A significant decrease in stereocontrol was observed between **new-1** (97.9%) and **new-3** (5.0%), the methyl and phenyl substituted Z-double bond. The lower selectivity of **new-3** was a result of the higher energy of the 'chair R' TS. The energy increased due to the unfavourable interaction between the phenyl substituent of the double-bond and the β-phenyl group attached to the 5-position of the catalyst. Figure 7-5 highlights the close proximity of the substituents.

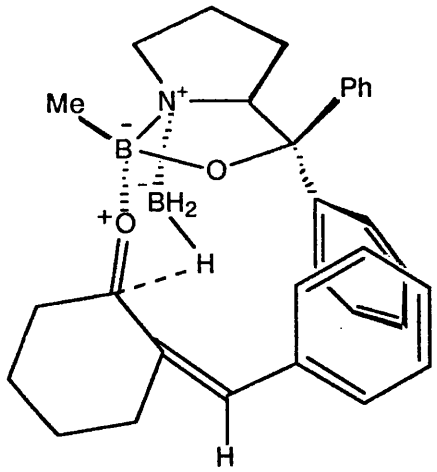

Figure 7-5

The ball-and-stick representations of the 'chair R' TSs of **new-1** and **new-3** are shown on the next page.

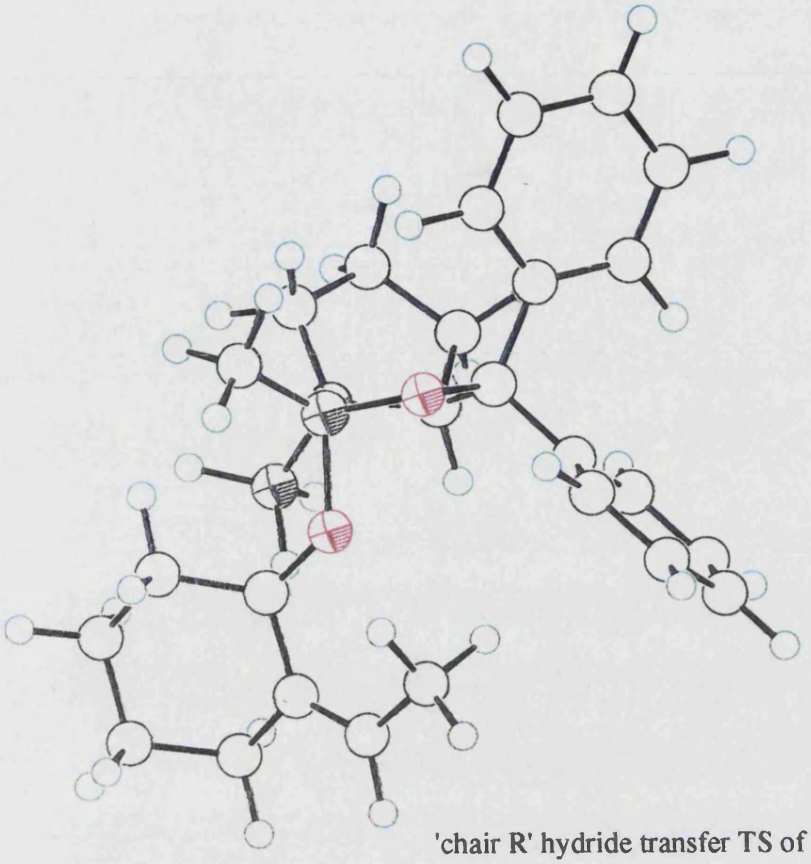

'chair R' hydride transfer TS of **new-1**

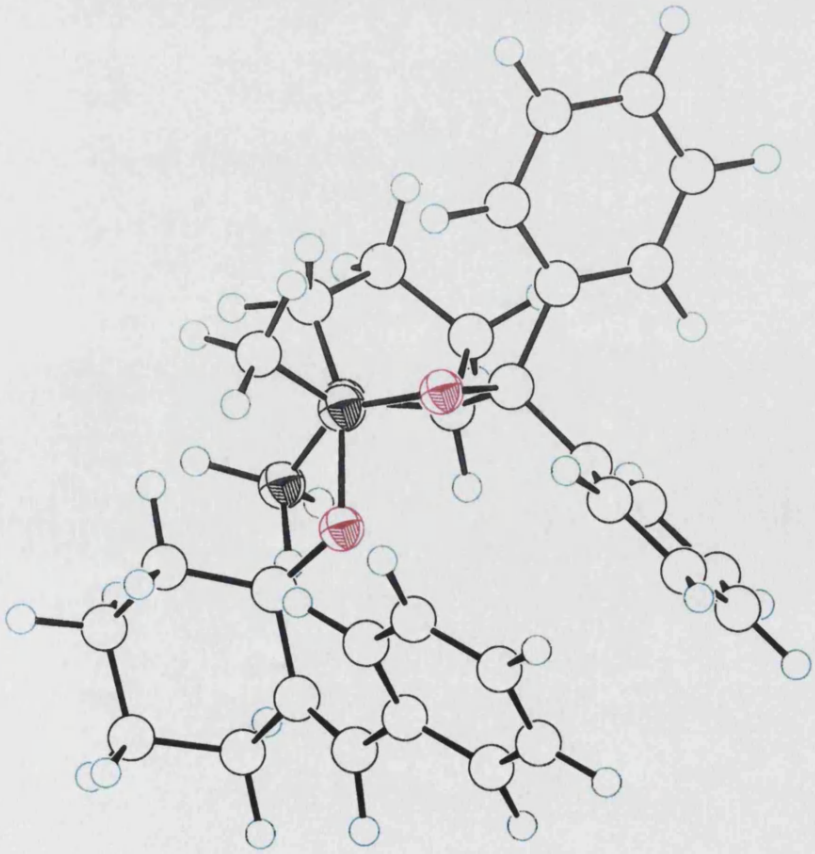

'chair' hydride transfer TS of **new-3**

The energetically less favoured 'chair R' TS, coupled with a large entropic differences (table 7-1) between this TS and the two S TSs, resulted in very low calculated e.e. (5.0 %).

The axial approach of a nucleophile to unsubstituted cyclohexanones is the preferred mode of attack, although whether this is due to steric or electronic effects is still subject to much debate.[56]

The approach of the hydride was from the axial position for the chair TSs. For the 'boat S' TSs, equatorial attack occurred except in **new-3** where the conformation of the cyclohexanone ring puckered to a twist-boat allowing axial attack. Ball-and-stick representations of the 'boat S' conformers of **new-1** and **new-3** are shown on the next page.

7.1.2 Reduction of Exo-Substituted Cyclopentanones

Table 7-3 summarises the important energetic changes and relative populations for all the hydride transfer TS located for the reduction of **new-5** to **new-9**, (figure 7-6).

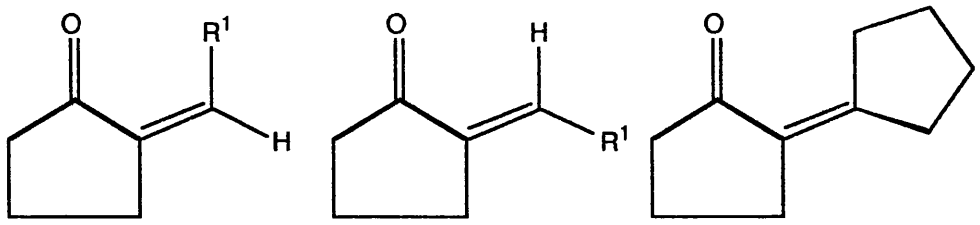

new-5: R^1 = Me **new-6:** R^1 = Me **new-9**

new-7: R^1 = Ph **new-8:** R^1 = Ph

Figure 7-6

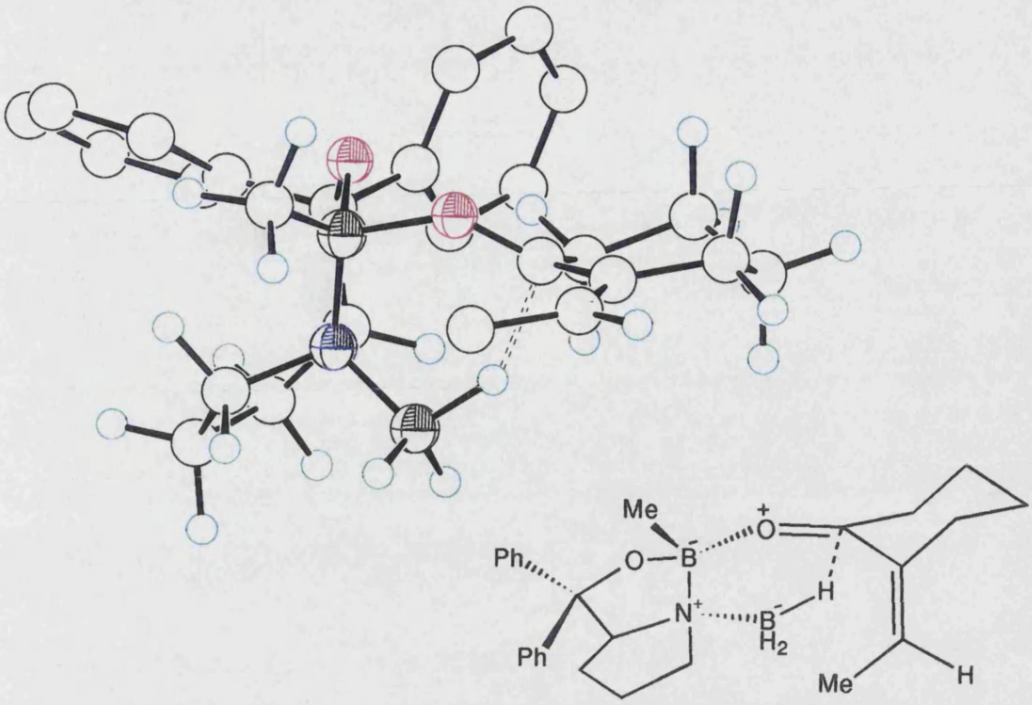

'boat S' hydride transfer TS of **new-1**
equatorial approach of the hydride

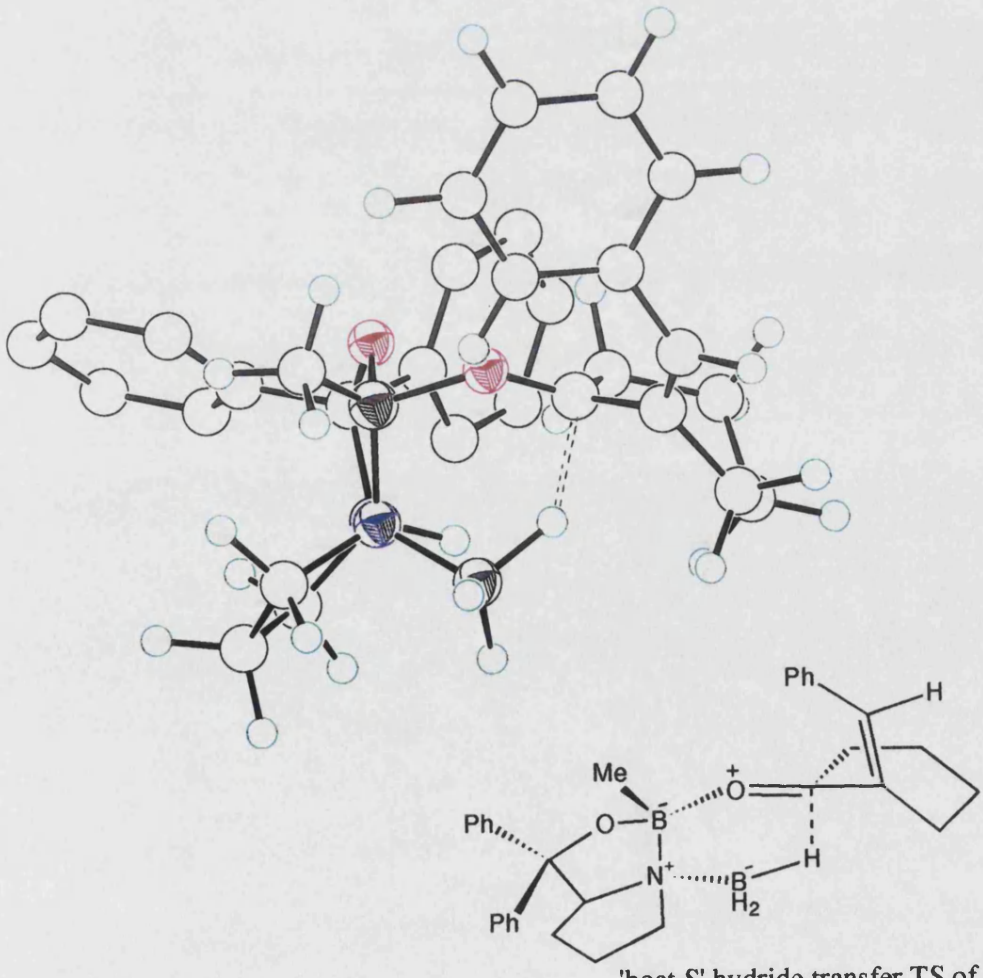

'boat S' hydride transfer TS of **new-3**
axial approach of the hydride

Table 7-3: The energetics for the reduction of **new-5, new-6, new-7, new-8** and **new-9** (kcal mol^{-1})

	ΔH_f	$\delta(\Delta H)$	$\delta(\Delta G_{273})$	population	$\upsilon^{\ddagger}$ (cm^{-1})
new-5					
BS	-50.08	1.00	0.95	0.1650	437*i*
BR	-40.68	10.40	11.49	0.0000	516*i*
CS	-42.70	8.38	8.26	0.0000	428*i*
CR	-51.08	0.00	0.00	0.8350	487*i*
new-6					
BS	-50.81	1.94	1.80	0.0448	435*i*
BR	-45.61	7.13	7.80	0.0000	458*i*
CS	-49.20	3.54	3.23	0.0039	432*i*
CR	-52.75	0.00	0.00	0.9513	458*i*
new-7					
BS	-13.63	0.00	0.00	0.9986	420*i*
BR	-2.83	10.80	11.86	0.0000	535*i*
CS	-8.50	5.13	4.88	0.0002	448*i*
CR	-11.25	2.38	3.95	0.0012	498*i*
new-8					
BS	-17.11	2.03	1.55	0.0664	428*i*
BR	-11.18	7.96	8.12	0.0000	460*i*
CS	-15.31	3.83	2.85	0.0072	434*i*
CR	-19.14	0.00	0.00	0.9264	448*i*
new-9					
BS	-63.49	0.65	0.56	0.2778	440*i*
BR	-52.29	11.85	12.14	0.0000	516*i* & 11.4*i*
CS	-53.42	10.72	10.89	0.0000	432*i*
CR	-64.14	0.00	0.00	0.7222	462*i*

Table 7-4 compares e.e. and the barrier for the reduction of the substituted cyclopentanones *via* the most populated conformers.

Table 7-4: A summary of the reduction of substituted cyclopentanones

	$\Delta H_{rel}(BS)^a$	$\Delta H_{rel}(CS)^a$	$\Delta H_{rel}(CR)^a$	e.e at 0°C
new-5	14.72	-	13.82	67.0% (R)
new-6	14.72	16.34	12.79	90.3% (R)
new-7	16.08	-	18.46	99.7% (S)
new-8	14.90	16.70	12.87	85.3% (R)
new-9	14.66	-	14.01	44.4% (R)

[a] Enthalpy relative to OAB-borane adduct [-24.70] + appropriate ketone [**new-5** = -40.23, **new-6** = -40.86, **new-7** = -5.04, **new-8** = -7.34, **new-9** = -53.48 kcal mol^{-1}]

For all ketones, the 'boat R' and 'chair S' epimers did not contribute to the calculated e.e. as they were significantly higher in energy. Compared to the cyclohexanone systems, the 'boat S' TSs were lower in energy for the cyclopentanone systems as there was less of steric clash between the enone ring and the β-phenyl group attached to the 5-position of the catalyst (figure 7-7).

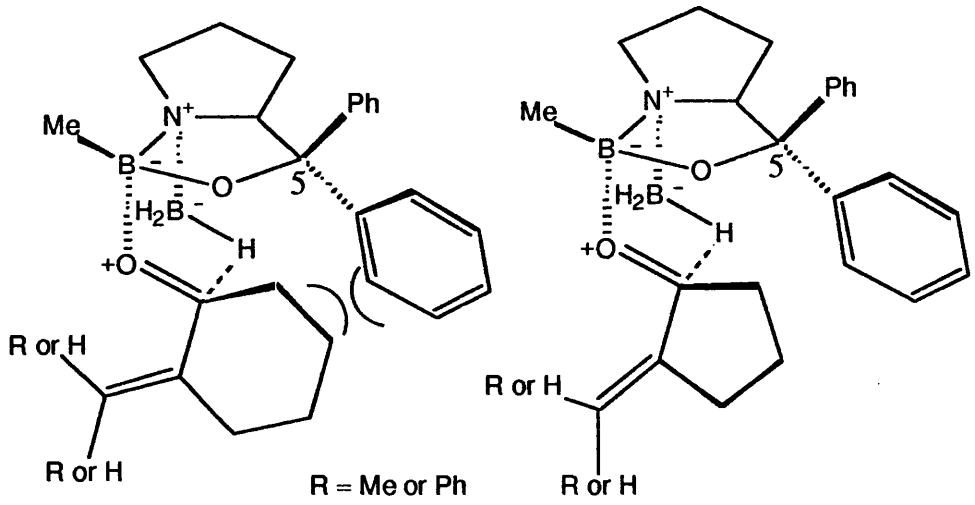

Figure 7-7

With the decrease in ring size, the angle between the *exo*-cyclic double bond and the carbonyl bond increased. In the 'chair S' TSs the increased bond angle

placed the enone-substituents further away from the boron-methyl substituent. The energetic advantage for minimising this interaction was reflected in the increased population of this conformer (table 7-3), with respect to the population calculated for the larger ring system (table 7-1).

Converting from the Z- to E-methylidenecyclopentanone, **new-5** to **new-6**, the enantiocontrol increased considerably, 67% to 90.3%. This increase was the result of a lower energy 'chair R' TS, not a higher energy 'boat S' TS. The energy decreased as the methyl group attached to the double bond was further from the β-phenyl on the 5-position of the catalyst.

The lower enantiocontrol exhibited by **new-9** (44.4%) than the either of the methyl-substituted systems resulted from the high energy 'chair R' TS due the close proximity of the double-bond substituent to the 5-β-Ph group. The differences in the position of the double bond substituents of **new-9** and **new-5** are highlighted in the ball-and-stick representation of both species, which can be found on the next page.

The reduction in e.e. on converting the methyl substituent to phenyl on the E-double bond, **new-6** (90.3%) to **new-8** (85.3) was due to large entropic difference between the R and S epimers of **new-8**.

For the Z-geometry of the *exo*-double bond, the change of double bond substituent from methyl to phenyl, **new-5** to **new-7**, resulted in the favouring of the S epimer. This was due to the increase in the energy of the 'chair R' TS, arising from the considerable steric clash between the phenyl group attached to the enone and the β-Phenyl group attached to the 5-position, rather than an decrease in the energy of the S epimer.

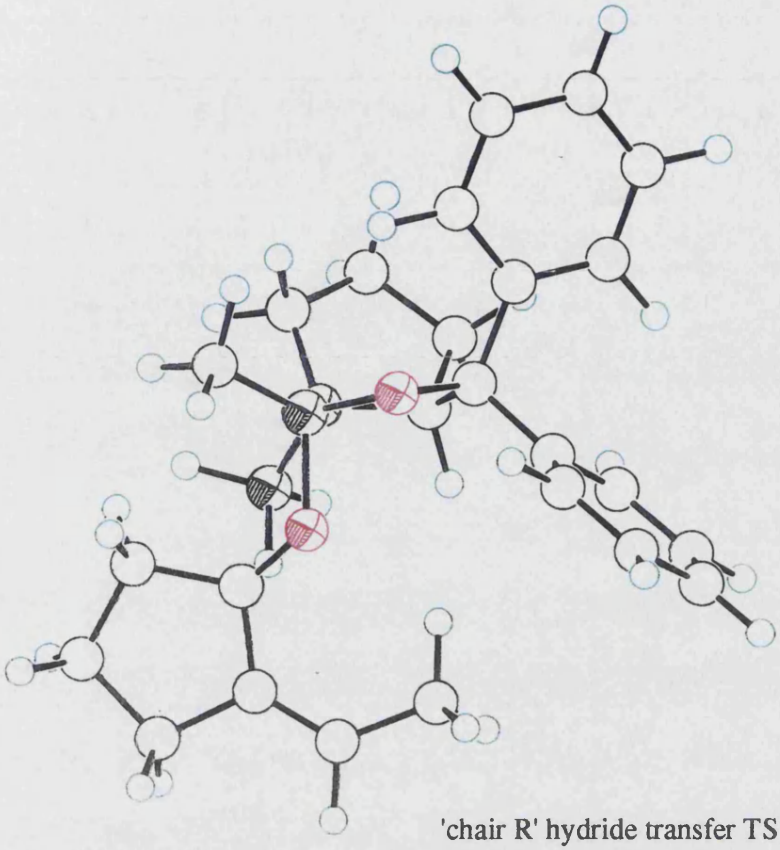

'chair R' hydride transfer TS of **new-5**

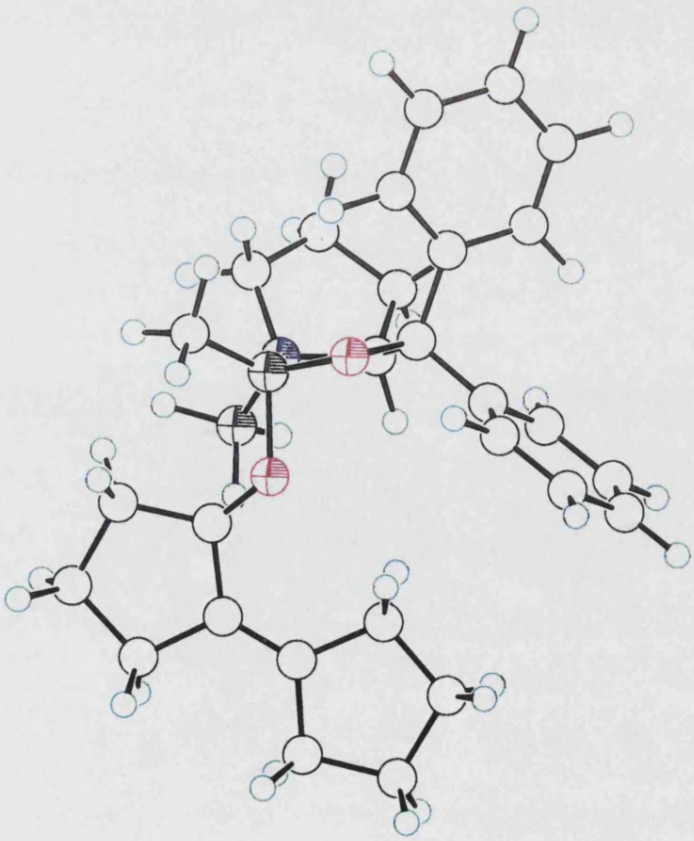

'chair R' hydride transfer TS of **new-9**

The 'boat S' TS of the cyclopentanone system **new-7** was more stable than that of the cyclohexanone system, **new-3**. The larger ring system was less stable as the cyclohexanone ring adopted a distorted boat-conformer, and the phenyl group attached to the enone was in closer proximity to the boron-methyl substituent. The differences between these two hydride transfer TSs can be seen in the ball-and-stick representations on the next page. In contrast, the 'chair R' conformer was higher in energy in **new-7** due to an increased steric clash between the ketone and β-phenyl group attached to the 5-position.

The experimental work, being performed by Prof. Gallagher's group, is underway and inital results look promising. For example, the reduction of **new-8** and **new-9** occurred with 86% and 46% e.e. compared with the predicted values of 85.3% and 44.4%.

7.2 The Design of a New Catalyst

The most important structural features of the OAB-borane adduct can be summarised as the close proximity of the ketone to a hydride source and bulky substituent which differentiates between the epimers in the rate-limiting hydride transfer step. The formation of this close spatial arrangement is also accompanied by a redistribution of electron density in such a fashion to promote hydride transfer.

Rather than change the boron atom, which provides an electron deficient binding site and the substituents which can be easily altered, systems with different neighbouring atoms were studied. Changing the boron to phosphorus had been studied by Buono and co-workers.[57] The complex (figure 7-8) was found to be a highly selective reducing agent at high temperatures.

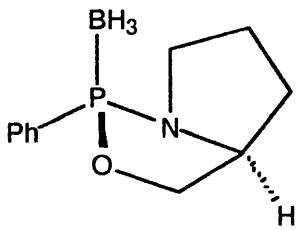

Figure 7-8

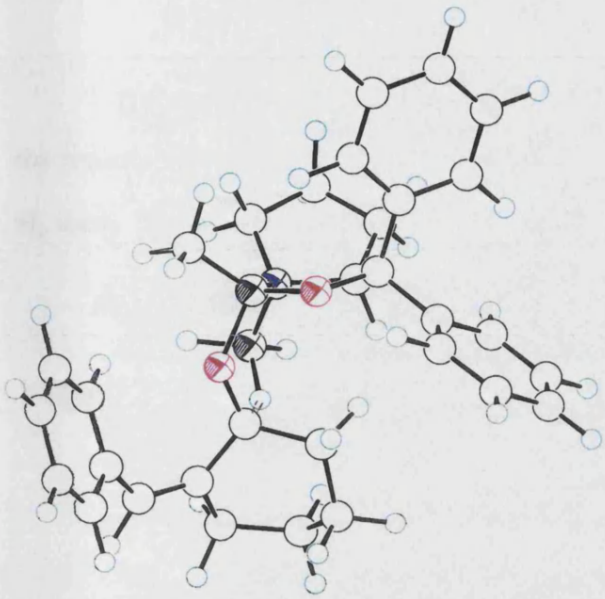

'boat S' hydride transfer TS of **new-3**
side view

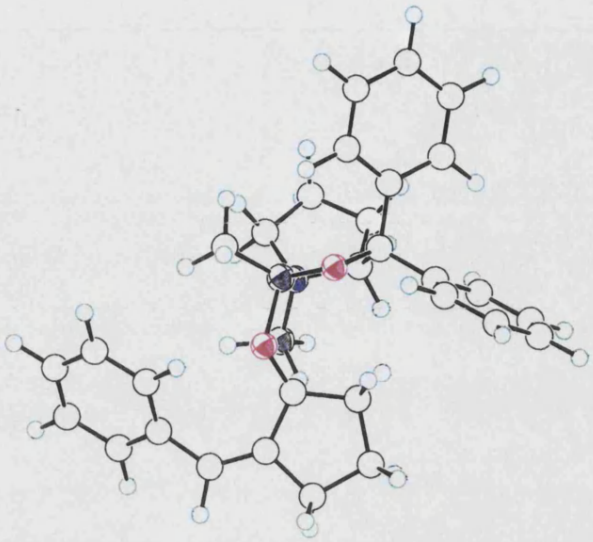

'boat S' hydride transfer TS of **new-7**
side view

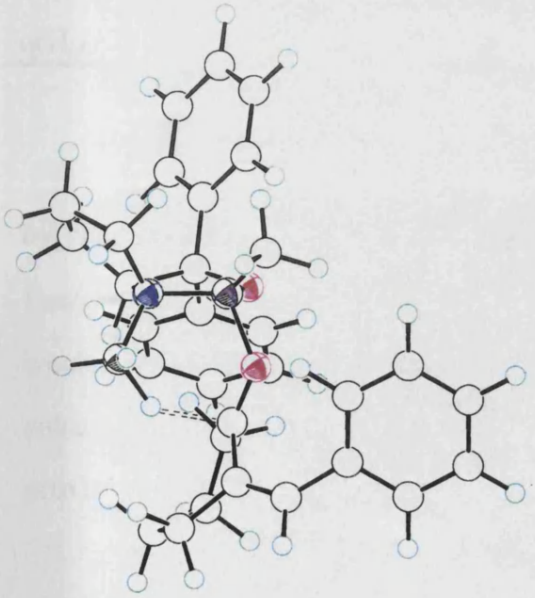

'boat S' hydride transfer TS of **new-3**
front view

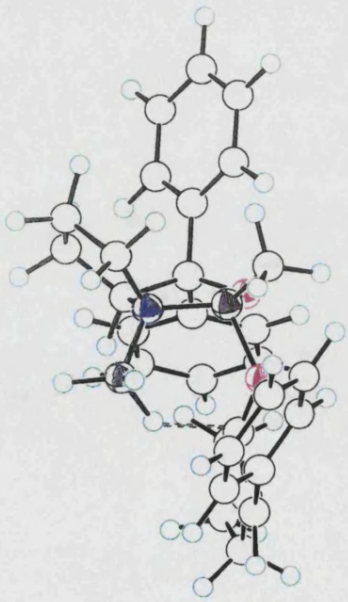

'boat S' hydride transfer TS of **new-7**
front view

7.2.1 P-B-O Catalysts

To determine which borane-adducts (figure 7-9) could act as a catalyst for the reduction of ketones, the charges of the ring boron B_r and transferring hydride H_t were calculated and is summarised in table 7-5.

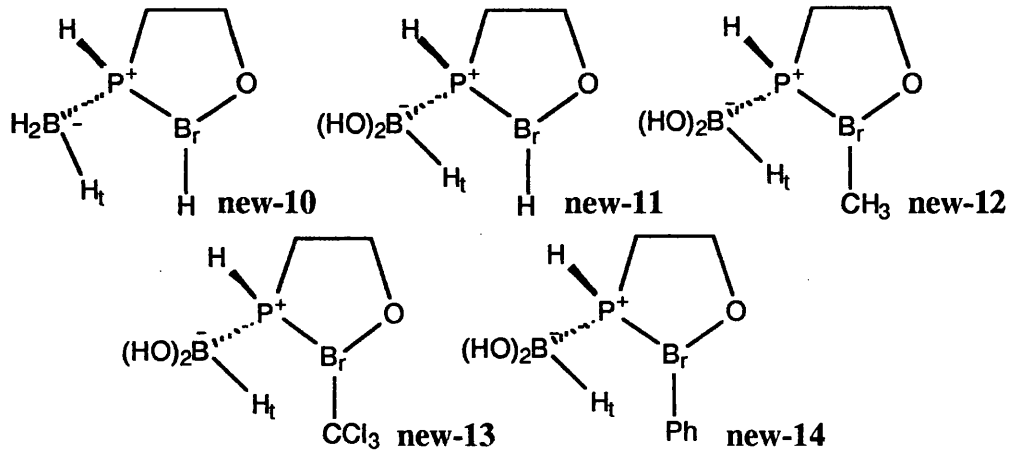

Figure 7-9

Table 7-5: The charges associated with the key atoms

	new-10	new-11	new-12	new-13	new-14
$q(B_r)$	-0.53	-0.55	-0.39	0.08	-0.52
$q(H_t)$	0.14	-0.09	-0.04	-0.04	-0.07

Whilst the electron density associated with the hydride could be increased by changing the substituents attached to the *exo*-boron, the ring boron B_r was Lewis-basic. If the boron was not electron-deficient, the rate determining step would be the binding of the ketone, not the hydride transfer, making it difficult to enhance the stereocontrol as the ketone and boron-substituent would not be in close proximity.

The only system with an electron deficient boron, B_r, was **new-13** but the reduction of acetophenone revealed only an 8.3% (S) enantioselectivity. The details of this reduction are given in table 7-6.

Table 7-6: A summary of the energetics (kcal mol^{-1}) for the reduction of acetophenone by **new-13**

	ΔH_f	$\delta(\Delta H)$	$\delta(\Delta G_{298})$	population
BS	-241.14	0.00	0.00	0.5400
BR	-240.15	0.99	0.73	0.1404
CS	-238.46	2.69	3.11	0.0017
CR	-240.85	0.30	0.29	0.3179

The 'chair S' epimer was the highest energy TS due to the close proximity of the aromatic ring of the ketone to the trichloro-group attached to boron. The unusual similarity in energies of the R conformers arose from the ability the five-membered ring to pucker. The ring puckering is shown in the ball-and-stick representations on the next page. This puckering could not occur in the OAB systems as the nitrogen effectively locked the conformation of the rings.

In view of the problems discussed, and the possibility of co-ordination of the ketone to the phosphorus, no further investigations of this type of system were carried out.

7.2.2 Nitrogen-Boron-Sulfur Systems

The charge distribution and pertinent bond lengths of the oxothiaborolidine (OTB) complex, **new-15**, and OTB-borane adduct, **new-16**, (figure 7-10) were compared with the appropriate OAB systems.

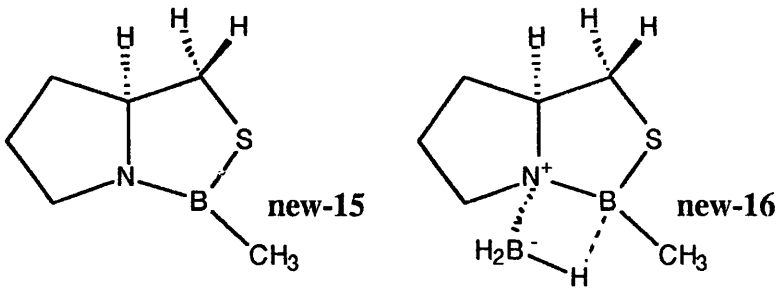

Figure 7-10

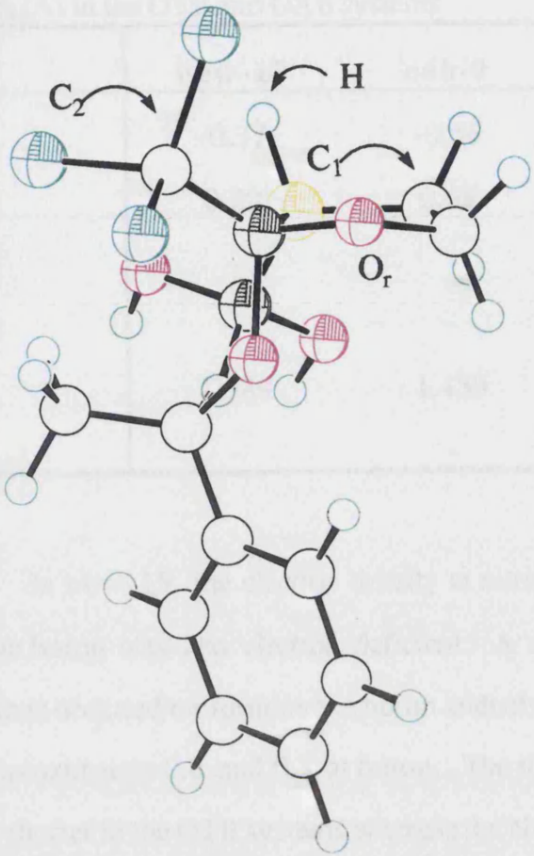

'chair R' hydride transfer TS
C_1-P-B-O_r = 7.4°
H-P-B-C_2 = 20.6°

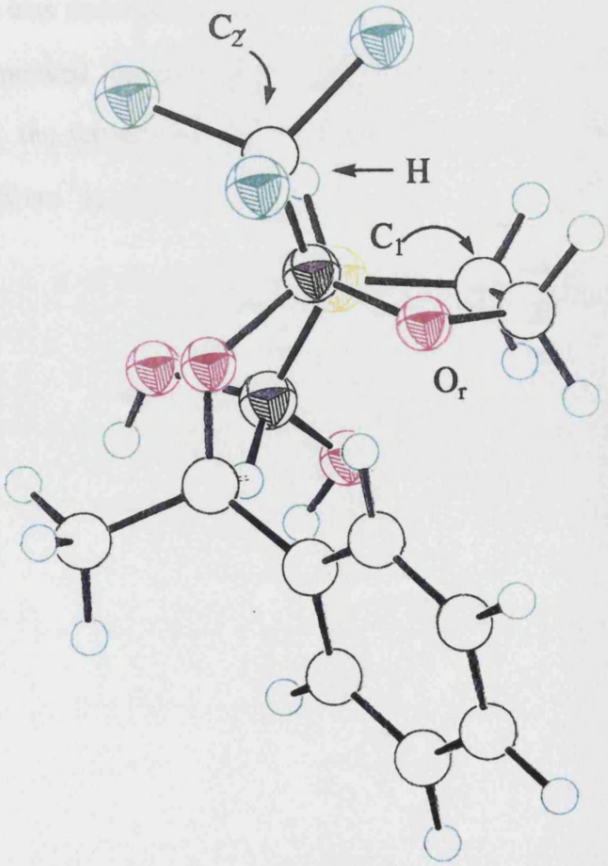

'boat R' hydride transfer TS
C_1-P-B-O_r = -21.2°
H-P-B-C_2 = -6.5°

Table 7-7: The comparison of charges of the important atoms and the key bond lengths (Å) in the OTB and OAB systems

	new-15	**oab-0**	**new-16**	**chi-2b**
q(N)	-0.37	-0.56	0.42	0.26
$q(B_r)$	0.29	0.58	0.01	0.27
$q(B_x)$	-	-	-0.24	-0.19
$q(H_t)$	-	-	0.03	-0.03
$N\text{-}B_r$	1.389	1.439	1.563	1.576
$N\text{-}B_x$	-	-	1.554	1.551

In **new-15**, the electron density at nitrogen was lower than in the **oab-0**, but the boron was less electron deficient. A similar amount of redistribution of electrons occurred on forming the boron adducts. The charge at nitrogen decreased by approximately 0.8 and 0.3 at boron. The nitrogen to boron B_r bond distances were shorter in the OTB systems whereas the $N\text{-}B_x$ bond was of a similar length to that in the OAB system.

The approach of the acetophenone was considered to boron B_r. Table 7-8 shows the important energetic and geometrical features relating to the ketone binding TS, **new-17**, ($\upsilon^{\ddagger} = 137i$ cm^{-1}), the ternary ketone complex, **new-18**, and 'chair R' hydride transfer TS($\upsilon^{\ddagger} = 386i$ cm^{-1}), **new-19**.

Table 7-8: The important energetic (kcal mol^{-1}) and geometric changes (Å) that occurred during ketone binding and hydride transfer

	new-17	new-18	new-19
ΔH_f	-40.92	-44.34	-40.45
ΔH_{rel} [a]	20.08	16.66	20.55
B_r-O_c	2.280	1.810	1.682
O_c-C_c	-	1.261	1.293
C_c-H_t	-	2.525	1.749
H_t-B_x	-	1.211	1.247
B_x-N	-	1.608	1.584
N-B_r	-	1.540	1.573

[a] Enthalpy relative to **new-16** [-45.89] + PhCOMe [-15.11] = -61.00 kcal mol^{-1}

The ketone binding TS was 0.47 kcal mol^{-1} lower in energy than the TS for hydride transfer. When entropic differences were included, the binding TS was 4.13 kcal mol^{-1} lower in energy, implying that the hydride transfer was rate limiting.

All the species were about 8 kcal mol^{-1} higher in energy than the equivalent OAB systems (see chapter 6.2.1 table 6-10), although the barriers from the ternary ketone complex to both hydride transfer and dissociation were about 1 kcal mol^{-1} lower. The conversions shown in figure 7-11 were considered to determine if the lower stability arose from a less stable borane-adduct than the comparable OAB-borane adduct.

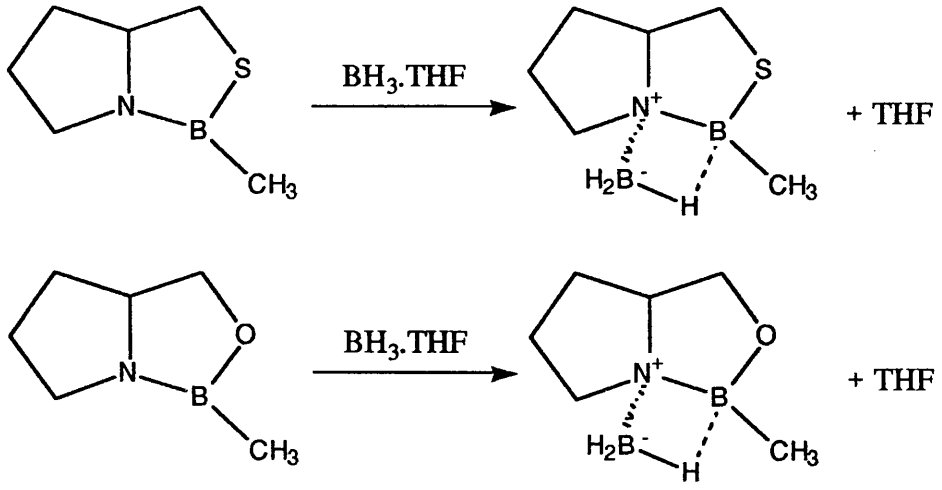

Figure 7-11

For the OTB system, 13.76 kcal mol^{-1} were released on the formation of the adduct compared to 15.04 kcal mol^{-1} for the OAB system. This analysis implied that the higher energy of the OTB-species was as a result of the lower Lewis acidity of the boron B_r and not an artefact of the reference point used to calculate the relative enthalpies.

With the hydride transfer confirmed as the rate determining step, the TS for the four usual configurations were located - the analysis of which is summarised in table 7-9.

Table 7-9: A summary of the energetic differences (kcal mol^{-1}) between the four conformers for hydride transfer

	ΔH_f	$\delta(\Delta H_f)$	$\delta(\Delta G_{298})$	population	$\upsilon^{\ddagger}$ (cm^{-1})
BS	-39.25	1.20	2.11	0.0261	439*i*
BR	-38.03	2.42	2.07	0.0280	410*i*
CS	-38.44	2.01	2.37	0.0169	413*i*
CR	-40.45	0.00	0.00	0.9290	396*i*
enantiomeric excess at 25°C = 91.4 % (R)					

The relative energetics of the hydride transfer TSs of the OTB system were compared with the energetics of **chi-1b** (table 6-2 in chapter 6.1.1). In the sulfur

system the 'boat S' TS was closer in energy to the 'chair R' TS than in the OAB system, $\delta(\Delta H)$ = 1.20 kcal mol^{-1} *versus* $\delta(\Delta H)$ = 1.62 kcal mol^{-1}. The 'boat R' TS was 0.68 kcal mol^{-1} higher in energy, relative to the 'chair R' TS, than in the OAB system. The 'chair S' systems had similar relative energies to the 'chair R' TSs in both systems, only 0.02 kcal mol^{-1} difference.

Comparing the geometries of the hydride transfer TSs, it was noted that in the OTB system, the N-B_r bond was on average 0.016 Å shorter than N-B_x bond. In the OAB system, the difference in bond lengths was similar but the N-B_x was the shorter of the two bonds. The B_x-H_t and B_r-O_c bond distances were slightly shorter in the OTB system, by 0.006 and 0.027 Å respectively.

The ten percent higher e.e. predicted for the sulfur system arose from a larger, negative entropy difference between the 'boat S' and 'chair R' TS than in the OAB system (-3.05 cal mol^{-1} K^{-1} *versus* -0.57 cal mol^{-1} K^{-1}). The negative entropy difference implied that in both systems the 'boat S' TS was tighter than in the 'chair R' TS. In such a complex system, trying to find a single bond distance which reflected this tighter TS was bound to be difficult, as in a cyclic system when one bond length decreases another will increase. The best 'measure' of the tighter bonding in the 'boat S' TS was in the comparison of sum of six key bond lengths in TS.

$$\Sigma_{BS} (B_r\text{-}O_c + O_c\text{-}C_c + C_c\text{-}H_t + B_x\text{-}H_t + B_x\text{-}N + N\text{-}B_r) = 9.082 \text{ Å}$$

$$\Sigma_{CR} (B_r\text{-}O_c + O_c\text{-}C_c + C_c\text{-}H_t + B_x\text{-}H_t + B_x\text{-}N + N\text{-}B_r) = 9.128 \text{ Å}$$

At the time of writing this thesis, the synthesis of **new-15** had been started by Dr. Chris Self. As the synthesis had not been completed, no reduction data was available.

Chapter 8: The Reduction of Ketones by Catalysts Containing the N-P=O Subunit: A Review of Experimental Results

Whilst oxazaborolidines have proved to be most successful catalysts, their preparation has often proved to be difficult and their enantiocontrol has been found to be sensitive to the presence of water and the nature of the substituents attached to the ketone.[50]

Wills and co-workers have investigated the use of borane-adducts of chiral phosphorus complexes as reduction catalysts. Whilst their results have indicated that these species are excellent catalysts, the design of a catalyst which imparts a high degree of enantiocontrol has yet to be achieved.

Their initial work focused on the borane adducts of α-methylbenzylamine (figure 8-1).[58]

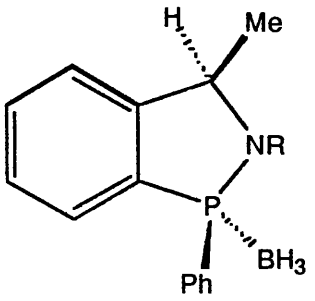

mw-1 R = H
mw-2 R = Me

Figure 8-1

The reduction of acetophenone by **mw-1** yielded the alcohol with a 23% (S) e.e. The use of **mw-2** did not increase the enantiocontrol. On the contrary, catalysis did not occur. Slight improvements in the stereoselectivity occurred with the use of phosphinamides (figure 8-2).[59]

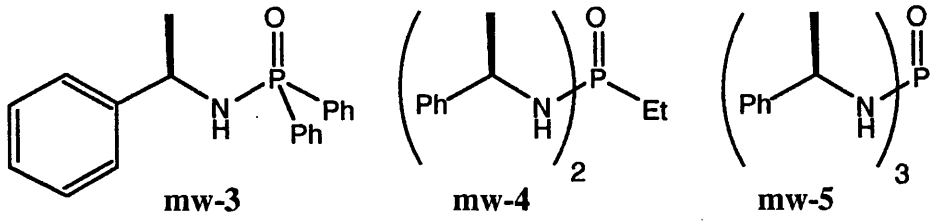

mw-3 mw-4 mw-5

Figure 8-2

The reductions were completed in under one hour and the optical purities of the products were 27% (S), 35% (S) and 20% (S) using the borane-adducts of **mw-3**, **mw-4** and **mw-5**, respectively.

Different analogues[60] of these catalysts were prepared (figure 8-3) to reveal which substituents affected the levels of induction.

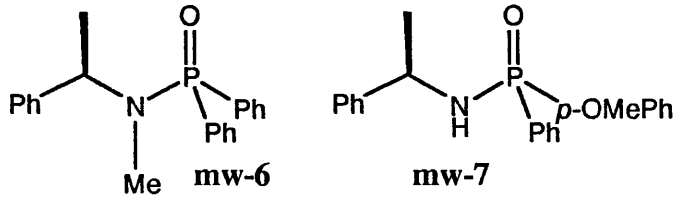

mw-6 mw-7

Figure 8-3

The borane adduct of **mw-6** was an effective catalyst with the reaction time being less than one hour. The e.e. was reduced to 10% (S), compared to 27% for **mw-3**. The reduction of acetophenone by the borane adduct of **mw-7** was complete in only fifteen minutes, with an optical purity of 24% (S) for the alcohol. From this Wills concluded that electron donation to the phosphinamide system was beneficial for catalysis, but did not affect the levels of induction.

Three rigid phosphinamides (figure 8-4) were also studied.[60]

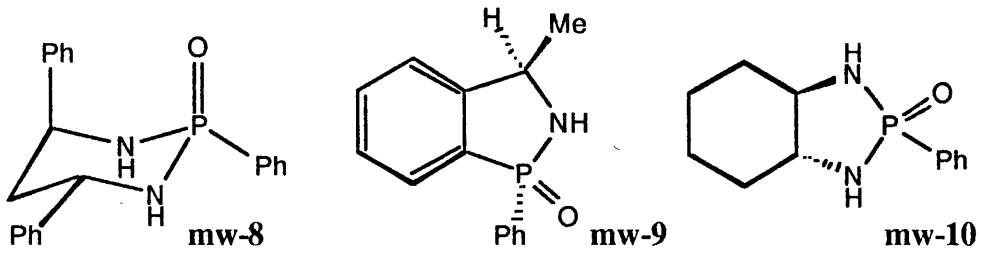

mw-8 mw-9 mw-10

Figure 8-4

Only the racemic form of **mw-8** was prepared. The rate of reduction by the borane adducts of **mw-8**, **mw-9** and **mw-10** was slow, the reduction of

acetophenone taking over three hours. It was concluded that the 'optimum geometry for catalytic activity was that in which the R_2NPO system can lie in a single plane and therefore electron donation from the nitrogen lone pair to the P=O bond was maximised.' Wills stated that this postulate was supported by the X-ray structures of related species[61] in which the nitrogen was sp^2-hybridised in systems which could attain planarity.

On the basis of the experimental observations, it was proposed that catalysis was achieved by activation of borane by a strong donation from the oxygen atom of the N–P=O system coupled with a weaker interaction of the substrate carbonyl lone pair with the phosphorus.[60] The hydride transfer TS is shown in figure 8-5.

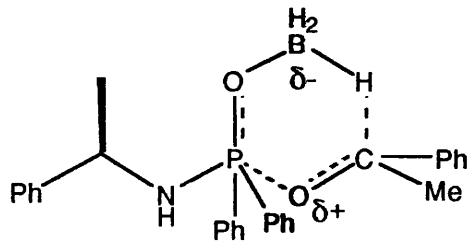

Figure 8-5

In a later study, Wills and co-workers investigated the use of an additive to improve selectivity.[62] A dioxoborolidine, in the presence of borane-dimethyl sulfide, slowly reduced acetophenone to yield the alcohol in 4% (S) e.e. The e.e. could be increased to 45% (S) by increasing the amount of dioxoborolidine from ten to one hundred mol percent. The addition of ten mol percent of **mw-3** to the reaction mixture increased the e.e. to 63% (S).

Wills proposed that the phosphinamide polarised the borane moiety whilst the dioxoborolidine bound the ketone. They are currently synthesising a catalyst (figure 8-6) which includes both the phosphinamide and the boron.

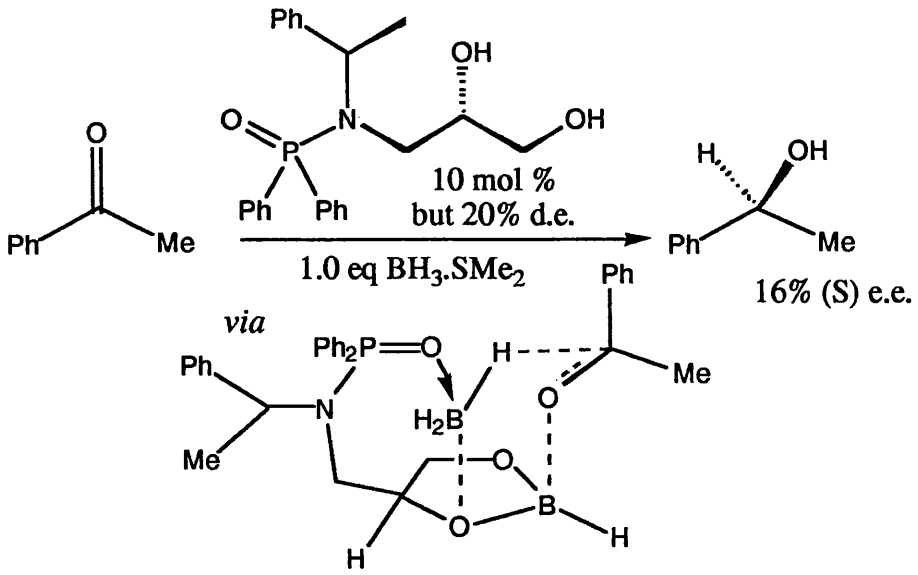

Figure 8-6

Early results look promising. A 20% diastereomeric excess of the catalyst reduced acetophenone with 16% (S) e.e.

Chapter 9: The Mechanism of the Reduction of Ketones by Phosphinamide-Borane Adducts: Computational Modelling

The mechanism for ketone reduction by borane adducts containing an N–P=O linkage was determined for the phosphinamide shown in figure 9-1. Figure 9-1 also shows the labelling scheme that will be used. If more than one of the molecules is present, the most recently added moiety will be denoted by 'n'.

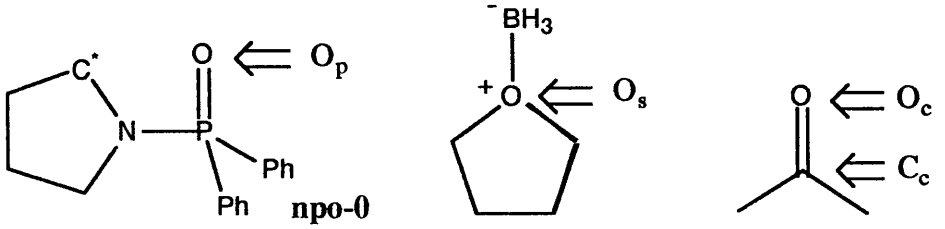

Figure 9-1

The phosphinamide **npo-0** was selected as it had only limited conformation freedom. Acetone was used as this allowed the important mechanistic details to be identified before considering the issue of enantioselectivity.

9.1 The Ligand

The ball-and-stick representation of **npo-0** is shown on the next page. In **npo-0** the dihedral angle C*-N-P-O_p was 16°. Wills and co-workers proposed that this angle had to be approximately zero for catalysis to occur.[60]

The phosphorus had a partial charge of 2.00, whilst nitrogen and oxygen were electron rich, -0.41 and -1.00. From these charges it was clear that the subsequent binding of borane-tetrahydrofuran (borane-THF) to the catalyst would be more likely to occur at the oxygen.

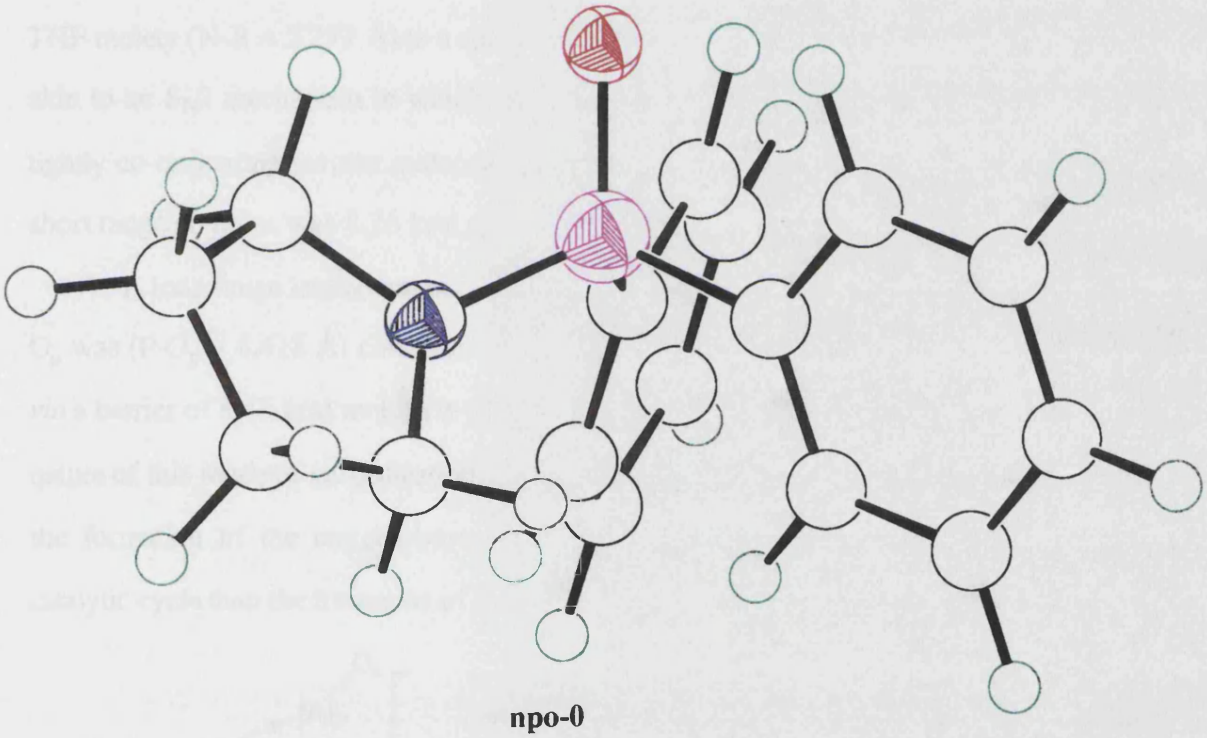

npo-0

In experimental investigations, it had been noted that the order of addition of ketone and borane-THF did not affect the enantioselectivity. In this investigation, the two possible pathways were considered.

9.1.1 Binding of the Borane-THF Prior to the Ketone

From the charge distribution in **npo-0**, donation of the lone pair on oxygen to the borane-THF was likely to be favoured over donation from the nitrogen. A barrier of 20.18 kcal mol^{-1} (N-B = 1.935Å, $\upsilon^{\ddagger}$ = 254*i* cm^{-1}) existed for the conversion of a long range interaction between nitrogen and boron of the borane-THF moiety (N-B = 5.277 Å) to a short range complex (N-B = 1.607Å). This was akin to an S_N2 mechanism in which the nitrogen acted as the nucleophile with the tightly co-ordinating solvent molecule of borane-THF as the leaving group. The short range complex was 8.26 kcal mol^{-1} less stable than the long range complex.

A long range interaction between borane-THF to the phosphinamide oxygen O_p was (P-O_p = 4.418 Å) converted to a short range interaction (P-O_p = 1.532 Å) *via* a barrier of 8.17 kcal mol^{-1} (B-O = 2.597Å, $\upsilon^{\ddagger}$ = 69*i* cm^{-1}). The exothermic nature of this mode of co-ordination (figure 9-2) and the lower barrier implied that the formation of the oxygen-boron bond was more likely to occur during the catalytic cycle than the formation of a nitrogen-boron bond.

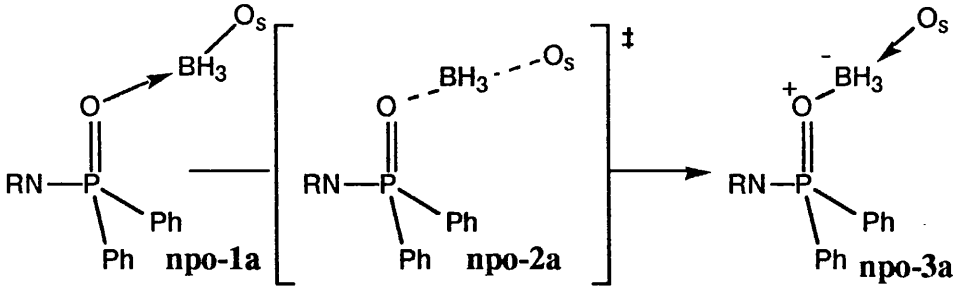

Figure 9-2

The ball-and-stick representations of these species are given on the next page.

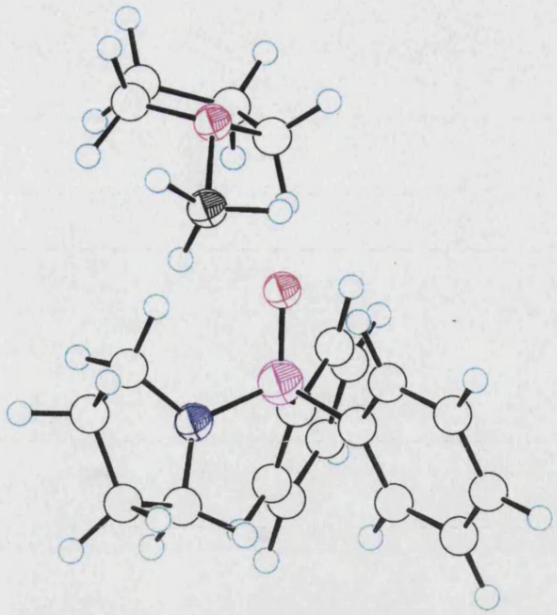

npo-1a

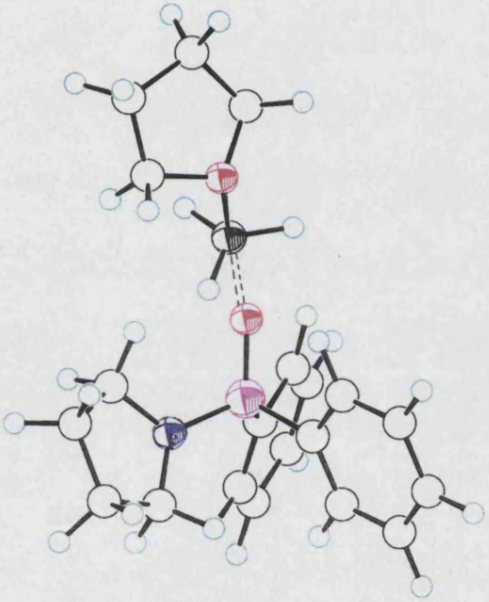

npo-2a

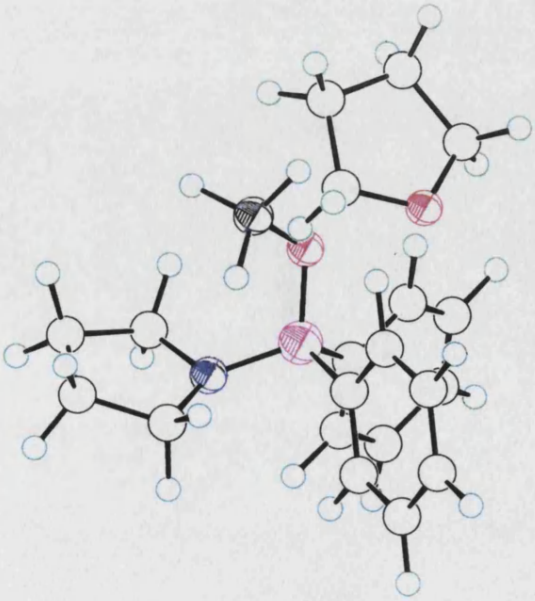

npo-3a

The important structural and the energetic changes that occurred during the conversion of long range O_p-B interaction, **npo-1a**, *via* the TS, **npo-2a**, to the short range O_p-B complex, **npo-3a**, are summarised in table 9-1.

Table 9-1: The energetic (kcal mol^{-1}) and geometrical changes (Å) associated with the binding of BH_3.THF to the phosphinamide oxygen

	npo-1a	**npo-2a**	**npo-3a**
ΔH_f	-83.35	-75.18	-100.05
ΔH_{rel} [a]	-5.51	.2.66	-22.21
O_p-B	4.418	2.597	1.532
B-O_s	1.752	1.849	4.127
P-O_p	1.484	1.481	1.551

[a] Enthalpy relative to **npo-0** [-30.18] + borane-THF [-47.66] = -77.84 kcal mol^{-1}

During the binding the C*-N-P-O angle had increased to 39.3°. The partial charge on the phosphinamide oxygen had decreased to -0.59 and the charge at phosphorus had decreased slightly to 1.85. The electron density on boron had increased, as reflected in the change in partial charge from 0.12 in isolated borane-THF to -0.24 in **npo-3a**. The electron density on the hydride source had decreased from an average of 0.13 in BH_3.THF to 0.03 in **npo-3a**.

A long range interaction between phosphorus P and the oxygen of the carbonyl O_c (P-O_c = 4.514 Å), a TS (P-O_c = 2.933 Å, $\upsilon^{\ddagger}$ = 272*i* cm^{-1}) and a short range P-O_c complex (P-O_c = 2.646 Å) were found for the binding of the ketone. The barrier for this process was 12.46 kcal mol^{-1}.

Figure 9-3 provides as schematic representation for conversion of the long range P-O_c, **npo-4a**, *via* the TS, **npo-5a**, to the short range P-O_c complex, **npo-6a**. Table 9-2 summarises the important energetic and structural changes.

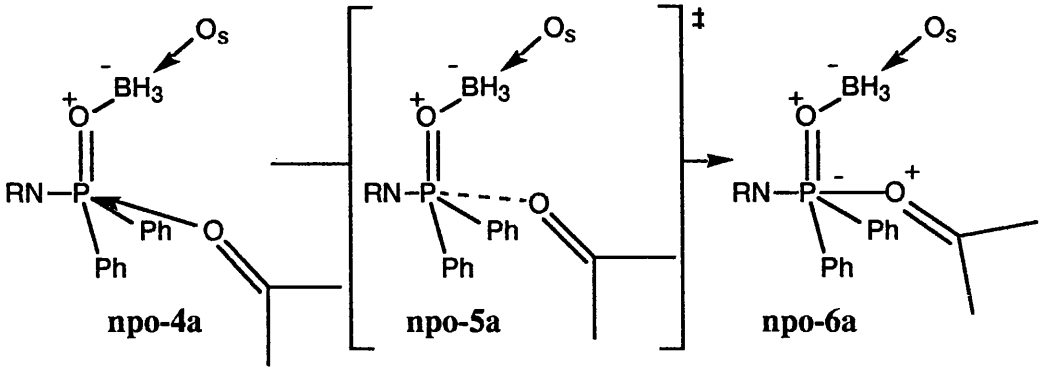

Figure 9-3

The ball-and-stick representations for these species are shown on the next page.

Table 9-2: The energetic (kcal mol^{-1}) and geometrical changes (Å) associated with the binding of acetone to the phosphinamide-borane adduct

	npo-4a	**npo-5a**	**npo-6a**
ΔH_f	-153.65	-141.19	-143.23
ΔH_{rel} [a]	-26.80	-14.34	-16.38
P-O_c	4.514	2.933	2.646

[a] Enthalpy relative to **npo-0** [-30.18] + borane-THF [-47.66] + MeCOMe [-49.01] = -126.85 kcal mol^{-1}

The P-O_c distance in **npo-6a** was considerably larger than the 1.8Å B-O_c distance observed in the ternary ketone-OAB-borane adducts.

The polarisation of the ketone increased making the carbon more electron deficient, 0.49 in isolated acetone to 0.66 in **npo-6a**, thus making it more susceptible to hydride transfer. During the binding of the ketone the electron density at the hydride source had increased to -0.14, which made the hydride slight more electron rich than isolated borane-THF. In **npo-6a**, the C*-N-P-O dihedral angle had increased to 47° and the carbonyl carbon was 2.631 Å from the hydride.

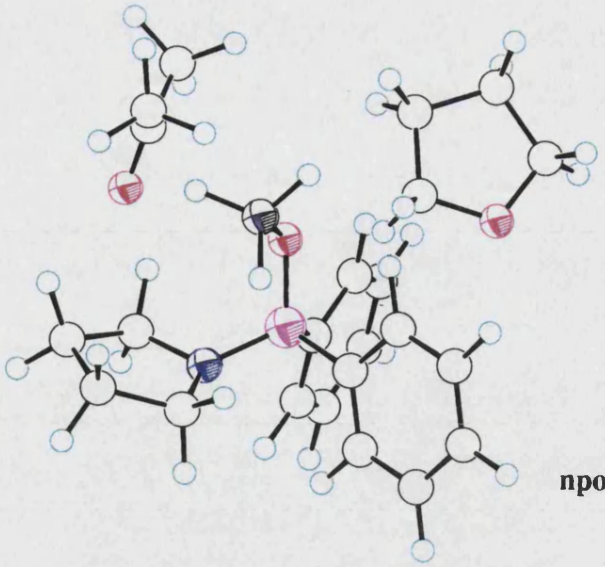

npo-4a

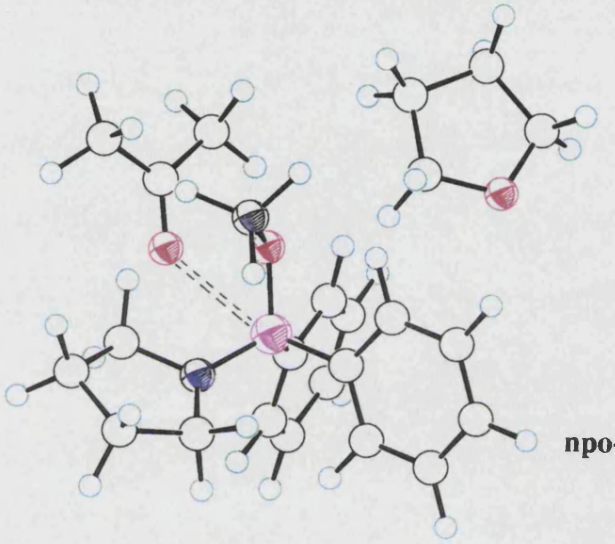

npo-5a

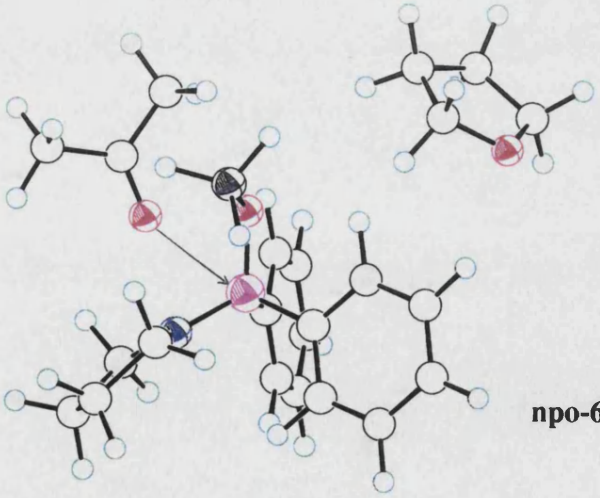

npo-6a

9.1.2 Binding of Acetone before the Hydride Source

The binding of the ketone to **npo-0** (figure 9-4) involved a long range interaction between phosphorus and the carbonyl oxygen O_c ($P\text{-}O_c$ = 4.639 Å) which was converted to a short range $P\text{-}O_c$ complex ($P\text{-}O_c$ = 2.613 Å) *via* a barrier of 13.40 kcal mol^{-1} (TS $P\text{-}O_c$ = 2.905 Å, $\upsilon^{\ddagger} = 255i\ cm^{-1}$).

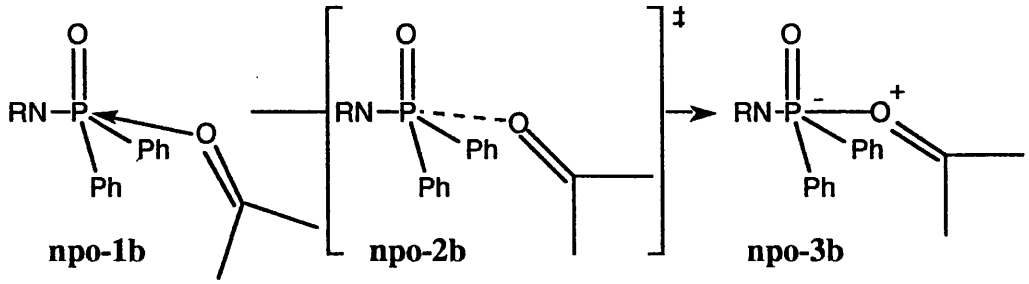

Figure 9-4

The ball-and-stick representations of these molecules are shown on the next page.

Table 9-3 summarises the important energetic and structural changes that accompanied the conversion of the long range $P\text{-}O_c$, **npo-1b**, *via* the TS, **npo-2b**, to the short range $P\text{-}O_c$ complex, **npo-3b**.

Table 9-3: The energetic (kcal mol^{-1}) and geometrical changes (Å) associated with the binding of acetone to the phosphinamide

	npo-1b	**npo-2b**	**npo-3b**
ΔH_f	-84.70	-71.30	-72.97
ΔH_{rel} [a]	-5.51	7.89	6.22
$P\text{-}O_c$	4.639	2.905	2.613

[a] Enthalpy relative to **npo-0** [-30.18] + MeCOMe [-49.01] = -79.19 kcal mol^{-1}

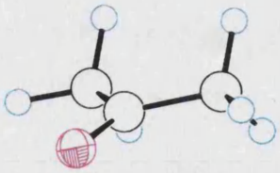

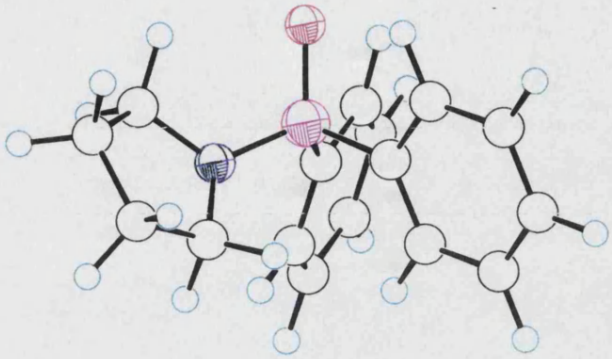

npo-1b

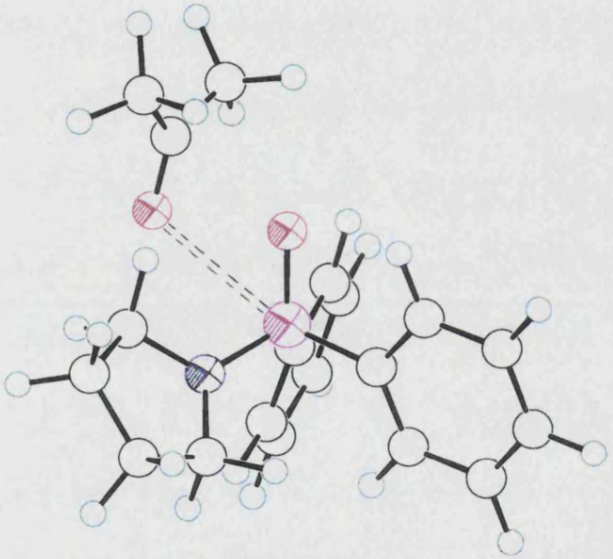

npo-2b

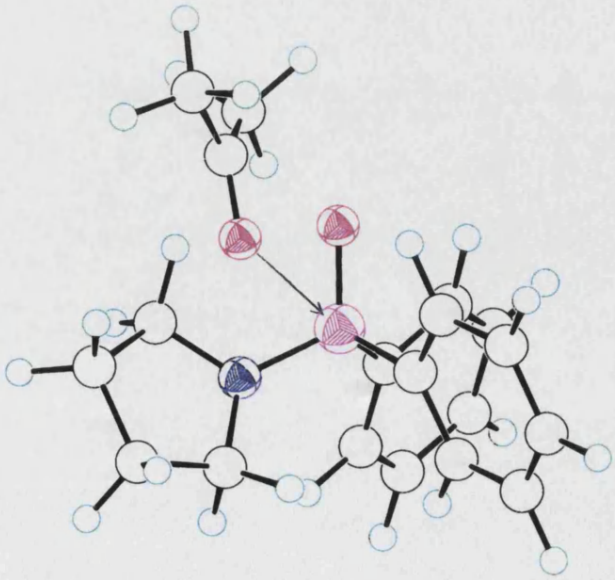

npo-3b

The nitrogen and oxygen O_p were both electron rich, as indicated by the charges of -0.20 and -0.95. Only donation from the lone pair on O_p to borane-THF was considered as the barrier the formation of the O_p-B bond was lower than that for N-B bond formation.

The barrier for converting a long range interaction between the oxygen O_p and boron of borane-THF (O_p-B = 5.106Å) to the tightly bound phosphinamide-borane adduct was 3.19 kcal mol^{-1} (TS O_p-B = 2.548 Å, $\upsilon^{\ddagger} = 81i\ cm^{-1}$). As **npo-6a** was found on both pathways it will be referred to as **npo-6** in subsequent discussions.

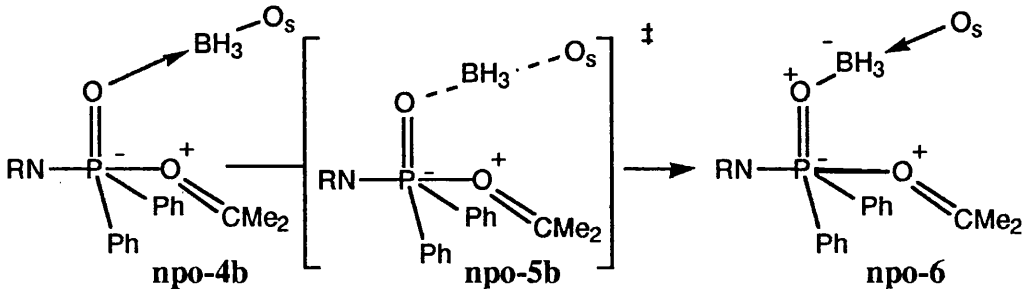

Figure 9-5

The ball-and-stick representations of these molecules are shown on the next page.

Table 9-4 summarises the important structural and energetic features of the **npo-4b**, **npo-5b** and **npo-6**.

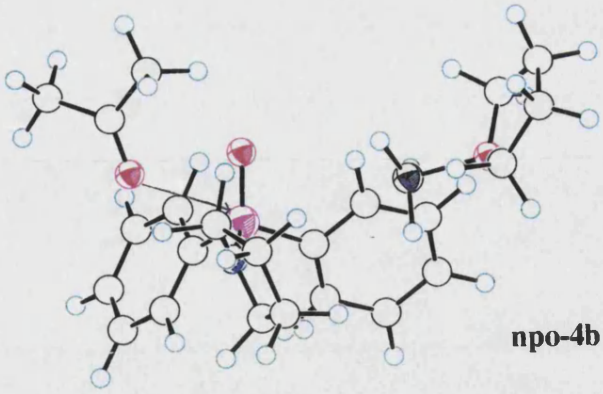

npo-4b

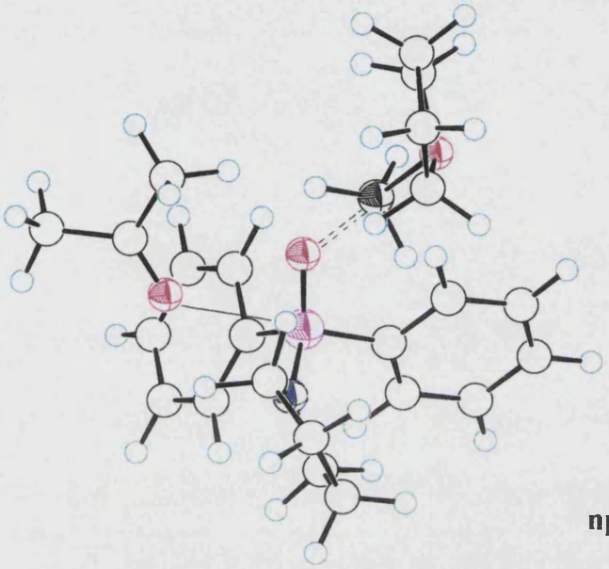

npo-5b

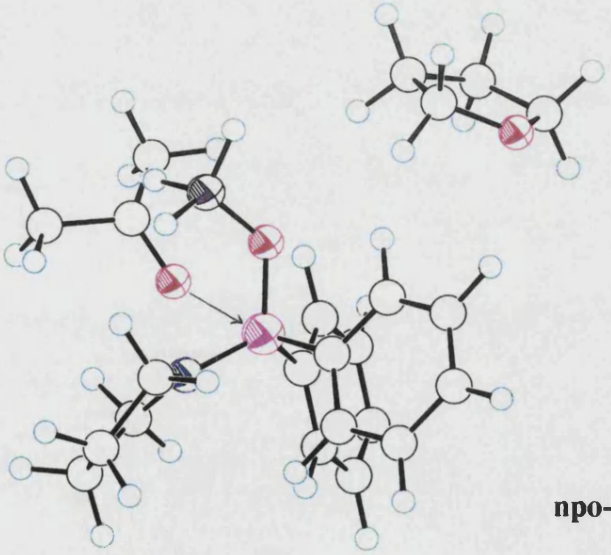

npo-6

Table 9-4: The energetic (kcal mol^{-1}) and geometrical changes (Å) arising from the binding of BH_3.THF to the phosphinamide-acetone complex

	npo-4b	npo-5b	npo-6
ΔH_f	-120.73	-117.54	-143.23
ΔH_{rel} [a]	6.12	9.31	-16.38
O_p-B	5.106	2.548	1.521
B-O_s	1.779	1.858	5.350
P-O_p	1.482	1.483	1.554
P-O_c	2.613	2.610	2.646

[a] Enthalpy relative to **npo-0** [-30.18] + borane-THF [-47.66] + MeCOMe [-49.01] = -126.85 kcal mol^{-1}

9.2 Hydride Transfer

Unlike the hydride transfer TS of OAB catalysts, only one conformer could be located for these systems. The six membered ring, comprising of P-O_p-B-H_t-C_c-O_c, adopted a distorted chair conformation (figure 9-6).

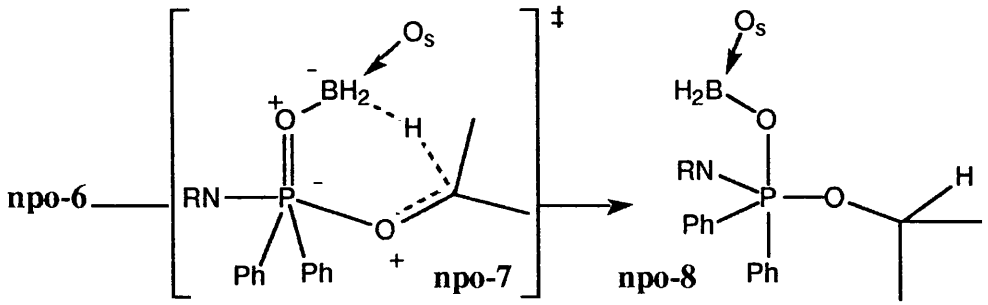

Figure 9-6

The ball-and-stick representations of these molecules are shown on the next page. After hydride transfer, **npo-8** adopted a trigonal bipyramidal geometry about phosphorus. The ball-and-stick view of **npo-8** has kept the pyrrolidine ring in the same orientation as in the hydride transfer TS. A clearer view of the trigonal bipyramidal structure is shown later, after the description of the next step of the mechanism.

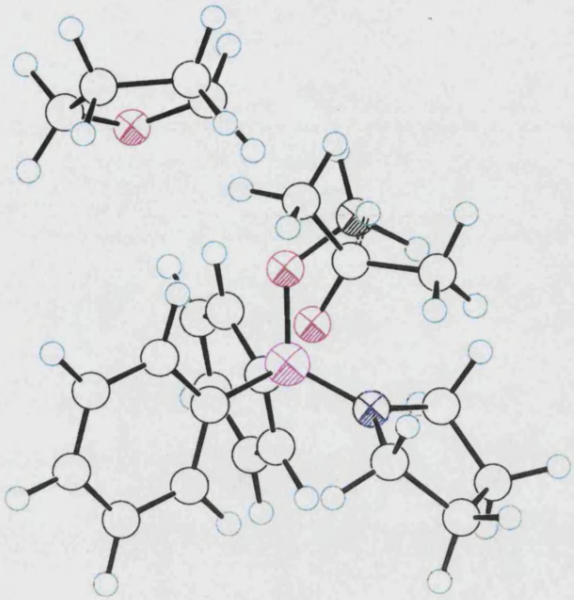

npo-7

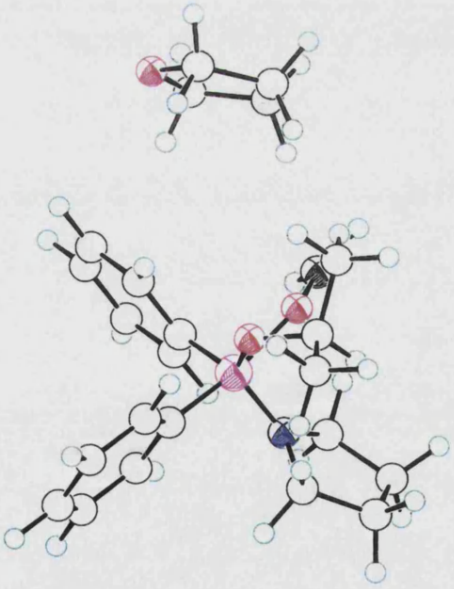

npo-8

The barrier to hydride transfer was 12.76 kcal mol^{-1} ($\upsilon^{\ddagger}$ = 378*i* cm^{-1}), a considerably larger barrier than the 5 kcals mol^{-1} typically found for hydride transfer in the OAB systems.

The important energetic and structural changes between the ketone complex, **npo-6**, the hydride transfer transition state, **npo-7**, and the minimum occurring directly after the transfer, **npo-8**, are summarised in table 9-5.

Table 9-5: The energetic (kcal mol^{-1}) and geometrical changes (Å) associated with hydride transfer

	npo-6	**npo-7**	**npo-8**
ΔH_f	-143.23	-130.47	-150.36
ΔH_{rel}[a]	-16.38	-3.62	-23.51
P-O_c	2.646	2.440	1.643
O_c-C_c	1.243	1.295	1.406
C_c-H_t	2.631	1.420	1.128
H_t-B	1.212	1.333	3.448
B-O_p	1.521	1.427	1.300
O_p-P	1.554	1.577	1.791

[a] Enthalpy relative to **npo-0** [-30.18] + borane-THF [-47.66] + MeCOMe [-49.01] = -126.85 kcal mol^{-1}

In **npo-7**, the C*-N-P-O dihedral angle had increased to 110° and the Pauling bond order **n** for the B-H_t bond was 0.49 indicating a much 'later' TS than either the OAB-systems or the uncatalysed reduction, both of which had **n** ≈ 0.7.

Although **npo-8** was located by following the IRC from **npo-7**, a more stable minimum was located by rotation about the P-O_p bond followed by the formation of a B-O_c bond. The barriers for these processes were 0.62 kcal mol^{-1} ($\upsilon^{\ddagger}$ = 73*i* cm^{-1}) and 1.82 kcal mol^{-1} ($\upsilon^{\ddagger}$ = 134*i* cm^{-1}) respectively. These two steps

(figure 9-8) converted the geometry about phosphorus from trigonal bipyramidal to pyramidal.

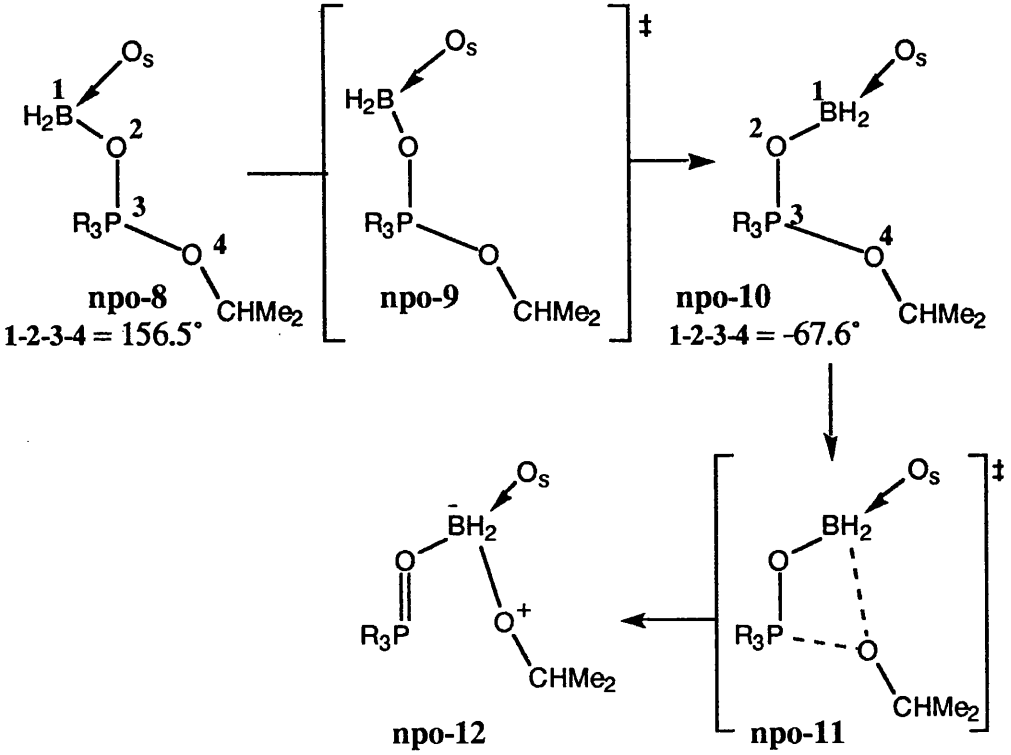

Figure 9-7

The ball-and-stick representations are shown on the next two pages. The orientation of **npo-8**, **npo-9** and **npo-10** shows the rotation about the P-O_p bond. A different orientation of **npo-10** is used the following page as this orientation to highlight the important changes during the bond formation step. Two views of **npo-12** are shown to make visualisation easier.

The structural and energetic changes that accompanied the rotation which converted **npo-8** *via* **npo-9** to **npo-10**, and the TS **npo-11** for formation of the B-O_c found in **npo-12** are summarised in table 9-6.

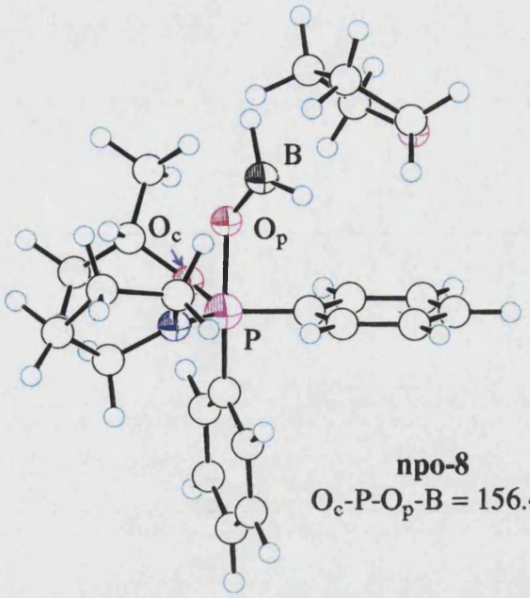

npo-8
O_c-P-O_p-B = 156.4°

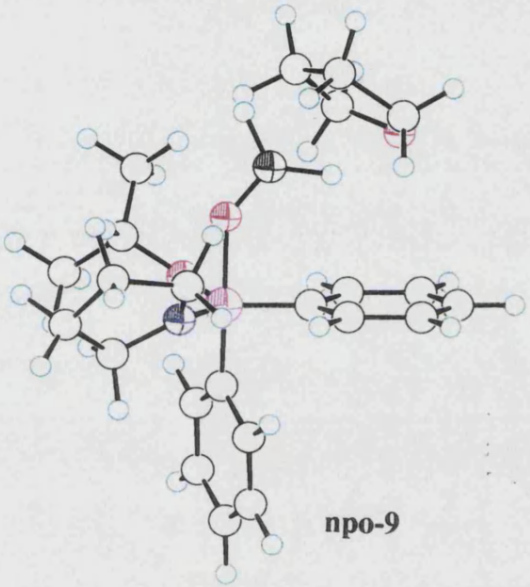

npo-9

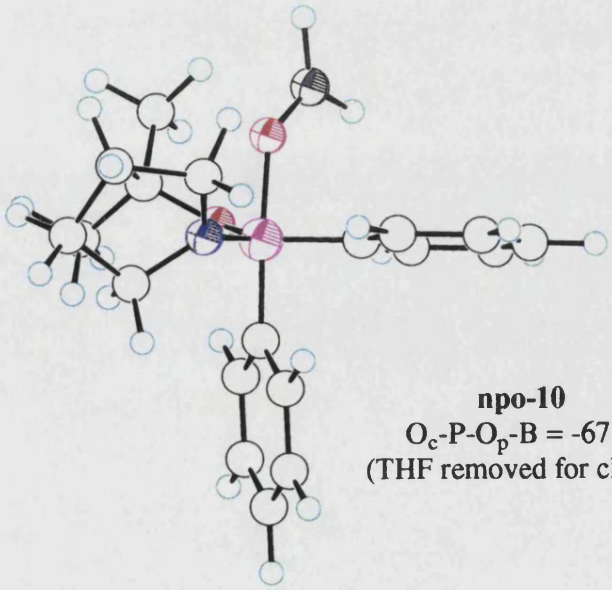

npo-10
O_c-P-O_p-B = -67.6°
(THF removed for clarity)

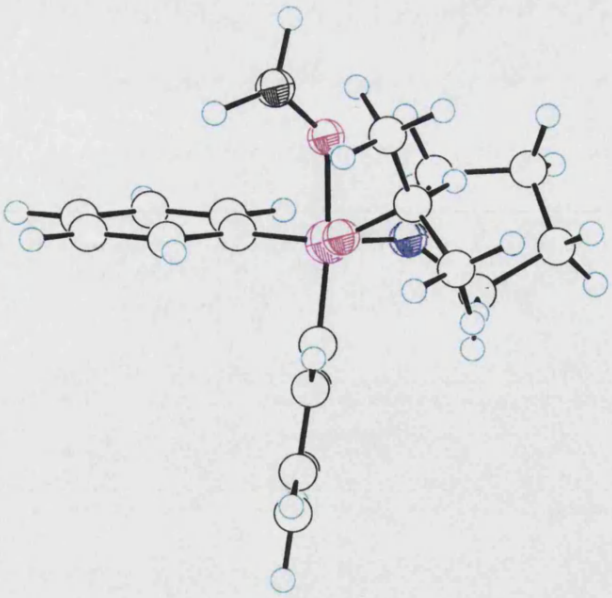

npo-10

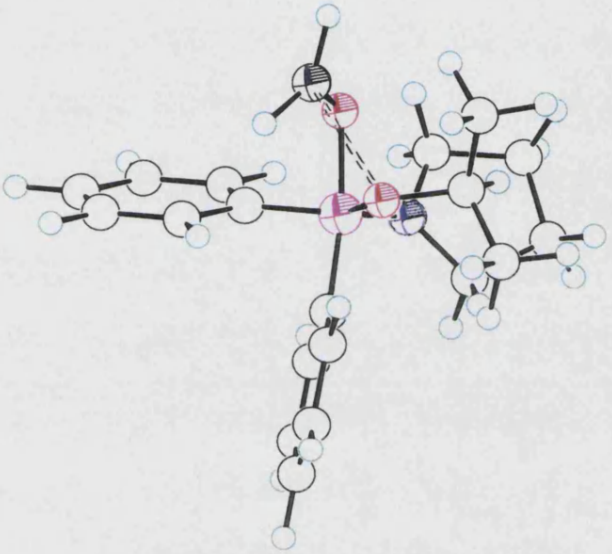

npo-11

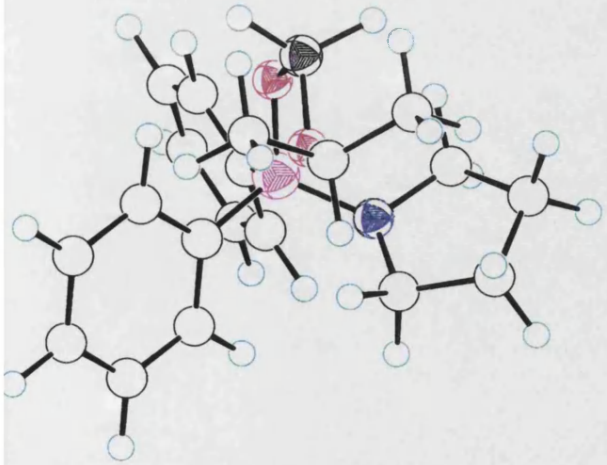

npo-12

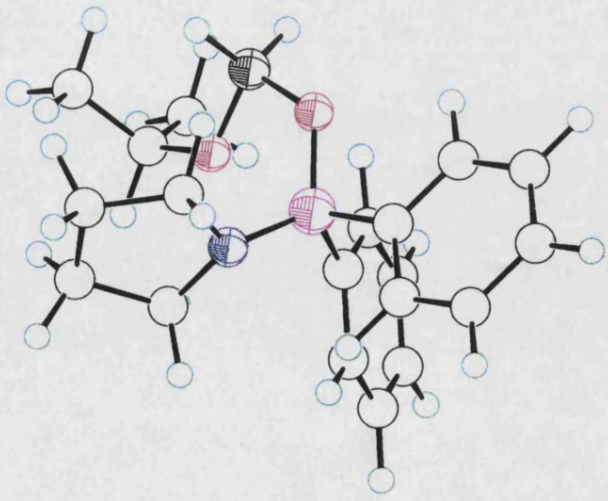

Table 9-6: The changes in the energetics (kcal mol^{-1}), geometry (Å) and charge distribution arising from bond rotation and formation of B-O_c bond

	npo-8	**npo-9**	**npo-10**	**npo-11**	**npo-12**
ΔH_f	-150.36	-149.74	-151.27	-149.45	-184.97
ΔH_{rel}[a]	-23.51	-22.89	-24.42	-22.26	-58.12
P-O_p	1.791	1.792	1.766	1.751	1.558
P-O_c	1.644	1.645	1.660	1.691	2.438
B-O_c	3.448	3.306	2.822	2.302	1.503
q(P)	1.84	2.06	0.58	0.77	1.62
q(H)[b]	-0.14	-0.14	-0.13	-0.12	-0.03
q(B)	0.24	0.29	0.23	0.25	-0.20

[a] Enthalpy relative to **npo-0** [-30.18] + borane-THF [-47.66] + MeCOMe [-49.01] = -126.85 kcal mol^{-1}; [b] Averaged over the remaining two hydrogens.

During these transformation the P-O_p interaction increased in double-bond character, which resulted in a decrease in electron density at phosphorous. Comparing the charges between **npo-12** and **npo-3a**, it was noted that phosphorus was less Lewis acidic (1.62 *versus* 1.85) and remaining hydrogens were only weakly nucleophilic (-0.02 *versus* -0.11).

The preference for the boron and the oxygen O_c interaction after hydride transfer posed the question of whether the proposed six-membered TS was correct. Attempts were made to locate a four-membered ring TS (figure 9-8) comprising of B-H_t-C_c-O_c, in which the only role of the phosphinamide was to polarise the borane moiety.

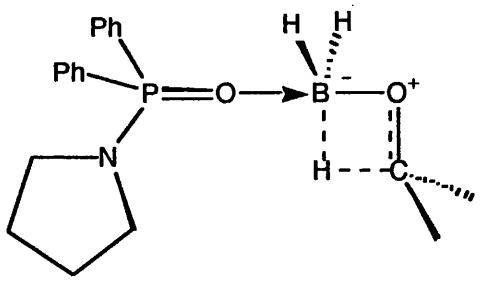

Figure 9-8

Despite the preference found for the B-O_c bond after hydride transfer, the more strained hydride transfer TS could not be located.

Experimental observations indicated that a second hydride transfer occurred. As no attempt had been made in the experiment to prevent this transfer from occurring, the second hydride transfer was also investigated in this modelling study. Whilst this step was not likely to be rate limiting, its investigation would provide insight into whether the second hydride transfer would result in a lowering of selectivity.

9.3 The Addition of a Second Ketone

As with the addition of the first ketone, structures containing either a long range or a short range interaction between phosphorus and the sp^2-hybridised oxygen were located. The barrier to the addition of the second molecule of acetone was 13.39 kcal mol^{-1} ($\upsilon^{\ddagger} = 246i\ cm^{-1}$), approximately 5 kcal mol^{-1} higher than the barrier for the co-ordination of the first ketone. This higher barrier was a result of the decreased Lewis acidity of the phosphorous.

The ball-and-stick representations of the long range complex, **npo-13**, the TS, **npo-14**, and the short range complex, **npo-15**, are shown on the next page (the THF molecule has been removed for clarity).

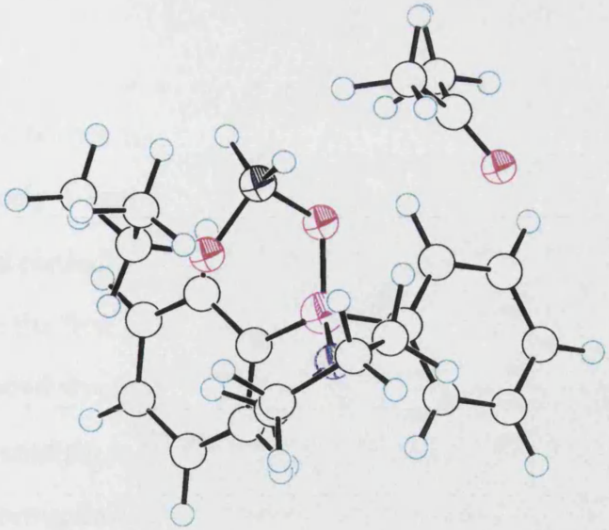

npo-13

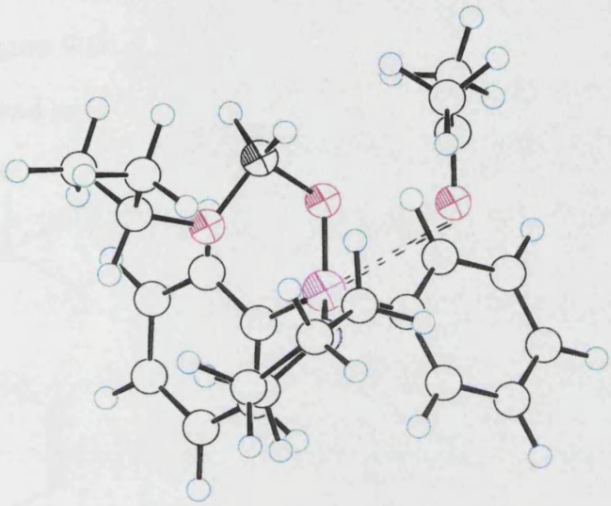

npo-14

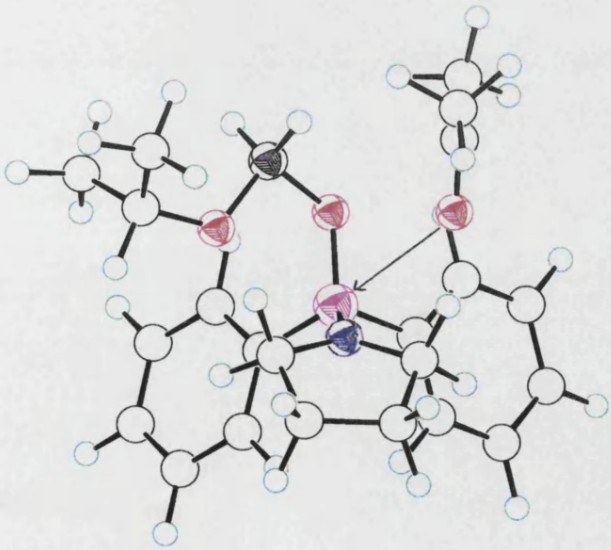

npo-15

The barrier to hydride transfer was 16.40 kcal mol^{-1} ($\upsilon^{\ddagger}$ = 455*i* cm^{-1}), approximately 4 kcal mol^{-1} higher than the first hydride transfer. Whilst this was mainly as a consequence of the reduced nucleophilicity of the hydride, the TS was 'later' than the first hydride transfer TS as reflected by the Pauling bond order for the B-H_t bond **n** = 0.39 *versus* 0.49.

In contrast to the OAB systems, the second hydride transfer TS was higher than the corresponding TS for ketone co-ordination. This implied that the second hydride transfer would not adversely affect the optical purity of the product.

Figure 9-9 provides a schematic for the conversion of **npo-13** through to **npo-17**, and table 9-7 summarises the important changes.

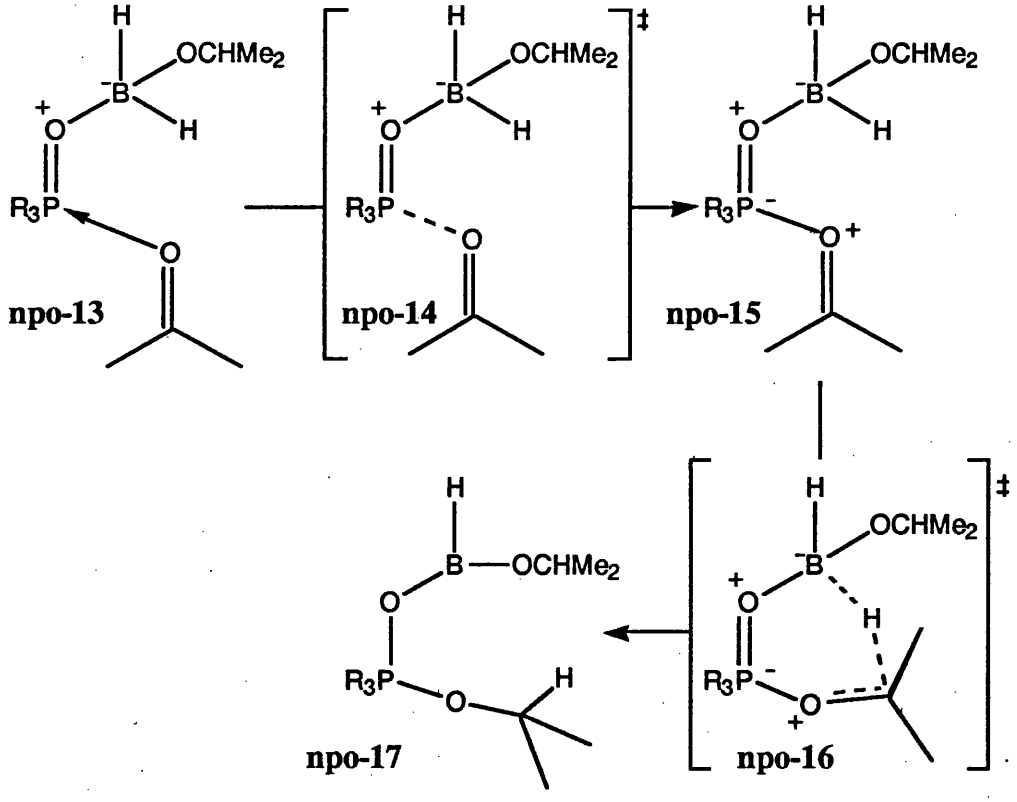

Figure 9-9

The ball-and-stick representations of **npo-16** and **npo-17** are shown on the next page.

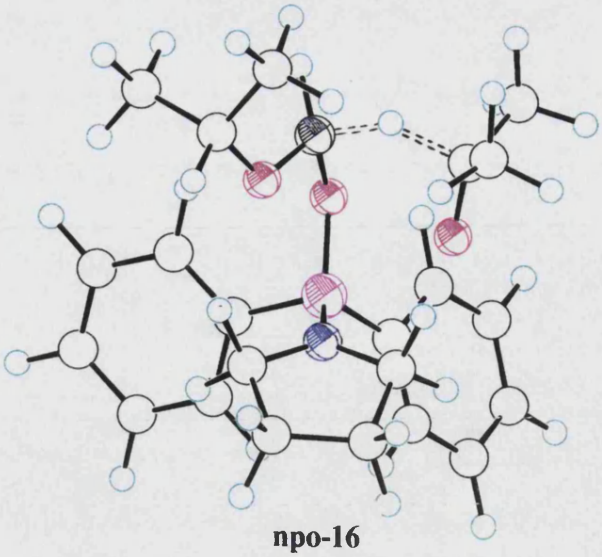

npo-16

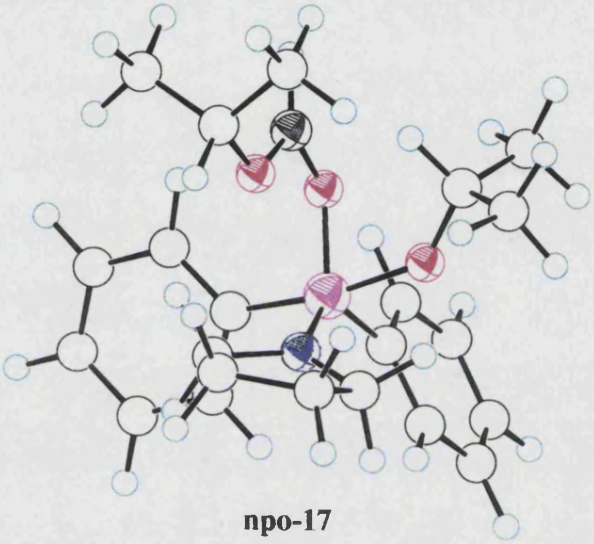

npo-17

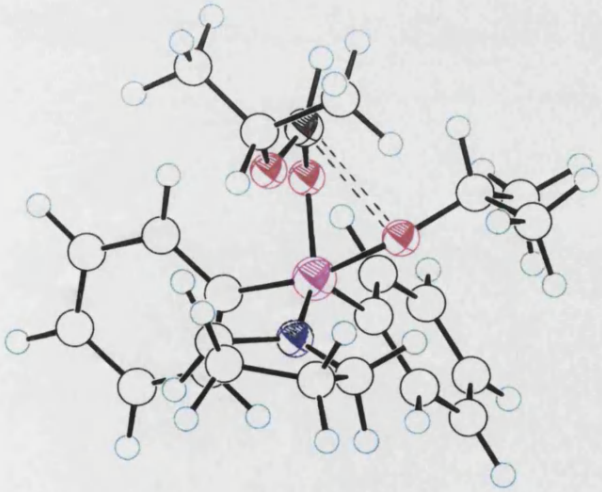

npo-18

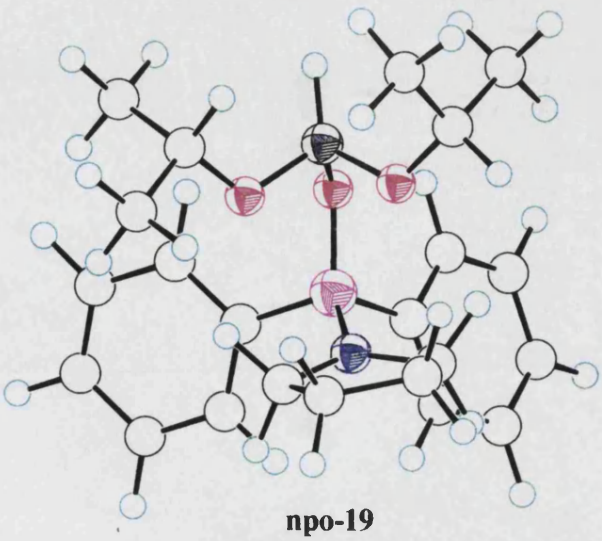

npo-19

Table 9-7: The energetic (kcal mol^{-1}) and geometrical changes (Å) arising from the binding of and hydride transfer to a second molecule of acetone

	npo-13	**npo-14**	**npo-15**	**npo-16**	**npo-17**
ΔH_f	-238.14	-224.75	-226.82	-210.42	-228.37
ΔH_{rel} [a]	-62.28	-48.89	-50.96	-34.56	-52.51
$P\text{-}O_{c(n)}$	4.965	2.908	2.649	2.393	1.741
$O_{c2}\text{-}C_{c(n)}$	-	-	1.242	1.303	1.388
$C_{c(n)}\text{-}H$	-	-	2.613	1.382	1.136
$H_t\text{-}B$	-	-	1.212	1.373	3.300
$B\text{-}O_p$	-	-	1.483	1.398	1.321
$O_p\text{-}P$	-	-	1.560	1.593	1.689

[a] Enthalpy relative to **npo-0** [-30.18] + borane-THF [-47.66] + 2 MeCOMe [-98.02] = -175.86 kcal mol^{-1}

As with the first hydride transfer, transfer of the alkoxy group from the phosphorus to boron led to a more stable minimum. Rotation about the $P\text{-}O_p$ bond was not needed prior to forming the $B\text{-}O_{c(n)}$ bond (figure 9-10). The barrier to bond formation was 2.03 kcal mol^{-1} ($\upsilon^{\ddagger} = 178i\ cm^{-1}$).

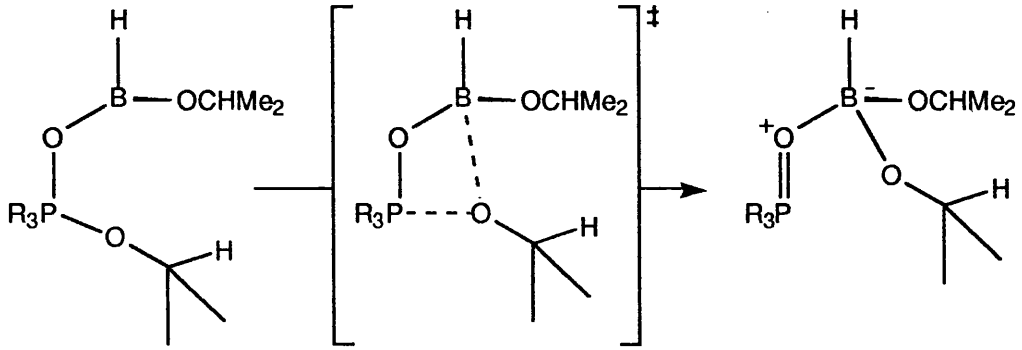

Figure 9-10

The ball-and-stick representations of **npo-18** and **npo-19** were shown on the previous page with those of **npo-16** and **npo-17**. The important structural and energetic changes associated with $B\text{-}O_c$ bond formation are summarised in table 9-8.

Table 9-8: The energetic (kcal mol^{-1}) and geometrical changes (Å) associated with the formation of a B-O_c bond

	npo-17	**npo-18**	**npo-19**
ΔH_f	-228.37	-226.34	-264.84
ΔH_{rel} [a]	-52.51	-50.48	-88.98
P-$O_{c(n)}$	1.741	1.776	2.586
P-O_p	1.689	1.686	1.566
O_p-B	1.321	1.331	1.458
B-$O_{c(n)}$	2.918	2.402	1.481

[a] Enthalpy relative to **npo-0** [-30.18] + borane-THF [-47.66] + 2 MeCOMe [-98.02] = -175.86 kcal mol^{-1}

The P-O_p bond increased in double-bond character. The remaining hydrogen on boron was found to be electron deficient, 0.20, making a third hydride transfer unlike, a postulate supported by experimental observations.

9.4 Regeneration of the Catalyst

As subsequent hydride transfers proved unlikely due to the electrophilic nature of the remaining hydride, any subsequent steps had to lead to the regenerated catalyst. Whilst the addition of a third ketone was possible, this was not envisaged to cause the removal of the dialkoxyborane species from the catalyst.

In order to achieve this cleavage, the introduction of a second borane-THF moiety was considered. Study of the charge distribution with in **npo-19** revealed that the former sp^2-hybridised oxygens and the phosphinamide oxygen were electron rich, O_c = -0.17, $O_{c(n)}$ = -0.11 and O_p = -0.03. This implied that the co-ordination of the borane-THF was favoured at O_c.

Although the reaction profile for O_c-B_n bond formation identified a maximum, refinement of the structure resulted in the location of a structure with only a long-range O_c-B_n interaction.

Optimisation of the maximum on the profile for the approach of the second moiety of the borane-THF to the phosphinamide oxygen, indicated that the barrier to this process (figure 9-11) was 5.45 kcal mol^{-1} (TS O_p-B = 1.774 Å, $\upsilon^{\ddagger}$ = 155*i* cm^{-1}).

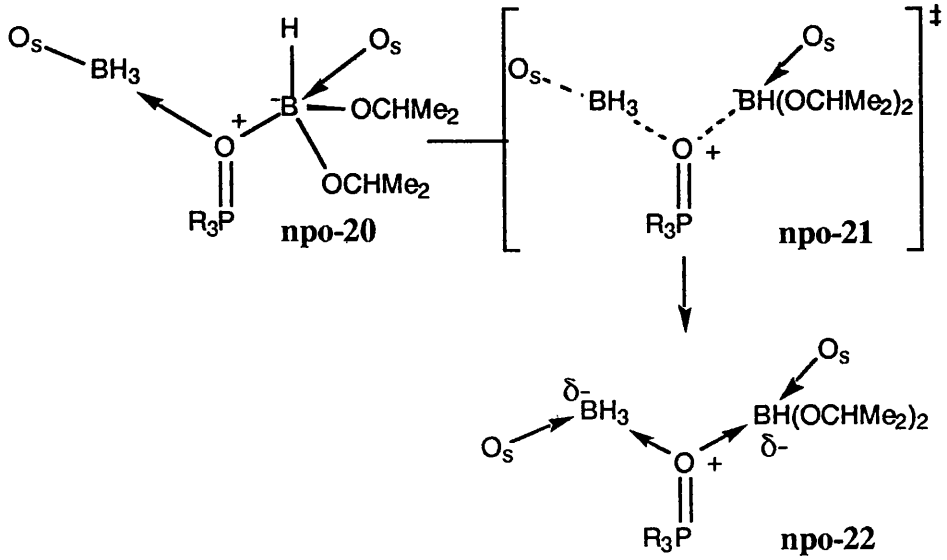

Figure 9-11

The ball-and-stick representations of these species are shown on the next page. The hydrogens of the THF associated with the original boron have been removed, so this THF can be distinguished from the one associated with borane-THF.

The reverse IRC from the TS did not locate a complex with long-range interaction O_p-B_n. The bond distance was 2.131 Å, compared to 1.659 Å for the structure proceeding the TS.

A reaction co-ordinate calculation, in which the bond length was increased from 2.131 in 0.2 Å steps up to 4 Å, revealed that energy decreased with increasing bond length. The energy at O_p-B_n = 4 Å was -312.50 kcal mol^{-1}, equal to **npo-19** [-264.84 kcal mol^{-1}] plus borane-THF [-47.66 kcal mol^{-1}].

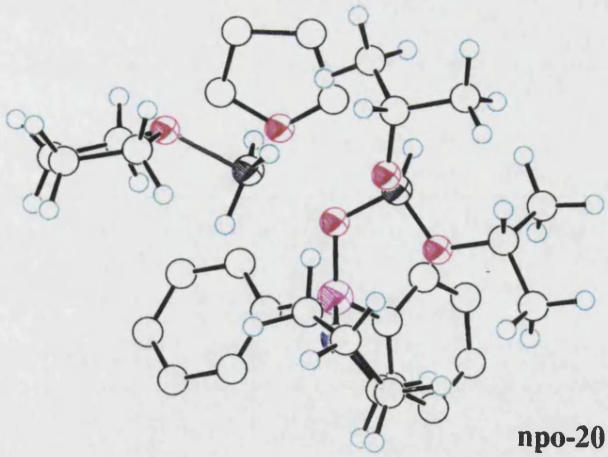

npo-20

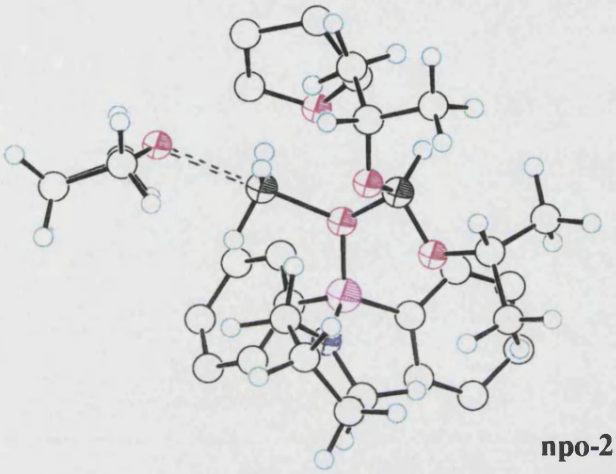

npo-21

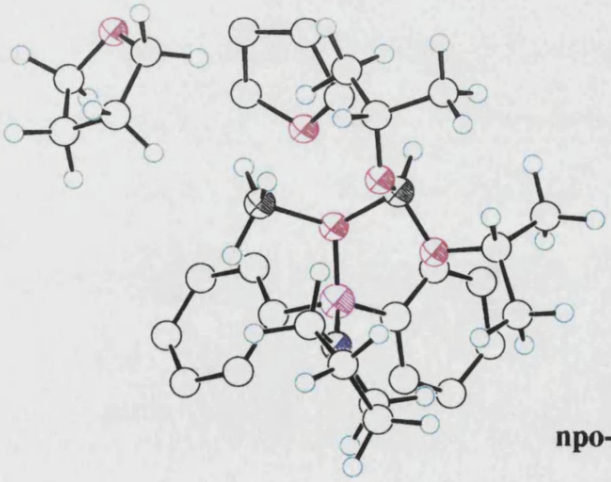

npo-22

The important energetic and structural changes for the conversion of the weaker complex **npo-17**, *via* the TS **npo-18**, to the complex with a stronger O_p-B_n interaction **npo-19** are summarised in table 9-9.

Table 9-9: The energetic (kcal mol^{-1}) and geometrical changes (Å) arising from the binding of a second BH_3.THF to the phosphinamide oxygen

	npo-20	**npo-21**	**npo-22**
ΔH_f	-308.01	-307.05	-314.82
ΔH_{rel} [a]	-84.49	-83.53	-91.30
O_p-B	1.507	1.575	1.639
O_p-B_n	2.131	1.774	1.659
B_n-O_s	1.905	2.292	4.881

[a] Enthalpy relative to **npo-0** [-30.18] + 2 borane-THF [-95.32] + 2 MeCOMe [-98.02] = -223.52 kcal mol^{-1}

The specific solvent interaction found in borane-THF was converted in a mechanism akin to an S_N2 reaction to a weak, non-specific interaction in **npo-22.**

Passage over the barrier of 4.49 kcal mol^{-1} ($\upsilon^{\ddagger}$ = 225*i* and 3.5*i* cm^{-1}) for the cleavage of the O_p-B bond led to a structure whose energy was equal to the sum of **npo-3a** and diisopropoxyborane-THF complex (figure 9-12). Further refinement of the TS, **npo-23**, failed to remove the small imaginary frequency, but this was not considered to be significant.

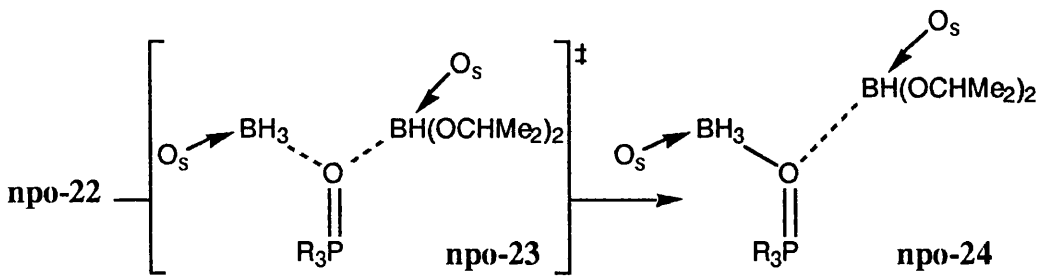

Figure 9-12

The ball-and-stick representations of these species are given on the next page.

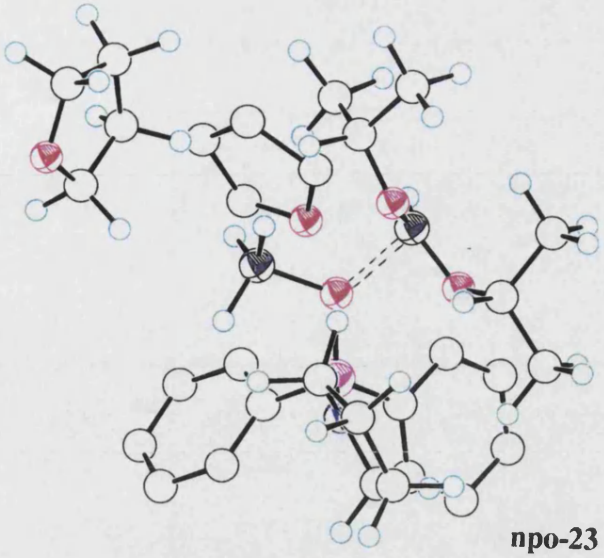

npo-23

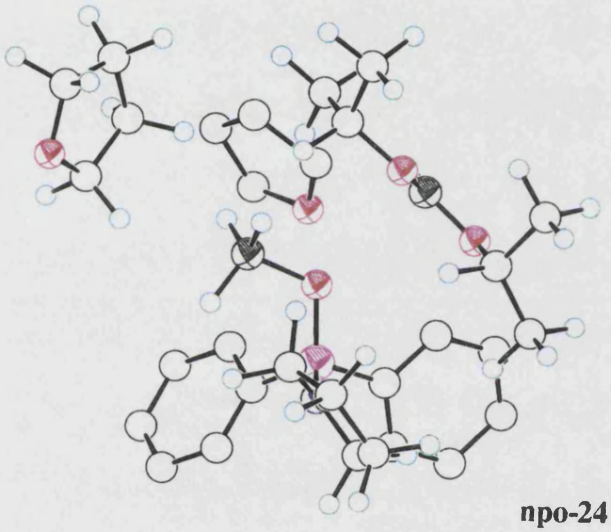

npo-24

The energetics and geometry for the final steps of this mechanism are given in table 9-10.

Table 9-10: The energetic (kcal mol^{-1}) and geometrical changes (Å) arising from the regeneration of the phosphinamide-borane adduct

	npo-22	**npo-23**	**npo-24**
ΔH_f	-314.82	-310.33	-324.19
ΔH_{rel} [a]	-91.30	-86.81	-100.67
O_p-B	1.639	1.938	3.085
O_p-B_n	1.659	1.574	1.529

[a] Enthalpy relative to **npo-0** [-30.18] + 2 borane-THF [-95.32] + 2 MeCOMe [-98.02] = -223.52 kcal mol^{-1}

9.5 Discussion of the Mechanism

This investigation revealed that the phosphinamide-borane complex **npo-3a** was the start-and-finish complex for a possible reduction mechanism. The lower barrier for the co-ordination of borane-THF to the phosphinamide compared to that for binding the ketone implied that in a competition reaction the formation of the borane adduct would be favoured. This explained the experimental observation that the order of the addition of the hydride source and the ketone did not affect the observed induction.

To compare the energetic changes during one catalytic turnover, the enthalpies relative of all the structures were calculated with respect to a chose baseline: **npo-3a** [-100.05], two molecules of acetone [-98.02] and one molecule of borane-THF [-47.66], the total energy being -245.73 kcal mol^{-1}. The relative enthalpies for all the species on the catalytic pathway are given in table 9-11 and plotted in figure 9-13. The reduction of acetone by the OAB-borane adduct proceeding *via* the chair conformer for the hydride transfer is also shown in figure 9-13, the reference point being the same as in chapter 4, table 4-16.

Table 9-11: The relative energetics (kcal mol^{-1}) for one catalytic turnover

Structure	npo-4a	npo-5a	npo-6	npo-7	npo-8	npo-9	npo-10
ΔH_{rel}	-3.24	9.22	7.18	19.94	0.05	0.07	-0.86
Structure	npo-11	npo-12	npo-13	npo-14	npo-15	npo-16	npo-17
ΔH_{rel}	0.96	-34.56	-38.72	-25.33	-27.40	-11.00	-28.95
Structure	npo-18	npo-19	npo-20	npo-21	npo-22	npo-23	npo-24
ΔH_{rel}	-26.92	-65.43	-60.94	-59.98	-67.75	-63.25	-77.11

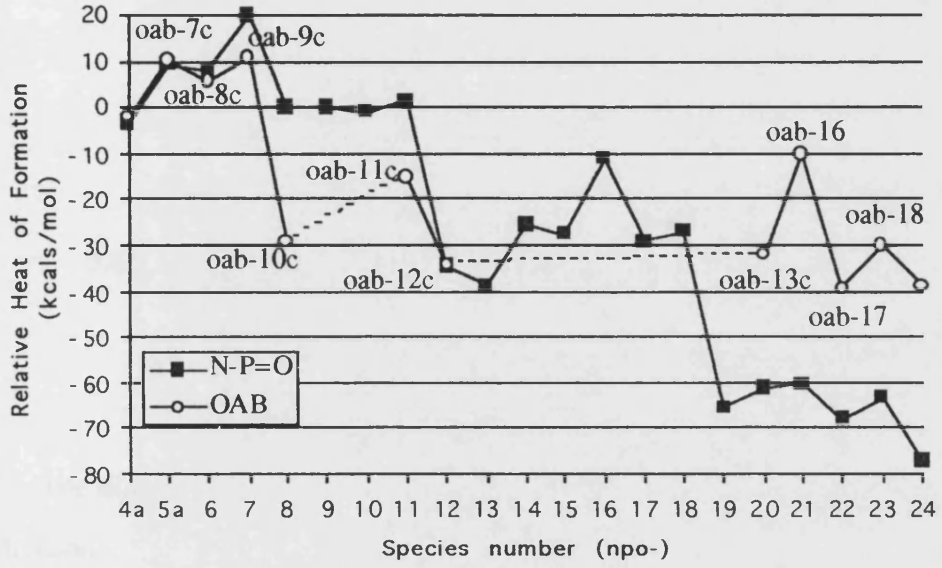

Figure 9-13

A larger rate enhancement occurred with the OAB-borane adduct than the NPO-borane adduct. The 9 kcal mol^{-1} energy difference between the two hydride transfer TS can be attributed to the transfer occurring later for the NPO system, figure 9-14.

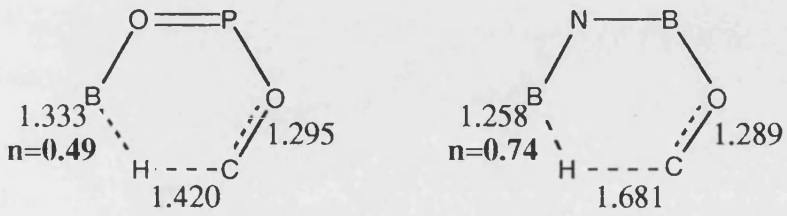

Figure 9-14

Both transition states were divided into two fragments, one representing the dipolar P=O or N-B bond and the other, a 'distorted' uncatalysed reduction of the ketone (figure 9-15). The charge distribution of each fragment was calculated. Note: the TSs had been re-optimised without THF molecules as the NPO system had one THF molecule whereas the OAB system had two.

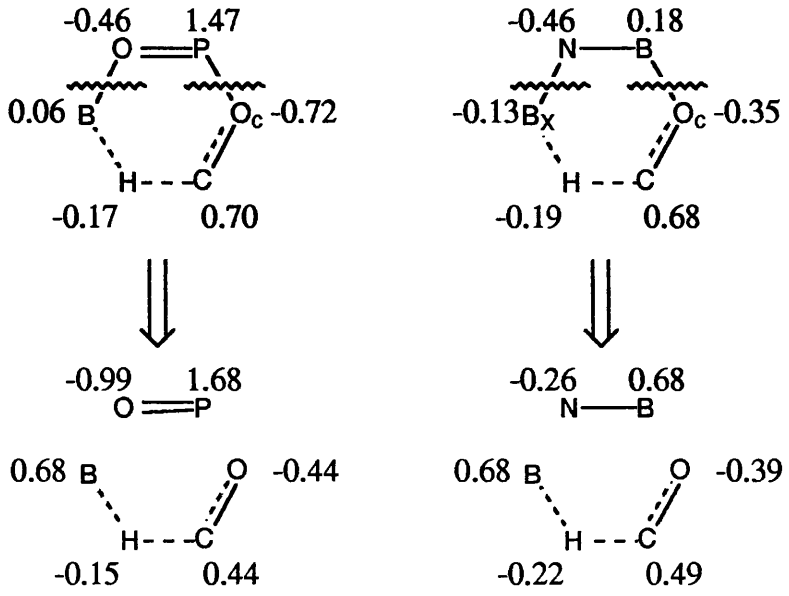

Figure 9-15

The dipolar interaction present in the OAB system provided better charge stabilisation. This was reflected by the lower electron density associated with the sp^2-oxygen O_c and the higher electron density on boron B_x. This provided insight into the later TS for the NPO system.

Although the phosphorus was electron deficient, it was possible that the ketone was hindered from binding by the presence of the bulky phenyl groups attached to phosphorous.

To address this issue, the hydride transfer TS shown in figure 9-16 were located. Note: the specific interaction between THF and boron were not included. It was anticipated that the barrier height would increase with the removal of the nitrogen substituent α-to phosphorous.

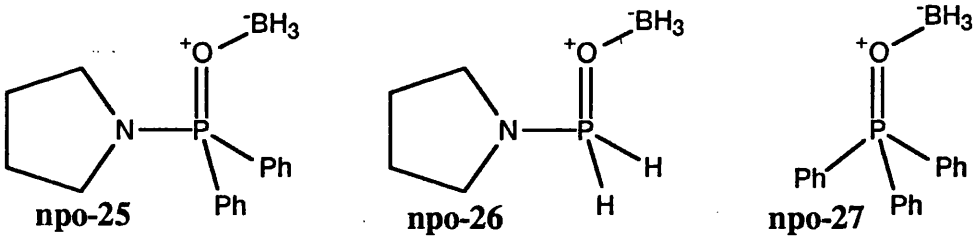

Figure 9-16

The barrier to hydride transfer was calculated by comparing the enthalpy difference between the relevant borane adduct and acetone with the hydride transfer TS. The difference in enthalpy and the interactions between the phosphorus and the carbonyl oxygen are noted in table 9-12.

Table 9-12: The energetic (kcal mol^{-1}) and geometrical changes (Å) associated with the hydride transfer from three different adducts

	npo-25	**npo-26**	**npo-27**
ΔH_f	-69.66[b]	-107.81[c]	-31.62[d]
ΔH_{rel}[a]	18.20	7.11	20.59
$P\text{-}O_c$	2.447	2.184	2.354

[a] Enthalpy relative to MeCOMe [-49.01] + appropriate borane adduct [**npo-25** = -69.66, **npo-26** = -65.91, **npo-27** = -3.20 kcal mol^{-1}], [b] $\upsilon^{\ddagger}$ = 389*i* cm^{-1}, [c] $\upsilon^{\ddagger}$ = 478*i* cm^{-1}, [d] $\upsilon^{\ddagger}$ = 452*i* cm^{-1}.

The presence of phenyl groups, **npo-26** *versus* **npo-25**, clearly weakened the interaction between the catalyst and the ketone, but this was not just due to steric factors alone. In **npo-25** the phosphorus was a weaker Lewis acid than in **npo-26**, as indicated by the charges: 1.85 *versus* 2.90. Therefore donation from the oxygen of the ketone was less favoured.

Contrasting the hydride transfer TSs (figure 9-17) derived from **npo-25** and **npo-27** revealed that the nitrogen substituent enhanced the rate by increasing the polarity of B-H bond.

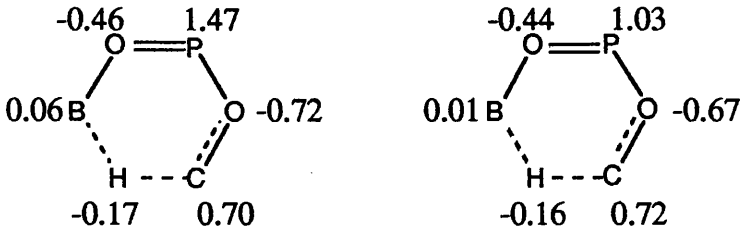

npo-25 **npo-27**

Figure 9-17

The presence of the nitrogen substituent also reduced the Lewis acidity of the phosphorus which explained the weaker P-O_c interaction.

9.6 Conclusion

Whilst phosphinamide systems were found to be excellent catalysts, enantiocontrol was hindered by the weak interaction between catalyst and ketone. The role of the phosphinamide was to polarise the borane moiety, which increased the nucleophilicity of the hydride source and thus increasing the rate of reaction.

About the time these conclusions were reached, the same conclusions had been obtained by the experimental observations of Wills and co-workers.[62] As their attentions were now focused on the use of phosphinamide-dioxoborolidines systems, a brief investigation of the ketone binding TS and the hydride transfer TS were made.

9.7 Phosphinamide-dioxoborolidines systems

The initial system to be studied was **npo-28**, a dioxoborolidine. The addition of borane to a solution of npo-28 would yield two borane adducts (figure 9-18).

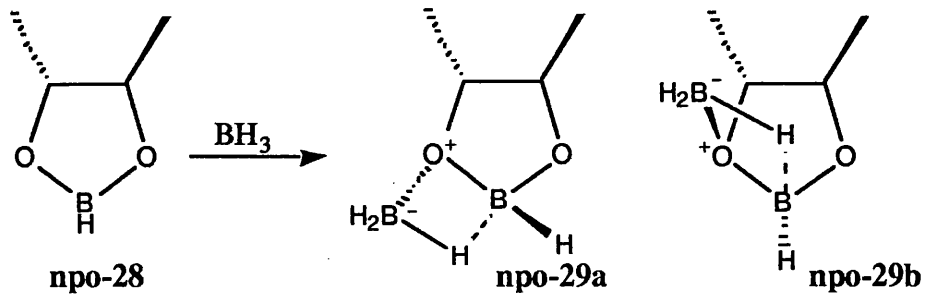

npo-28 **npo-29a** **npo-29b**

Figure 9-18

The borane adduct **npo-29b** was about 6 kcal mol^{-1} more stable than **npo-29a.**

Of the eight possible conformers for hydride transfer, the 'chair S' diastereomer with the trans-borane adduct, **npo-29b**, was the most stable, and 2.05 kcal mol^{-1} more stable than the ketone binding TS. This implied that the ketone binding TS was the rate determining step.

The weak interaction between the ketone and the catalyst in the rate determing step implies that it will not be possible to exert significant enantiocontrol with the combined phosphinamide-dioxoborolidine system, shown in figure 9-19.

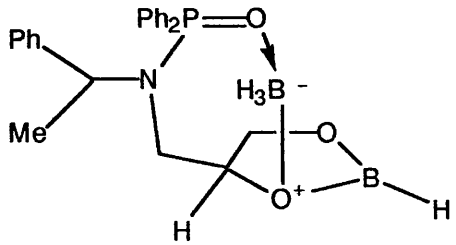

Figure 9-19

If possible to synthesise, it would be interesting to see if a phosphinamide-oxazaborolidine system is a superior catalyst to the normal OAB system. This could enhance the rate of an already proven, highly selective catalyst.

Chapter 10: The Use of Diethylzinc as an Alkylating agent: A Review of the Literature

Alkylation of an aldehyde provides a complementary route to the reduction of a ketone for the formation of secondary alcohols. This method may create a chiral centre during the formation of the carbon skeleton of the alcohol. This is often achieved by the use of organometallic reagents, such a methyl magnesium or methyl lithium.

The use of organozinc chemistry had been limited as the reaction rates were very slow and often unwanted side reactions occurred. The applicability of dialkylzinc chemistry to alkylation reactions was expanded by the use of chiral auxiliaries which enhance the reactivity at the same time as controlling the stereochemical outcome of the reaction. This methodology is known as *ligand accelerated control.*

10.1 The Use of Chiral Amino Alcohols as Catalysts

Mukaiyama determined that a chiral diamino alcohol (figure 10-1) could be used in conjunction with alkyl lithium and dialkyl magnesium species to yield optically pure alcohols in greater than 90% enantiomeric excess.[63] Whilst the combination of this ligand with diethylzinc did result in a rate enhancement, no stereocontrol was exhibited.[64]

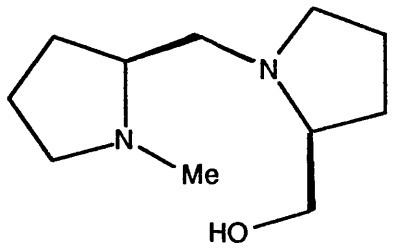

Figure 10-1

The first highly enantioselective addition of diethylzinc to aldehydes was achieved by Noyori and co-workers (figure 10-2).[65] The camphor-derived, (-)-3-*exo*-(dimethyl-amino)isoborneol, [(-)-DAIB], catalysed the alkylation of benzophenone to yield (1)-phenyl-propan-1-ol in 98% (R) e.e.

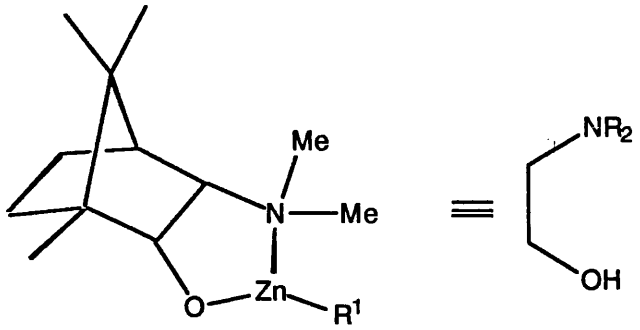

Figure 10-2

The system worked equally well for other aromatic aldehydes, but only gave moderate enantioselectivity in additions to aliphatic aldehydes, typically about 61% e.e.

Whilst most catalysts have contained two zinc atoms,[66] the use of an alternative Lewis acidic site has also been studied. Corey[67] stated that as long as the six-membered ring assembly could be formed, the catalysts would impart the required control. On this basis the lithium complex shown in figure 10-3 was synthesised.

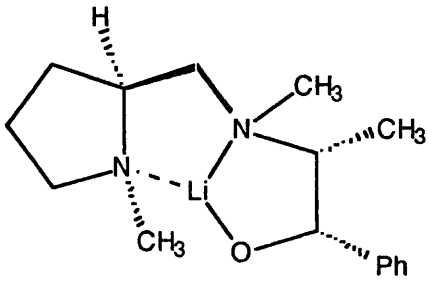

Figure 10-3

10.2 The Use of Oxazaborolidines as Chiral Catalysts

As with the reduction of prochiral ketones, oxazaborolidines have been used in alkylation reactions. Brown and co-workers[68] studied the complexes formed between ephedrine and zinc, aluminium, lithium and boron, as shown in figure 10-4.

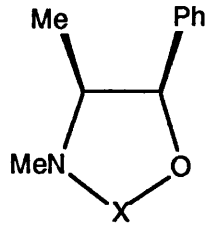

X = Zn, Al, Li, B

Figure 10-4

The catalyst which had incorporated boron exhibited a higher degree of enantioselectivity: alkylation of benzophenone occurred in 86% (R) e.e. with the boron catalyst, 58% for the aluminium catalyst, 70% for lithium and 71% for zinc.

As the structure had not been determined, it was assumed that the metals were bound in the same position, namely between the nitrogen and oxygen of ephedrine. Working on this premise, the superiority of the boron catalysts was attributed the shorter B-O and B-N bonds than the other metal-O and -N interactions.

Both the selectivity and the rate decreased with increasing substitution on boron. It was postulated that the diethylzinc was co-ordinated to either the nitrogen or oxygen of the oxazaborolidine ring. Whilst the system worked well for aromatic aldehydes, the results for the aliphatic aldehydes were less successful.

Brown noted that unlike the organozinc catalysts, no precatalyst-catalyst equilibrium existed, and a linear relationship between the optical purity of the catalyst and the e.e. of the product was found.

Caze and co-workers[69] recently tried to improve the scope of this catalyst by using a polymeric support which was bound to the catalyst *via* the boron atom.

Whilst their results found that a polymeric support did not enhance the selectivity, they noted that the enantioselectivity was dependent on the nitrogen substituent. Without a polymeric support, altering the nitrogen substituent from methyl to hydrogen decreased the level of induction from 75 to 62% e.e.

10.3 The Proposed Mechanism for Catalysis by Chiral Amino Alcohols

Noyori proposed the mechanism shown in figure 10-5.[70]

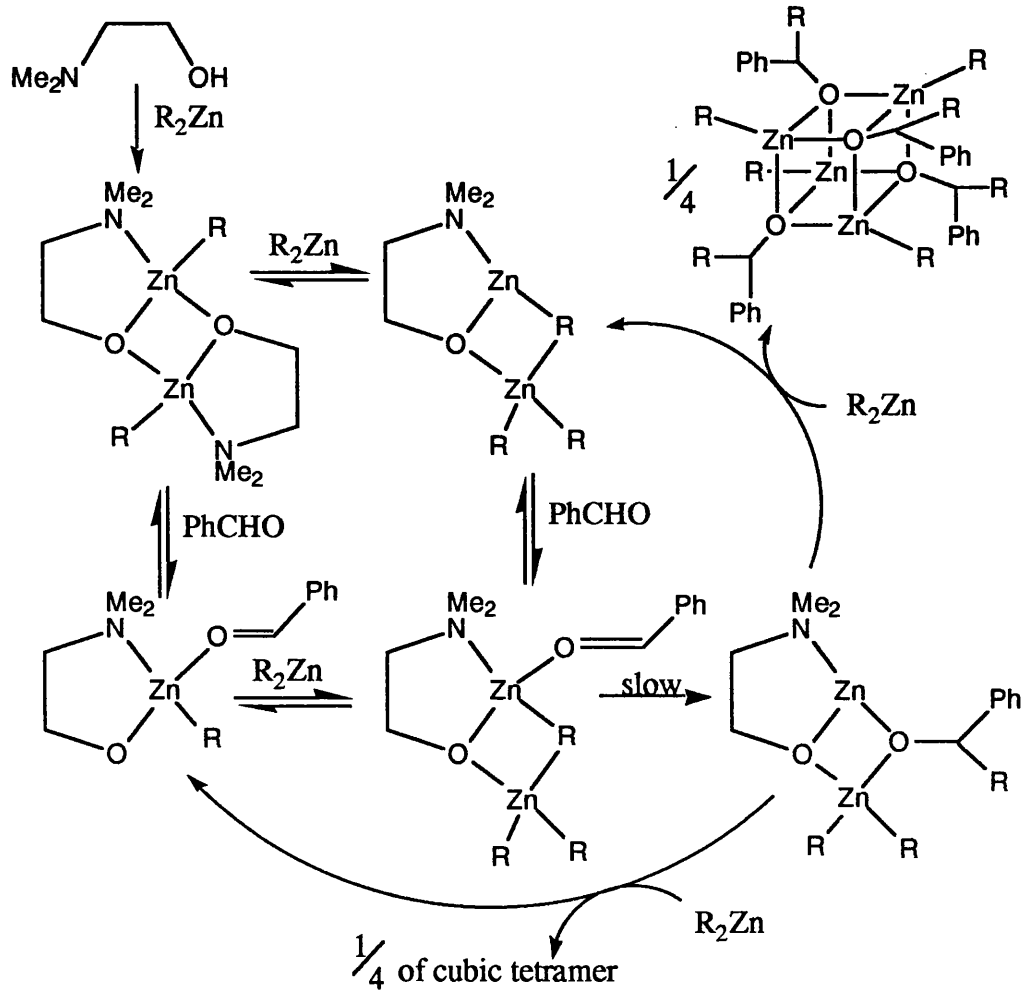

Figure 10-5

Different groups have proposed a variety of transition structures for the alkyl transfer. Noyori and co-workers[70] proposed that was aldehyde bound to the more Lewis acidic *endo*-zinc (figure 10-6) which resulted in an increase of the

electrophilicity of the sp^2-hybridised carbon centre. The bridging alkyl group, rather than one of the alkyl groups attached to the *exo*-zinc, was then transferred.

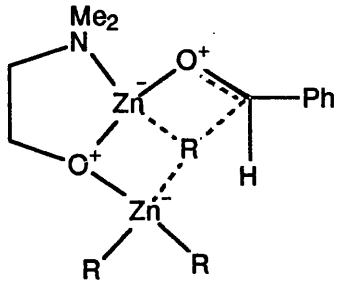

Figure 10-6

The concept of the transfer of a tri-coordinated alkyl group was supported by the findings of Houk and co-workers.[71] In their *ab initio* calculations on the addition of methyl lithium to formaldehyde they found that the an early TS (figure 10-7), with the trajectory of approach of the alkyl group being controlled by the lithium.

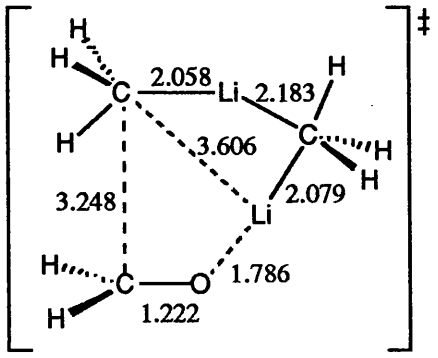

Figure 10-7

Itsuno and co-workers proposed that the mechanism involved transfer of one of the terminal alkyl groups,[72] (figure 10-8) an arrangement which was postulated by Mole for the reaction of trimethylaluminium with benzophenone.[73]

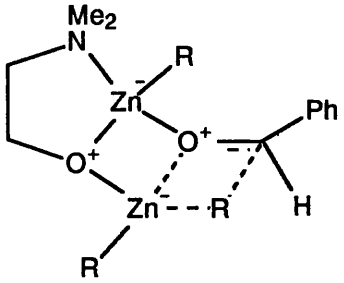

Figure 10-8

A similar arrangement was proposed by Corey and Hannon,[74] the only difference being that transfer occurred *via* a six-membered ring transition state as shown in figure 10-9.

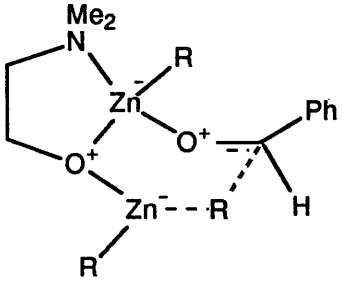

Figure 10-9

Soai's postulated mechanism[75] involved alkyl transfer from the *exo*- to the *endo*-zinc (figure 10-10) followed by co-ordination of the aldehyde co-ordination to the *exo*-zinc which would be the more Lewis acidic site as the result of the alkyl transfer. The subsequent transfer of the alkyl group to the aldehyde was proposed to occur *via* a six-membered ring TS.

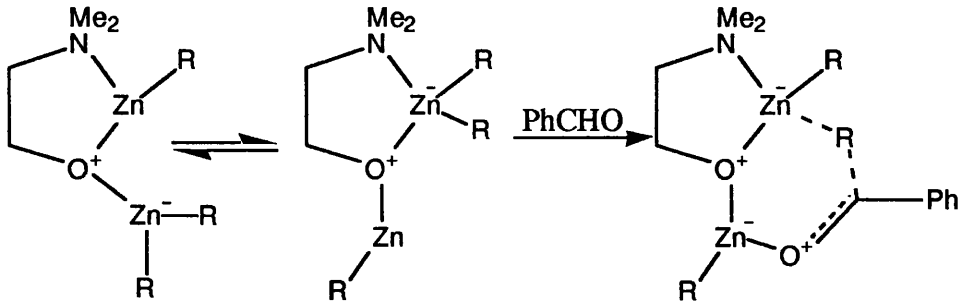

Figure 10-10

Analysis of by-products, together with these speculations concerning TS structure, represents the total experimental mechanistic investigation which has been performed on these systems to date. The main focus of attention has been on chiral

amplification by these catalysts,[76] for example, 15% e.e (-)-DAIB can yield products with 98% e.e.

Noyori first noted that the dependence of the e.e. of the alkylation product was non-linear with respect to the e.e. of the DAIB.[70]

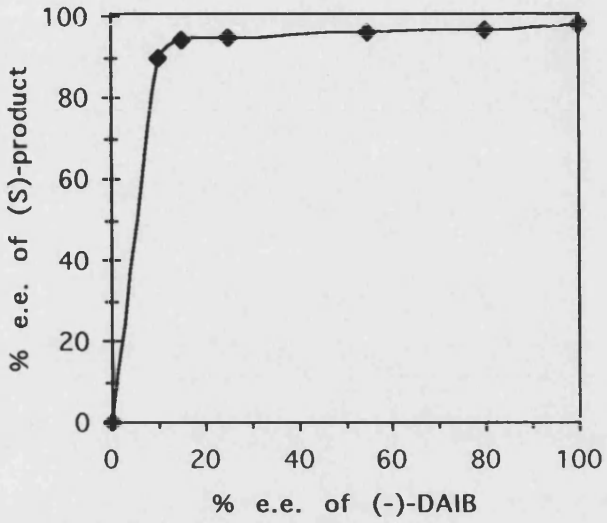

Figure 10-11

After careful investigation, Noyori found that a thermodynamic equilibrium (figure 10-12) existed between the various diastereoisomers.

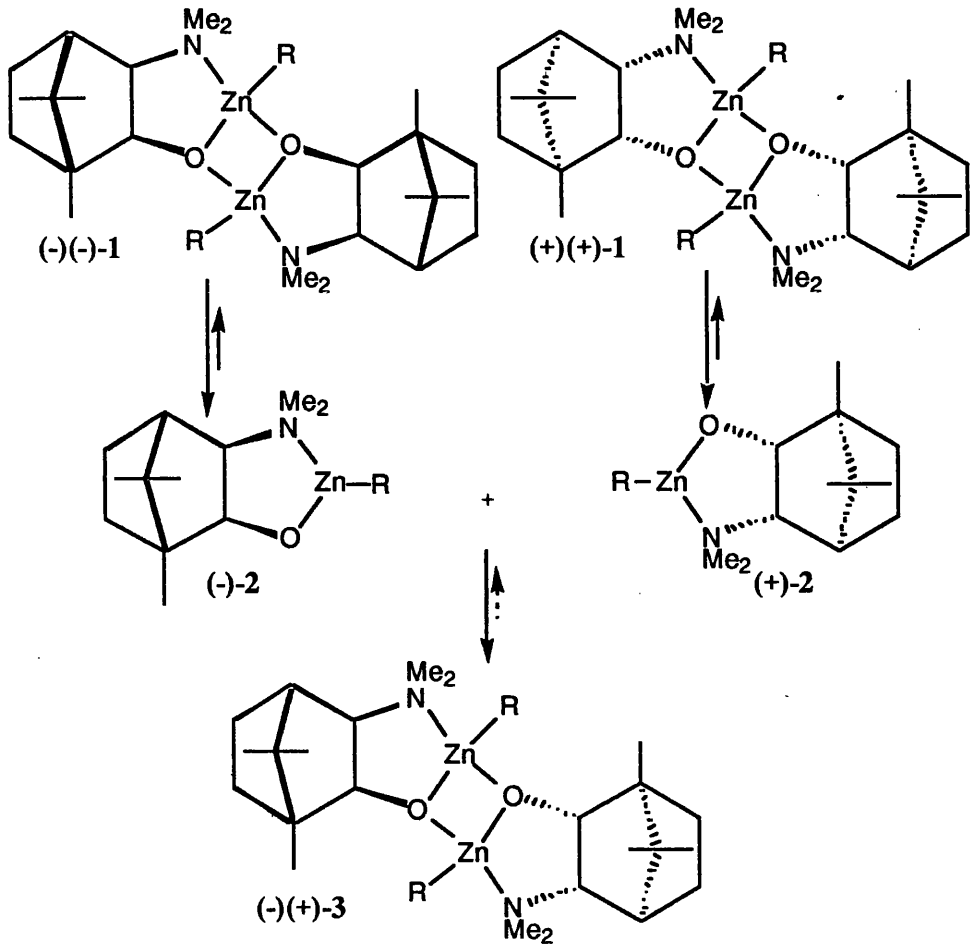

Figure 10-12

Both the major isomer (-)-2 and minor isomer (+)-2 of DAIB were found to be catalytic, but the minor isomer was removed from the cycle by combination with the major isomer to form a relatively stable dimeric (-)(+)-3 which did not catalyse the reduction. This complex was considerably more stable than either (-)(-)-1 or (+)(+)-1, which dissociate back to the reactive isomers.

So in a 15% e.e. solution of DAIB, there would be 42.5% of (+)-2 and 57.5% of (-)-2. All of (+)-2 and 42.5% of (-)-2 would be used to form the inactive *meso* complex and the remaining 15% of (-)-2 would act as the chiral catalyst.

Whilst this scheme explains the observed 'chiral amplification' it does not address the origins of the enantiocontrol exhibited by these catalysts, a subject has yet to be considered using a rational approach.

10.4 *Ab Initio* Study of the Catalysed Reaction of Dialkylzinc and Aldehydes

Yamakawa and Noyori[77] undertook an *ab initio* study on a cut-down model of DAIB to address the origins of the catalytic efficiency and chirality amplification. They performed full geometry optimisations at the Hartree-Fock level using a [8s4p2d]/(14s9p5d) basis for zinc and 3-21G for the remaining atoms. The energy was obtained *via* single point, second-order Møller-Plesset calculation using the same basis set for zinc as in the RHF calculations and 6-31G* for the other atoms. Dimethylzinc was used instead of diethylzinc, and formaldehyde was used to represent an aldehyde.

10.4.1 Forming the Ternary Methylzinc-formaldehyde-aminoalkoxide Adduct

Starting from dimethylzinc aminoalkoxide, which was planar about the ring zinc Zn_r, the formation of the ternary complex can be achieved by co-ordination of the aldehyde followed by the binding of the dimethylzinc, or *vice-versa*, as shown in figure 10-13.

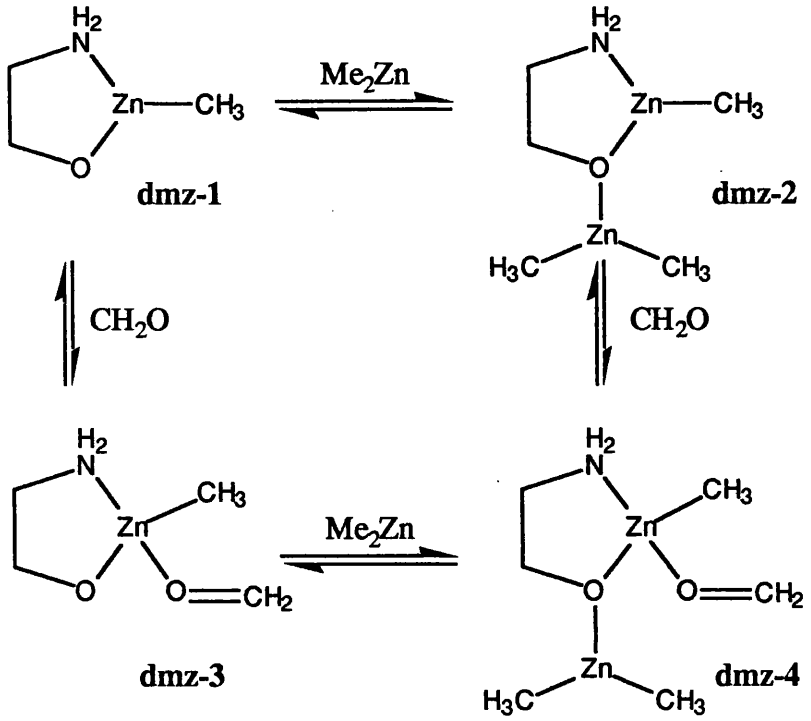

Figure 10-13

No TSs were found for these equilibria, but **dmz-4** was 26.6 kcal mol^{-1} lower in energy than a 1:1:1 mixture of **dmz-1**, dimethylzinc and formaldehyde. The amount of energy released at each step on the binding of the alkyl source and the aldehyde was dependent on the order, as shown in table 10-1.

Table 10-1: The energetics for binding dimethylzinc and formaldehyde to amino-alcohol zinc complex **dmz-1**

	Binding Me_2Zn	Binding OCH_2
dmz-1 → -2 → -4	-16.0	-10.6
dmz-1 → -3 → -4	-15.2	-11.4

The conformation adopted in **dmz-4** was similar to alkyl transfer TS proposed by Corey and Hannon.[74] The ternary complex **dmz-4'**, which resembled the TS proposed by Itsuno,[72] was 6.2 kcal mol^{-1} less stable than **dmz-4**. The conformations are shown in figure 10-14.

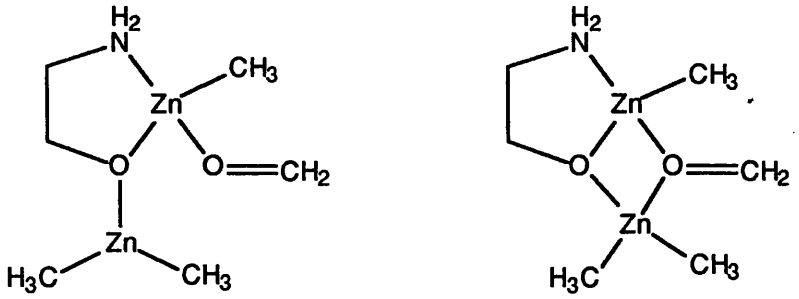

dmz-4 **dmz-4'**

Figure 10-14

In both **dmz-4** and **dmz-4'**, the O_c-C_c carbonyl bond was longer than in free formaldehyde and the distance between the *exo*-zinc Zn_x to methyl group had increased.

10.4.2 Alkyl Transfer

Three possible TSs (figure 10-15) were located for the formation of the 5/4-fused bicyclic product, **dmz-6**.

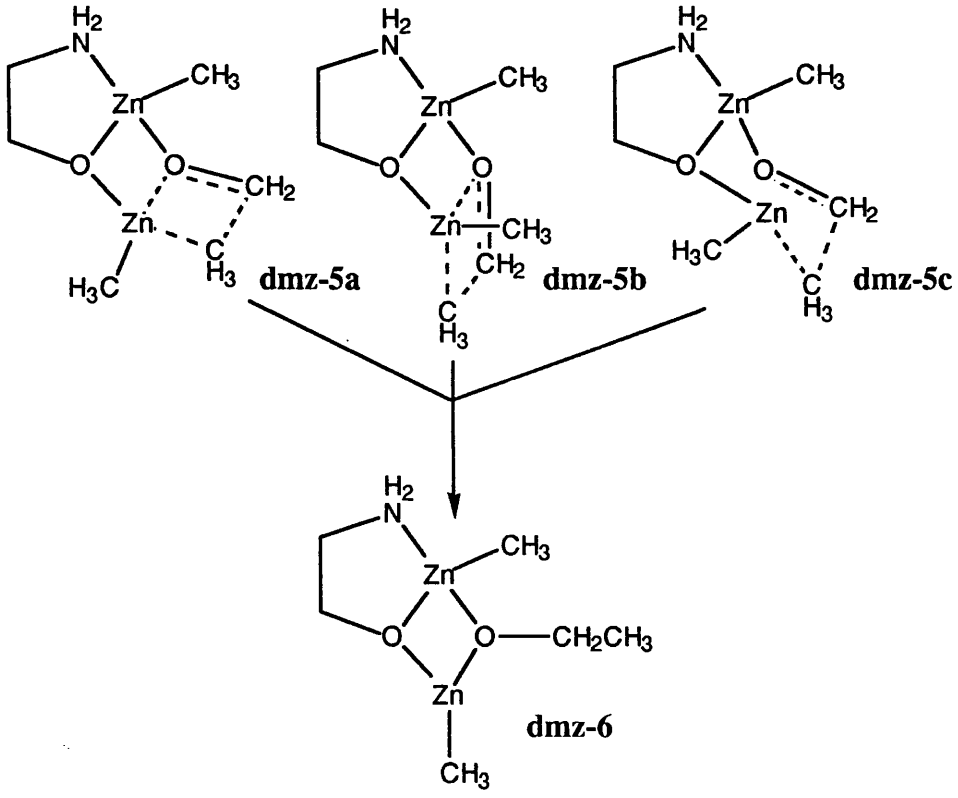

Figure 10-15

The barrier to alkyl transfer from **dmz-4** *via* **dmz-5a** was 12.4 kcal mol^{-1} and 15.3 kcal mol^{-1} *via* **dmz-5b**. Noyori noted that the methyl migration occurred with retention of stereochemistry. The interaction between the *exo*-zinc and the oxygen of the aldehyde was purely electrostatic in nature.

The chair conformer **dmz-5c** was higher in energy with the a 19.2 kcal mol^{-1} barrier for alkyl transfer. The methyl migration was predicted to occur with inversion of configuration. No simple boat-like or flat six-membered TS could be located.

To assess the key issue of the efficiency of the catalysis, the uncatalysed reaction between dimethylzinc and formaldehyde was studied. This reaction does not occur experimentally, a fact which Noyori attributed to the 29.2 kcal mol^{-1} activation barrier. The energetics of the uncatalysed reaction are summarised in figure 10-16.

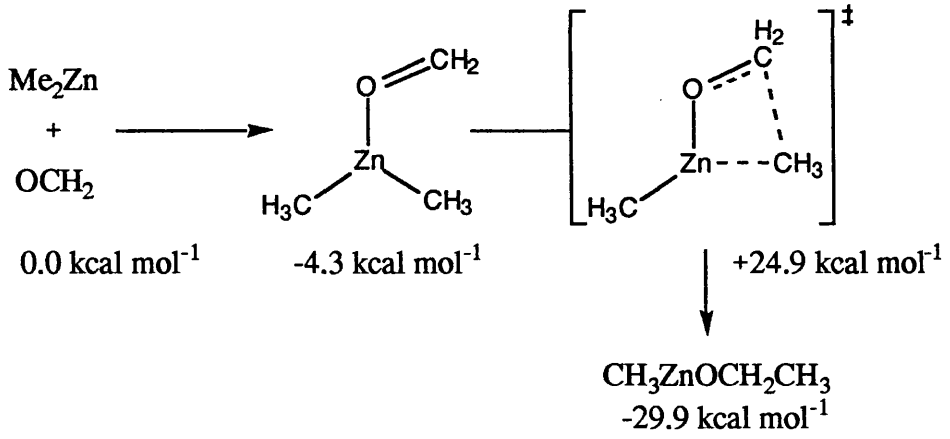

Figure 10-16

The activation barrier for the catalysed reaction was 12.5 kcal mol^{-1} lower than that of the uncatalysed reaction.

It was noted that whilst complex **dmz-1** was an excellent catalyst it could not act as the alkyl donor. The barrier for methyl transfer from the ring zinc was 32.2 kcal mol^{-1}.

10.4.3 The Regeneration Pathway

As with the formation of the ternary adduct, the regeneration was considered *via* two pathways, (figure 10-17) namely addition of dimethyl zinc to yield **dmz-2** or addition of formaldehyde to yield **dmz-3.**

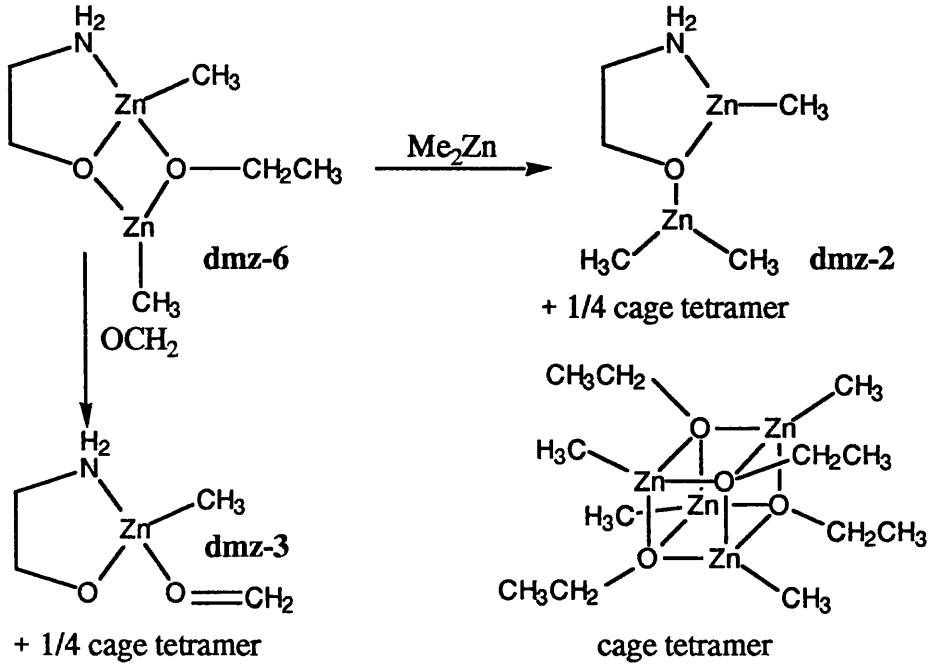

Figure 10-17

Both pathways produced a caged tetramer. The reaction with the dimethylzinc was exothermic by 5.5 kcal mol^{-1} compared to 10.0 kcal mol^{-1} for the addition of formaldehyde. No barriers were found for these processes.

10.4.4 Chirality Amplification

The dimerisation of **dmz-1** was found to enthalpically favoured with the *anti*-configuration being 3.1 kcal mol^{-1} more stable than the *syn*-isomer. From this it was concluded that the 'thermodynamic difference coupled with the reaction conditions results in the enormous chirality amplification.'

Whilst this study highlighted important mechanistic features, the origins of the selectivity has not been addressed.

Chapter 11: Computational Modelling of the Catalytic Alkylation of Aromatic Aldehydes by Organozinc Reagents

This chapter will focus on two areas of interest, namely alkyl transfer from organozinc-dialkylzinc and oxazaborolidine-dialkylzinc complexes.

11.1 Alkyl-Transfer from Organozinc-Dialkylzinc Complexes

Before studying the possible alkyl transition states, the crystal structure of DAIB (figure 11-1) was compared with the fully optimised structures found using the AM1 and the PM3 hamiltonians. Table 11-1 compares the important bond lengths.

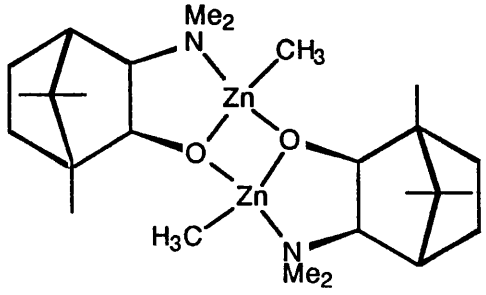

Figure 11-1

Table 11-1: The calculated and experimental DAIB bond lengths (Å)

	Crystal Structure	AM1	PM3
Zn-O (*intra.*)	2.028	2.162	2.119
Zn-O (*inter*)	2.001	2.217	2.207
Zn-N	2.168	2.370	2.134
Zn-C	2.020	1.917	2.012

The geometry located using the PM3 hamiltonian was in closer agreement with the crystal structure than the AM1 structure. In the theoretical structures, the strength of the interaction between zinc and oxygen was underestimated, whereas the zinc to carbon interaction was predicted to be stronger than observed in the crystal environment. From these findings, it was proposed that the PM3 hamiltonian would be used to study the organozinc complexes. The AM1 hamiltonian would be employed for the oxazaborolidine study as PM3 has not yet been parameterised for boron.

In the discussion, the labelling scheme shown in figure 11-2 will be used.

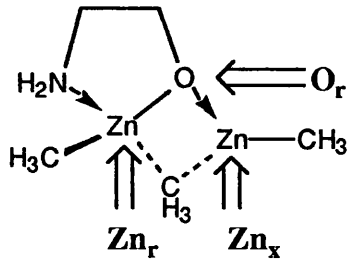

Figure 11-2

O_c will denote the sp^2-hybridsed carbonyl oxygen, C_c the carbon of the ketone and C_t the carbon of the alkyl group which is transferred.

11.1.1 Organozinc-dialkylzinc Adducts

The mode of co-ordination of dialkylzinc to an organozinc complex was addressed by the study of the four adducts shown in figure 11-3. Dimethylzinc was chosen as the alkyl transfer agent as this had fewer degrees of freedom than diethylzinc; experimental observations do not differ between zinc species. A zinc-ephedrine complex was used as model for the DAIB-camphor system as it contained all the important interactions.

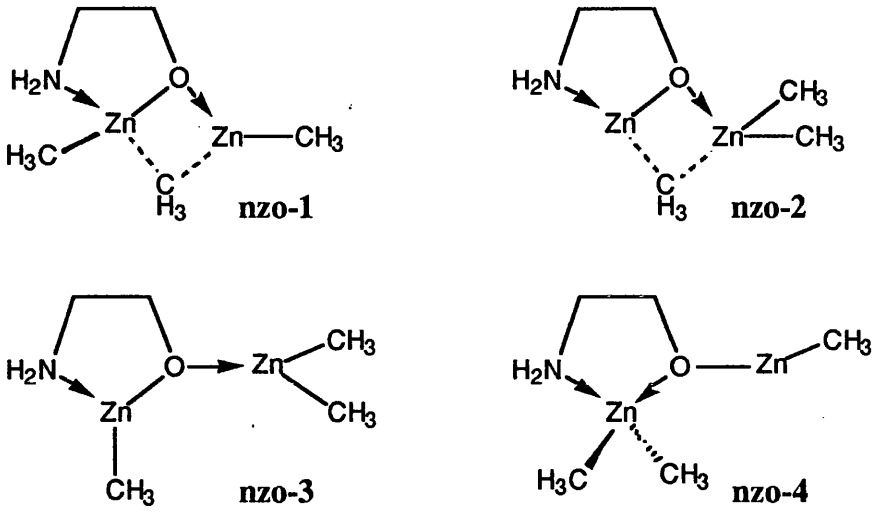

Figure 11-3

The ball-and-stick representations of these complexes are shown on the next page.

Of the four structures, **nzo-1** and **nzo-3** were the only minima which could be fully optimised. **nzo-1** was about 35 kcal mol^{-1} lower in energy than **nzo-3**, their heat of formations being -51.50 and -16.79 kcal mol^{-1}, respectively. A species similar to **nzo-2** was found, but all attempts to reduce the gradient norm to beneath 4 kcal mol^{-1} $Å^{-1}$ failed with the optimiser returning an error message. The final structure obtained was 46 kcal mol^{-1} higher in energy than **nzo-1** and had a small imaginary frequency of $29i$ cm^{-1} associated with motion of methyl groups attached to the *exo*-zinc.

A TS (figure 11-4) was the only species found having a conformation similar to that of **nzo-4**.

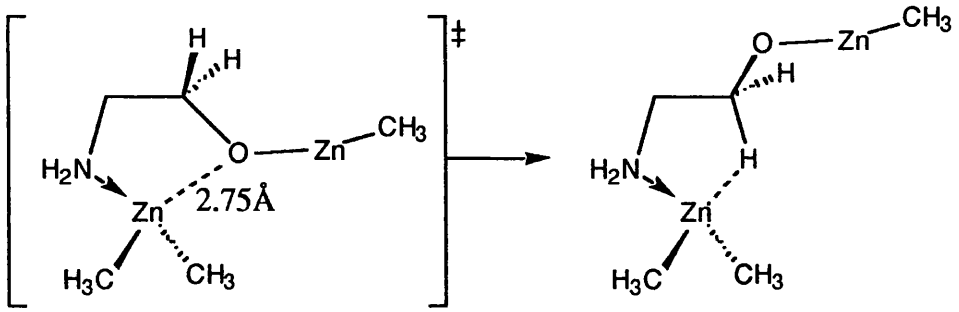

Figure 11-4

The barrier to the rotation was 11 kcal mol^{-1} ($\upsilon^{\ddagger} = 64i$ cm^{-1}).

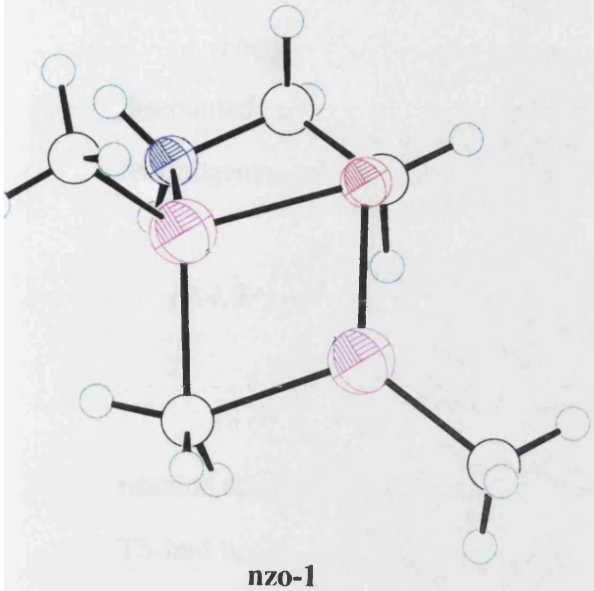

nzo-1

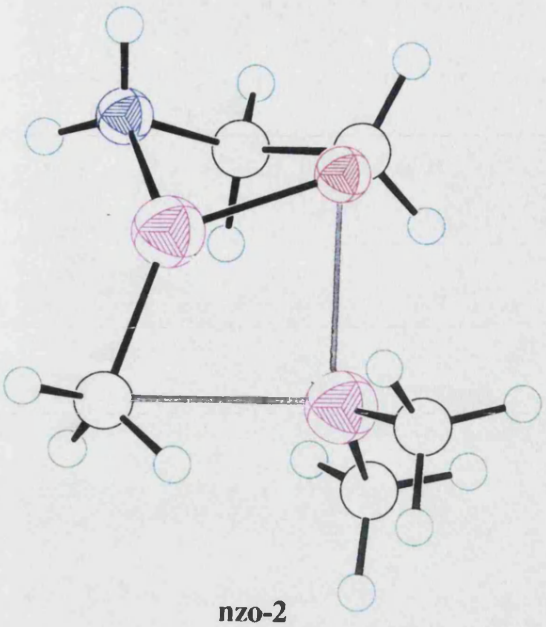

nzo-2

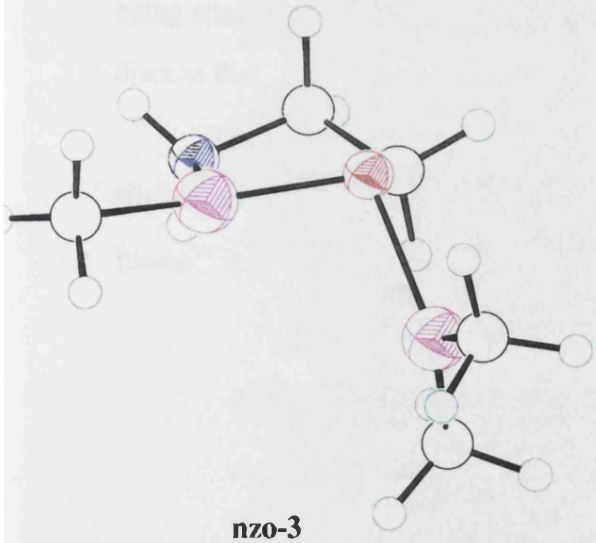

nzo-3

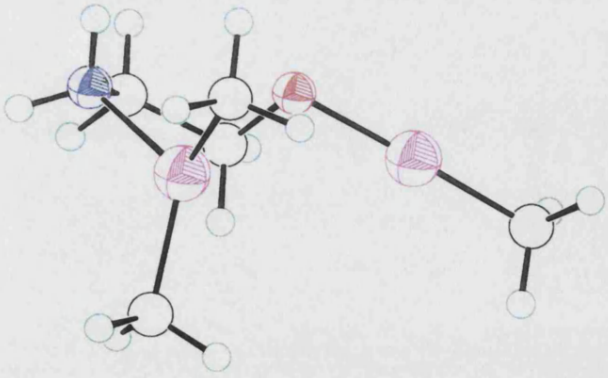

nzo-4

The most probable organozinc-dimethyl zinc adduct was **nzo-1**. This result discounted the TS proposed by Noyori and co-workers[70] as this demanded rearrangement of the zinc adduct to a less favoured conformer.

11.1.2 Alkyl Transfer TS

In chapters 4 and 9, the hydride transfer TSs were located by the means of a reaction co-ordinate calculation from a proposed ternary ketone complex. Once the TS had been located, the reverse IRC calculation was used to identify the actual ketone complex. From this structure, the dissociation of the ternary complex to the borane adduct plus ketone was studied. In the discussion of the mechanism, it was logical to present the forward reaction, with the binding of the ketone being discussed prior to the hydride transfer.

In this section, the same approach was followed with the alkyl transfer step being studied first. For reasons that will become apparent, it was not appropriate to discuss the binding of the aldehyde.

The addition of formaldehyde to **nzo-1** could lead to alkyl transfer TSs (figure 11-5) adopting conformations similar to those proposed by Corey,[74] Itsuno[72] and Soai.[75]

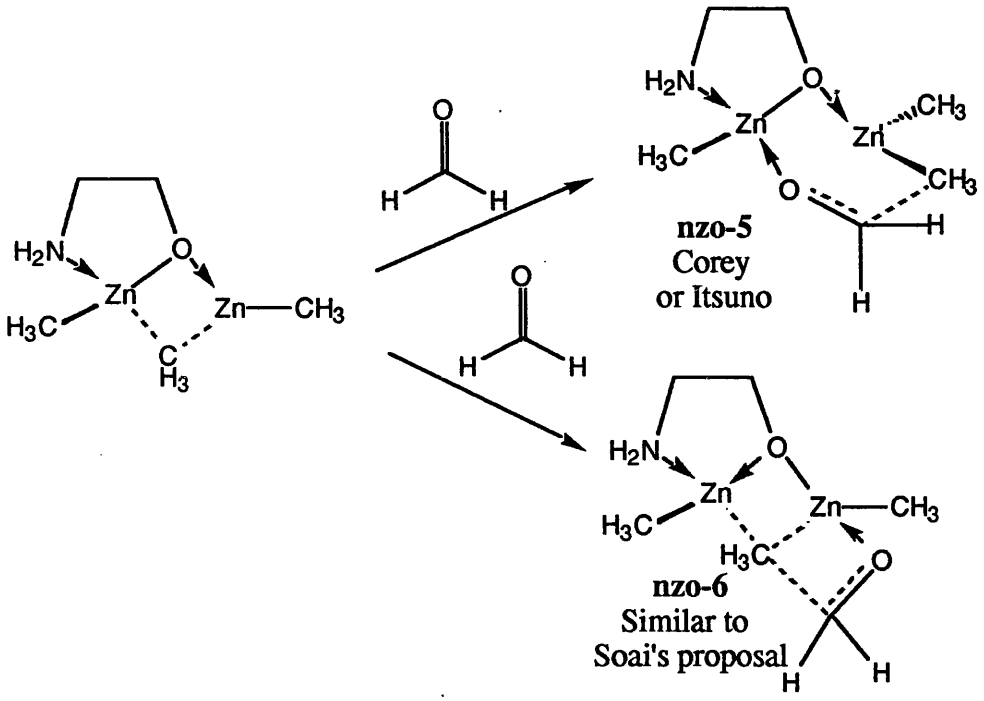

Figure 11-5

The TSs were of similar energies, -28.50 kcal mol^{-1} ($\upsilon^{\ddagger}$ = 563*i* cm^{-1}) and -28.13 kcal mol^{-1} ($\upsilon^{\ddagger}$ = 471*i* cm^{-1}) for **nzo-5** and **nzo-6** respectively, but the barriers were 21.42 kcal mol^{-1} and 60.13 kcal mol^{-1}.

The reverse IRC calculation from **nzo-6** did not lead to the expected ternary-ketone complex, but a species with an interaction between the *exo*-zinc Zn_x and the sp^2-hybridised carbon of the carbonyl group, as shown in figure 11-6. The ball-and-stick representations of species shown in figure 11-6 are given on the next page.

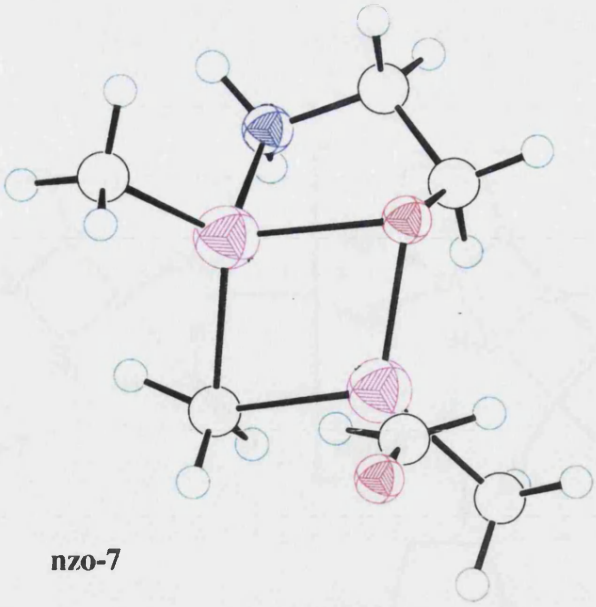

nzo-7

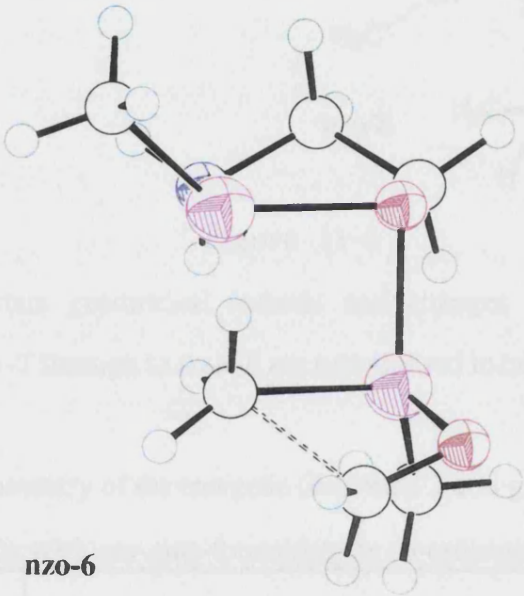

nzo-6

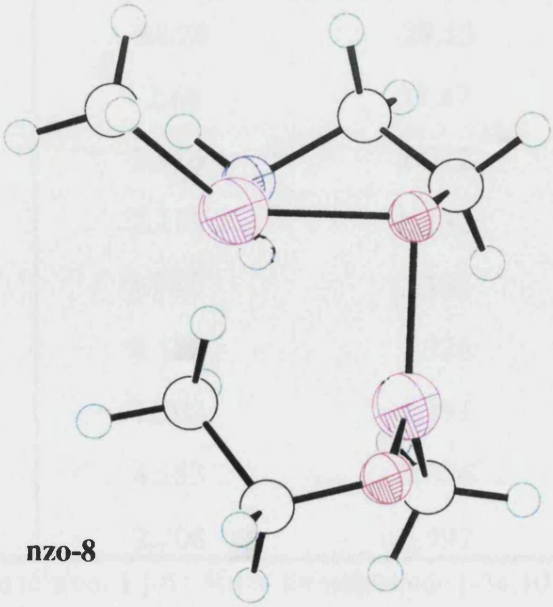

nzo-8

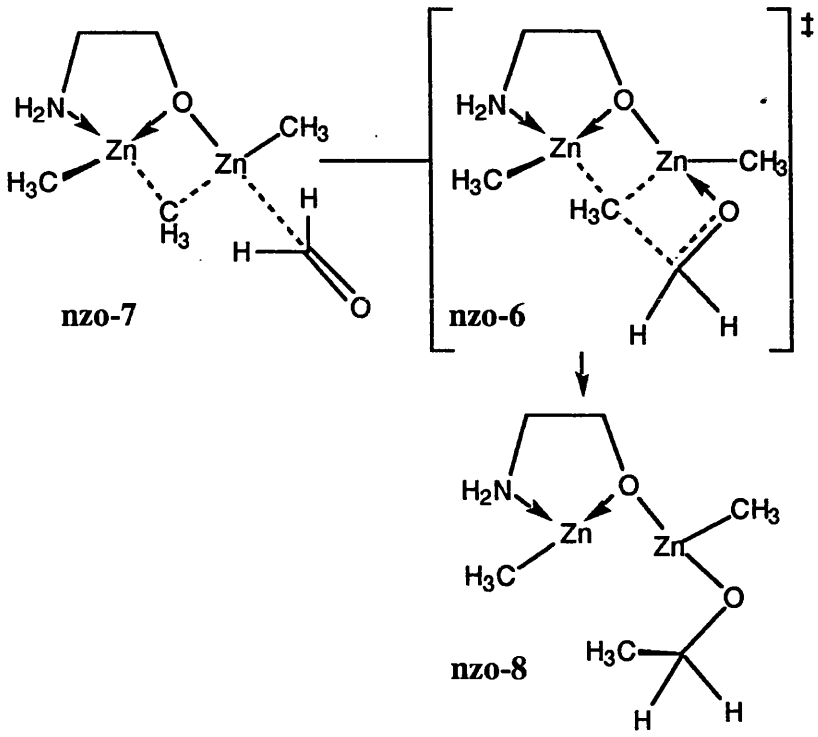

Figure 11-6

The important geometrical features and changes in energetics for the conversion of **nzo-7** through to **nzo-8** are summarised in table 11-2.

Table 11-2: A summary of the energetic (kcal mol^{-1}) and geometrical changes (Å) during alkyl transfer with *exo*-zinc-formaldehyde co-ordination

	nzo-7	**nzo-6**	**nzo-8**
ΔH_f	-88.26	-28.13	-50.24
ΔH_{rel} [a]	-2.66	57.47	35.36
Zn_r-O_r	2.236	2.072	2.042
O_r-Zn_x	2.112	2.132	2.166
Zn_x-O_c	3.787[b]	2.139	1.960
Zn_x-C_t	2.185	2.326	2.721
O_c-C_c	1.202	1.291	1.390
C_c-C_t	4.183	2.056	1.555
C_t-Zn_r	2.208	2.497	2.603

[a] Enthalpy relative to **nzo-1** [-51.50] + formaldehyde [-34.10] = -85.60 kcal mol^{-1}

[b] Zn_x-C_c = 2.649 Å

The expected ketone complex was located by the reverse IRC calculation from **nzo-5**, but attempts to locate the TS for the binding of the ketone did not have the anticipated interaction between O_c and the *endo*-zinc Zn_r.

As with **nzo-5**, the anticipated bond formation was replaced by a carbon-zinc interaction (figure 11-7).

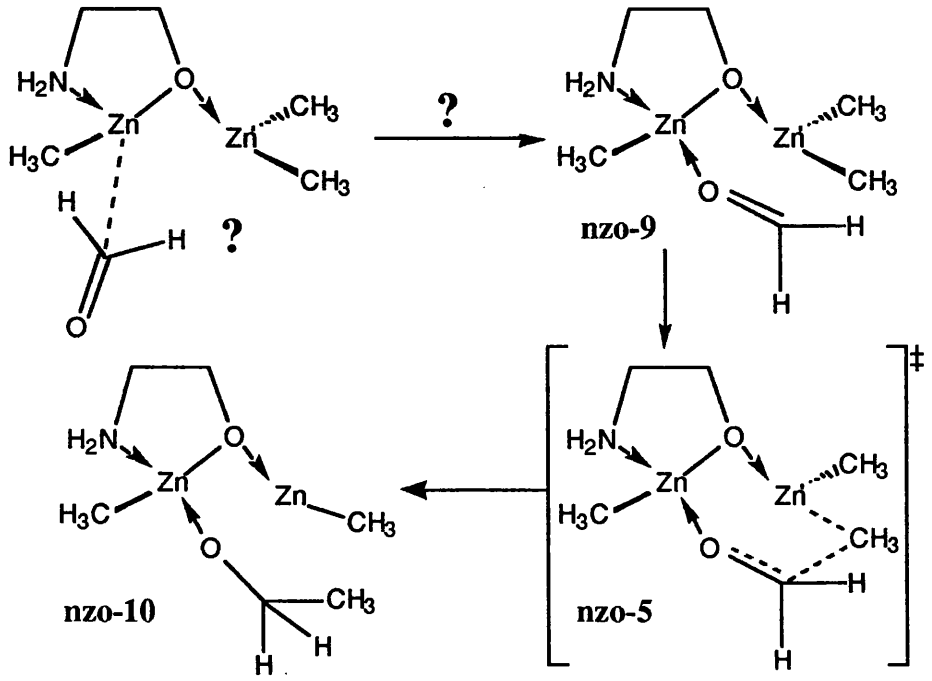

Figure 11-7

The ball-and-stick representations of these molecules are given on the next page. Table 11-3 provides the geometric and energetic data for the alkyl transfer.

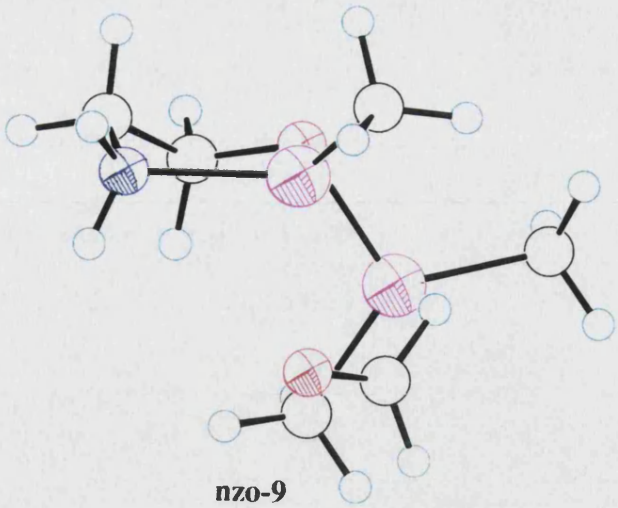

nzo-9

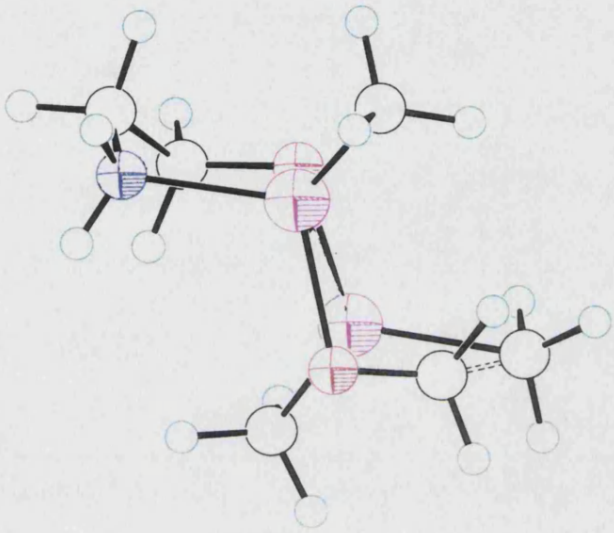

nzo-5

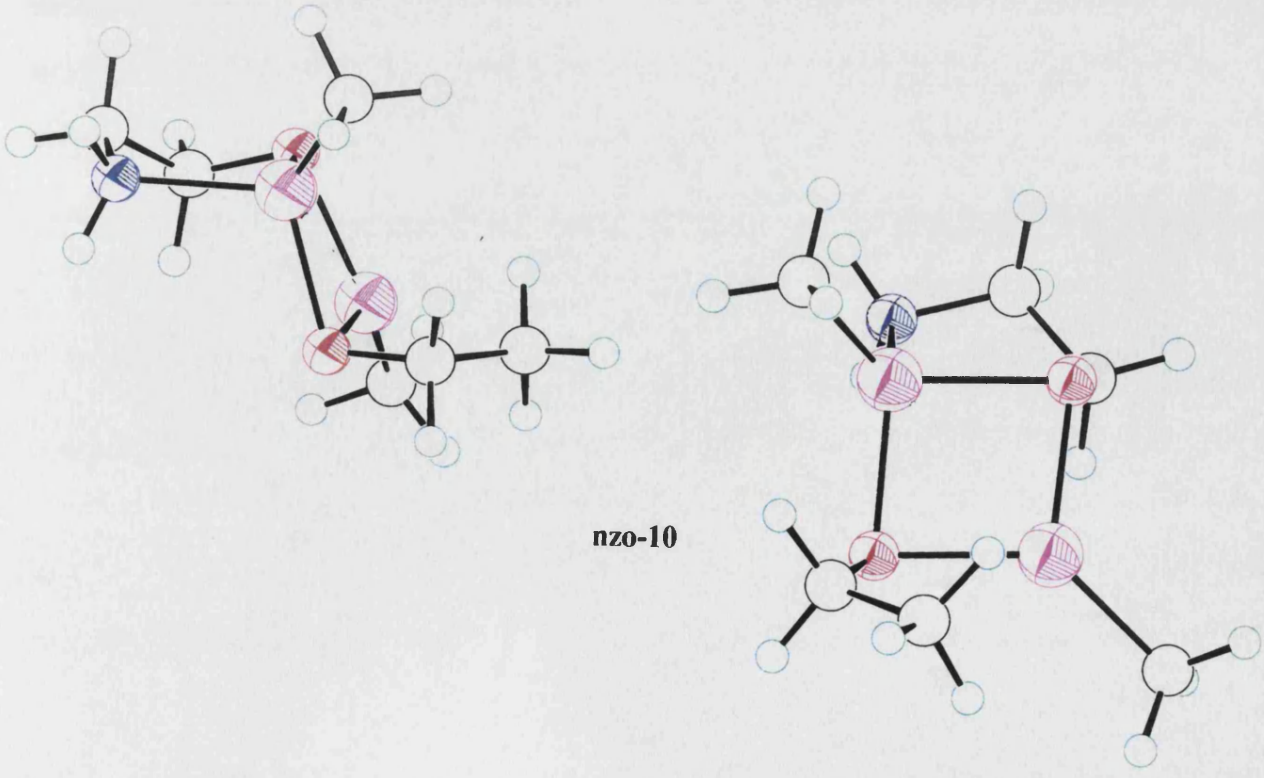

nzo-10

Table 11-3: A summary of the energetic (kcal mol^{-1}) and geometrical changes (Å) for alkyl transfer with *endo*-zinc-formaldehyde co-ordination

	nzo-9	**nzo-5**	**nzo-10**
ΔH_f	-49.92	-28.50	-64.03
ΔH_{rel} [a]	35.68	57.10	21.57
Zn_r-O_r	2.011	2.129	2.160
O_r-Zn_x	2.162	2.071	2.102
Zn_r-O_c	2.497	2.124	2.104
O_c-C_c	1.219	1.310	1.416
C_c-C_t	3.794	2.119	1.536
C_t-Zn_x	1.993	2.143	2.574

[a] Enthalpy relative to **nzo-1** [-51.50] + formaldehyde [-34.10] = -85.60 kcal mol^{-1}

In both these systems, the approach of the formaldehyde to the adduct was *via* the sp^2-hybrised carbon, C_c. This atom was electron deficient, as indicated by the charge of 0.24, and therefore likely to interact with electron rich sites. Study of the charge distribution within **nzo-1** showed that both the zinc atoms were electron deficient, $q(Zn_r) = 0.42$ and $q(Zn_x) = 0.80$. No further investigation of these systems was undertaken as a mechanism which involved electrophilic attack at an electron-deficient site was not a reasonable suggestion.

11.2 The Alkylation of Formaldehyde by OAB-dimethylzinc complexes

As the OAB-zinc adducts did not contain any Zn-O_c interactions, the mechanism for the alkyl transfer from these systems was investigated. Brown and co-workers[68] had found that the OAB derived from ephedrine proved an excellent catalyst for alkylation reactions. The complex shown in figure 11-8 was used to investigate the mechanism, with the intention of adding the ring substituents when the issue of stereoselectivity was addressed.

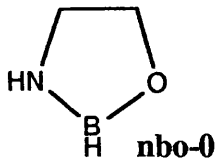

nbo-0

Figure 11-8

11.2.1 The Formation of OAB-$ZnMe_2$ adducts

As Brown's study had not discovered whether the dimethylzinc was bonded to the nitrogen or the oxygen of the oxazaborolidine, the zinc adducts shown in figure 11-9 were studied.

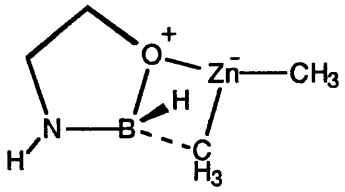

nbo-1

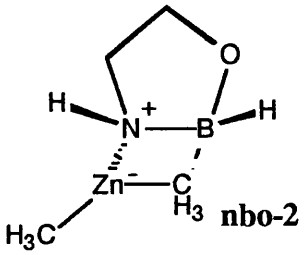

nbo-2

Figure 11-9

The heat of formation of **nbo-1** was -37.61 kcal mol^{-1} compared to -59.68 kcal mol^{-1} for **nbo-2**. A non-alkyl-bridged analogue of **nbo-2** was about 4.5 kcal mol^{-1} less stable than **nbo-2** and the barrier for the rotation about the N-Zn bond was 20.60 kcal mol^{-1} ($\upsilon^{\ddagger} = 550i\ cm^{-1}$). It was not possible to locate a non-bridged version of **nbo-1**.

From this study, **nbo-2** was identified as the more stable conformer. A barrier of 5.31 kcal mol^{-1} ($\upsilon^{\ddagger} = 76i\ cm^{-1}$) had to be overcome to convert a complex with a long-range interaction between nitrogen and zinc, **nbo-3**, to **nbo-2**.

Figure 11-10 represents this elementary step and table 11-4 summarises the important energetic and geometrical changes.

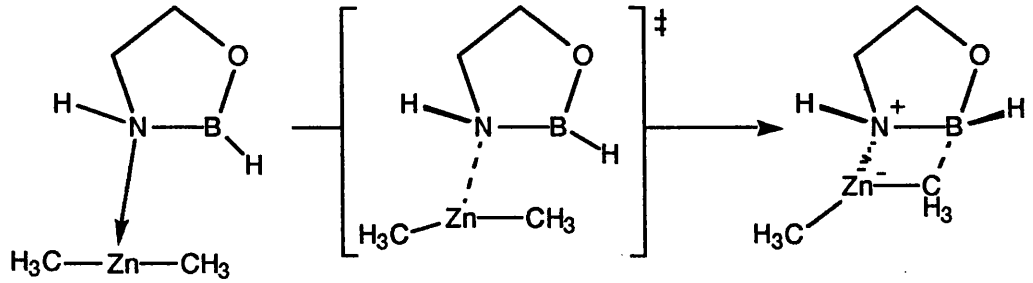

nbo-3 **nbo-4** **nbo-2**

Figure 11-10

Table 11-4: A summary of the energetic (kcal mol^{-1}) and geometrical changes (Å) for the formation of the OAB-$ZnMe_2$ adduct.

	nbo-3	nbo-4	nbo-2
ΔH_f	-62.60	-57.29	-59.64
ΔH_{rel} [a]	-0.03	5.28	2.93
N-Zn	7.846	3.105	2.661
N-B	1.382	1.404	1.448

[a] Enthalpy relative to **nbo-0** [-82.38] + $ZnMe_2$ [19.81] = -62.57 kcal mol^{-1}

All the species involved in this elementary step were thermodynamically less stable than the isolated species. As with the binding of borane-THF (chapter 4.4), the donation of electrons from nitrogen to zinc decreased the availability of the electrons for resonance stabilisation between the nitrogen, boron and oxygen of the OAB. This decrease of electrons in the N-B bond was reflected in the reduction N-B bond order[20] in **nbo-2** (1.023) with respect to **nbo-0** (1.208).

11.2.2 The Binding of Formaldehyde

As with the reduction of ketones, two distinct conformers existed for the alkyl transfer and the differences in the pathways were visible in the TS for the formation of the bond between boron and the oxygen of the ketone. The two

conformers were distorted-boat and distorted-chair six membered ring comprising N-B-O_c-C_c-C_t-Zn.

The barrier for binding the ketone in a distorted-boat conformer was 3.6 kcal mol^{-1} ($\upsilon^{\ddagger}$ = 156*i* cm^{-1}) and 4.0 kcal mol^{-1} ($\upsilon^{\ddagger}$ = 142*i* cm^{-1}) for the distorted chair. The energetic changes for the binding (figure 11-11) are given in table 11-5 where the suffix b indicates the distorted-boat conformer and c indicates the distorted-chair.

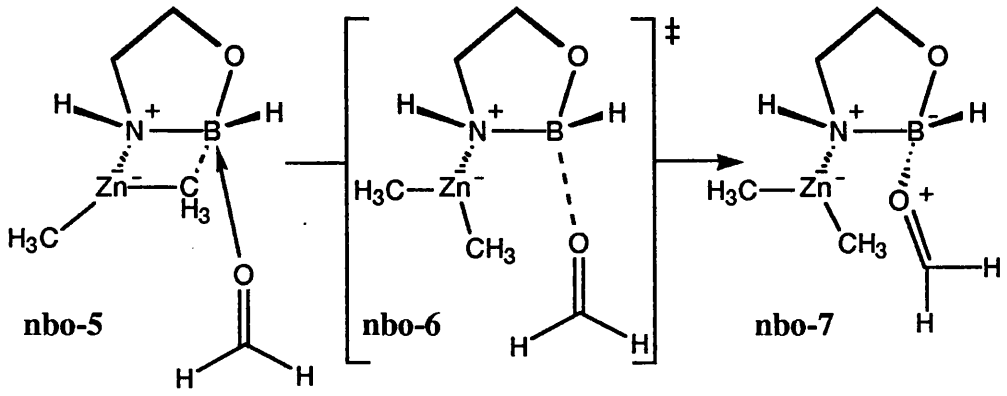

Figure 11-11

The ball-and-stick representations of both conformers of **nbo-6** and **nbo-7** are shown on the next page.

Table 11-5: A summary of the energetic (kcal mol^{-1}) and geometrical changes (Å) during the binding of formaldehyde

	via a distorted-boat conformer			*via a distorted-chair conformer*		
	nbo-5b	**nbo-6b**	**nbo-7b**	**nbo-5c**	**nbo-6c**	**nbo-7c**
ΔH_f	-92.14	-88.14	-94.37	-90.04	-86.44	-92.80
ΔH_{rel} [a]	1.94	5.94	-0.29	4.04	7.64	1.28
O_c-B	3.514	2.393	1.823	4.555	2.477	1.850
B-N	1.453	1.466	1.497	1.453	1.469	1.502
N-Zn	2.400	2.391	2.372	2.401	2.407	2.378

[a] Enthalpy relative to **nbo-0** [-82.38] + $ZnMe_2$ [19.81] + H_2CO [-31.51] = -94.08 kcal mol^{-1}

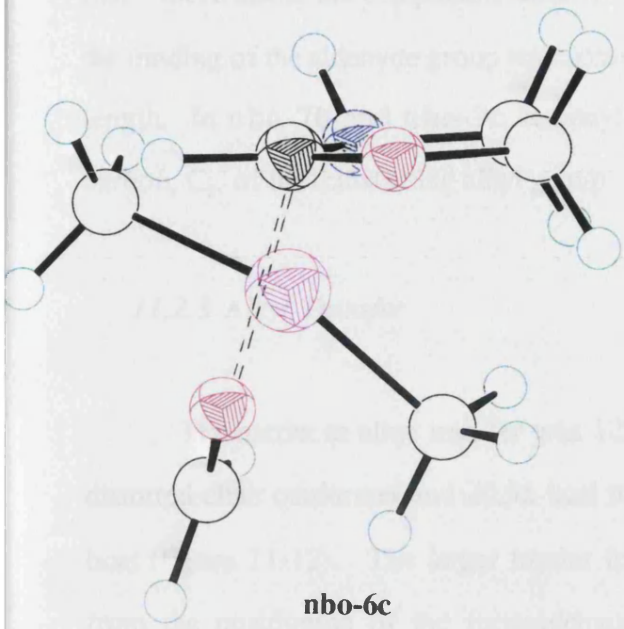

nbo-6c

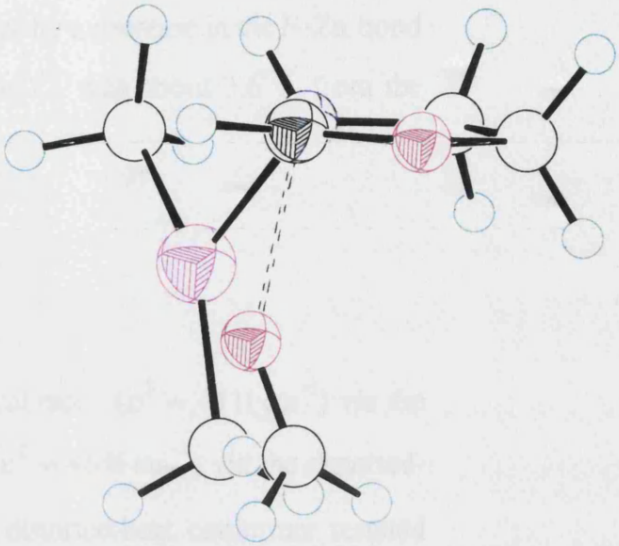

nbo-6b

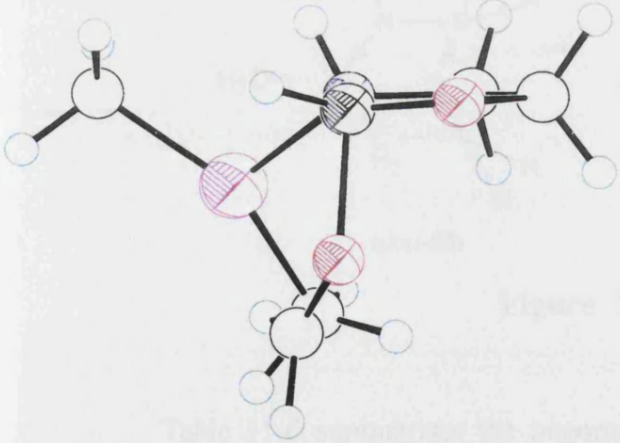

nbo-7c

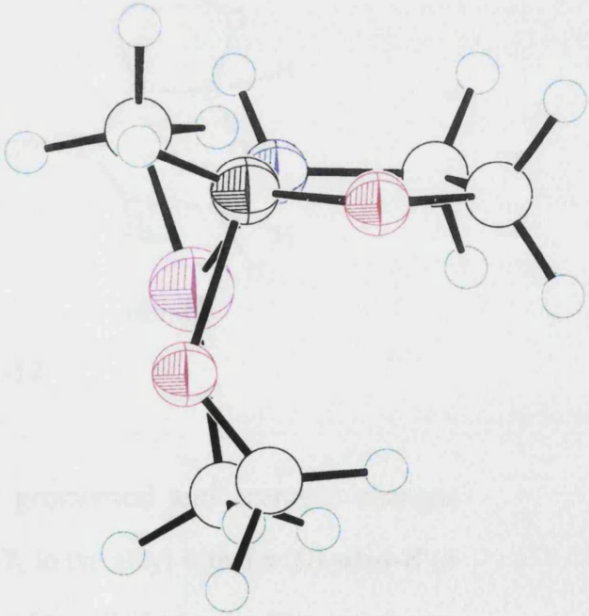

nbo-7b

In all the species, the distorted-boat conformer was approximately 2 kcal mol^{-1} more stable the comparable distorted-chair conformer. In both conformers, the binding of the aldehyde group was accompanied by a decrease in the N-Zn bond length. In **nbo-7b** and **nbo-7c** carbonyl carbon C_c was about 3.6 Å from the carbon, C_t, of the transferring alkyl group.

11.2.3 Alkyl Transfer

The barrier to alkyl transfer was 12.34 kcal mol^{-1} ($\upsilon^{\ddagger}$ = 411*i* cm^{-1}) *via* the distorted-chair conformer and 20.56 kcal mol^{-1} ($\upsilon^{\ddagger}$ = 463*i* cm^{-1}) *via* the distorted-boat (figure 11-12). The larger barrier for the distorted-boat conformer resulted from the positioning of the formaldehyde beneath the OAB ring, creating an unfavourable energetic interaction.

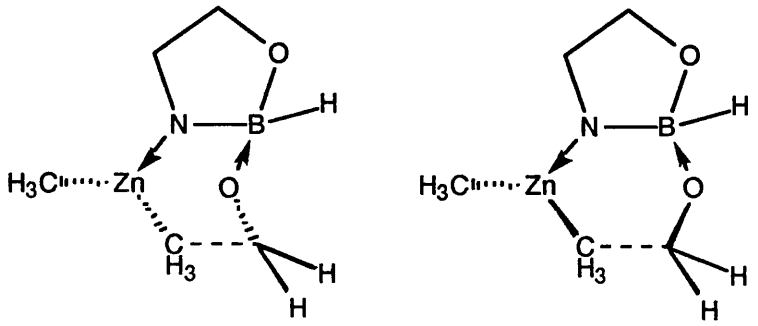

nbo-8b **nbo-8c**

Figure 11-12

Table 11-6 summarises the important geometrical and energetic changes going from the ternary ketone complexes **nbo-7**, to the alkyl transfer TS **nbo-8** to the next intermediate **nbo-9**. Two orientations of the alkyl transfer TSs are shown in ball-and-stick representations on the next page. The intermediate **nbo-9** is also shown.

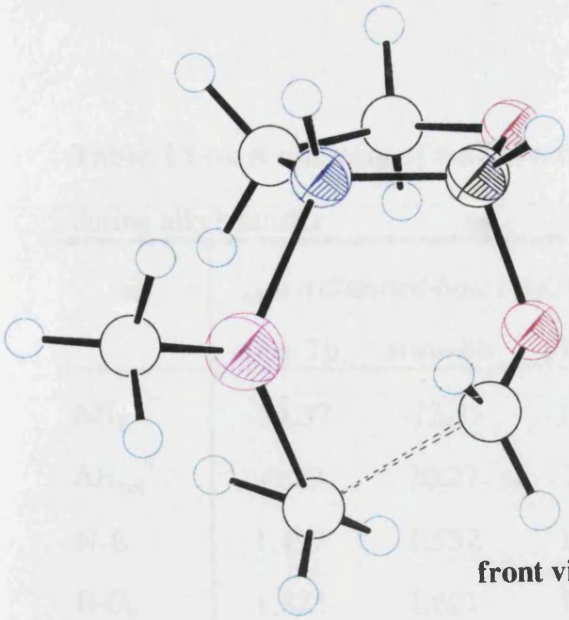

front view

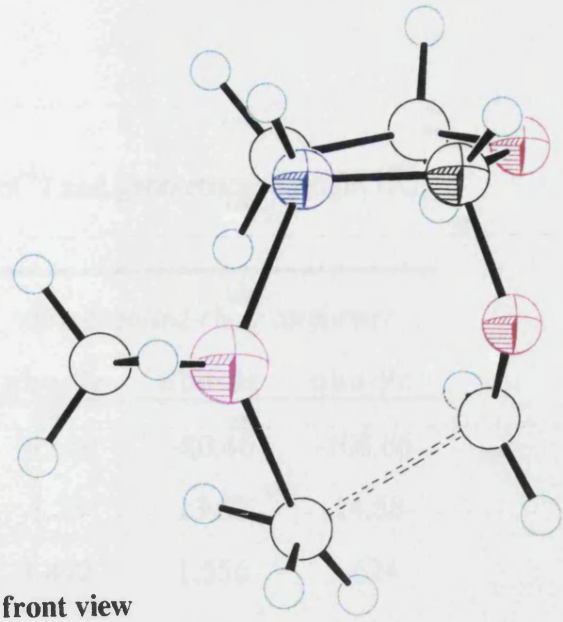

front view

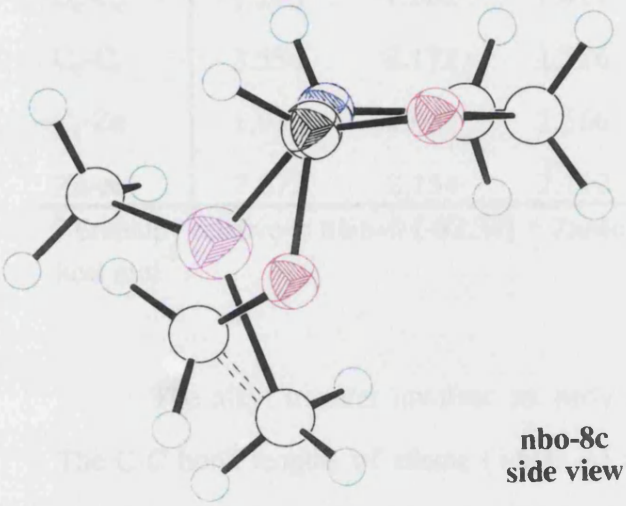

nbo-8c
side view

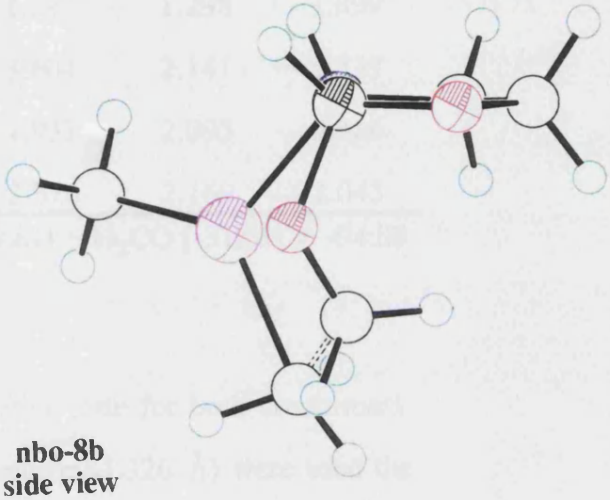

nbo-8b
side view

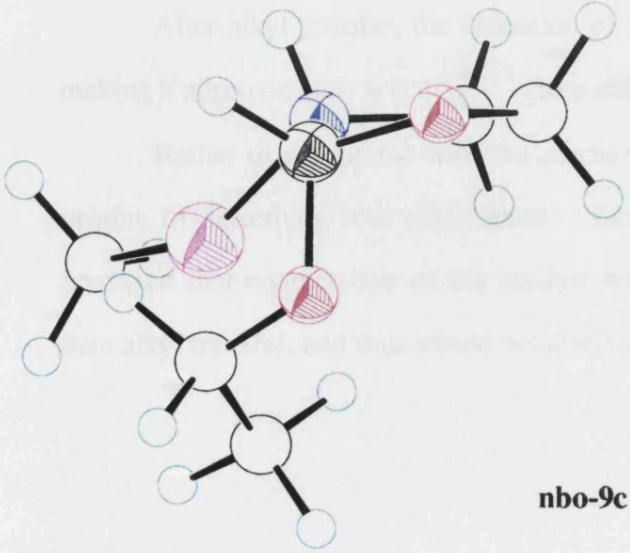

nbo-9c

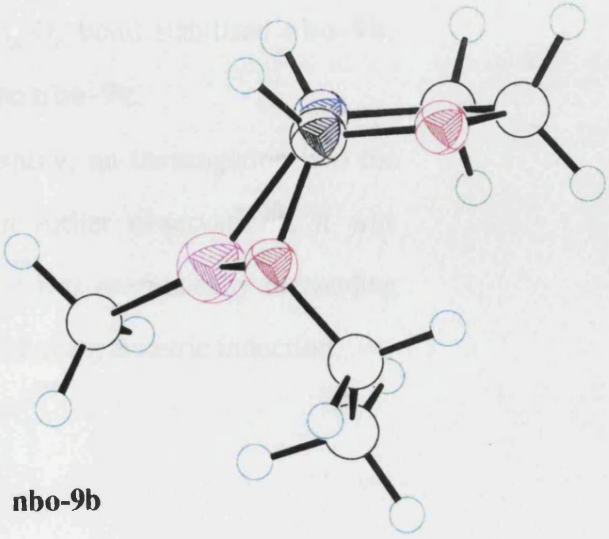

nbo-9b

Table 11-6: A summary of the energetic (kcal mol^{-1}) and geometrical changes (Å) during alkyl transfer

	via a distorted-boat conformer			*via a distorted-chair conformer*		
	nbo-7b	**nbo-8b**	**nbo-9b**	**nbo-7c**	**nbo-8c**	**nbo-9c**
ΔH_f	-94.37	-73.81	-114.90	-92.80	-80.46	-108.66
ΔH_{rel}[a]	-0.29	20.27	-20.82	1.28	13.62	-14.58
N-B	1.497	1.552	1.591	1.472	1.556	1.624
B-O_c	1.823	1.621	1.542	1.850	1.661	1.496
O_c-C_c	1.243	1.302	1.417	1.241	1.298	1.399
C_c-C_t	3.554	2.172	1.526	3.604	2.141	1.537
C_t-Zn	1.933	2.082	2.566	1.932	2.095	2.486
Zn-N	2.372	2.154	2.110	2.376	2.169	2.043

[a] Enthalpy relative to **nbo-0** [-82.38] + $ZnMe_2$ [19.81] + H_2CO [-31.51] = -94.08 kcal mol^{-1}

The alkyl transfer involved an early transition state for both conformers. The C-C bond lengths of ethane (1.500 Å) and ethene (1.326 Å) were used the derive the value of the constant c=0.25 needed to calculate the Pauling bond order **n**. In both TSs, the C_c-C_t bond order was less than 0.1, 0.07 and 0.08 for **nbo-8b** and **nbo-8c** respectively.

After alkyl transfer, the formation of the Zn_x-O_c bond stabilised **nbo-9b**, making it approximately 6 kcal mol^{-1} more stable than **nbo-9c**.

Rather than continue with the mechanistic study, an investigation into the origins of selectivity was undertaken. Based on earlier observations, it was predicted that regeneration of the catalyst would be less energetically demanding than alkyl transfer, and thus would not affect the level of asymmetric induction.

11.3 The Alkylation of Benzophenone

Substituents were added to the 3-, 4- and 5-positions of **nbo-0** so that the theoretical e.e. could be compared with that observed by Brown and co-workers.[68] Dimethylzinc was replaced by diethylzinc, the resulting adduct being shown in figure 11-13.

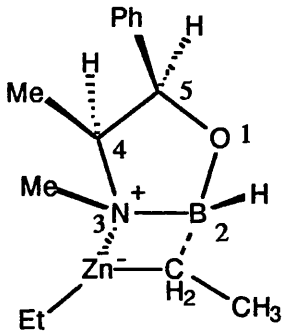

nbo-10

Figure 11-13

Four TSs were located which were thought to relate to alkyl transfer to benzophenone *via* distorted-boat and distorted-chair conformers in both the R and S epimeric forms (BS $\upsilon^{\ddagger} = 408i$ cm^{-1}, BR $\upsilon^{\ddagger} = 329i$ cm^{-1}, CS $\upsilon^{\ddagger} = 346i$ cm^{-1} and CR $\upsilon^{\ddagger} = 400i$ cm^{-1}). The geometries obtained were similar to those obtained for the alkylation of formaldehyde by **nbo-2** but the reverse IRC did not locate the ternary ketone complex. Rather than being bonded to the nitrogen, the diethylzinc was associated with the hydrogens of the methyl group attached to nitrogen (figure 11-14).

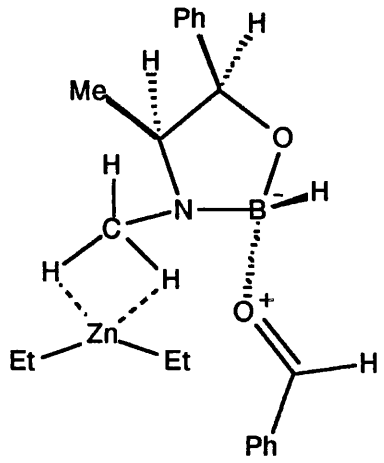

Figure 11-14

Two ball-and-stick representations of this molecule are given on the next page.

Starting from the methyl transfer TS, **nbo-8** (either conformer), the substituents were added and the TS located. The addition of the substituents to the 4- and 5- positions nor the alteration of dimethyl to dimethylzinc affected the TS. On the addition the methyl substituent to nitrogen, the zinc preferred to interact with the hydrogens rather than the nitrogen.

No further attempts were made to study the enantioselective alkylation of benzophenone.

11.4 The Parameterisation of Zinc

After the failures of these investigations, the applicability of the zinc parameters to these systems was questioned. The AM1[78] and PM3[79] parameters were determined from dialkyl and dihalide zinc species, and polymeric zinc oxide.

The lack of zinc-nitrogen or zinc-oxygen (sp^2-hybridised) interactions in the parameterisation complexes explained the preference for the zinc-carbon and zinc-hydrogen interactions exhibited in these calculations. Therefore, all the results in this chapter should be treated with caution.

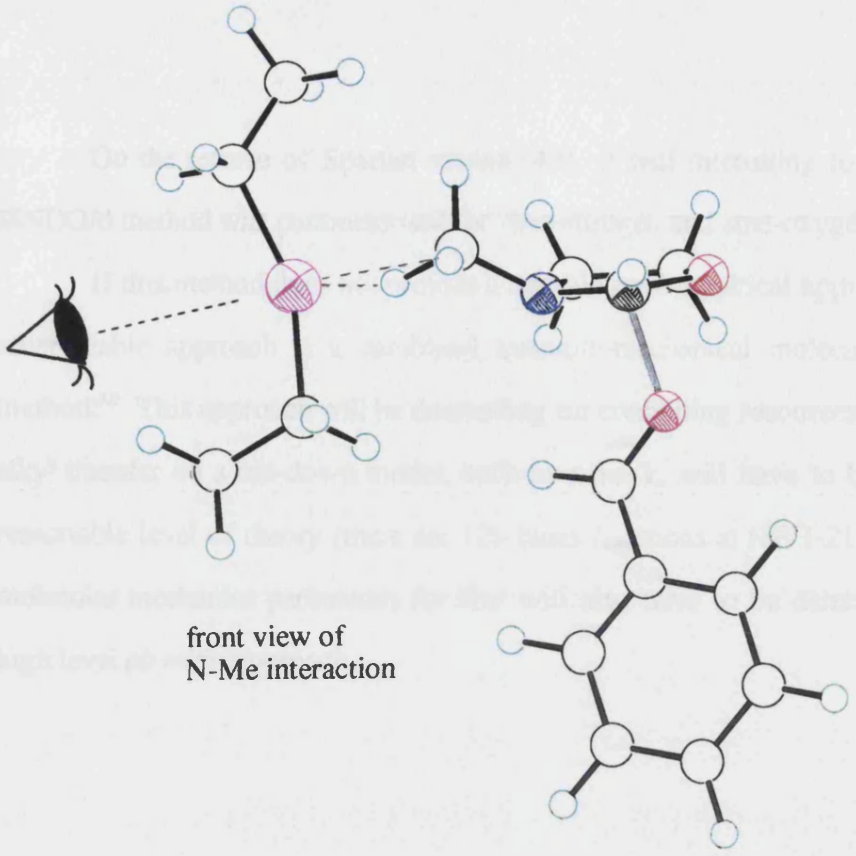

front view of
N-Me interaction

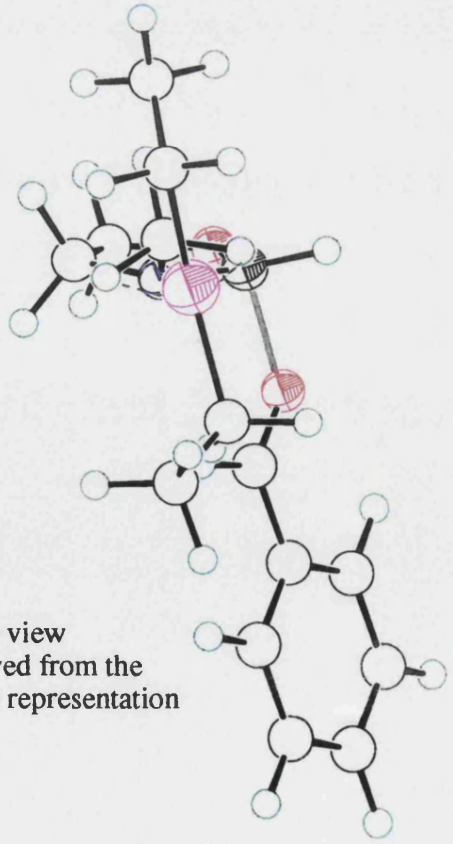

side view
i.e. as viewed from the
eye in the top representation

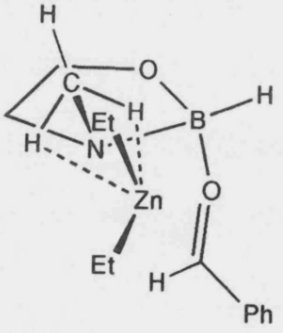

On the release of Spartan version 4.0, it will interesting to see if Thiel's MNDO/d method was parameterised for zinc-nitrogen and zinc-oxygen interactions.

If this method does not provide a suitable semi-empirical approach, the only other viable approach is a combined quantum-mechanical molecular-mechanical method.[80] This approach will be demanding on computing resources as the TS for alkyl transfer on a cut-down model, such as **nbo-1**, will have to be located at a reasonable level of theory (there are 125 basis functions at HF/3-21G level). The molecular mechanics parameters for zinc will also have to be determined using a high level *ab initio* approach.

Chapter 12: 'Loose Ends'

It was hoped that *ab initio* calculations on simple OAB-borane adducts could have provided further insight into some aspects of the catalytic mechanism.

One such area was the existence of the ring opened form of the catalyst (figure 16-1).

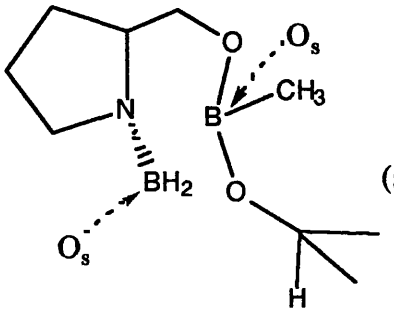

oab-10c
(see chapter 4-6)

Figure 16-1

A study was started on a cut-down model (figure 16-2) using the 3-21G basis set, the demands of disk space preventing the use of a higher basis set.

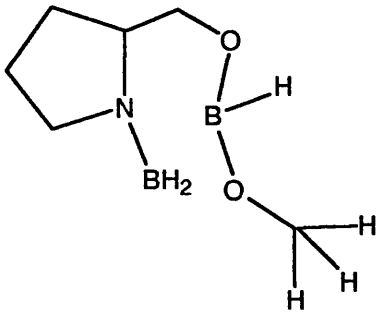

Figure 16-2

An unsuccessful starting geometry was selected and the optimisation did not provide a relevant structure. Insufficient time was available to rectify the problem. In hindsight, following the IRC from the chair hydride transfer TS (which has been located using Gaussian 92) would have been a more successful approach. This method was not selected initially as IRC calculations are very time demanding.

The other area in which it was hoped that *ab initio* work would provide guidance was the enantiocontrol. The majority of the e.e.s determined in chapter 6 were lower than the experimental values. Whilst this was true for the aromatic ketones, the alkyl systems were in very close agreement with the experimental work. It was postulated that there may be an inherent flaw in the AM1 geometries of aromatic ketones.

As there are no published high level *ab initio* calculations on the structure of acetophenone, an optimisation at the MP2/6-31G** basis set was started. It was hoped that the structure obtained would highlight any deficiencies in the AM1 description. After three months on an Indigo 2 workstation, elapsed time not CPU, convergence had still not been achieved.

If the comparison of the structures does not provide any insight into the prediction of lower e.e.s, a combined quantum-mechanical molecular-mechanical study might provide an alternative method. Attempts were made to model cut-down hydride transfer TSs (figure 16-3). A structure for the chair conformer has been located and fully optimised but even at HF/3-21G with an excellent starting geometry, the routines in Gaussian 92 failed to locate the boat conformer.

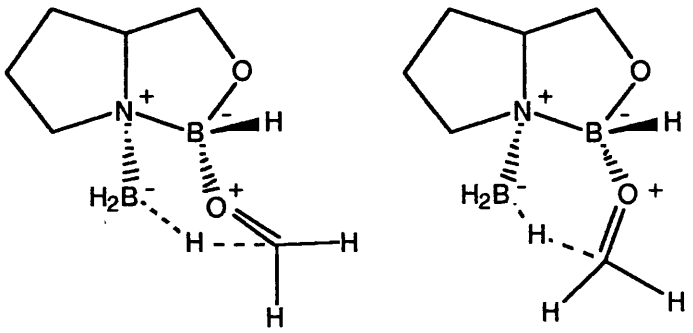

Boat conformer Chair conformer

Figure 16-3

If Gaussian 94 does not provide any better algorithms for the locations of TSs, the use of the GAMESS program would be an alternative. As this program tends to handle CPU resources more successfully, optimisation at a higher level, for

example MP2/6-31G**, would be desirable especially after the observations made about the failures of HF-level (chapter 4-4, table 4-7).

A final approach would be in the pain-staking parameterisation of MM2 molecular mechanics method. At the present time, MM2 does not contain all the parameters needed to describe the bonding interactions present in oxazaborolidines. For example, there are no nitrogen to boron interactions. Therefore, several AM1 MO calculations would be required to determine the N-B bond term. Parameters for the bond and torsion angles about the N-B bond would also need to be calculated.

Once all the missing parameters were determined, over one hundred of them, an optimisation of the OAB-borane-ketone complex could be performed, the result being compared to the AM1 structure. If there was a good correlation between structures, other related systems would also be investigated to check the validity of the parameters.

If all of this was successful, free energy perturbation calculations[81] could provide an alternative theoretical e.e. Free energy perturbation calculations start from one epimer, calculate the free energy, and then convert the structure to that of the other epimer by a series of structural perturbations about a defined bond. Each structure is fully optimised and the free energy calculated. In the oxazaborolidine systems, rotation about the carbonyl O_c-C_c double bond would 'convert' the R epimer to the S epimer, the free energy difference between these stereoisomers being directly related to the e.e.

Hopefully, the experimental observations of Prof. Gallagher's group and Dr Chris Self will support the predictions made in chapter 7. Further work will probably arise from their studies.

The future of the phosphinamide-borane adduct work really depends on experimental chemists and the avenue pursued by them.

The only real failure of this research was in the dialkylzinc work described in chapter 11. The most likely route to success with this work would be the QM/MM approach. The geometries published by Noyori, the publication of which

occurred after the semi-empirical work was undertaken, provide an excellent starting point.

Chapter 13: Acknowledgements

Trying to remember everybody who has helped me throughout my Ph. D. is quite challenging!

The main recipient of my thanks has got to be Prof. Ian Williams, my supervisor, without whose trust three years ago I would have never embarked on a Ph. D. He really has been an excellent supervisor - there when I needed him, but giving me freedom to explore my own ideas.

Dr. Chris Self was an excellent industrial-case award supervisor. He provided a lot of helpful input into the project. Most important to me personally, was the mountains he managed to move to arrangement my placement and the help and support he provided whilst I was at Roche.

I would like to thank all the past members of the Ian's group: Dr. John Wilkie for his help with MOPAC and grasping the basics of system management, Dr. John Barnes for his help with MOPAC, Dr Mick Hand for the help with Gaussian and Dr. David Buttar for generally trying to wind me up!

I'd like to thank the Ph. D. synthetic organic chemists at Bath for their contributions. The study of the phosphinamide systems would not have been possible without Martin Wills and John Studley. Also, to the Wills and Armstrong groups for daily reminding me why I gave up synthetic chemistry.

Thanks to Prof. Tim Gallagher, University of Bristol, for the joint collaboration with the enone systems.

Apologies and thanks to Dr. Paul Sherwood at Daresbury for his time explaining how to use the combined codes, work that was never undertaken as I couldn't find the relvevant *ab initio* TSs!

I would like to thank everyone at Roche with putting up with yet another case-award student, one who seemed to be there for ages. Thanks to Dr. Brad Sherborne for his help with Moloc and Texsan, and being the systems' manager - a

whole eight months without "Lynda, it doesn't work ..." was bliss. Special thanks to Dr. Glyn Williams and Pete Simpson for making me feel welcome and part of the team.

And finally thanks to Ian (hubby) who convinced me into staying poor for another three years. I'd never have managed without his encouragement, support, love and his regular reminders that I wasn't a proper chemist!!

I suppose the acknowledgements would not be complete without mentioning *Medici* and *Leonardo* for without their (?) willingness to work 24 hours a day, 7 days a week, the project would never have been completed in 3 years.

Chapter 14: References

1. N. L. Allinger, Y. H. Yuh and J. -H. Lii, *J. Am. Chem. Soc.*, 1989, **111**, 8551; N. L. Allinger, and J. -H. Lii, *ibid*, 8566; N. L. Allinger, Y. H. Yuh and J. -H. Lii, *ibid*, 8576; N. L. Allinger, Y. H. Yuh and J. -H. Lii, *J. Comput. Chem.*, 1990, **11**, 848.

2. P. K. Weiner and P. A. Kollman, *J. Comput. Chem.*, 1981, **2**, 287. S. J. Weiner and P. A. Kollman, *J. Am. Chem. Soc.*, 1984, **106**, 765.

3. B. R. Brooks, R. E. Bruccoleri, B. D. Olafson, D. J. States, S. Swaminathan and M. Karplus, *J. Comput. Chem.*, 1983, **4**, 187.

4. Only a brief review of the theory is provided in this section. A more detailed description is provided in the following texts: T. Clarke, *A Handbook in Computational Chemistry: A Practial Guide to Chemical Structure and Energy Calculations*, Wiley, New York, 1985. V. F. Traven, *Frontier Orbitals and Properties of Organic Molecules*, Ellis Horwood, New York, 1992, p 13. J. J. P. Stewart, in *Reviews in Computational Chemistry*, ed. K. B. Lipowitz and D. B. Boyd, VCH, New York, 1990, vol. 1, p 45. M. C. Zerner, in *Reviews in Computational Chemistry*, ed. K. B. Lipowitz and D. B. Boyd, VCH, New York, 1991, vol. 2 p 313. W. J. Hehre, L. Radam, P. v. R. Schleyer, *Ab Initio Molecular Orbital Theory*, Wiley, New York, 1986. A. Szabo and N. S. Ostlund, *Modern Quantum Chemistry: Introduction to Advanced Electronic Structure Theory*, London Free Press, New York, 1982. I. N. Levine, *Quantum Chemistry*, Prentice Hall, New Jersey, 1991.

5 (a) J. A. Pople, D. P. Santry and G. A. Segal, *J. Chem. Phys.*, 1965, **43**, S129. J. A. Pople, and G. A. Segal, *J. Chem. Phys.*, 1965, **43**, S136.

6. J. A. Pople, D. L. Beveridge and P. A. Dobosh, *J. Chem. Phys.*, 1967, **47**, 2026.

7. R. C. Bingham, M. J. S. Dewar and D. H. Lo, *J. Am. Chem. Soc.*, 1975, **97**, 1285.

8. M. J. S. Dewar and W. J. Thiel, *J. Am. Chem. Soc.*, 977, **99**, 4899.

9. M. J. S. Dewar, E. G. Zoebisch, E. F. Healy and J. J. P. Stewart, *J. Am. Chem. Soc.*, 1985, **107**, 3902; M. J. S. Dewar, C. Jie and E. G. Zoebisch, *Organometallics*, 1985, **4**, 1964.

10. J. J. P. Stewart, *J. Comput.Chem.*, 1989, **10**, 209; J. J. P. Stewart, *J. Comput. Chem.*, 1989, **10**, 221.

11. R. S. Mulliken, *J. Chem. Phys.*, 1955, **23**, 1833; *ibid*, 1841; *ibid*, 2338; *ibid*, 2345.

12. MOPAC 93, J. J. P. Stewart and Fujitsu Limited, Tokyo, 1993.

13. B. H. Besler, K. M. Merz, Jr. and P. Kollman, *J. Comput. Chem.*, 1990, **4**, 431.

14. A more detailed discussion of kinetics can be found in J. Moore, *Physical Chemistry*, Longman, London, 1972. P. W. Atkins, *Physical Chemistry*, Oxford University Press, Oxford, 1986.

15. (a) AMPAC 4.0, 1992, © Semichem, 12751W, 66th Terrace, Shawnee, KS66216; (b) AMPAC 4.5, 1993, © Semichem, 12751W, 66th Terrace, Shawnee, KS66216.

16. (a) C. G. Broyden, *J. Inst. Mathem. Appl.*, 1970, **6**, 222; (b) R. Fletcher, *Comput. J.*, 1965, **8**, 33; (c) D. Goldfarb, *Mathem. Comput.*, 1970, **24**, 23; (d) D. F. Shanno, *Mathem. Comput.*, 1970, **24**, 647; (e) D. F. Shanno, *Optim. Theory Appl.*, 1985, **46**, 87.

17. R. H. Bartels, University of Texas, Center for Numerical Analysis, Report CNA-44, Austin, 1972.

18. J. Baker, *J. Comput. Chem.*, 1986, **7**, 385.

19. M. J. S. Dewar, E. F. Healy, J. J. P. Stewart, *J. Chem. Soc., Faraday Trans. II*, 1984, **3**, 227.

20. Review of intrinsic reaction coordinates: D.G. Truhlar, R. Steckler and M.S. Gordon, *Chem. Rev.*, 1987, **87**, 217 and the references cited therein.

21. A more detailed discussion in given by H. Maskill, *The Physical Basis of Organic Chemistry*, Oxford Science Publications, Oxford, 1985, p293.

22. (a) I. H. Williams, *Chem. Phys. Lett.*, 1982, **88**, 462. (b) I. H. Williams, *J. Mol. Struct., THEOCHEM*, 1983, **94**, 275.

23. Physical Organic texts: C. D. Ritchie, *Physical Organic Chemistry: The Fundamental Concepts*, Marcel Dekker Inc., New York, 1990. T. H. Lowry and K. Scheuller Richardson, *Mechanism and Theory in Organic Chemistry*, Harper Collins, New York, 1987. J. March, *Advanced Organic Chemistry*, Wiley, New York, 1985, p 179.

24. Recent review articles: V. K. Singh, *Synthesis*, 1992, 605; S. Wallbaum and J. Martens, *Tetrahedron: Asymmetry*, 1992, **3**, 1475; L. Deloux and M. Srebnik, *Chem. Rev.*, 1993, **93**, 763.

25. D. Sartor, J. Saffrich and G. Helmchen, *Synlett*, 1990, 197; M. Takasu and H. Yamamoto, *Synlett*, 1990, 194; D. Sartor, J. Saffrich, G. Helmchen, C. J. Richards and H. Lambert, *Tetrahedron: Asymmetry*, 1991, **2**, 639; E. J. Corey and T. -P. Loh, *J. Am. Chem. Soc.*, 1991, **113**, 8966.

26. N. N. Joshi, M. Srebnik and H. C. Brown, *Tetrahedron Lett.*, 1989, **30**, 5551; E. J. Corey and K. A. Cimprich, *J. Am. Chem. Soc.*, 1994, **116**, 3151.

27. (a) A. Hirao, S. Itsuno, S. Nakahama and N. Yamazaki, *J. Chem. Soc., Chem. Commun.*, 1981, 315; (b) S. Itsuno, A. Hirao, S. Nakahama and N. Yamazaki, *J. Chem. Soc., Perkin Trans. 1*, 1983, 1673; (c) S. Itsuno, K. Ito, A. Hirao and S. Nakahama, *J. Chem. Soc., Chem. Commun.*, 1983, 469; (d) S. Itsuno, K. Ito, A. Hirao and S. Nakahama, *J. Org. Chem.*, 1984, **49**, 555; (e) S. Itsuno, Y. Sakurai, A. Hirao and S. Nakahama, *Bull. Chem. Soc. Jpn.*, 1987, **60**, 395.

28. E. J. Corey, M. Azimioara and S. Sarshar, *Tetrahedron Lett.*, 1992, **33**, 3429.

29. E. J. Corey, R. K. Bakshi and S. Shibata, *J. Am. Chem. Soc.*, 1987, **109**, 5551.

30. (a) E. J. Corey, R. K. Bakshi, S. Shibata, C. -P. Chen and V. K. Singh *J. Am. Chem. Soc.*, 1987, **109**, 7925; (b) G. B. Stone, *Tetrahedron: Asymmetry*, 1994, **5**, 465. (c) see reference 27a (d) J. M. Brunel, M. Maffei and G. Buono, *Tetrahedron: Asymmetry*, 1993, **4**, 2255. (e) J. G. H. Willems, F. Jan Dommerholt, J. B. Hammink, A. M. Vaarhorst, L. Thijs and B. Zwanenburg, *Tetrahedron Lett.*, 1995, **36**, 603. (f) A. V. R. Rao, M. K. Gurjar and V. Kaiwar, *Tetrahedron: Asymmetry*, 1992, **3**, 859. (g) A. V. R. Rao, M. K. Gurjar, P. A. Sharma and V. Kaiwar, *Tetrahedron Lett.*, 1990, **31**, 2341. (h) W. Behnen, Ch. Dauelsber, S. Wallbaum and J. Martens, *Synth. Commun.*, 1992, **22**, 2143. (i) E. Didier, B. Loubinoux, G. M. Ramos Tombo and G. Rihs, *Tetrahedron*, 1991, **47**, 4941.

31. D. J. Mathre, A. S. Thompson, A. W. Douglas, K. Hoogsteen, J. D. Carroll, E. G. Corley and E. J. J. Grabowski, *J. Org. Chem.*, 1993, **58**, 2880.

32. H. Tlahuext and R. Contreras, *Tetrahedron: Asymmetry*, 1992, **3**, 1145.

33. E. J. Corey, J. O. Link and R. K. Bakshi, *Tetrahedron Lett.*, 1992, **33**, 7107.

34. (a) V. Nevalainen, *Tetrahedron: Asymmetry*, 1991, **2**, 63. (b) *ibid*, 1991, **2**, 429. (c) *ibid*, 1991, **2**, 827. (d) *ibid*, 1991, **2**, 1133. (e) *ibid*, 1992, **3**, 921. (f) *ibid*, 1992, **3**, 933. (g) *ibid*, 1992, **3**, 1441. (h) *ibid*, 1992, **3**, 1563, (i) *ibid*, 1993, **4**, 1505. (j) *ibid*, 1993, **4**, 1565. (k) *ibid*, 1993, **4**, 1569. (l) *ibid*, 1993, **4**, 1597. (m) *ibid*, 1993, **4**, 2001. (n) *ibid*, 1993, **4**, 2517. (o) *ibid*, 1994, **5**, 289. (p) *ibid*, 1994, **5**, 387. (q) *ibid*, 1994, **5**, 395.

35. J. Hine, *Adv. Phys. Org. Chem.*, 1977, **15**, 1.

36. H. C. Brown, H. I. Schlesinger and A. B. Burg, *J. Am. Chem. Soc.*, 1939, **92**, 1637.

37. S. S. White and H. C. Kelly, *J. Am. Chem. Soc.*, 1970, **92**, 4203.

38. M. F. Hawthorne and E. S. Lewis, *J. Am. Chem. Soc.*, 1958, **80**, 4296.

39. R. E. Davis and R. E. Keson, *J. Am. Chem. Soc.*, 1967, **89**, 1384.

40. D. C. Wigfield and F. W. Gowland, *Tetrahderon Lett.*, 1979, **24**, 2205

41. D. M. Ferguson, I. R. Gould, W. A. Glauser, S. Scroeder and P. A. Kollman, *J. Comput. Chem.*, 1992, **13**, 525.

42. D. R. Armstrong, P. G. Perkins and J. J. P. Stewart, *J. Chem. Soc., Dalton Trans.*, 1973, 838.

43. Gaussian 92 Revision C.4, MJ. Frisch, G.W. Trucks, M. Head-Gordon, P.M.W. Gill, M.W. Wong, J.B. Foresman, B.G. Johnson, H.B. Schlegel, M.A. Robb, E.S. Replogle, R. Gomperts, J.L. Andres, K. Raghavachari, J.S. Binkley, C. Gonzalez, R.L. Martin, D.J. Fox, D.J. Defrees, J. Baker, J.J.P. Stewart and J.A. Pople, Gaussian Inc., Pittsburgh PA, 1992.

44. (a) D. Cai, D. Tschaen, Y. -J. Shi, T. R. Verhoeven, R. A. Reamer and A. W. Douglas, *Tetrahedron Lett.*, 1993, **34**, 3243; (b) Y. -J. Shi, D. Cai, U. -H. Dolling, A. W. Douglas, D. M. Tschaen and T. R. Verhoeven, *Tetrahedron Lett.*, 1994, **35**, 6409.

45. R. Berenguer, J. Garcia, M. Gonzàlez and J. Vilarrasa, *Tetrahedron: Asymmetry*, 1993, **4**, 13.

46. B. T. Cho and M. H. Ryu, *Bull. Korean. Chem. Soc.*, 1994, **15**, 1080

47. G. B. Stone, *Tetrahedron: Asymmetry*, 1994, **5**, 465.

48. J. M. Brunel, M. Maffei and G. Buono, *Tetrahedron: Asymmetry*, 1993, **4**, 2255.

49. J. M. Brown, G. C. Lloyd-Jones and T. P. Layzell, *Tetrahedron: Asymmetry*, 1993, **4**, 2151.

50. T. K. Jones, J. J. Mohan, L. C. Xavier, T. J. Blacklock, D. J. Mathre, P. Sohar, E. T. Turner Jones, R. A. Reamer, F. E. Roberts and E. J. J. Grabowski, *J. Org. Chem.*, 1991, **56**, 763.

51. D. K. Jones, D. C. Liotta, I. Shinkai and D. J. Mathre, *J. Org. Chem.*, 1993, **58**, 799.

52. G. J. Quallich, J. F. Blake and T. M. Woodall, *J. Am. Chem. Soc.*, 1994, **116**, 8516.

53. E. J. Corey, J. O. Link, S. Sarshar and Y. Shao, *Tetrahedron Lett.*, 1992, **33**, 7103.

54. G. Fronza, C. Fuganti, S. Lanati, R. Rallo and S. Servi, *Tetrahedron Lett.*, 1995, **36**, 123.

55. G. Iwasaki, M. Sano, M. Sodeoka, K. Yoshida and M. Shibasaki, *J. Am. Chem. Soc.*, 1988, **53**, 4864.

56. (a) Y. -D. Wu, J. A. Tucker and K. N. Houk, *J. Am. Chem. Soc.*, 1991, **113**, 5018 and references cited therein. (b) A. S. Cieplak, *J. Am. Chem. Soc.*, 1988, **103**, 4550.

57. J. M. Brunel, O. Pardigon, B. Faure and G. Buono, *J. Chem. Soc., Chem. Commun.*, 1992, 287; G. Buono, J. M. Brunel, B. Faure and O. Pardigon, *Phosphorus Sulfur Silicon*, 1993, 43; J. M. Brunel, G. Buono, A. Baldy, J. Feneau-Dupont and J. -P. Declerq, *Acta Cryst. C.*, 1994, **C50**, 954.

58. B. Burns, E. Merifield, M. F. Mahon, K. C. Molloy and M. Wills, *J. Chem. Soc., Perkin Trans. 1*, 1993, 2243.

59. B. Burns, J. R. Studley and M. Wills, *Tetrahedron: Lett.*, 1993, **34**, 7105.

60. B. Burns, P. King, J. R. Studley, H. Tye and M. Wills, *Tetrahedron: Asymmetry*, 1994, **5**, 801.

61. Reference 60: see references 9, 10 and 11 contained therein.

62. J. R. Studley and M. Wills, *unpublished work.*

63. T. Mukaiyama, K. Soai and S. Kobayashi, *Chem. Lett.*, 1978, 219. K. Soai and T. Mukaiyama, *Chem. Lett.*, 1978, 491. T. Sato, K. Soai, K. Suzuki and T. Mukaiyama, *Chem. Lett.*, 1978, 601.

64. T. Mukaiyama, K. Soai, T. Sato, H. Shimizu and K. Suzuki, *J. Am. Chem. Soc.*, 1979, **101**, 1455.

65. M. Kitamura, S. Suga, K. Kawai and R. Noyori, *J. Am. Chem. Soc.*, 1986, **108**, 6071.

66. Review articles and the references cited therein: R. Noyori and M. Kitamura, *Angew. Chem. Int. Ed. Engl.*, 1991, **30**, 49. K. Soai and S. Niwa, *Chem. Rev.*, 1992, **92**, 833.

67. E. J. Corey and F. J. Hannon, *Tetrahedron Lett.*, 1987, **28**, 5233.

68. N. N. Joshi, M. Srebnik and H. C. Brown, *Tetrahedron Lett.*, 1989, **30**, 5551.

69. N. E. Moualij and C. Caze, *Eur. Polym. J.*, 1995, **31**, 193.

70. M. Kitamura, S. Okada, S. Suga and R. Noyori, *J. Am. Chem. Soc.*, 1989, **111**, 4028.

71. E. Kaufmann, P. v. R. Schleyer, K. N. Houk and Y. -D. Wu, *J. Am. Chem. Soc.*, 1985, **107**, 5560.

72. S. Itsuno, J. M. J. Frèchet, *J. Org. Chem.*, 1987, **52**, 4140.

73. Reference 63 in R. Noyori and M. Kitamura, *Angew. Chem. Int. Ed. Engl.*, 1991, **30**, 49.

74. E. J. Corey, P. -W. Yuen, F. J. Hannon and D. A. Wierda, *J. Am. Chem. Soc.*, 1990, **55**, 784.

75. K. Soai, A. Ookawa, T. Kaba and K. Ogawa, *J. Am. Chem. Soc.*, 1987, **109**, 7111.

76. M. Kitamura, S. Suga, M. Niwa and R. Noyori, *J. Am. Chem. Soc.*, 1995, **117**, 4832.

77. M. Yamakawa and R. Noyori, *J. Am. Chem. Soc.*, 1995, **117**, 6327.

78. M. J. S. Dewar and K. M. Merz, *Organometallics*, 1988, 7, 522.

79. J. J. P. Stewart, *J. Comp. Chem.*, 1991, **12**, 320.

80. It is envisaged that this work could be carried out as part of a colloboration with Dr. Paul Sherwood at Daresbury who is developing CHEMSH, a combined QM/MM program.

81. Free energy calculations can be performed using the current version of Macromodel. For further details see the references cited within the manual.